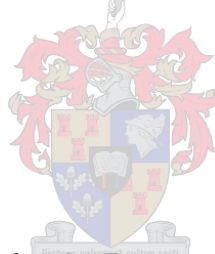


Synthesis of magnetite nanoparticles and their  
potential application in transition and platinum  
group metal ion extraction

Laura Lisa Vatta



Dissertation presented for the Degree of Doctor of Philosophy  
at the University of Stellenbosch

Promoter: Professor Klaus R. Koch

Co-promoter: Professor Ron D. Sanderson

March 2007

**I, the undersigned, hereby declare that the work contained in this dissertation is my own original work and that I have not previously in its entirety or in part submitted it at any university for a degree.**

**SIGNATURE:**

\_\_\_\_\_

**Laura L Vatta**

**DATE:**

**February 2007**

## Summary

---

This thesis comprises of the following main sections:

### *Synthesis of magnetite nanoparticles*

Parameters that are potentially important for the industrial-scale synthesis of magnetite nanoparticles were investigated in a factorial design experiment. It was found that the Fe(III):Fe(II) ratio specifically should be controlled in an industrial environment while small variations in the iron and ammonia solution concentrations do not significantly affect precipitate properties. These parameters were incorporated into a study on the large-scale synthesis of 8 – 12 nm magnetite particles using high pressure impinging stream reactors. The magnetite material was synthesised at rates of between 30 g min<sup>-1</sup> at 200 kPa and 50 g min<sup>-1</sup> at 500 kPa.

### *Applications of magnetite nanoparticles in transition metal ion extraction*

The use of magnetite, a magnetic liquid and the extractants Aliquat 336 and methyl isobutyl ketone incorporated into a magnetic liquid were investigated in the extraction of Co(II) from a model [Co(SCN)<sub>4</sub>]<sup>2-</sup> system. The magnetically modified systems were found to compare favourably with or extract more [Co(SCN)<sub>4</sub>]<sup>2-</sup> than the conventional extractant systems as a result of the added potential for anion extraction by the cationic magnetite surface in acidic media. Commercial solvent extractants (Cyanex 272, D2EHPA and LIX 984N) incorporated into a magnetic liquid showed an increased rate of phase separation after solvent extraction when using an externally applied magnetic field as compared to a non-magnetic system.

### *Applications of magnetite nanoparticles in platinum group metal ion extraction*

Magnetite nanoparticles coated with silica and functionalised with diethylenetriamine were shown to be capable of selective Pd(II) extraction over Cu(II) (at pH < 4) as well as showing an improved resistance of up to 80 % as compared to bare magnetite in acidic media. Degradation of ion exchanger material of up to 55 % was observed when the ion exchanger was used in four successive recovery cycles and under harsh desorption conditions. Alternative desorbents should decrease this iron dissolution.

## Opsomming

---

Die verhandeling bevat die volgende hoof tema's:

### *Sintese van magnetiet nanopartikels*

Die belangrikste proses eienskappe vir die industriële skaal sintese van magnetiet nanopartikels is ondersoek deur gebruik te maak van 'n faktoriale ekperimentele ontwerp benadering. Die Fe(III):Fe(II) verhouding is van kritiese belang en moet noukeurig gekontroleer word in die industriële skaal sintese, terwyl klein variasies in die magnetiet en ammoniak oplossing konsentrasies nie 'n waarneembare invloed op die presipitasie eienskappe van die nanopartikels het nie. Die resultate van die ondersoek is in ag geneem tydens die grootskaalse sintese van 8 – 12 nm magnetiet partikels met behulp van 'n hoëdruk stroomreaktor. Die magnetiet nanopartikels is gesintetiseer met vloeitempo's tussen 30 g min<sup>-1</sup> by 200 kPa en 50 g min<sup>-1</sup> by 500 kPa.

### *Gebruik van magnetiet nanopartikels in oorgangsmetaal ion ekstraksie*

Magnetiet, magnetiese vloeistof, en die gemodifiseerde magnetiese vloeistof bestaan uit die ekstraktant Aliquat 336 en metiel isobutiel ketoon, was gebruik om die ekstraksie van Co(II) uit die model [Co(SCN)<sub>4</sub>]<sup>2-</sup> stelsel te ondersoek. Die gemodifiseerde magnetiese vloeistof stelsel vergelyk gunstig, of ekstraheer meer [Co(SCN)<sub>4</sub>]<sup>2-</sup>, as konvensionele ekstraksie. Dit is waarskynlik as gevolg van die affiniteit vir anioon ekstraksie deur die kationiese magnetiet oppervlakte in 'n suur medium. Met die toevoeging van kommersiële ekstraheer middels (Cyanex 272, D2EHPA en LIX 984N) word die faseskeiding van die magnetiese vloeistof na die ekstraksie onder die invloed van 'n eksterne magnetiese veld verhoog in vergelyking met die nie-magnetiese sisteme.

### *Gebuike van magnetiet nanopartikels in platinum groep metal ion ekstraksie*

Deur die silika bedekte magnetiet nanopartikels te funksionaliseer met di-etileentriamien toon die nanopartikels 'n selektiewe ekstraksie vir Pd(II) oor Cu(II) by 'n pH < 4. Verder vertoon die nanopartikels 'n verhoogde weerstand teen degradasie in 'n suur medium van tot 80 %. Onder desorpsie kondisies toon die funksionele nanopartikels 'n degradasie van tot 55 % na vier agtereenvolgende desorpsie siklusse. Die gebruik van alternatiewe desorpsie materiaal kan die degradasie van die magnetiet verder verminder.

## Acknowledgements

---

I would like to express my sincere gratitude towards:

Prof Klaus Koch for his enthusiasm and encouragement, support, guidance, technical assistance and infectious passion for work. Thank you for giving me the opportunity to work in such a super group.

Prof Ron Sanderson for providing me with the opportunity to study at Stellenbosch University and for his strong belief in my ability.

The students and staff of the Department of Chemistry and Polymer Science, especially members of the Platinum Metals Research Group for their friendship, support and academic assistance: Adam, Annelie, Arjan, Bettinah, Mr Bonthuys, Calvin, Elsa, Erinda, Gavin, Jean, Jessica, Jos, Jovita, Jurjen, Lebo, Liezel, Lisinda, Lyndal, Marco, Maggie, Margie, Marlene, Nagaraju, Portia, Shafiek, Sibule, Sonto and Ursula.

The following people without whose valuable technical support and assistance, much of the work would have been impossible:

- George Langefeld, Dr Leon Krüger, Dr Vasile Murariu and Dr Staffan Tapper from the Research Group at De Beers Consolidated Mines
- Prof Andre Strydom from the Physics Department at the University of Johannesburg
- Mohamed Jaffer from the Microscopy Unit at the University of Cape Town
- Jannie Barnard, Anton Cordier, Prof Jacques Eksteen, Dr Raymond Els, Prof Leon Lorenzen, Esmé Spicer and Riana Roussouw from Process Engineering and the Central Analytical Facility at the University of Stellenbosch
- Dr Kathy Sole from Anglo Research
- Dr Dave Robinson from Anglo Platinum

The Harry Crossley Foundation (University of Stellenbosch), National Research Foundation (GUN2053351), THRIP (Project 2921) and Anglo Platinum for financial support.

My family and friends especially Tony, Adriano, Mark and my parents, especially my mom for their emotional support and encouragement.

## Contents

---

### Chapter 1

Introduction and thesis outline 1

### Chapter 2

A factorial design investigation into the effect of selected parameters on the precipitation of nanosized magnetite particles 6

### Chapter 3

An investigation into the potential large-scale continuous magnetite nanoparticle synthesis by high pressure impinging stream reactors 25

### Chapter 4

Magnetic liquids, magnetic liquid/Aliquat 336 and magnetic liquid/methyl isobutyl ketone mixtures for the extraction of  $[\text{Co}(\text{SCN})_4]^{2-}$  from an aqueous solution by solvent extraction 46

### Chapter 5

Sterically stabilised magnetic nanoparticle liquids for magnetically assisted base metal solvent extraction 70

### Chapter 6

The preparation of silica-coated, diethylenetriamine functionalized magnetic nanoparticle ion exchangers 111

### Chapter 7

Diethylenetriamine-functionalised silica-coated magnetite nanoparticles for selective palladium (II) ion extraction from chloride-rich aqueous solutions 138

### Chapter 8

Project summary, evaluation and general discussion 154

## Chapter 1

### Introduction and thesis outline

---

#### 1. Properties of magnetic nanoparticles

Scientists have become increasingly interested in the field of nanoscience and nanotechnology<sup>1</sup>, a broad interdisciplinary area of research involving chemistry, physics, metallurgy and engineering and with the emphasis on materials in the range of 1 – 100 nm.

Nanoparticles are defined as solid well-characterised materials being less than 100 nm in all dimensions and are more often defined as spherical particles of the order of 10 nm or less<sup>2</sup>. They may have unique electrical, chemical, structural and magnetic properties<sup>3</sup> and are becoming increasingly important in a variety of different fields. Nanosized magnetic particles are already being used in a number of applications<sup>2, 4-14</sup>: as surface functionalised particles for biosensing applications, in magnetic storage media, in catalysis, for investigations into surface effects and magnetism, in magnetic liquids, in sensors and in medical applications. Interesting medical applications include their use as contrast agents in magnetic resonance imaging, cell separation and targeted drug delivery where the magnetic properties of the particles allow for the directed movement and retention of a biological effector at the required point of action.

The properties of the magnetic nanoparticles are highly dependent on their size, morphology and chemical composition<sup>2</sup>. Bulk ferromagnetic materials are subdivided into areas known as domains<sup>15</sup>. In an unmagnetised sample and below the Curie temperature, the moments of these domains are randomly orientated but will tend to align themselves in the direction of an external applied magnetic field. The magnetisation and subsequent reversal of magnetisation occurs through the motion of the domain walls. As the particle size approaches a certain minimum critical size, often in the nanometre range, the formation of domain walls becomes energetically unfavourable. Changes in magnetization occur through the coherent rotation of spins rather than through the motion of domain walls. Particles of this size that exhibit these properties are called single domain particles. The critical volume for single domain magnetite particles<sup>11</sup>, is calculated to be approximately 50 nm.

As size is decreased further (and depending on the particle anisotropy), the particles become superparamagnetic<sup>2, 3, 13</sup>. Superparamagnetic materials can be magnetised when exposed to an external applied magnetic field but exhibit no hysteresis in their magnetisation curve and have zero magnetisation at zero applied field<sup>16</sup>. Superparamagnetism is often only displayed at room temperature<sup>11</sup> when the particle size is in the region of 10 nm. Because of the size of the particles, thermal energy is normally sufficient to overcome magnetic coupling moments by causing atomic magnetic moments to fluctuate randomly. In the absence of a magnetic field, the particles exhibit a random distribution of magnetic moments so that the collection of particles have no net magnetisation. In an applied

magnetic field, the moments experience an induced torque and align in the direction of the field either by rotation of the particle itself or by rotation of the magnetic vector of the particles. The relaxation mechanism is a function of the particles' anisotropy and thermal energy<sup>2</sup> and occurs either by Néel relaxation (relaxation of the internal magnetization vector) or Brownian relaxation (rotational diffusion of the particle)<sup>10, 17, 18</sup>.

The superparamagnetic phenomenon essentially allows one to use these materials as conventional “unmagnetised” materials but with the added advantage that one can control and transport them when and as required by judicious application of an external applied magnetic field produced by an electromagnet or permanent magnet<sup>3, 5, 19</sup>.

In addition, the small particle size provides a large surface area for functionalisation or attachment of a high concentration of the species of interest and allows for the use of these particles in applications where small dimensions are required (see as a comparison the sizes of commonly occurring small objects, Fig. 1)<sup>20</sup>. With a decrease in particle size, the available surface area increases (i.e. surface to volume ratio increases)<sup>13</sup>. As an illustration, a 3 nm particle has 50 % of its atoms on its surface as compared to the 20 and 5 % surface atoms possessed by 10 and 30 nm particles, respectively<sup>20</sup>. (It may, however, be more difficult to manipulate very small particles if they possess a low magnetic susceptibility<sup>9</sup>.) The surface area of 1 g of magnetite nanoparticles increases from approximately 100 to 1000 m<sup>2</sup> as the particle diameter decreases from 10 to 1 nm.

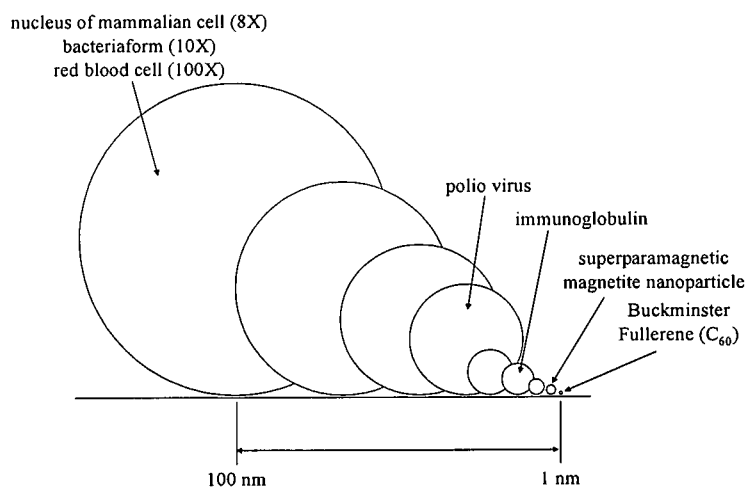


**Figure 1** Size comparison of magnetite nanoparticles with other common small objects<sup>20</sup>

## 2. Magnetite nanoparticles

Magnetite ( $\text{Fe}_3\text{O}_4$ ) is one of the sixteen natural and commonly occurring hydroxides or oxide hydroxides and is used for interesting purposes such as by salmon, honey bees and pigeons for navigation and by bacteria for magnetotaxis<sup>7</sup>.

Magnetite is a black material with a crystalline inverse spinel structure<sup>7</sup>. It differs from most iron oxides in that it contains both divalent and trivalent iron, with structure  $Y[XY]O_4$  where  $X = \text{Fe(II)}$  and  $Y = \text{Fe(III)}$  and the brackets denote octahedral sites. The trivalent ions occupy both tetrahedral and octahedral sites<sup>7</sup> as shown in Fig. 2. Stoichiometric magnetite has Fe(III) in a ratio of 2:1 to Fe(II) but in practice, magnetite is frequently non-stoichiometric with a cation deficient Fe(III) sublattice<sup>18</sup>. The divalent ion may be replaced by other divalent species such as Mn(II) or Zn(II) as the oxygen framework is flexible, allowing for a change in shape to accommodate cations different in size from the Fe(II) ions. In magnetite, the occupation of tetrahedral and octahedral sites by trivalent iron and the occupation of octahedral sites by divalent iron, allows for a system of two interpenetrating magnetic sublattices. The spins on the octahedral and tetrahedral sites are antiparallel and of unequal magnitude resulting in a ferromagnetic order<sup>7</sup>. Magnetite has a density of  $5.18 \text{ g cm}^{-3}$ , a Curie temperature of 850 K and a saturation magnetisation<sup>7,10</sup> ranging from 300 to 480  $\text{kA m}^{-1}$ .

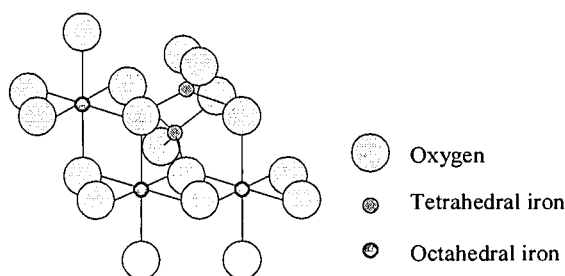


**Figure 2** Ball and stick model showing arrangement of octahedral and tetrahedral sites in magnetite<sup>7</sup>

### 3. Research goals and thesis outline

We have become interested in the use of magnetite nanoparticles for a variety of potential industrial applications including transition and platinum group metal ion extraction. The research aims of this thesis were:

1. The large-scale synthesis and characterisation of magnetite nanoparticles,
2. the synthesis and investigation of the use of a magnetic liquid system for transition metal ion extraction and
3. the synthesis and investigation of a superparamagnetic ion exchanger for transition and/or platinum group metal ion extraction

In **Chapter 2**, work focuses on the importance of selected parameters for the industrial scale precipitation of magnetite. These parameters are then taken into consideration in **Chapter 3** in the investigation of the use of high pressure impinging stream reactors for the large-scale, continuous precipitation of magnetite.

In **Chapter 4**, a model system is studied for the extraction of  $[\text{Co}(\text{SCN})_4]^{2-}$  from an aqueous phase onto the surface of bare magnetite and into a magnetic organic phase. The results are compared to the extraction into a conventional non-magnetic organic phase.

Work is extended in **Chapter 5** to investigate the percentage metal ion extraction and rate of organic/aqueous phase separation after solvent extraction by comparison of a conventional solvent extraction system with a system in which commercial liquid organic extractants are incorporated into a magnetic liquid, thereby conferring magnetic properties to the extractants.

The synthesis of a silica-coated diethylenetriamine functionalised acid resistant magnetite ion exchanger is discussed in **Chapter 6** and the use of these particles in the selective extraction of Pd(II) over Cu(II) is discussed in **Chapter 7**.

**Chapter 8** concludes with the main findings and recommendations and evaluates the systems discussed in the thesis.

The following papers are based in part on this thesis:

- Vatta, L. L.; Sanderson, R. D.; Koch, K. R., Magnetic nanoparticles: Properties and potential applications. *Pure Appl. Chem.* 2006, **78**, (9), 1791-1799.
- Vatta, L. L.; Sanderson, R. D.; Koch, K. R., An investigation into the potential large-scale continuous magnetite nanoparticle synthesis by high pressure impinging stream reactors. In press. *Journal of Magnetism and Magnetic Materials* 2007.
- Vatta, L. L.; Kramer, J.; Koch, K. R., Diethylenetriamine functionalised silica coated magnetite nanoparticles for selective palladium ion extraction from aqueous solutions. In press. *Separation Science and Technology* 2007.
- Vatta, L. L.; Koch, K. R., The extraction of  $[\text{Co}(\text{SCN})_4]^{2-}$  from an aqueous solution by solvent extraction using a magnetic liquid and a magnetic liquid/Aliquat 336 mixture. Manuscript in preparation 2007.
- Vatta, L. L.; Sole, K. C.; Koch, K. R., Sterically stabilised nanoparticle magnetic liquids for magnetically assisted base metal solvent extraction. Manuscript in preparation 2007.

## References

1. Horng, H. E., *J. Phys. Chem. Solids* 2001, **62**, 1749.
2. Willard, M. A.; Kurihara, L. K.; Carpenter, E. E.; Calvin, S.; Harris, V. G., *Encycl. Nanosci. Nanotech.* 2004, **1**, 815.
3. Leslie-Pelecky, D. L.; Rieke, R. D., *Chem. Mater.* 1996, **8**, 1770.
4. Charles, S. W.; Popplewell, J., *Ferromagnetic liquids, ferromagnetic materials: a handbook on the properties of magnetically ordered substances* North-Holland Publishing Company, Amsterdam, 1980.
5. Buske, N.; Sonntag, H.; Götze, T., *Colloids Surf.* 1984, **12**, 195.
6. Charles, S. W.; Popplewell, J., *IEEE Trans. Magn.* 1980, **Mag-16**, 172.

7. Cornell, R. M.; Schwertmann, U., *The iron oxides* VCH Publishers, New York, 1996.
8. Farkas, J., *Sep. Sci. Technol.* 1983, **18**, 787.
9. Häfeli, U. O., *Int. J. Pharm.* 2004, **277**, 19.
10. Matusevich, N. P.; Orlov, L. P.; Samoilov, V. B.; Fertman, V. E., *Heat Transfer - Soviet Research* 1987, **19**, 25.
11. Rosensweig, R. E., *Ferrohydrodynamics* Cambridge University Press, Cambridge, 1985.
12. Reimers, G. W.; Khalafalla, S. E., *Preparing magnetic fluids by a peptizing method* U. S. Department of the Interior, Twin Cities Metallurgy Research Centre, Minneapolis, 1972, 1.
13. Hilgendorff, M., *Encycl. Nanosci. Nanotech.* 2004, **1**, 213.
14. Bönnemann, H.; Nagabhushana, K. S., *Encycl. Nanosci. Nanotech.* 2004, **1**, 777.
15. Jakubovics, J. P., *Magnetism and magnetic materials*, Cambridge University Press, Cambridge, 1994.
16. Craik, D., *Magnetism: principles and applications* John Wiley and Sons Ltd, Chichester, 1995.
17. Nakatsuka, K.; B., J., *IEEE Trans. Magn.* 1994, **30**, 4671.
18. Tartaj, P., *Encycl. Nanosc. Nanotech.* 2004, **6**, 823.
19. Ahn, C. H.; Choi, J.-W.; Hyong, J. C., *Encycl. Nanosc. Nanotech.* 2004, **6**, 815.
20. Klabunde, K. J., *Nanoscale materials in chemistry* Wiley-Interscience, New York, 2001.

## Chapter 2

### A factorial design investigation into the effect of selected parameters on the precipitation of nanosized magnetite particles

---

#### Abstract

Optimum ranges of various factors important for magnetite precipitation, such as iron and ammonia solution concentration, temperature, reagent addition time, pH and ionic strength, have been defined by various research groups. Slight variations in such parameters can be expected in a potential industrial environment where magnetite is precipitated on a larger scale. A factorial design experiment was conducted to determine the sensitivity and effect on the saturation magnetisation, percentage magnetite precipitated (as opposed to the precipitation of other non-magnetic iron oxides) and particle size for variations within the suggested parametric range for iron and ammonia solution concentrations and Fe(III)/Fe(II) molar ratio. The Fe(III)/Fe(II) molar ratio was found to be the most important factor affecting saturation magnetisation and the precipitation of magnetite. For industrial scale precipitation, an Fe(III):Fe(II) molar ratio of 2 should be used and the iron solution should be prepared immediately prior to use, to prevent Fe(II) oxidation and subsequent variations in Fe(III):Fe(II) molar ratio. The iron and ammonia solution concentrations, the Fe(III):Fe(II) molar ratio and the interaction between the Fe(III):Fe(II) molar ratio and iron solution concentration were found to have an effect on the particle size. However, the maximum change in particle size was approximately  $\pm 2$  nm which is not significant for our applications. Variations within the suggested ranges should not adversely affect the precipitation of magnetite of a certain size, and the iron and ammonia solution concentrations can therefore be maintained within the range of 0.5 – 1.5 and 8.3 – 13.5 mol l<sup>-1</sup>, respectively.

#### 1. Introduction

##### *1.1 Methods for the synthesis of magnetic particles*

Three methods are commonly used for the preparation of magnetic nanoparticles: physical vapour deposition<sup>1</sup> (assembly of individual atoms to form nanostructures), mechanical attritioning<sup>1,2</sup> (fracturing of larger coarse-grained structures) and chemical routes from solution which may include precipitation, reduction, hydrothermal means, micelle routes, decomposition of transition organometallic complexes by thermolysis, photolysis or sonolysis, sol-gel methods, polyol methods and electrochemical or electrodeposition methods<sup>1-3</sup>. Chemical routes for the preparation of magnetic nanoparticles are advantageous in that enhanced homogeneity may be achieved more easily using solution chemistry as opposed to using mechanical forces such as attritioning and the method lends itself to the cost-effective production of large quantities of material.

Although a variety of chemical syntheses routes exist, it was decided in this study to prepare magnetic nanoparticles by a precipitation route for a number of reasons:

- As mentioned in Chapter 1, nanoparticle composition and size impact on magnetic properties and the ideal synthesis technique should therefore offer control over these parameters<sup>4</sup>. In certain chemical syntheses methods such as the sol-gel method, reactions may be difficult to control resulting in undefined particle composition, size, size distribution, morphology, agglomerate size etc.<sup>5</sup> whilst precipitation methods usually allow for the control of these particle properties through the manipulation of parameters such as pH, metal cation type and concentration, temperature and type of precipitating agent<sup>5-7</sup>.
- Particle size could be controlled accurately in, for example, micelle synthesis or using thermolysis, photolysis or sonolysis synthesis methods where a polymer, surfactants, capping agents or ligands are used to limit space available for growth<sup>8,9</sup>. However, it may be difficult to free the particle from these reagents<sup>4</sup> and interaction of these agents with the particle surface may result in an alteration of their magnetic properties<sup>1</sup>. Precipitation reactions provide minimal contamination from additional reagents used to control particle size<sup>5</sup>.
- Precipitation in aqueous solutions is relatively simple, rapid and cost effective<sup>5,6</sup>. Syntheses by, for example, reduction or hydrothermal means are complex or have complex chemistry<sup>1</sup>.
- Surface modification during or after synthesis is easy to accomplish after precipitation and allows for added functionality<sup>1,6</sup>.
- Relatively large volumes of homogeneous material can be produced by precipitation<sup>1,5</sup>.

Magnetite (Fe<sub>3</sub>O<sub>4</sub>) is often chosen as the preferred magnetic nanoparticle precipitate as it is relatively easily prepared in aqueous solution and can be doped with Co(II), Mn(II), Zn(II) or Ni(II) (which allows for the manipulation of the magnetic hardness of the material)<sup>10</sup>. Pure ferromagnetic elements such as Fe, Co or Ni nanoparticles may exhibit a higher magnetisation<sup>11</sup> as compared to magnetite, however, they are more susceptible to oxidation<sup>12,13</sup>. In addition, magnetite offers other advantages in that there is potential for it to be manufactured at low cost using effluents containing iron compounds<sup>14</sup> (such as spent pickle liquor). The presence of other metal ions is not overly detrimental to magnetite precipitation provided they are present in relatively small amounts<sup>15</sup>. Magnetite is also of general interest because, along with maghemite (γ-Fe<sub>2</sub>O<sub>3</sub>), it is one of the only magnetic materials accepted for medical applications<sup>12,16</sup>.

### 1.2 The synthesis of magnetite nanoparticles by precipitation

Magnetic nanoparticle ferrites with the spinel structure, MFe<sub>2</sub>O<sub>4</sub> where M is a divalent metal cation, e.g., Co(II), Mn(II), Fe(II), can be prepared by addition of a base to an aqueous mixture of the metal salts<sup>12</sup>:



Fe(II) is a popular choice for coprecipitation with Fe(III) ions. The minimum Fe(III):M(II) molar ratio for  $MFe_2O_4$  precipitation (where M(II) is Fe(II), Co(II), Cu(II), Mn(II), Ni(II) or Zn(II)) is 10 for Fe(II), 3.3 for Co(II) or Cu(II) and 2 for Mn(II), Ni(II) or Zn(II), i.e., less Fe(II) is required than Co(II), Cu(II), Mn(II), Ni(II) or Zn(II) for  $MFe_2O_4$  precipitation. This is because the Fe(III)/Fe(II) system has the advantage of being able to exchange the identities of the M(III) and M(II) sites by electron transfer whilst particles are growing<sup>5, 6, 17, 18</sup>. In addition, aging is required for coprecipitation of Fe(III) with other divalent cations, because spinel can only form by redissolution-crystallisation equilibria (Ostwald ripening). Massart<sup>17</sup> first precipitated magnetite from an aqueous solution of Fe(III) and Fe(II) cations by addition of an alkaline solution. The formation and transformation pathways<sup>19</sup> of the iron oxides that can be produced by this method under various pH conditions are shown in Fig. 1. Because of the number of diverse iron oxides that could precipitate, control of certain important factors is required to obtain the magnetite spinel structure.

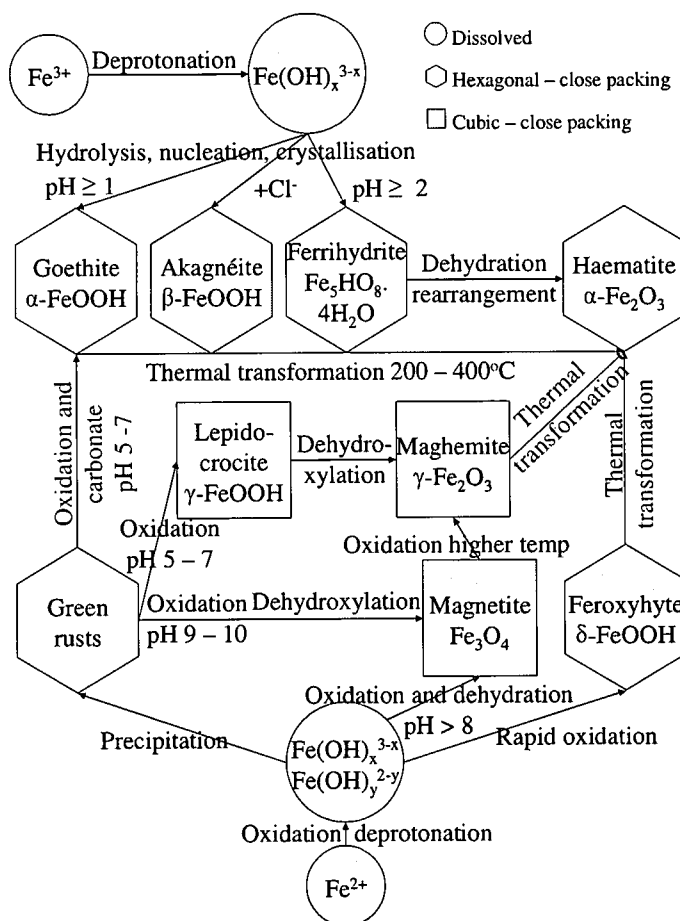


**Figure 1** Formation and transformation pathways of the iron oxides at various different pH conditions<sup>19</sup>

Much work has been performed to determine the effect of various parameters on the precipitation of the correct species of iron oxide from aqueous Fe(III)/Fe(II) solutions. Although certain conditions for the optimised

precipitation of magnetite, such as rate and intensity of mixing, temperature, nature of precipitator, presence of a surfactant and type of metal precursor salt used (chlorides, nitrates, perchlorates, etc.)<sup>6, 20, 21</sup>, can be found in literature, in general, these are for controlled laboratory conditions.

In Chapter 3 the use of impinging stream reactors is investigated for the precipitation of magnetite with the envisaged aim of using these reactors on a large commercial scale. In industry, depending on quality control practices, there may be variations in reagent quality. For example, ammonia solubility in an ammonium hydroxide solution is dependent on temperature and could vary according to environmental temperature changes thereby affecting the solution concentration. Alternatively, Fe(II) in a Fe(III)/Fe(II) reagent feed solution may oxidise with time thereby altering the iron solution concentration. (It has been suggested that a 1.5 molar ratio of Fe(III) to Fe(II) be used in practice instead of the stoichiometric value of 2 because of the potential oxidation of Fe(II)<sup>15</sup>.)

The importance of parameters such as Fe(III):Fe(II) molar ratio, iron concentration and ammonia concentration on nanosized magnetite precipitation has been determined over a wide range<sup>5, 6, 8, 22, 23</sup>. For example:

- An Fe(III):Fe(II) molar ratio smaller than or equal to 3 is suggested for magnetite precipitation.
- A final solution pH in the range of ~8 – 12 (from ammonia solution addition) is required not only for the precipitation of magnetite as opposed to other iron oxides but also allows for the precipitation of small magnetite particles.
- Media with high ionic strength (~0.5 – 3 mol l<sup>-1</sup>) allow for the precipitation of small particles.

It is, however, not clear what the effect would be on percentage magnetite precipitated (as a function of the total magnetic and non-magnetic iron oxide precipitated), saturation magnetisation and precipitate particle size within these defined ranges and with variations in reagent quality. A factorial design experiment was conducted in order to determine the sensitivity to variations in iron and ammonia solution concentrations and Fe(III):Fe(II) molar ratio within the suggested optimum ranges on magnetite precipitation. Once these effects have been established, variations in magnetite precipitation when using the impinging stream reactors (Chapter 3) can be ascribed to reactor parameters rather than to variations in reagent composition and the sensitivity of these factors on magnetite precipitation on an industrial scale can be established.

## 2. Experimental

### 2.1 Reagents and analytical methods

All reagents and solvents were purchased from commercial sources and were used without further purification. FeCl<sub>3</sub>·6H<sub>2</sub>O, FeSO<sub>4</sub>·7H<sub>2</sub>O and a 25 % NH<sub>4</sub>OH solution (Merck) were used for the precipitation of magnetite. Deionised water was used for the preparation of aqueous solutions.

Magnetisation curves (and saturation magnetization at a maximum field of  $1.35 \times 10^6 \text{ A m}^{-1}$ ) were obtained on an LDJ 9600 Vibrating Sample Magnetometer (VSM) while field emission scanning electron micrographs (FESEM) were obtained using a JEOL JSM-6000F Field Emission Scanning Electron Microscope. Densities of precipitates measured at  $20^\circ \text{C}$  were determined using an Anton Paar Densitometer. X-ray diffraction (XRD) measurements were obtained on a Siemens D501 Diffractometer with qualitative sample percentage composition determined using the reference intensity ratio and peak height. Particle size was determined in two manners: firstly using ImageJ, a public domain image processing program<sup>24</sup> and secondly through the method of Chantrell et al.<sup>25</sup> where an approximation of the magnetite particle size is determined indirectly from the magnetisation curve. There is evidence that the distribution of precipitate particle size is given by a log normal distribution while the total magnetisation is given by the sum of the contribution from each particle size weighted using the distribution function. Formulae have been derived for the median diameter ( $D_v$ ) and the standard ( $\sigma$ ) deviation of the log normal distribution:

$$D_v = \left[ \frac{18kT}{\pi I_s'} \sqrt{\frac{\chi_i}{3 \varepsilon I_s' H_o}} \right]^{\frac{1}{3}} \quad (2)$$

$$\sigma = \frac{\sqrt{\ln \left( \frac{3\chi_i}{\varepsilon I_s' \frac{1}{H_o}} \right)}}{3} \quad (3)$$

with  $k$  the Boltzmann constant,  $T$  the temperature,  $I_s'$  the saturation magnetisation for the bulk magnetic particles,  $\varepsilon$  the volumetric particle packing fraction,  $\chi_i$  the initial susceptibility and  $\frac{1}{H_o}$  the reciprocal field at  $I = 0$ . This method of particle size determination should be considered as an approximate one as a discrepancy could arise from the assumption of the validity of the log normal distribution of particle sizes.

## 2.2 Factorial design

A 3-factor full factorial experiment was designed where the effect of the following variable factors on magnetite precipitation were investigated: Fe(III):Fe(II) molar ratio (varied from 1 – 3), total iron concentration (varied from  $0.5 - 1.5 \text{ mol l}^{-1}$ ) and ammonia concentration (varied from  $8.3 - 13.5 \text{ mol l}^{-1}$ , the concentration of which was determined by titration with HCl). As responses to the experiments, the saturation magnetization, particle size (and standard deviation) and percentage magnetite (as a function of the total magnetic and non-magnetic iron oxide

precipitated) were determined. An analysis of variance (ANOVA) was performed to determine significant parameters in the model.

The conditions for each run in the factorial designed experiment with masses and volumes of reagents used in the experiments are given in Table 1. High and low levels in all possible combinations (runs 3 to 10) were investigated for each factor, i.e., at low and high levels 1 and 3 for the Fe(III):Fe(II) molar ratio, 0.5 and 1.5 mol l<sup>-1</sup> for the total iron concentration and 8.3 and 13.5 mol l<sup>-1</sup> for the ammonia concentration. Runs 1 and 2 are replicates with factors that are at the centre points of the design space (average of the high and low levels for each factor), i.e., the factors are set at an Fe(III):Fe(II) molar ratio of 2 (average of 1 and 3), a total iron concentration of 1 mol l<sup>-1</sup> (average of 0.5 and 1.5 mol l<sup>-1</sup>) and an ammonia concentration of 10.9 mol l<sup>-1</sup> (average of 8.3 and 13.5 mol l<sup>-1</sup>).

**Table 1** Conditions at each run for the factorial designed experiment

Run	Factor 1 Fe(III)/Fe(II) molar ratio	Factor 2 Iron conc (mol l <sup>-1</sup> )	Factor 3 Ammonia conc (mol l <sup>-1</sup> )	FeCl <sub>3</sub> .6H <sub>2</sub> O mass (g)	FeSO <sub>4</sub> .7H <sub>2</sub> O mass (g)	NH <sub>4</sub> OH solution volume (ml)
1	2	1	10.9	9.0	4.6	24.4
2	2	1	10.9	9.0	4.6	24.4
3	1	0.5	13.5	3.4	3.5	9.9
4	1	1.5	8.3	10.1	10.4	48.0
5	3	1.5	8.3	15.2	5.2	48.0
6	1	1.5	13.5	10.1	10.4	29.7
7	3	0.5	13.5	5.1	1.7	9.9
8	3	0.5	8.3	5.1	1.7	16.0
9	1	0.5	8.3	3.4	3.5	16.0
10	3	1.5	13.5	15.2	5.2	29.7

The required masses of FeCl<sub>3</sub>.6H<sub>2</sub>O and FeSO<sub>4</sub>.7H<sub>2</sub>O were dissolved in 50 ml water. Two times excess NH<sub>4</sub>OH solution was added rapidly to the iron solution with intense mixing. The precipitate was stirred for 10 minutes.

Saturation magnetizations were compared at a density of 1.4 g cm<sup>-3</sup> (diluted by addition of deionised water if required). If the sample could not be diluted to exactly 1.4 g cm<sup>-3</sup>, the saturation magnetization at 1.4 g cm<sup>-3</sup> was determined by the interpolation of the densities of two of the same samples of approximately 1.4 g cm<sup>-3</sup>.

For the preparation of samples for FESEM, the required mass of lauric acid (40 % by mass<sup>26</sup>, Sigma-Aldrich) and 5 ml 25 % NH<sub>4</sub>OH were added to 3X20 ml samples to prevent agglomeration of particles. (Excess ammonia is used to form a carboxylate with the surfactant because of its low solubility<sup>26</sup> although it is also possible to add the

dispersing agent in ammoniated form, e.g., as ammonium laurate<sup>15</sup>.) The flask was heated to 80 °C with mixing to promote dissolution of the lauric acid. Samples were suspended on carbon stubs and allowed to dry.

For the XRD measurements, the precipitate was washed with two portions of 200 ml water through which nitrogen had been bubbled. The wash water was decanted (non-magnetically so as to retain all precipitated material) each time between washing after allowing the material to settle.

Certain samples were aged for 8 days to determine the effect on sample composition and particle size. The samples were covered whilst stirring to limit the entry of air. FESEM and XRD sample preparation was conducted in the same way as for the samples where no aging was performed.

### 3. Results and discussion

The responses as given in Table 2 (average size and unbiased standard deviation determined using the VSM, average size and unbiased standard deviation determined using the FESEM, saturation magnetisation and percentage magnetite precipitated) were obtained for use in the factorial design analysis of variance (ANOVA).

**Table 2** Factorial design responses: average size and standard deviation, saturation magnetisation and percentage magnetite

Run	Average size (determined using VSM) (nm)	Standard deviation (VSM data) (nm)	Average size (determined using FESEM) (nm)	Standard deviation (FESEM data) (nm)	Saturation magnetisation (A m <sup>-1</sup> )	Percentage magnetite (%)
1	11.2	0.6	7.3	1.7	3355	53
2	11.6	0.6	6.7	1.8	3414	67
3	11.3	0.7	8.7	2.5	3525	100
4	11.0	0.6	7.5	2.1	3456	100
5	9.5	0.7	6.3	1.2	2635	55
6	10.6	0.7	7.6	2.1	3600	53
7	10.3	0.8	6.3	1.6	2917	52
8	10.5	0.8	5.8	1.0	2543	60
9	11.6	0.7	9.0	2.1	3846	100
10	9.2	0.7	6.7	1.3	2770	26

Once the ANOVA had been performed to determine significant parameters, one factor or interaction graphs were plotted. One factor graphs (Fig. 2 (a)) are plotted only for those factors that do not show any interactions with one another and display for example, a linear effect of Response B at low and high levels of Factor A.

An interaction between two factors occurs when the measured response is different, depending on the high or low settings of the two factors. Interaction graphs (e.g., Fig. 2 (b)) show two non-parallel lines and indicate for example, that the Response B to Factor A differs depending on whether Factor C is at a high or low level.

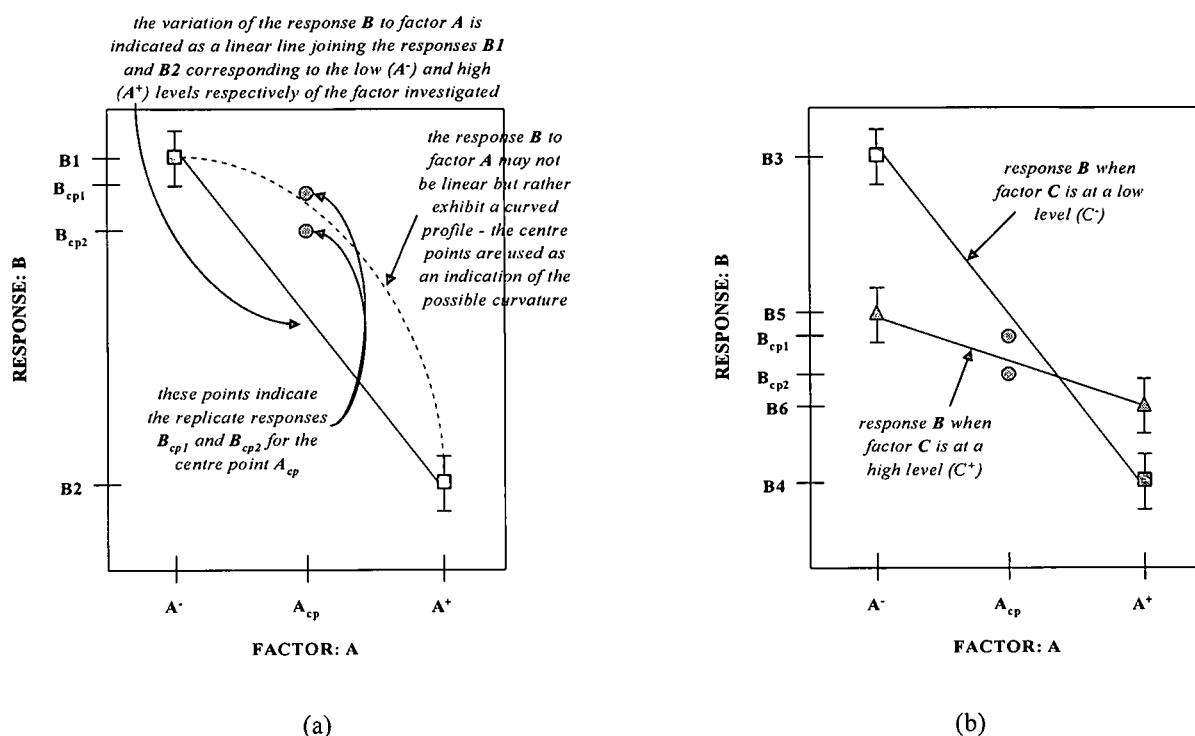


**Figure 2** (a) One factor graph and (b) interaction graph showing factors A<sup>-</sup> (low level), A<sub>cp</sub> (centre point) and A<sup>+</sup> (high level) and responses B1 (response for A<sup>-</sup>), B<sub>cp1</sub> (response for A<sub>cp</sub>, first replicate), B<sub>cp2</sub> (response for A<sub>cp</sub>, second replicate), B2 (response for A<sup>+</sup>), B3 (response for A<sup>-</sup> when factor C is at a low level), B4 (response for A<sup>+</sup> when factor C is at a low level), B5 (response for A<sup>-</sup> when factor C is at a high level) and B6 (response for A<sup>+</sup> when factor C is at a high level)

The responses are plotted at the factor low and high levels only, and therefore appear to be linear even if in practice there is curvature in the response at points in between the factor low and high level. In order to provide an estimate of this curvature and to indicate the pure error, runs are conducted at centre points of the factors (see for example Runs 1 and 2, Table 1, which were conducted at the centre points of the factors). These responses can be plotted as points on the factor or interaction graphs thereby providing an estimate of this curvature. The ‘curvature F-value’ calculated as part of the ANOVA indicates the difference between the average of the center points responses and the average of the calculated factorial points and gives an indication of the deviation from the assumed linear response.

'p-values' reported for the data indicate the statistical significance of the results and represent the probability of error that is involved in accepting the observed result as valid, e.g., a p-value of 0.05 indicates that there is a 5 % probability that the relation between the variables found in the sample is coincidental. For these studies, a p-value of 0.05 was treated as an acceptable error level. The concepts as discussed above are explained graphically in Fig. 2.

### 3.1 Effect of the three factors investigated on the saturation magnetisation and percentage magnetite precipitated

The ANOVA from our studies indicated the importance of the Fe(III)/Fe(II) molar ratio in magnetite formation as the only factor out of the three factors investigated that affected the saturation magnetisation significantly (p-value of 0.010) and percentage magnetite in the samples (p-value of 0.011) (see Figs 3 (a) and (b), respectively). The percentage magnetite is related to the saturation magnetisation as samples containing magnetite (which has a higher saturation magnetisation as compared to the other iron oxides<sup>19</sup>) would contribute most to the magnetic nature of the sample. The centre points lie within the experimental error of the factor plots and the curvature in the model was not found to be significant relative to the noise (a curvature F-value of 3.3 was obtained as measured by the difference between the average of the center points and the prediction from a linear relation between the factorial points).

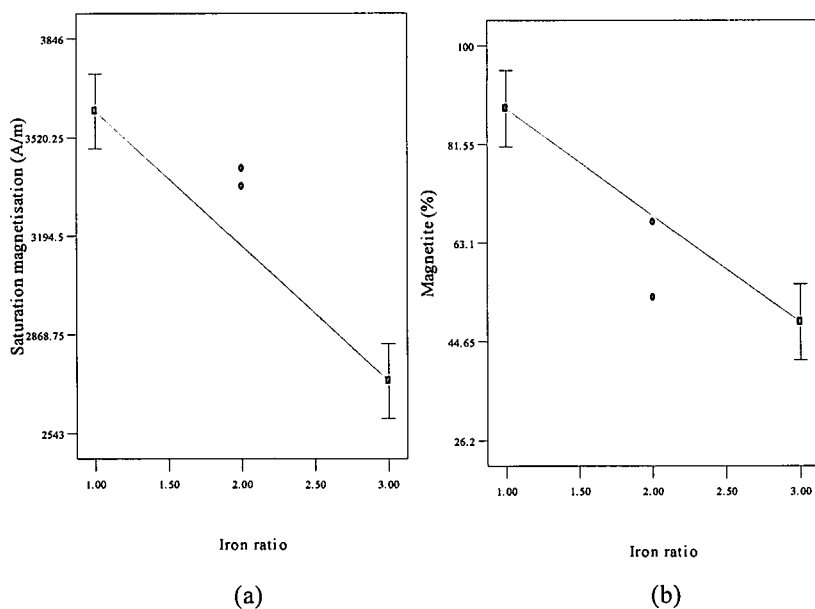


**Figure 3** One factor plot of (a) saturation magnetisation and (b) percentage magnetite versus Fe(III)/Fe(II) molar ratio (● represents the response for the centre points in the design)

In order to understand the importance of the Fe(III)/Fe(II) molar ratio, the mechanism of magnetite formation will be discussed briefly.

The **addition of a base to an Fe(III) solution** results in the displacement of water molecules from the coordination sphere of the hexa-aqua ion,  $[\text{Fe}(\text{H}_2\text{O})_6]^{3+}$  or displacement of other complexing anions such as  $\text{Cl}^-$ . Above pH 1, species such as  $[\text{Fe}(\text{OH})(\text{L}_5)]^{2+}$ ,  $[\text{Fe}(\text{OH})_2(\text{L}_4)]^+$  or  $[\text{L}_5\text{FeOFeL}_5]^{4+}$  (where L represents a complexing ligand) may form. Above pH 2, more condensed species and colloidal gels form. Bridging through hydroxo (Fe-OH-Fe) and oxo (Fe-O-Fe) species is favoured at high pH ( $> 8$ ) and can result in the formation of polymeric iron oxohydroxo species<sup>19</sup> with general formula  $\text{Fe}_3\text{O}_r(\text{OH})_s^{9-(2r+s)}$ . (The formation of these oxyhydroxides is often observed visually in the laboratory: the precipitate appears gelatinous and viscous immediately after addition of the base to the aqueous solution.) The most common of the oxyhydroxide species is ferrihydrite, with a low degree of cross-linking, poorly ordered association of  $\text{Fe}(\text{O},\text{OH})_6$  octahedra and of which the structure is not clearly understood. Ferrihydrites are therefore often referred to as 'Fe(OH)<sub>3</sub>'. Thermodynamically, ferrihydrite could transform to other crystalline ferric oxides such as hematite (see Fig. 1), however, it is stabilised kinetically as a result of its slow dissolution/precipitation transformation reaction<sup>19</sup>.

The **addition of a base to a mixed Fe(III)/Fe(II) solution**, results in the formation of  $\text{Fe}(\text{OH})_2$  from the Fe(II) which could be oxidised in the presence of air to a variety of iron oxides, but is likely to react with the ferrihydrite formed from the Fe(III) (with its poorly ordered arrangement of atoms, fairly high-energy state and relatively easy electron movement) to form green 'rusts'<sup>18, 27</sup>. The green 'rusts' consist of sheets of positively charged  $\text{Fe}^{2+}(\text{OH})_6$  in which some of the Fe(II) is replaced by Fe(III). The sheets are held together electrostatically by anions located between the layers allowing for ion mobility and rearrangement<sup>28</sup>. Growth of magnetite particles<sup>19</sup> may take place through contact re-crystallisation of small primary particles that nucleate on or near the surface of these plates.

In summary therefore, for magnetite precipitation, ferrihydrites from Fe(III) and  $\text{Fe}(\text{OH})_2$  from Fe(II) must combine to form green 'rusts'. The extent to which the Fe(III) is present in relation to the Fe(II) (or vice versa) will govern this precipitation reaction and determine the form of the resultant iron oxides. According to literature, if the Fe(III):Fe(II) molar ratio is greater than 10 (i.e., low Fe(II) concentration), ferric hydroxide ( $\text{Fe}(\text{O}/\text{OH}/\text{OH}_2)_6$ ) octahedra form, but the only stable phase that is recrystallised is goethite<sup>18</sup>. If the ratio is between 3 and 10, goethite formation is suppressed and two different phases form, a non-stoichiometric magnetite enriched with Fe(II) and a poorly ordered, hydrated oxyhydroxide species with low Fe(II). As the Fe(III):Fe(II) molar ratio decreases further, the amount of non-stoichiometric magnetite increases relative to the oxyhydroxide species until finally, when this ratio is less than or equal to 3, there is complete crystallisation of spinel. Therefore, above an Fe(III):Fe(II) molar ratio of 3, the percentage magnetite, and therefore the resultant saturation magnetisation, would be low.

The results from the factorial design are in accordance with information from literature: from the factor plots in Fig. 3 it can be seen that as the Fe(III):Fe(II) molar ratio increases, the saturation magnetisation and the percentage magnetite decrease. A decrease in Fe(III):Fe(II) molar ratio shows a constant linear increase in saturation magnetisation and the percentage magnetite. However, with a decreasing Fe(III):Fe(II) molar ratio, it is more likely that a point will be reached, possibly outside the investigated design space, at which the saturation magnetisation

will decrease and magnetite formation become limited. This should occur because the formation of ferrihydrite will become limited and the potential for electron transfer between the Fe(II) and Fe(III) and subsequent transformation to spinel will decrease<sup>18</sup>.

It appears that variations in total iron concentration of between 0.5 and 1.5 mol l<sup>-1</sup> will not affect magnetite precipitation significantly. This implies that as long as the Fe(III):Fe(II) molar ratio is correct, if the solution concentrations are over or underdiluted from the norm within this operating range, the quality of the resultant precipitate will not be affected deleteriously. Similarly, as long as the volume of ammonia solution added to the iron solution is in excess, variations in the ammonia solution concentration (owing to temperature effects, reagent quality, etc.) should not affect magnetite precipitation significantly.

Most FESEM images obtained using the JEOL JSM-6000F microscope showed a predominance of rounded nanoparticles in the order of 10 nm in size. This is the common morphology for magnetite synthesized in aqueous systems below 100 °C<sup>19</sup>. Examples of these FESEM micrographs are given in Figs 4 (a) to (c) for runs 4, 6 and 9 (see Tables 1 and 2), respectively.

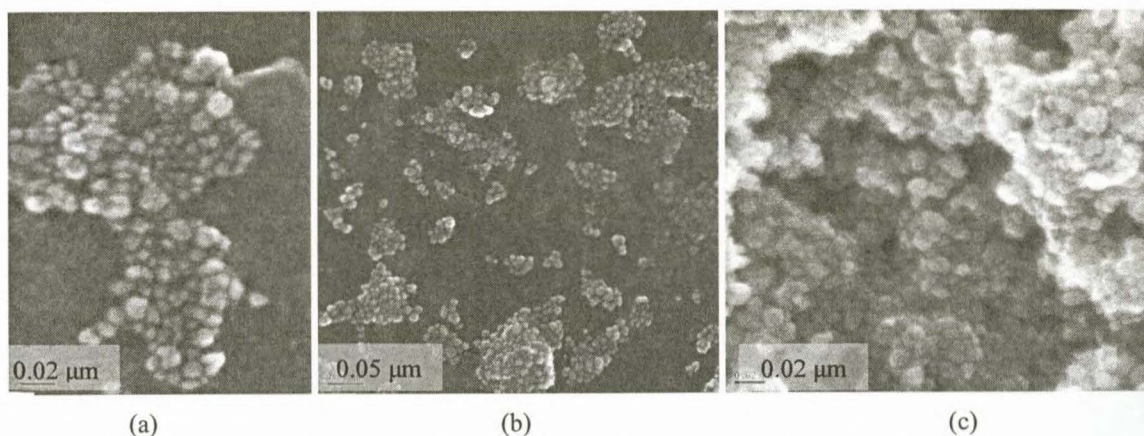


**Figure 4** FESEM micrographs of runs (a) 4, (b) 6 and (c) 9

Some slightly irregularly-shaped particles which are visible in the FESEM micrographs (Fig. 4) may be maghemite material<sup>19</sup>. There are a variety of possible interconversions between iron oxide phases and maghemite may form by oxidation and solid state transformation from stoichiometric or nearly stoichiometric magnetites<sup>18</sup>. (Maghemite is a red-brown ferromagnetic material isostructural with magnetite, with all or most of its iron in the trivalent state and octahedral cation deficient sites<sup>19</sup>.) If magnetite is oxidized to maghemite, either cubic or irregular particles form as the magnetite morphology is usually adopted. In addition, although XRD data may show the presence of only magnetite, it is often difficult to distinguish between magnetite and maghemite structures because of the broadness of the peaks and because their peak positions are similar<sup>29</sup> (see for example, the X-ray diffractogram in Fig. 5 and the comparative X-ray diffractograms of magnetite and maghemite in the picture inset<sup>19</sup>). Some maghemite may therefore also be present in the samples.

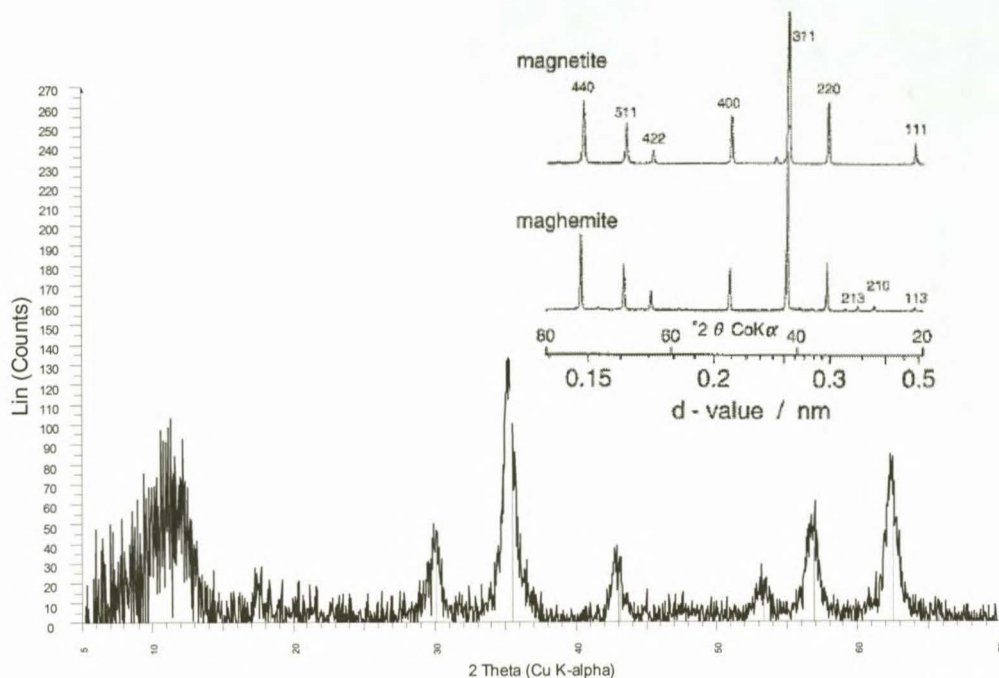


**Figure 5** X-ray diffractogram obtained for magnetite showing broad peaks with comparative X-ray diffractograms for magnetite and maghemite shown in the inset<sup>19</sup>

FESEM micrographs of runs 5, 7 and 10 (see Tables 1 and 2) are given in Figs 6 (a) to (d). These samples (as well as run 8) were prepared with an excess of Fe(III) to Fe(II). Rod-like structures are visible in the figures (and in FESEM micrographs from run 8) possibly indicating the presence of haematite ( $\gamma\text{-Fe}_2\text{O}_3$ ) or goethite ( $\alpha\text{-FeOOH}$ ) which may have long and rodlike morphology and can form in Fe(II)-poor media<sup>18, 30</sup>. Oxidation of ferrihydrites at lower pH could also lead to the formation of goethite (or lepidocrocite)<sup>19</sup> while these species may also form from the decomposition of the green 'rust' complex<sup>27, 28</sup>. Examples of possible haematite morphology<sup>19</sup> are given in Fig. 7.

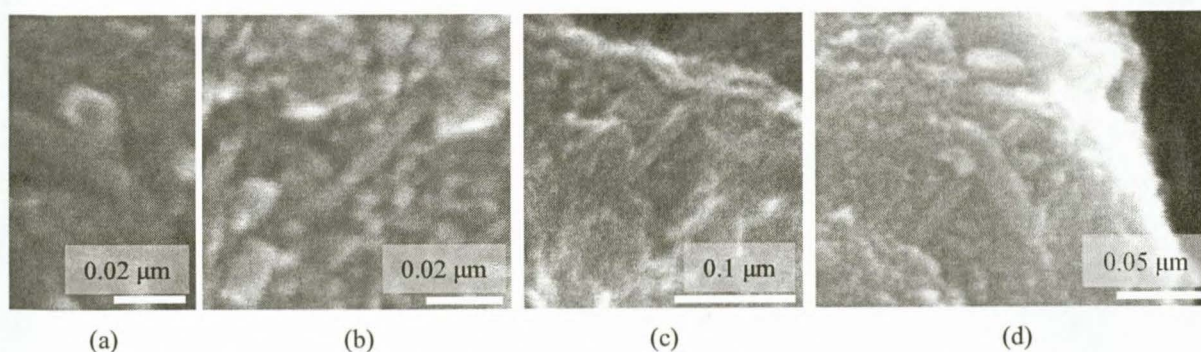


**Figure 6** FESEM micrographs of runs (a) 5, (b) 7 and (c and d) 10

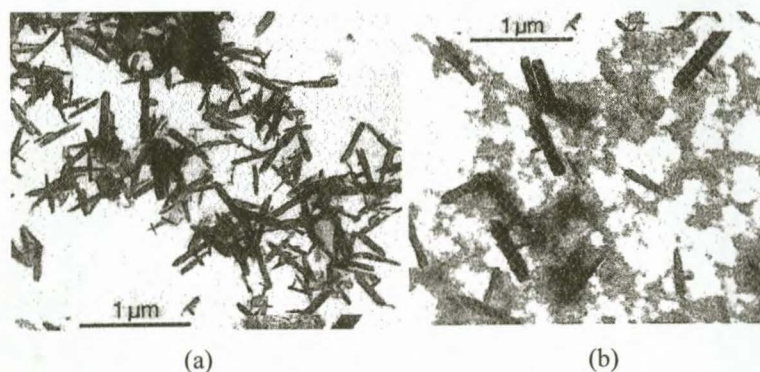


**Figure 7** Rod-like haematite particles with granular ferrihydrate visible in (b)<sup>19</sup>

Hexagonal plates and rods were visible in aged samples with an Fe(III):Fe(II) molar ratio of 2 or 3 (Fig. 8), e.g., in samples 1, 2, 5 and 8 (see Tables 1 and 2). It is suspected that the hexagonal plates are also haematite crystals which can form, for example, from ferrihydrate gels<sup>19</sup> at pH 8 to 15. Rods could be produced from forced hydrolysis of acidic Fe(III) solutions and spheroids from forced hydrolysis of dilute Fe(III) in the presence of chloride<sup>19</sup> as shown in Fig. 9. Morphologies of synthetic haematite include plates, discs, rods, spindles, spheres, ellipsoids, double ellipsoids, rhombohedra, stars and cubes. In addition, Fe(OH)<sub>2</sub> and green 'rusts' exist as hexagonal plates and the hexagonal-shaped structures could therefore be these forms of iron oxide<sup>19</sup>.

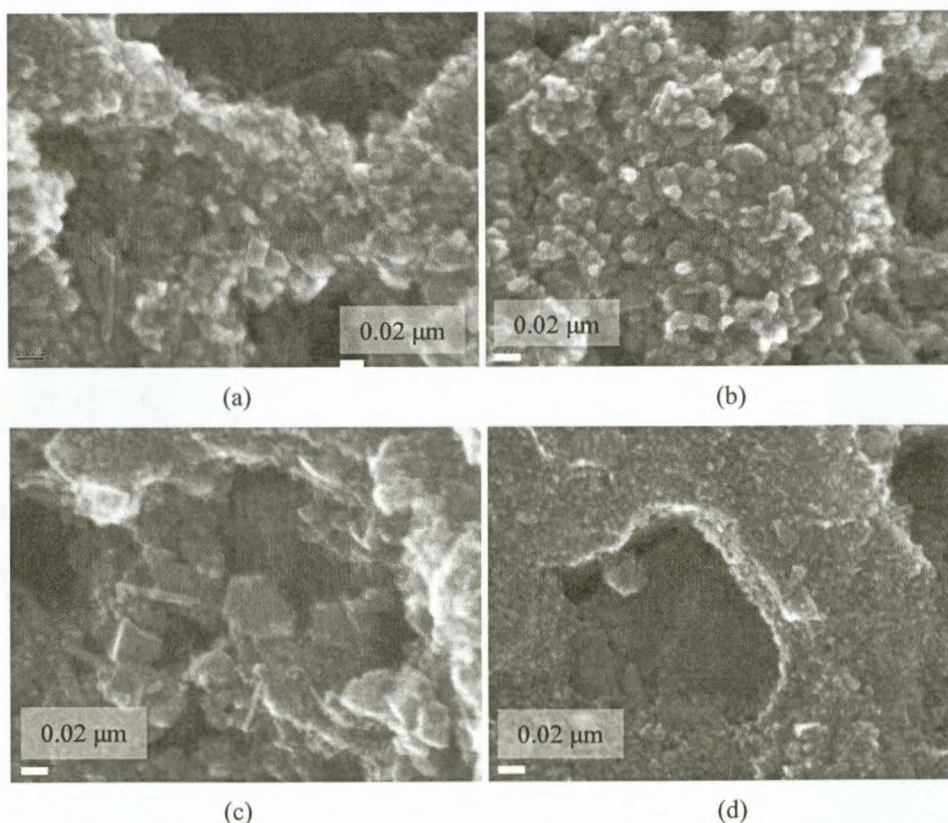


**Figure 8** FESEM micrographs of aged samples from runs (a) 1, (b) 2, (c) 5 and (d) 8

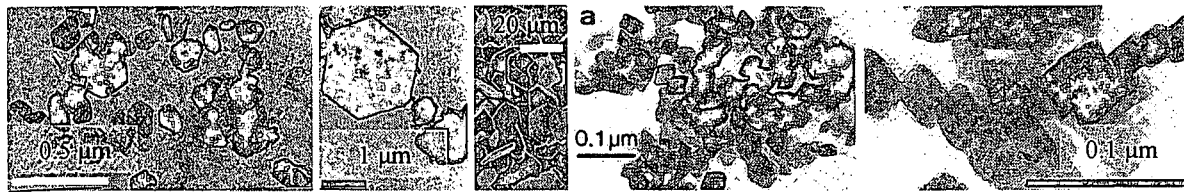


**Figure 9** Examples of hexagonal/straight-edged haematite particles<sup>19</sup>

### 3.2 Effect of the three factors investigated on the precipitate particle size

The results from the ANOVA indicated that the Fe(III)/Fe(II) molar ratio and iron and ammonia solution concentrations affected the average particle size of the samples significantly as determined from VSM measurements (p-values of 0.0002, 0.0011 and 0.055, respectively). The analysis shows that there is significant curvature in the design space (curvature F-value of 35.98) indicating that there is a difference between the average of the center points and the prediction from a linear relation between the factorial points. Figs 10 (a), (b) and (c), the one factor plots of average size (determined from VSM measurements) versus Fe(III)/Fe(II) molar ratio, iron solution concentration and ammonia solution concentration, respectively, show that as these factors are increased, the average size decreases.

By comparison, the average particle size determined by FESEM also indicated that the Fe(III)/Fe(II) molar ratio (p-value of 0.003) and interaction of the Fe(III)/Fe(II) molar ratio and iron concentration (p-value of 0.027), affect the particle size (see Figs 11 (a) and (b), respectively). At a high iron concentration, the effect on average particle size as a function of iron ratio appears to be less significant than that at lower iron concentration. The model curvature (a curvature F-value of 1.05) was found to be insignificant relative to noise.

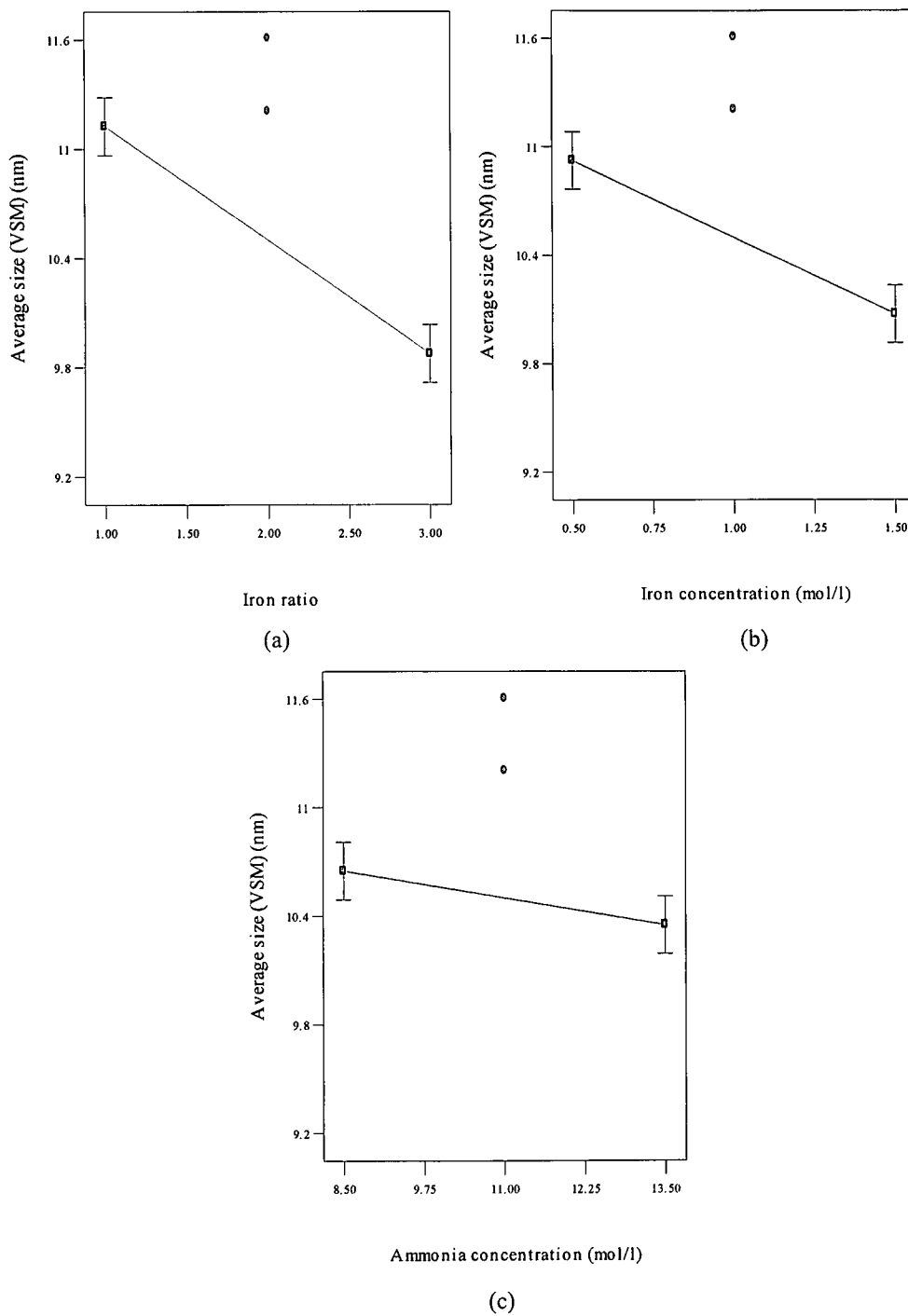


**Figure 10** One factor plot of average size determined from VSM measurements versus (a) Fe(III)/Fe(II) molar ratio, (b) iron concentration and (c) ammonia solution concentration (◐ represents the response for the centre points in the design)

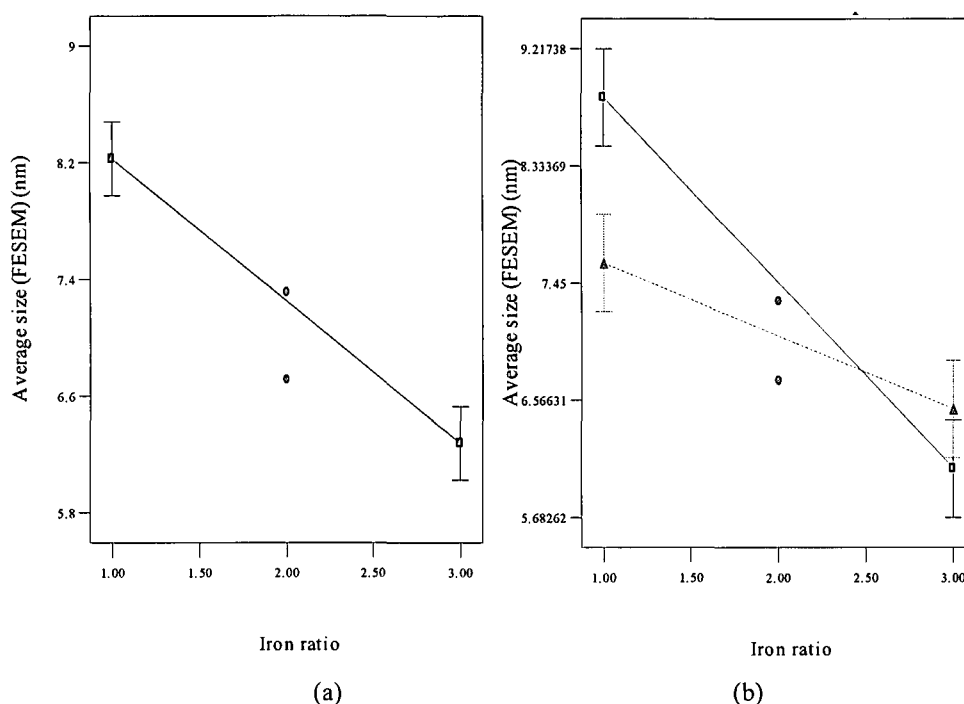


**Figure 11** (a) One factor plot of average size determined from FESEM measurements versus Fe(III)/Fe(II) molar ratio and (b) interaction plot of average size versus Fe(III)/Fe(II) molar ratio and iron concentration ( $\circ$  represents the response for the centre points in the design and in (b),  $\square$  represents the iron concentration at a low level of  $0.5 \text{ mol l}^{-1}$  while  $\triangle$  is the iron concentration at a high level of  $1.5 \text{ mol l}^{-1}$ )

The observation that particle size decreases with increasing Fe(III)/Fe(II) molar ratio concurs with data from literature<sup>18</sup>. The most likely reason for an increase in Fe(III)/Fe(II) molar ratio (Figs 10 (a) and 11 (a)) resulting in a decrease in particle size is that the depletion of available Fe(II) limits the potential for Ostwald ripening and subsequent increase in particle size. It has been found that for ratios of Fe(III):Fe(II) greater than 10, amorphous material results<sup>6</sup>. As the ratio decreases, the morphological order increases with an increase in particle growth.

The observations made in these studies as to the increasing total iron and ammonia solution concentrations (Figs 10 (b) and (c), respectively) resulting in a decrease in average particle size also concur with previously reported results stating that the particle size decreases with increasing ionic strength<sup>6</sup>. Changes in ionic strength affect interfacial tension which controls particle surface area as discussed below.

The point of zero charge (PZC) of a particle is that pH at which the charge on the particle surface is zero and the extent of adsorption of positively charged species equals that of negatively charged species. (The PZC of magnetite has been reported to be in the range of 6 to 8.2<sup>19, 31-34</sup>.) In an aqueous environment, magnetite surface hydroxyl groups arise from adsorption of water<sup>19</sup>. Changes in pH affect the protonation-deprotonation equilibria of the surface hydroxylated sites and can result in the formation of cationic magnetite particles in acidic media and anionic particles in alkaline media<sup>35</sup>. Excess ammonium hydroxide solution is used in magnetite precipitation resulting in a

final solution pH of approximately 8 to 11. The excess hydroxyl groups allow for the deprotonation of the magnetite surface hydroxyl groups according to:



These anionic magnetite particles can adsorb cationic species from solution in high ionic strength media (high iron and ammonia concentration), increasing  $\Gamma_i$ , the density of adsorbed species  $i$  with chemical potential  $\mu_i$ <sup>5,8</sup>. This results in a decrease of the interfacial tension ( $\gamma$ ) as compared to the value at the PZC where the net surface charge is zero<sup>6,8</sup>:

$$d\gamma = -\Gamma_i d\mu_i \quad (5)$$

A decrease in the interfacial tension leads to a lowering of the free enthalpy of formation<sup>8</sup>,  $dG = \gamma dA$ , thereby allowing for an increase in the surface area of the system,  $A$ , which equates to a lower magnetite particle size<sup>5,8</sup>.

Although the higher ionic strength media yields smaller particles, the decrease of approximately 2 nm over the range investigated is not significant for our application and it would therefore be possible to operate comfortably within the ranges selected for the factorial design without any significant effect on particle size.

It was also observed that the iron solution of higher concentration (higher ionic strength medium) has a lesser effect on the average magnetite particle size with increasing Fe(III)/Fe(II) molar ratio than the iron solution of lower concentration (Fig. 11 (b)). As discussed above (see eq. (4)), a higher pH results in the formation of anionic surfaces and a resultant increase in adsorbed cationic species which decreases the interfacial tension and final particle size. The iron solution of higher concentration effectively results in a lower solution pH (the iron solution pH is approximately 2) which may negate the effect that an increased pH has on reducing particle size. Again, however, the effects of Fe(III)/Fe(II) molar ratio and iron concentration result in a particle size variation of only approximately 2 nm which is insignificant for our application.

#### 4. Conclusions

A precipitation route for the preparation of magnetite was selected because of various cost- and flexibility-related issues such as ease of synthesis and subsequent functionalisation of materials.

From the factorial experiment, the Fe(III)/Fe(II) molar ratio (but not the iron and ammonia solution concentrations) appears to have an effect on the saturation magnetisation and percentage magnetite precipitated, with a lower

Fe(III):Fe(II) molar ratio (< 3) favouring magnetite formation. Although the factor plot appears to indicate that the saturation magnetisation and percentage magnetite increase indefinitely with a decrease in Fe(III):Fe(II) molar ratio (Fig. 3), at some point there will be insufficient Fe(II) for stoichiometric magnetite formation and rod-like structures (as observed when an excess of Fe(III) was used) may form. It has therefore been decided to select an Fe(III):Fe(II) molar ratio of 2 for subsequent impinging stream reactor test work. It has also been suggested that homogeneous particles form when a stoichiometry as close as possible to that of magnetite is used<sup>6, 17</sup>. Because of the importance of the Fe(III):Fe(II) molar ratio in solution, for the tests in Chapter 3 (and on an industrial scale) the iron solution should be prepared and used immediately to prevent Fe(II) oxidation. The precipitated magnetite should be used for subsequent processing soon after formation to avoid oxidation of magnetite to maghemite or haematite as is believed to have occurred in aged samples. Oxygen removal from the system and solutions may also assist in the prevention of oxidation of Fe(II) but this may not be practical and cost-effective on a large scale.

The Fe(III)/Fe(II) molar ratio and iron and ammonia solution concentrations were found to be significant in terms of the particle size of materials. The actual particle size variation was, however, found to be only 2 nm which would be insignificant for our applications. This therefore implies that variations within the factor ranges selected (0.5 – 1.5 mol l<sup>-1</sup> and 8.3 – 13.5 mol l<sup>-1</sup> for the iron and ammonia solution concentrations, respectively, whilst maintaining the Fe(III)/Fe(II) molar ratio at 2) should not result in the precipitation of particles with great size variations.

In summary then, the following factors are suggested for acceptable magnetite precipitation in Chapter 3:

- an Fe(III):Fe(II) molar ratio equal to 2,
- an iron solution concentration within the range of 0.5 – 1.5 mol l<sup>-1</sup> and
- an ammonia solution concentration within the range of 8.3 – 13.5 mol l<sup>-1</sup>.

## References

1. Willard, M. A.; Kurihara, L. K.; Carpenter, E. E.; Calvin, S.; Harris, V. G., *Encycl. Nanosci. Nanotech.* 2004, **1**, 815.
2. Bönnemann, H.; Nagabhushana, K. S., *Encycl. Nanosci. Nanotech.* 2004, **1**, 777.
3. Inouye, K.; Endo, R.; Otsuka, Y.; Miyashiro, K.; Kaneko, K.; Ishikawa, T., *J. Phys. Chem.* 1982, **86**, 1465.
4. Seip, C. T.; Carpenter, E. E.; O'Connor, C. J., *IEEE Trans. Magn.* 1998, **34**, 1111.
5. Jolivet, J.-P.; Tronc, E.; Chanéac, C., *C. R. Chimie* 2002, **5**, 659.
6. Jolivet, J.-P.; Tronc, E.; Vaysierres, L., *Formation of magnetic spinel iron oxide solution in Nanophase Materials*, Kluwer, 1994.
7. Babes, L.; Denizot, B.; Tanguy, G.; Le Jeune, J. J.; Jallet, P., *J. Colloid Interface Sci.* 1999, **212**, 474.
8. Vayssières, L.; Chantrell, R. W.; Tronc, E.; Jolivet, J.-P., *J. Colloid Interface Sci.* 1998, **205**, 205.
9. Zhou, Z. H.; Wang, J.; Liu, X.; Chan, H. S. O., *J. Mater. Chem.* 2001, **11**, 1704.
10. Hilgendorff, M., *Encycl. Nanosci. Nanotech.* 2004, **1**, 213.
11. Nakatani, I.; Furubayashi, T.; Takahashi, T.; Hanaoka, H., *J. Magn. Mater.* 1987, **65**, 261.
12. Tartaj, P., *Encycl. Nanosci. Nanotech.* 2004, **6**, 823.
13. Kilner, M., *IEEE Transactions on Magnetism* 1984, **Mag-20**, 1735.

14. Farkas, J., *Sep. Sci. Technol.* 1983, **18**, 787.
15. Reimers, G. W.; Khalafalla, S. E., US patent 3 843 540, 1973.
16. Müller, R.; Steinmetz, H.; Hiergeist, R.; Gawalek, W., *J. Magn. Magn. Mater.* 2004, **272-276**, 1539.
17. Massart, R.; Cabuil, V., *Journal de Chimie Physique et de Physico-Chimie Biologique* 1987, **84**, 967.
18. Tronc, E.; Belleville, P.; Jolivet, J.-P.; Livage, J., *Langmuir* 1992, **8**, 313.
19. Cornell, R. M.; Schwertmann, U., *The iron oxides* VCH Publishers, New York, 1996.
20. Feltin, N.; Pileni, M. P., *Langmuir* 1997, **13**, 3927.
21. Gribanov, N. M.; Bibik, E. E.; Buzunov, O. V.; Naumov, V. N., *J. Magn. Magn. Mater.* 1990, **85**, 7.
22. Jolivet, J.-P.; Belleville, P.; Tronc, E.; Livage, J., *Clays Clay Miner.* 1992, **40**, 531.
23. Reimers, G. W.; Khalafalla, S. E. Technical progress report 56, U. S. Department of the Interior, Twin Cities Metallurgy Research Centre: Minneapolis, 1972, 1.
24. Rasband, W. ImageJ: Image processing and analysis in Java <http://rsb.info.nih.gov/ij/>.
25. Chantrell, R. W.; Popplewell, J.; Charles, S. W., *IEEE Transactions on Magnetism* 1978, **Mag-14**, 975.
26. Khalafalla, S. E.; Reimers, G. W.; Rholi, S. A., US Patent 4 208 294, 1980.
27. Misawa, T.; Hashimoto, K.; Shimodaira, S., *J. Inorg. Nucl. Chem.* 1973, **35**, 4167.
28. Schwertmann, U.; Fechter, H., *Clays Clay Miner.* 1994, **29**, 87.
29. Sjögren, C. E.; Johansson, C.; Naevestad, A.; Sontum, P. C.; Briley-Saebo, K.; Fahlvik, A. K., *Magnetic Resonance Imaging* 1997, **15**, 55.
30. Sugimoto, T.; Matijević, E., *J. Colloid Interface Sci.* 1980, **74**, 227.
31. Milonjic, S. K.; Kopenci, M. M.; Ilic, Z. E., *J. Radioanal. Chem.* 1983, **78**, 15.
32. Kosmulski, M., *J. Colloid Interface Sci.* 2004, **275**, 214.
33. Sun, Z.-X.; Su, F.-W.; Forsling, W.; Samskog, P.-O., *J. Colloid Interface Sci.* 1998, **197**, 151.
34. Wesolowski, D. J.; Machesky, M. L.; Palmer, D. A.; Anovitz, L. M., *Chem. Geol.* 2000, **167**, 193.
35. Lefebure, S.; Dubois, E.; Cabuil, V.; Neveu, S.; Massart, R., *J. Mater. Res.* 1998, **13**, 2975.

## Chapter 3\*

### An investigation into the potential large-scale continuous magnetite nanoparticle synthesis by high pressure impinging stream reactors

---

#### Abstract

Scale-up of current batch, laboratory magnetite precipitation techniques involving relatively small volumes may be problematic as large stirred vessels can yield areas of localised low pH upon addition of a base to an iron solution resulting in the precipitation of undesired non-magnetic iron oxides. The use of five high pressure impinging stream (IS) reactors of different designs for the potential large-scale continuous precipitation of magnetite nanoparticles is presented. The small, inexpensive IS reactor system is ideal for providing a large interfacial area and high mass transfer as compared to conventional mixing systems such as, for example, a conventional stirred tank reactor. Reactor shape and volume were found to be critical for efficient magnetite precipitation of which the experimental system described here is capable of producing predominantly 8 – 12 nm diameter magnetite precipitate particles at rates of between 30 g min<sup>-1</sup> at 200 kPa and 50 g min<sup>-1</sup> at 500 kPa. It would be relatively easy to scale-up to higher throughputs using larger capacity nozzles or increased pressures. In addition, commercially available dosing pumps could be used for continuous reagent feed.

#### 1. Introduction

##### 1.1 Batch versus continuous magnetite precipitation

Magnetic nanoparticles are becoming increasingly important in a variety of different fields, e.g., in magnetic storage media<sup>1</sup>, catalysis<sup>2</sup> and medical applications<sup>1, 3, 4</sup>. In Chapter 1, the discussion of the magnetic properties of superparamagnetic magnetite nanoparticles highlighted that one of their defining characteristics is their size<sup>1</sup>. The ability to produce nanometre-sized particles in large quantities for commercial use is a research challenge with important potential technological consequences and a simple method for large-scale continuous magnetite synthesis may become increasingly desirable as applications develop further<sup>5</sup>. It is relatively easy to precipitate magnetite nanoparticles in a batchwise manner in the laboratory using a stirred vessel and small reactor volumes: fast manual ammonia solution addition and rapid mixing is used during synthesis to disperse reagents, thereby preventing adverse side reactions, magnetite agglomeration and crystal growth<sup>6</sup>. The precipitation mixture pH should exceed a

---

\* Based in part on the paper, Vatta, L. L.; Sanderson, R. D.; Koch, K. R., *An investigation into the potential large-scale continuous magnetite nanoparticle synthesis by high pressure impinging stream reactors*. In press. *Journal of Magnetism and Magnetic Materials* 2007.

critical value (~8), for magnetite ( $\text{Fe}_3\text{O}_4$ ) precipitation. However, in an industrial environment, scale-up to large volumes of reagents and addition times in the order of minutes could result in inhomogeneous agitation, areas of localised pH and the resulting precipitation of non-magnetic iron oxides<sup>7</sup> such as  $\text{FeOOH}$  and  $\text{Fe}(\text{OH})_2$  (see Fig. 1, Chapter 2). An alternative batch synthesis route to prevent the formation of localised areas of low pH, would be to add the iron solution to excess ammonia solution with intensive mixing, thereby maintaining the pH at suitable levels for magnetite precipitation<sup>8</sup>. Ideally, however, a continuous method of reagent contact yielding highly turbulent mixing would be most desirable.

### 1.2 Theory of impinging stream reactors

Reagent contact in mass transfer operations forms a vital part of process engineering. Many reactions are characterized by the overall interfacial area available for mass transfer and by the fact that mass transfer limits the transport rates of reagents to each other<sup>9</sup>.

The mass transfer coefficient,  $k$ , is defined by<sup>10</sup>:

$$k = \frac{N_a}{A\Delta C_a} \quad (1)$$

where  $N_a$  is the rate of mass transfer of component  $a$  ( $\text{kg s}^{-1}$ ),  $A$  is the mass transfer area ( $\text{m}^2$ ) and  $\Delta C_a$ , the driving force for mass transfer, is the change in concentration of component  $a$  ( $\text{kg m}^{-3}$ ). Mass transfer is governed by certain resistances and if these resistances can be reduced or if the mass transfer coefficient can be increased, mass transfer can be improved. For example, in eq. 1, the mass transfer rate can be increased by increasing the concentration gradient and by increasing the area (e.g., by decreasing the size of the reagent droplets)<sup>10</sup>.

Many attempts have been made in various designs to promote intense, turbulent mixing to generate high shear rates and promote interfacial area production and mass transfer. Mechanically agitated reactors equipped with multiple impellers or turbine blades, jets and venturis and multiphase systems involving small gas bubbles to provide a larger surface area<sup>9</sup> are some of the processes that have been investigated over conventional items used for mass transfer such as packed and bubble columns. Improved reagent contact may offer possible economic gain: higher mass transfer rates may allow for the use of smaller items of equipment at a possible lower cost and in the case of competing chemical reactions, an increase in the mass transfer rate may result in a decrease in the undesired product produced if the desired product has a higher intrinsic reaction rate (increased mass transfer favours the reaction with the higher intrinsic reaction rate)<sup>9, 11, 12</sup>.

Impinging stream (IS) reactors, also known as jet reactors, consist of small reactor volumes fed by reagent streams directed towards one another<sup>10</sup>. Feed streams are supplied at high pressure and velocity to the reactor volumes via

nozzles directed towards each another. The kinetic energy of the feed streams creates highly turbulent conditions inside the reactor volume. The streams impinge at the midpoint of their flow, known as the impingement plane (see Fig. 1), resulting in<sup>10</sup>:

- an increase in the relative velocities between the penetrating particles and the opposing stream: a particle penetrating into an opposing stream could achieve a relative velocity twice that of the penetrated stream velocity thereby decreasing the resistance to mass transfer.
- an increase in the mean residence time of the particle in the system as a result of penetration and circulation in the opposing stream: this could allow for a decrease in the geometric size of the system.
- an increase in the shear forces and pressure pulsations between reagents: this leads to a breakup of droplets or bubbles resulting in an increased interfacial area and an increase in surface renewal leading to an increase in mass transfer rates.
- good mixing and an increased probability of collisions because of pressure pulsations between reagents and the multiple circulation of particles: the collision of the opposing streams leads to intense radial and axial velocity components in the turbulent flow.

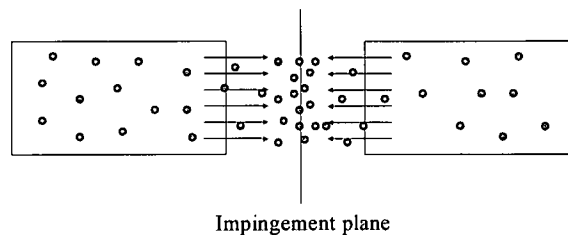


**Figure 1** Impingement plane at which opposing reagent streams collide in an impinging stream reactor<sup>10</sup>

There is a repeated penetration of the one stream into the opposing stream through the impingement plane owing to the inertia of the incoming feed stream. This continues until the material is discharged<sup>10</sup>.

It has been shown that using an impinging stream jet reactor can result in a significant improvement in mass transfer in gas-liquid, liquid-liquid and liquid-solid systems<sup>10</sup>. Tamir and Herskowitz compared an impinging stream (Fig. 2 (a)) and single stream absorber (Fig. 2 (b)) by investigating the absorption rates of carbon dioxide into water and acetone into water and the desorption of acetone from water by air<sup>13</sup>. In the single stream absorber, the impingement effect is eliminated by including a partition to separate the reactor streams as shown schematically in Fig. 2 (b).

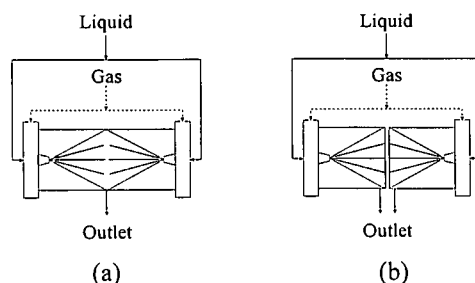


**Figure 2** Impinging streams (a) without partition and (b) with a partition

From their studies, it was found that the ratio as given in eq. 2, where  $R_i$  and  $R_p$  denote the absorption rate of the gas in the impinging stream and partitioned absorber, respectively, was greater than 1, implying that the impinging stream absorber is more efficient than two equivalent single stream absorbers<sup>9</sup>. A 65 % improvement was obtained for carbon dioxide absorption into water (ratio of 1.65) and a ratio of between 2 and 4 was obtained for acetone absorption into water<sup>9</sup>.

$$\frac{R_i}{2R_p} > 1 \quad (2)$$

IS reactor technology was initially implemented by Elperin in the 1960s in the former USSR for the drying of solid particles and solutions, combustion of gases, creation of emulsions and evaporative cooling of air<sup>10</sup>. Tamir, who subsequently became a champion of the technology, believes that almost any chemical process could be performed using IS reactor technology with a higher efficiency and lower power input in comparison to conventional processes<sup>10</sup>. He has suggested that IS reactors could be used for homogeneous or heterogeneous systems in drying, dust collection, mixing, adsorption, ion exchange and extraction. He has broadened test work to applications such as swirling IS reactors and jet loop reactors for, amongst others, the absorption and desorption of gases from liquids, the combustion of gas and coal, the creation of emulsions, for liquid-liquid extraction and for the dissolution of solids<sup>10</sup>.

Despite the fact that IS reactors could contribute to process intensification (the view that for a given duty, a drastic reduction in the size of process equipment may benefit safety, capital cost and the environment whilst possibly offering significant energy savings)<sup>14</sup>, IS reactors have not been widely implemented. This is probably because of industrial resistance to modifying large-scale processes and potentially affecting production. Many processes are also often based on scale-up from a stirred beaker resulting in the predominant use of stirred tank reactors for the past 200 years.

IS reactors have been tested at the University of Stellenbosch for the washing of diesel-contaminated soil<sup>12</sup>, for the leaching of gold from various ore types<sup>15</sup> and for the absorption of CO<sub>2</sub> into a sodium hydroxide solution<sup>16, 17</sup>.

Table 1 compares the mass transfer parameters ( $k_L$ , the mass transfer coefficient,  $a$ , the interfacial area and  $k_L a$ , the combined mass transfer coefficient) and the power required for mechanically agitated reactors, venturis and IS reactors. The highest combined mass transfer coefficient is obtained for the IS reactors. From these studies and from the comparison of experimental results with literature data for conventional systems, it was found that these reactors showed a significant improvement in terms of the mass transfer coefficient and value of interfacial area per unit of energy dissipated in the reactors<sup>9</sup>.

**Table 1** Mass transfer parameters for different reactor systems<sup>9,16</sup>

Type of reactor	$k_L$ ( $\text{m s}^{-1} \times 10^4$ )	$a$ ( $\text{m}^2 \text{m}^{-3}$ )	$k_L a$ ( $\text{s}^{-1}$ )	Power ( $\text{kW m}^{-3}$ )
Mechanically agitated reactors	0.3 – 4.0	100 – 2000	0.003 – 0.8	0.5 – 4
Venturi scrubbers	5.0 – 10.0	160 – 250	0.08 – 0.25	10 – 700
Impinging stream absorbers	2.9 – 6.6	90 – 2050	0.025 – 1.22	0.8 – 140
Impinging stream reactors as tested by Kleingeld <sup>9</sup> and Botes <sup>16</sup>	2.6 – 22.2	1500 – 16000	1.0 – 14.2	

Because IS reactors offer a turbulent environment for high mass transfer and interfacial area and could potentially allow for the continuous large-scale precipitation of magnetite, it was decided to investigate iron oxide precipitation using such reactors as an alternative to the batch precipitation of iron oxides using a stirred tank reactor in the laboratory or on an industrial scale.

## 2. Experimental

### 2.1 Reagents and analytical methods

All reagents and solvents were purchased from commercial sources and were used without further purification. Chloride ( $\text{FeCl}_3 \cdot 6\text{H}_2\text{O}$ ) and sulphate ( $\text{FeSO}_4 \cdot 7\text{H}_2\text{O}$ ) salts which are readily available and affordable and 25 %  $\text{NH}_4\text{OH}$  (Merck) were used for iron oxide precipitation. Deionised water was used for the preparation of aqueous solutions.

Magnetisation curves (and saturation magnetization) were obtained on an LDJ 9600 Vibrating Sample Magnetometer (VSM). Field emission scanning electron micrographs were obtained using a JEOL JSM-6000F Field Emission Scanning Electron Microscope (FESEM). X-ray diffraction (XRD) measurements were obtained on a Siemens D501 Diffractometer. Qualitative sample percentage composition was determined using the reference intensity ratio and peak height. Particle size was determined using the FESEM micrographs and ImageJ, a public domain image processing program<sup>18</sup>, through the method of Chantrell et al.<sup>19</sup>, where an approximation of particle size is determined indirectly from the magnetisation curve, and by analysis of XRD peak broadening data<sup>20</sup> using the

Scherrer formula (where  $t$  is the nanocrystal size,  $\lambda$  is the wavelength,  $B$  is the width of the peak at an intensity equal to half the maximum intensity, and  $\theta_B$  is half the angle at which the peak exists)<sup>20,21</sup>:

$$t = \frac{0.9\lambda}{B \cos \theta_B} \quad (3)$$

## 2.2 Impinging stream reactors and experimental setup

Three iron oxide replicate samples were precipitated at 200, 300, 400 and 500 kPa pressures using four IS reactors of varying reactor shape and volume as illustrated in Fig. 3 (the Y-shaped reactor does not conform as such to the definition of an IS reactor: the reactor does not possess a small reactor volume in which material may circulate and precipitated material exits immediately from the reactor after impingement):

- Two kite-shaped reactors of volumes  $\sim 20$  and  $\sim 8$  cm<sup>3</sup>,
- circular reactor of volume  $\sim 20$  cm<sup>3</sup>,
- triangular reactor of volume  $\sim 8$  cm<sup>3</sup> and
- Y-shaped reactor.

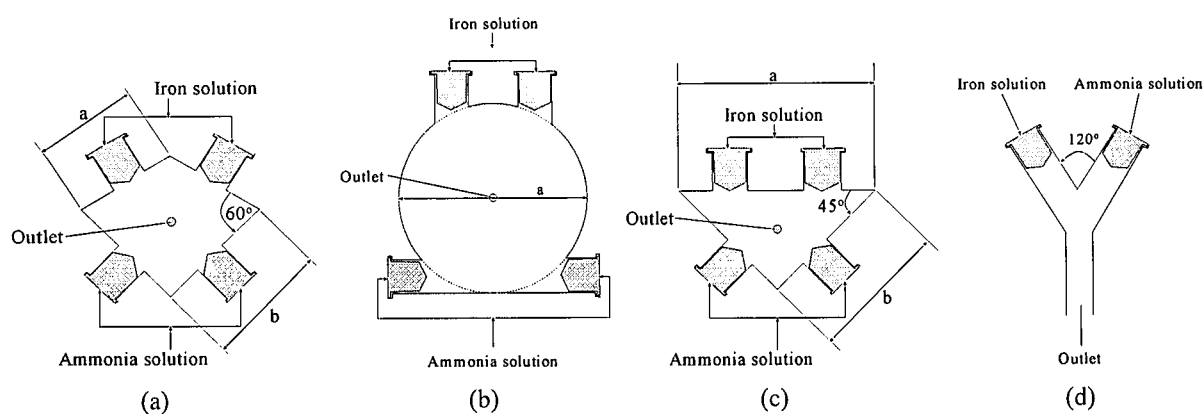


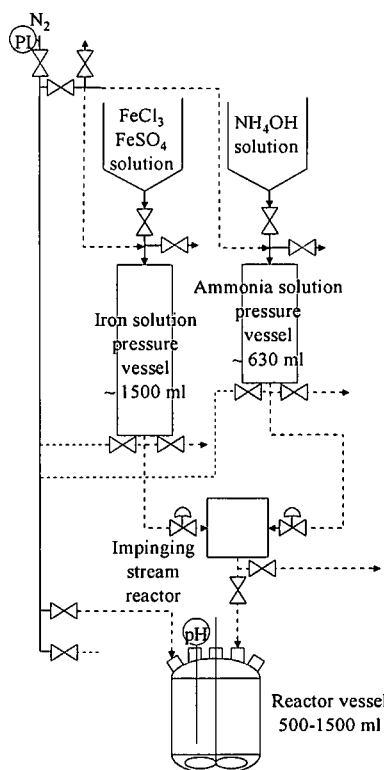
**Figure 3** (a) Kite-shaped ( $a = 42$  mm and  $b = 30$  mm for the larger volume reactor and  $a = 25$  mm and  $b = 18.5$  mm for the smaller volume reactor), (b) circular ( $a = 36$  mm), (c) triangular ( $a = 40$  mm and  $b = 29$  mm) and (d) Y-shaped reactor

Inlets were via UniJet® full cone small capacity spray nozzles with reactor volume outlets perpendicular to the inlet plane (with the exception of the Y-shaped reactor). Nozzles of 0.7 capacity (0.76 mm orifice diameter, 0.51 mm maximum free passage) and 0.3 capacity (0.51 mm orifice diameter, 0.41 mm maximum free passage) were used for supplying the iron and ammonia solutions, respectively, with flow rates (as a function of pressure) as given in Table 2. The required reagent volumes were adjusted relative to the nozzle capacity and precipitation time to provide a two times molar excess of ammonia to iron solution.

**Table 2** Nozzle capacities within the pressure range of interest

Pressure (kPa)	0.7 mm nozzle capacity (l min <sup>-1</sup> )	0.3 mm nozzle capacity (l min <sup>-1</sup> )
200	0.43	0.19
300	0.52	0.22
400	0.6	0.25
500	0.66	0.28

The experimental setup is given in Fig. 4. The  $\text{FeCl}_3 \cdot 6\text{H}_2\text{O}$  and  $\text{FeSO}_4 \cdot 7\text{H}_2\text{O}$  salts (Fe(III):Fe(II) molar ratio 2:1) were added to the required volume of water. The iron and a 25% ammonia solutions were added to the relevant pressure storage vessel and pressurised using nitrogen gas. The feed valves to the reactor were opened simultaneously and the liquid volumes fed to the IS reactor by the nitrogen gas over a precipitation time of 10 seconds. The first and last fractions (unsteady state) were diverted to waste while the mid fraction (steady state) was collected in an unstirred vessel.

**Figure 4** Impinging stream reactor experimental setup

A sample was collected immediately for determination of the magnetisation curve with the maximum magnetisation at  $1.35 \times 10^6 \text{ A m}^{-1}$  recorded for each sample. A 20 ml sample of precipitate was placed in a flask to which 5 ml  $\text{NH}_4\text{OH}$  and lauric acid (40 % by mass<sup>22</sup>, Sigma-Aldrich) for coating of the sample was added. The mixture was heated to  $80^\circ\text{C}$  with mixing to improve lauric acid solubility. These samples were used for FESEM measurements. The remaining precipitate was washed with three portions of 50 ml water. The wash water was decanted after each wash once the material had settled and these samples were used for XRD measurements. In some cases, a factorial analysis of variance (ANOVA) was used to determine whether results were statistically significantly different. The p-value reported for these data indicates the statistical significance of the result and represents the probability of error that is involved in accepting the observed result as valid, e.g., a p-value of 0.05 indicates that there is a 5 % probability that the relation between the variables found in the sample is coincidental. For these studies, a p-value of 0.05 was treated as an acceptable error level

### 2.3 High speed filming

A Photron Fastcam Ultima APX camera (capable of filming at 120 000 frames per second (fps) and with a maximum resolution of 1024 by 1024 pixels) was used to identify material flow and areas of low turbulence in the reactors. Two systems were used where compressed air or nitrogen was fed via the ammonia solution nozzle and water via the iron solution nozzle. (A two phase liquid-gas system was used to be able to differentiate between incoming streams although, ideally, liquid systems should have been used. The use of solid particles suspended in a liquid stream or immiscible or coloured liquids was also investigated, however, solids resulted in blockages of the nozzles while liquid flows were indistinguishable from one another.) In the first system (Fig. 5 (a)), mains water pressure was maintained at 150 kPa while the compressed air pressure was increased through 150, 200, 300, 400 and 500 kPa. The second system (Fig. 5 (b)) made use of the IS reactor setup where both the liquid and gas flow pressures were increased through 150, 200, 300, 400 and 500 kPa. Filming was performed at 4 000 fps.

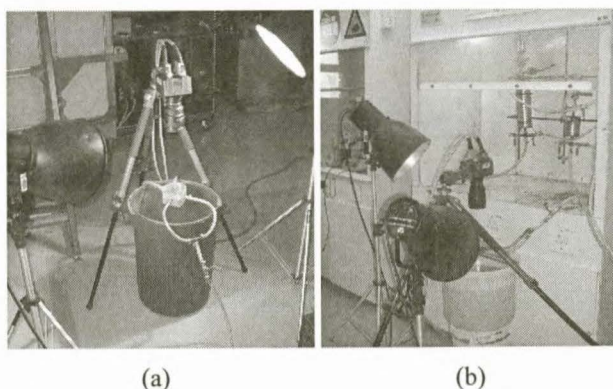


**Figure 5** Two high speed filming setups used to investigate stream flow inside the reactors. In (a), mains water (pressure maintained at 150 kPa) and compressed air (up to a pressure of 500 kPa) were fed to the reactors. In (b), the impinging stream reactor setup was used and both the liquid and gas flow pressures were increased to 500 kPa.

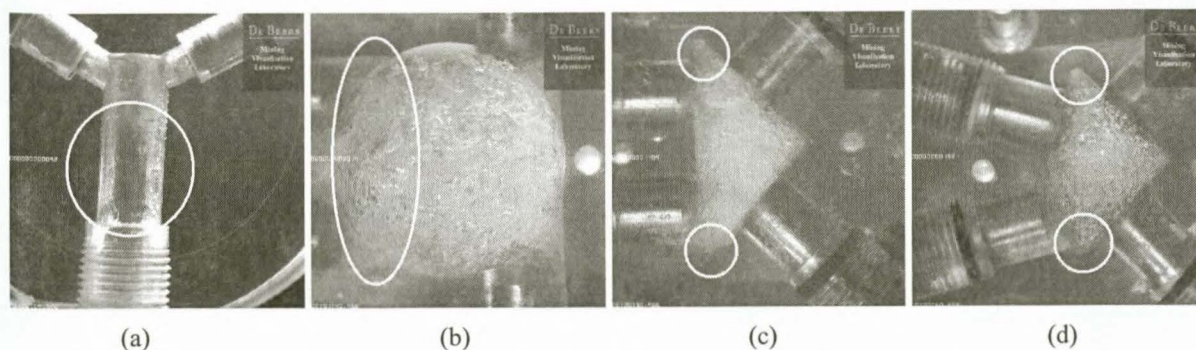
### 3. Results and discussion

#### 3.1 High speed filming

High speed filming using a model gas bubble system indicated that there is extremely poor mixing in the lower section of the Y-shaped reactor (Fig. 6 (a)). This is expected as the reactor does not form a closed volume in accordance with the definition of IS reactors. After the impinging streams collide, the precipitate emerges directly from the reactor stem, with no residence time and further reagent contact being possible.

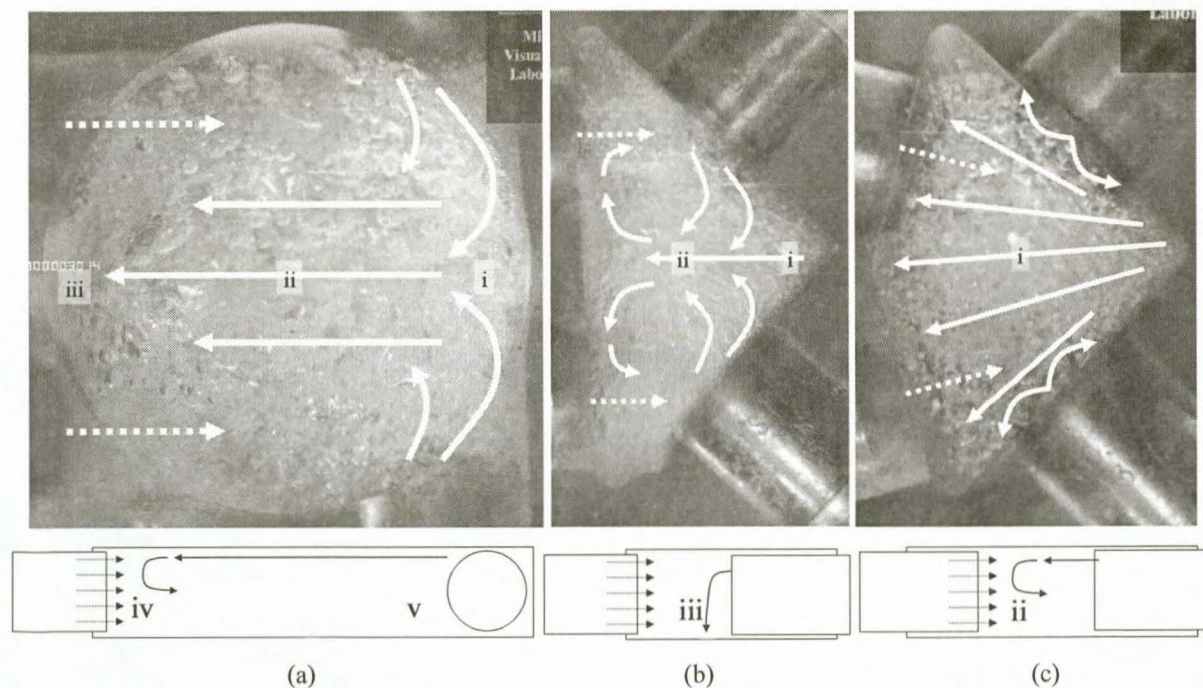
In the remaining reactors, the liquid can be seen to shear off the bubbles from the entering gas stream and transport the bubbles to the bulk of the reactor. The kinetic energy of the entering liquid streams must be dissipated by the liquid and therefore intense small scale turbulence is created in the liquid phase. Small scale turbulence and bubbles in the bulk interact causing bubble breakup and increase the interfacial area for mass transfer. Macro flow patterns distribute the random turbulence through the reactor<sup>11</sup>.

Although the circular reactor (Fig. 6 (b)) should be capable of high mass transfer because of the observed centrifugal acceleration of the fluid in the chamber, and although the triangular and kite-shaped reactors (Figs 6 (c) and (d), respectively) appear to provide a high interfacial area as a result of the collisions of streams with the reactor walls, there still appear to be stagnant zones towards the base of the circular reactor and in the base angles of the triangular and kite reactors. Potential areas of lower pH in these low turbulence zones (in the case of magnetite precipitation) could possibly be eliminated in the circular reactor by increasing the reagent inlet velocities and in the kite and triangular reactors by minimising the sharp angles inside the reactor volume thereby maintaining small scale turbulence created in the vicinity of the nozzles but increasing the forceful macro flow pattern. An ideal reactor would combine the mass transfer characteristics of the rounded reactor chamber with the enhanced interfacial area produced by the angular reactor as a compromise between reactor shapes.



**Figure 6** Potentially stagnant zones (areas of lower turbulence) in (a) the Y-shaped, (b) circular, (c) triangular and (d) small kite-shaped impinging stream reactors

Fig. 7 depicts cross-sectional photographs and longitudinal schematics of the liquid and gas flow patterns inside the reactors as determined by observation of the flow patterns from the high speed filming footage. In the circular reactor (Fig. 7 (a)), the incoming liquid stream shears off gas bubbles, creating a centrifugal acceleration of the gas within the reactor volume. The gas is forced towards the centre (Fig. 7 (a) i) and down the middle of the circular reactor (Fig. 7 (a) ii). When it reaches the opposite side of the reactor (Fig. 7 (a) iii), the gas moves perpendicularly to the original direction of flow and towards the reactor base (Fig. 7 (a) iv) before changing direction and heading towards the gas nozzles (Fig. 7 (a) v). There may be a circulation of this gas in the reactor before it exits via the base of the reactor. In the triangular reactor (Fig. 7 (b)), the liquid stream also shears off gas bubbles and forces the gas towards the middle (Fig. 7 (b) i) and down the centre of the reactor (Fig. 7 (b) ii). However, the liquid stream is not reflected effectively and many of the gas bubbles exit directly through the outlet at the base of the reactor as shown in the longitudinal figure (Fig. 7 (b) iii). This direct exiting of material results in a reduced residence time of material inside the reactor. The kite-shaped reactor (Fig. 7 (c)) exhibits much the same flow pattern as the circular reactor, with gas flowing across the reactor (Fig. 7 (c) i) and then downwards (Fig. 7 (c) ii) towards the base of the reactor thereby increasing the residence time before exiting the reactor.



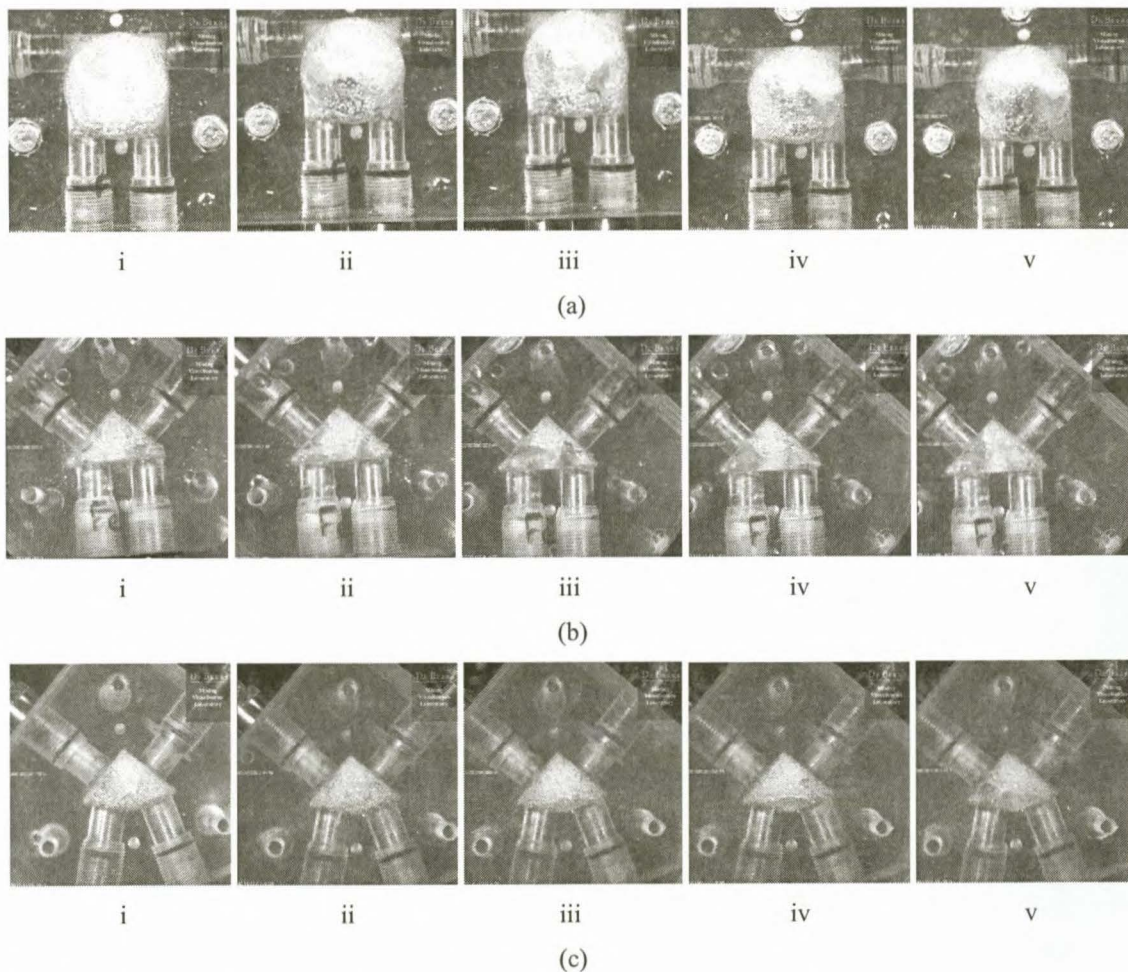
**Figure 7** Cross-sectional photograph (above) and longitudinal schematic diagram (below) depicting flow patterns in the (a) circular, (b) triangular and (c) small kite-shaped impinging stream reactors (---- liquid flow, — gas flow)

Fig. 8 shows the static flow pattern inside the circular, triangular and kite-shaped reactors for increasing gas pressures of 150, 200, 300, 400 and 500 kPa (liquid pressure maintained at 150 kPa). The gas voidage in the reactor increases as shown in Figs 8 (a) to (c), especially in the base of the circular reactor, while the liquid holdup

decreases. With an increase in gas pressure, more bubbles are ruptured and a larger interfacial area is created. This should result in an increase in the rate of energy dissipation per unit mass of liquid, increasing the degree of turbulence and enhancing the mass transfer. The combined mass transfer coefficient should increase with an increase in gas flow rate because it is directly proportional to the energy  $\epsilon$  dissipated in the reactor (where  $\epsilon$  is the energy dissipation rate per mass in  $\text{J kg}^{-1}$  and the exponent  $\alpha$  varies according to the contacting device)<sup>9</sup>:

$$k_L a \propto \epsilon^\alpha \quad (4)$$

It appears, however, that the gas voidage at a pressure above 200 kPa (Figs 8 (a-c) ii-v) may be excessively high resulting in a decrease in liquid/gas phase contact



**Figure 8** Flow inside (a) circular, (b) triangular and (c) kite reactor at increasing gas pressures of (i) 150, (ii) 200, (iii) 300, (iv) 400 and (v) 500 kPa with constant liquid pressure of 150 kPa

When both liquid and gas pressures are increased from 200 to 500 kPa (Fig. 9), the turbulence again increases while the bubble size decreases. This should result in an increased mass transfer and interfacial area. The gas voidage in these reactors is not as significant as that observed in Fig. 8.

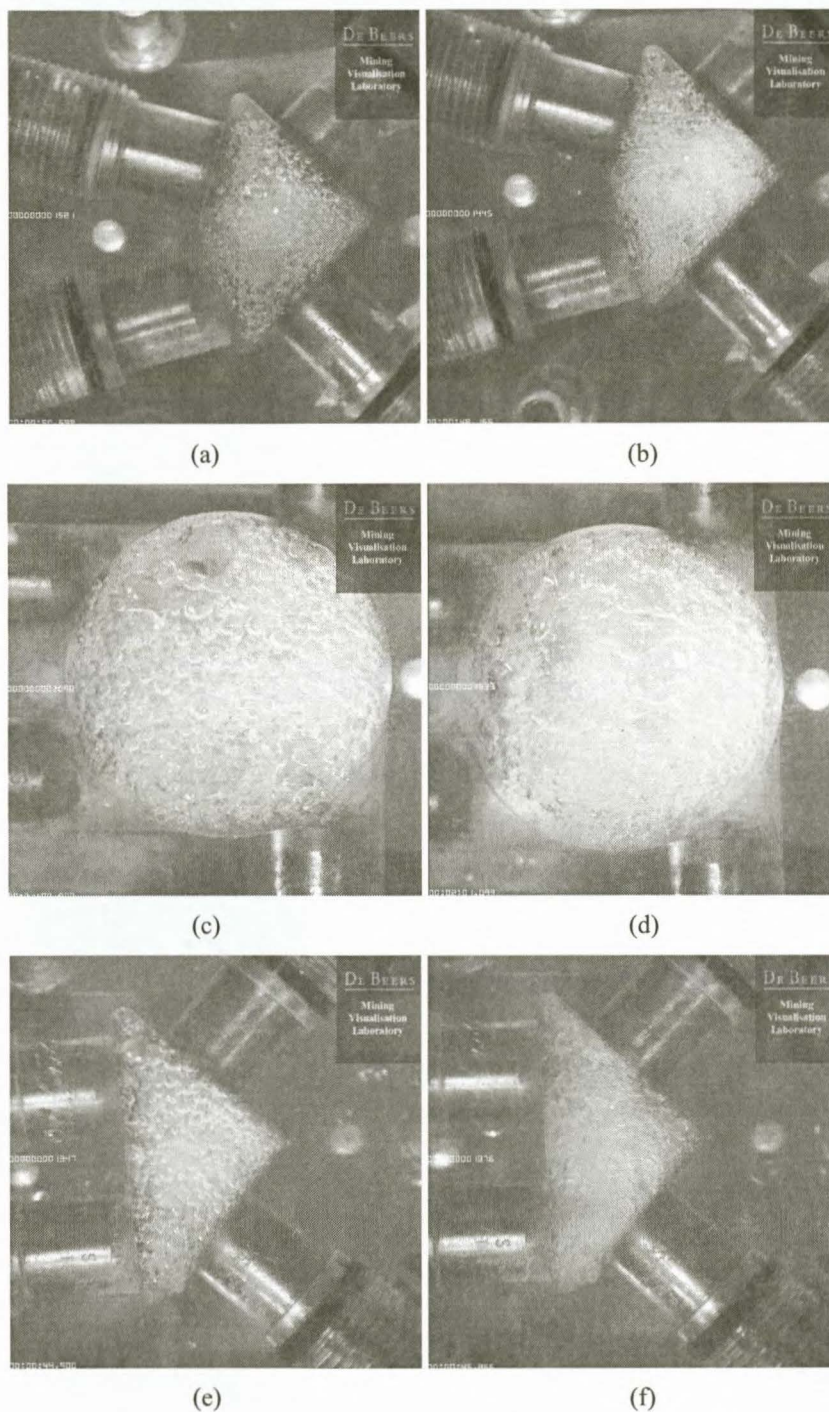


**Figure 9** (a) Kite reactor at 200 and (b) 500 kPa, (c) circular reactor at 200 and (d) 500 kPa and (e) triangular reactor at 200 and (f) 500 kPa gas and liquid pressures

### 3.2 X-ray diffraction analysis

The XRD data (Table 3) for the iron oxide precipitate obtained from each reactor show clearly that the kite and circular reactors produce a precipitate of highest magnetite content while the triangular and Y-shaped reactors produce a precipitate of lowest magnetite content, across the pressure range (it must be borne in mind that it is sometime difficult to distinguish between magnetite and maghemite in XRD as mentioned in Chapter 2, section 3.1). XRD data indicate that the balance of material is mainly haematite. However, it was found that the values in Table 3 are not statistically significantly different ( $p$ -value = 0.24) and it cannot be concluded from these data whether more magnetite is precipitated using one reactor over another (the XRD results are qualitative as only single measurements of the sample compositions were determined).

**Table 3** Percentage magnetite in samples precipitated by the small kite, circular, triangular and Y-shaped reactors as determined by XRD

Pressure (kPa)	200	300	400	500
	Percentage magnetite (%)			
Small Kite	100	100	100	75
Circular	100	84	85	100
Triangular	79	63	100	84
Y-shaped reactor	65	89	79	82

### 3.3 Field emission scanning electron microscopy micrographs

From the XRD data (which in general shows greater than 60 % magnetite composition), it is concluded that the rounded nanoparticles in the FESEM micrographs obtained for the small kite, circular, triangular and Y-shaped reactors (Figs 10 (a) to (d)) are magnetite particles. The observation by Cornell and Schwertmann<sup>7</sup> that the synthesis of magnetite particles in aqueous solutions at temperatures less than 100 °C produces fine-grained (< 0.1  $\mu\text{m}$ ) rounded, cubic or octahedral crystals further supports this conclusion.

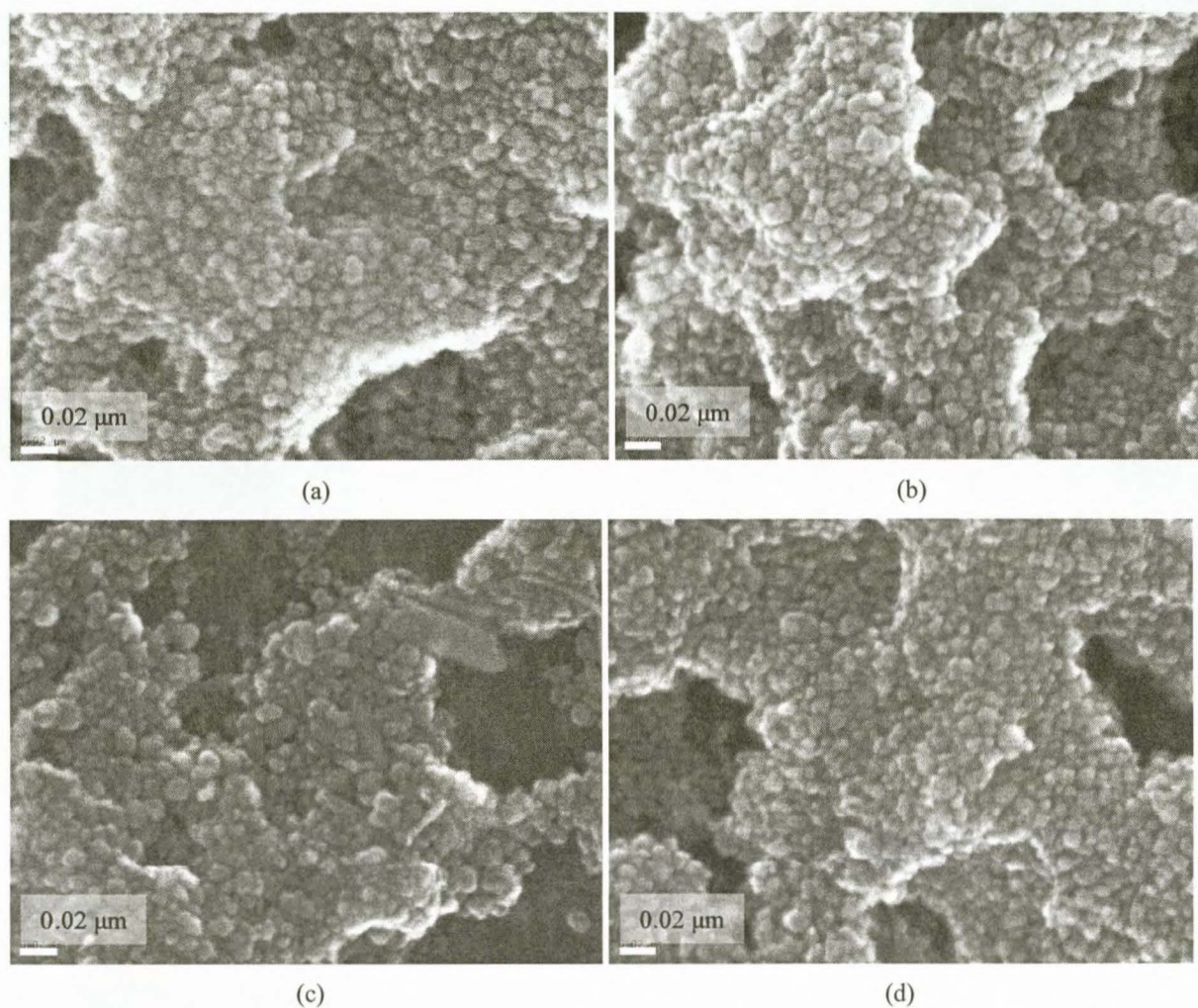


**Figure 10** Examples of particle morphology of iron oxide precipitate as produced by the (a) small kite, (b) circular, (c) triangular and (d) Y-shaped reactors

The precipitate produced by the triangular reactor (Fig. 10 (c)) shows the occurrence of rod-like structures which, from comparison with morphology in the literature (examples of which are given in Fig. 11, also reproduced in Chapter 2), are believed to be haematite rods<sup>7</sup>. Although XRD data for the Y-shaped reactor also indicated the presence of haematite, in most samples, a variation in morphology, potentially indicative of a variation in iron oxide composition was not observed.

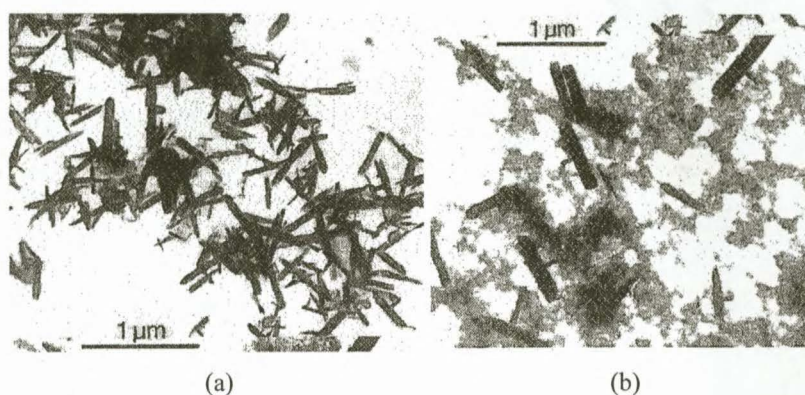


**Figure 11** Rod-like haematite particles as prepared from ferrihydrite at pH 11<sup>7</sup>

### 3.4 Particle size

Average particle sizes as determined by VSM and FESEM (with unbiased standard deviation) were  $12 \pm 1$  and  $8 \pm 2$  nm, respectively (see Table 4), while XRD data indicated an average particle size of  $11 \pm 3$  nm. These values indicate that the particles are single domain (the estimated diameter below which magnetite is single domain is approximately 80 - 130 nm)<sup>23, 24</sup>.

**Table 4** Average particle size as a function of pressure and reactor type (unbiased standard deviation in parentheses) as determined from VSM and FESEM measurements

Particle size	Determined from VSM measurements				Determined from FESEM micrographs			
	200	300	400	500	200	300	400	500
Large kite	12.2 (0.6)	11.7 (0.6)	11.7 (0.6)	11.8 (0.6)	Not determined			
Small kite	11.2 (0.7)	12.1 (0.6)	11.8 (0.6)	11.6 (0.6)	7.4 (1.7)	8.4 (1.7)	8.0 (1.7)	8.0 (1.7)
Circular	12.4 (0.6)	13.4 (0.6)	12.8 (0.6)	12.8 (0.6)	7.3 (2.1)	7.6 (1.6)	7.3 (1.7)	7.6 (1.7)
Triangle	11.1 (0.9)	14.5 (0.9)	11.8 (0.9)	12.4 (0.9)	8.6 (2.0)	9.7 (2.4)	7.8 (2.0)	8.5 (2.2)
Y-shape	Not determined				7.5 (1.8)	7.7 (1.6)	7.8 (1.7)	7.5 (1.7)

The average particle size as determined from VSM measurements is approximately 4 nm larger than that determined from the FESEM micrographs. This is in contradiction with literature findings: the particle size as given by the magnetisation curve is often smaller (by up to 10 %)<sup>25</sup> as compared to that determined from electron micrographs as a result of the chemical reaction of the surfactant at the magnetite surface or from surface oxidation<sup>24-30</sup> (see Fig. 12). In this study, however, a surfactant was not used for VSM samples and instead, samples were measured immediately after precipitation with the intention of minimising any possible magnetite oxidation. It is more likely that particle overlap in the FESEM images resulted in an under estimation of particle diameter. The unbiased standard deviation determined from FESEM micrographs is also higher than that for the VSM measurements indicating that a greater degree of inaccuracy may be incurred with manual particle measurement.

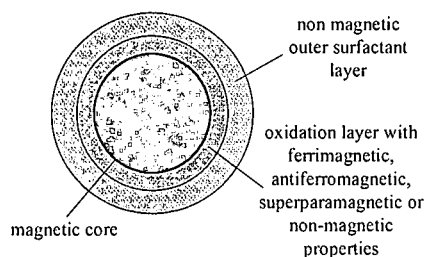


**Figure 12** Schematic representation of the non-magnetic shell between the magnetic core and the surfactant usually resulting in an underestimation of particle size from VSM measurements

### 3.5 Magnetic characterisation

Magnetisation curves for the samples produced by the kite and circular reactors (examples of which are given in Figs 13 (a) to (c) for the 20 and 8 cm<sup>3</sup> kite and 20 cm<sup>3</sup> circular reactors, respectively, at varying pressures) confirm that the precipitate is superparamagnetic and exhibits zero magnetisation at zero applied field. Because high speed filming did not show turbulent reactor mixing and XRD data showed low magnetite precipitate percentages, magnetisation measurements were not performed for the Y-shaped reactor.

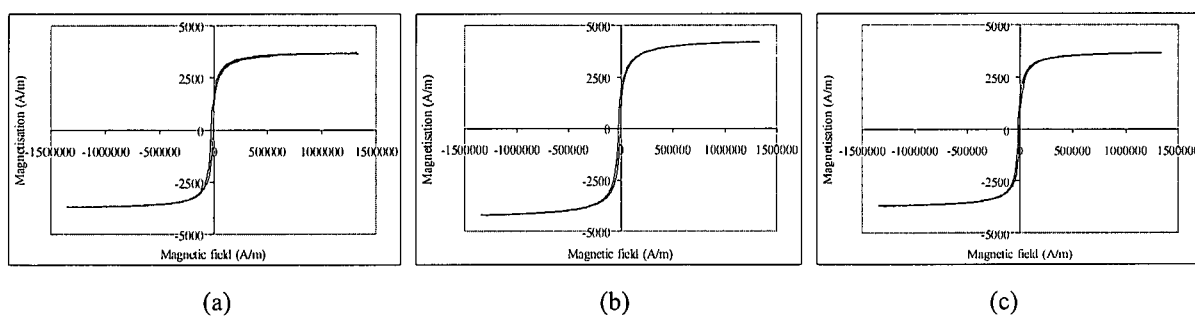


**Figure 13** Magnetisation curves for the samples precipitated by the (a) large kite (200 kPa), (b) small kite (300 kPa) and (c) circular reactor (300 kPa)

The saturation magnetisation for the 8 and 20 cm<sup>3</sup> kite and 20 cm<sup>3</sup> circular reactors lies predominantly between 4200 to 4800 A m<sup>-1</sup> across the pressure range investigated (Fig. 14) suggesting that the precipitate produced by these reactors consists of material of similar magnetic properties. The saturation magnetisation agrees reasonably well with the calculated value of 4800 A m<sup>-1</sup> for a sample of 1 % magnetite by volume (with saturation magnetisation of pure magnetite taken to be equal to 4.8X10<sup>5</sup> A m<sup>-1</sup>). The factorial analysis of variance (ANOVA) indicated that the interaction between the reactor type and the pressure was not statistically significant (p-value = 0.15). Furthermore the ANOVA showed no significant difference between the kite and circular reactor mean values of saturation magnetization (p-value = 0.13). This suggests that the precipitate produced by the circular and that produced by the

kite reactors does not differ significantly in terms of saturation magnetization as a function of the shape of these reactors.

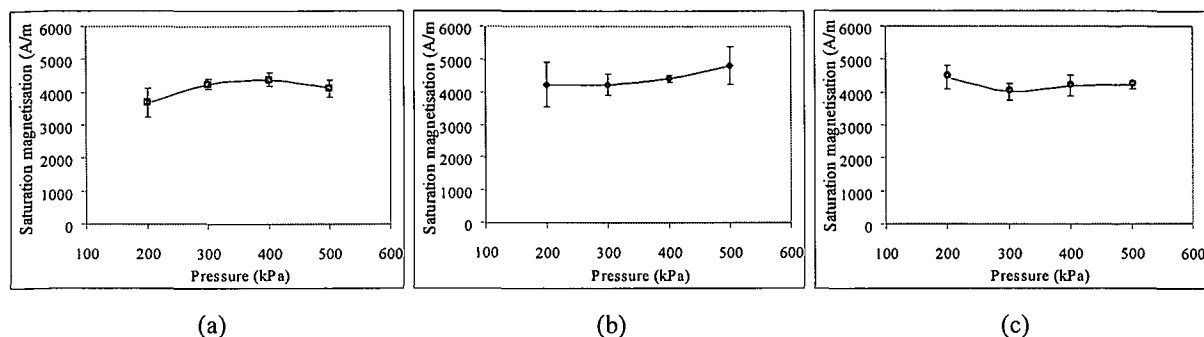


**Figure 14** Saturation magnetisation of samples precipitated at pressures of 200 to 500 kPa for the (a) large kite, (b) small kite and (c) circular reactor

The magnetisation curves obtained for the triangular reactor showed great variation in maximum magnetisation and curve shape across the pressure range investigated (Fig. 15). In many cases, the precipitate did not saturate within the magnetic field range (see for example, Fig. 15 (a)). The variability and inconsistency in the precipitate produced was confirmed visually by the variation in precipitate colour (ochre or red-brown to black) produced at identical replicate conditions. These observations may indicate the precipitation of a variety of iron oxides such as goethite, haematite or ferrihydrite<sup>7</sup>. In the triangular reactor, in some cases, a viscous, gelatinous precipitate was produced possibly as a result of the formation of Fe(III) hydroxides<sup>31</sup>. The initial magnetisation curve of such a sample precipitated at 200 kPa and that of the same sample after 30 minutes are shown in Figs 15 (b) and (c). The slow conversion of these gels to form magnetite may have occurred in situ in the VSM sample holder which showed an increase in maximum magnetisation with time.

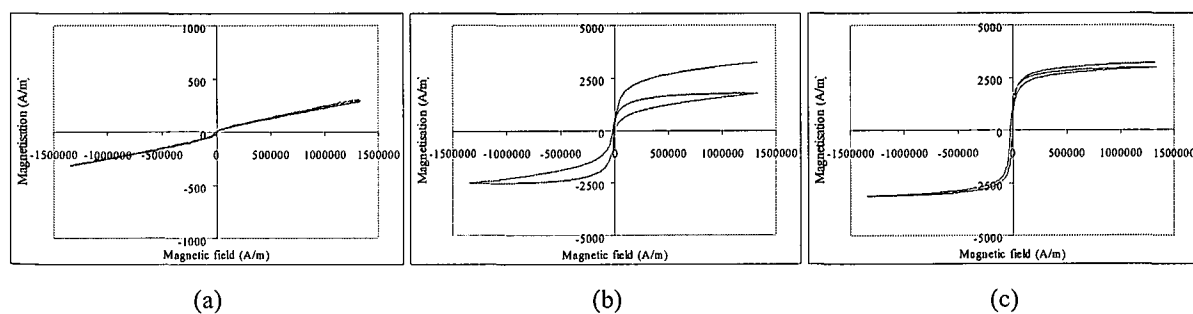


**Figure 15** Magnetisation curves produced by the triangular reactor at (a) 500 kPa (note the scale as compared to (b) and (c)), (b) 200 kPa and (c) the same 200 kPa sample measured 30 minutes later

From high speed filming and XRD and VSM data, it appears that the choice of reactor shape and volume are critical for magnetite precipitation. The 8 cm<sup>3</sup> kite-shaped reactor produces a precipitate of higher magnetic content than the 8 cm<sup>3</sup> triangular reactor. It is possible that the angle of impingement between the reagent streams and their impact

on the reactor wall in the small kite-shaped reactor as compared to the triangular reactor is such that turbulence in the reactor is more easily established and maintained. The larger corner angles ( $60^\circ$ ) of the kite reactor appear to allow for more fluid movement within the reactor while the triangle with smaller sharper corners ( $45^\circ$ ) is more likely to exhibit stagnant volumes. Moreover, it is possible that there is insufficient reactor residence time and poor mixing because of the smaller volume of the triangular reactor compared to the larger  $20\text{ cm}^3$  circular and kite-shaped reactors. Limitations as a result of the shape and volume of the triangular reactor appear to result in localised pH gradients, variations in hydrolysed species, poor magnetite precipitation and irreproducible results<sup>7</sup>.

The observations that the kite and circular reactors are capable of producing a precipitate of higher magnetic material content is confirmed by the studies performed by Botes<sup>16</sup> and Kleingeld<sup>17</sup>. Botes tested an opposing jet, spherical and hemispherical reactor (Figs 16 (a) to (c)) for the absorption of  $\text{CO}_2$  into a sodium hydroxide solution.

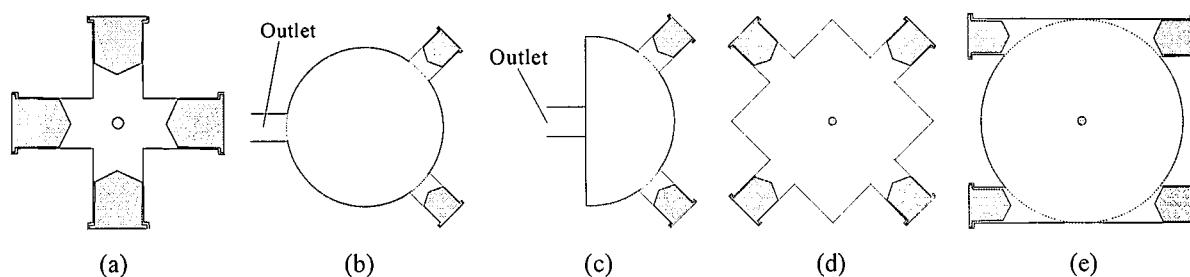


**Figure 16** (a) Opposing jets, (b) spherical, (c) hemispherical, (d) square and (e)  $\sigma$ -shaped circular reactor

Based on the main conclusions from this work, namely, that opposing jets resulted in a larger impingement effect between feed streams, that nozzles should be positioned in such a fashion as to create a forceful directed flow inside the reactor and that nozzle placement should eliminate plug flow, Botes then tested a square (Fig. 16 (d)), triangular (Fig. 3 (c)) and kite-shaped reactor (Fig. 3 (a)). The square reactor exhibited similar behaviour as for the first three reactors tested (opposing jets, spherical and hemispherical reactors). The kite and triangular reactors exhibited similar trends for interfacial area production and the combined mass transfer coefficient but the kite exhibited higher values overall. This was ascribed to the angle of impingement of reagent streams and the angle of incidence on the reactor walls which results in the creation of random turbulence in the reactor.

Kleingeld then compared the kite-shaped reactor to two circular reactors termed the  $\pi$ - (Fig. 3 (b)) and  $\sigma$ -reactors (Fig. 16 (e)). Because of concerns as to potential nozzle blockages from precipitation with head-on impingement of streams, the  $\sigma$ -shaped circular reactor was not tested for the precipitation of magnetite. Kleingeld found that the circular reactors exhibited a higher mass transfer coefficient than the kite reactor as a result of the centrifugal acceleration in the reactor volume. This is in accordance with eq. 5 which gives the mass transfer coefficient as a function of fluid acceleration,  $a$  ( $\rho_L$  and  $\rho_G$  are the liquid and gas densities, respectively, and  $\mu_L$  is the liquid viscosity)<sup>3</sup>:

$$k_L \propto \left( \frac{(\rho_L - \rho_G) \mu_L a}{\rho_L^2} \right)^{\frac{1}{3}} \quad (5)$$

By comparison, however, energy is used in the kite reactor for the division of opposing streams rather than in changing stream direction and momentum. The kite-shaped reactor yielded a higher interfacial area and was found to display a higher combined mass transfer coefficient  $k_L a$ , as compared to the  $\pi$ -shaped circular reactor. The combined mass transfer coefficients for these investigations were a maximum of 8, 12 and 22  $\text{s}^{-1}$  for the triangular, circular and kite-shaped reactors, respectively.

The observations made for the magnetite precipitation are in accordance with the observations by Botes<sup>16</sup> and Kleingeld<sup>17</sup>. The circular and kite-shaped reactors produced a good magnetite precipitate of similar saturation magnetisations. In addition, particle size and FESEM and XRD data were similar for the two reactors. The triangular reactor with the lower mass transfer coefficient produced a precipitate with lowest magnetic content according to VSM and XRD data.

#### 4. Conclusions and general discussion

Five impinging stream reactors of different shapes and volumes for the potential large-scale, continuous precipitation of magnetite were tested. The circular reactor, which promotes mass transfer, and the kite-shaped reactors, which provide a high interfacial area for reaction, allow for the precipitation of predominantly good magnetite material while the triangular and Y-shaped reactors tend to produce higher quantities of non-magnetic iron oxides. The Y-shaped and triangular reactors could be used for initial precipitation of gelatinous oxyhydroxides with final magnetite formation occurring in a subsequent stirred tank. However, it has been seen that magnetite can be precipitated directly from the other reactors and an additional stirred tank would be an unnecessary item of equipment.

Not only reactor shape, but also reactor volume is critical for efficient magnetite precipitation: the 8  $\text{cm}^3$  triangular reactor of the same small volume as the kite-shaped reactor produced precipitates with low magnetic material content probably as a result of the low reactor residence time. To obtain further information on the influence of reactor shape and volume, precipitation using a 20  $\text{cm}^3$  triangular and 8  $\text{cm}^3$  circular reactor should be investigated. In addition, and based on the fact that no nozzle blockages were experienced during the test work, the  $\sigma$ -shaped circular reactor could also be tested as this reactor showed higher mass transfer coefficients than the  $\pi$ - and kite-shaped reactors in test work on  $\text{CO}_2$  absorption<sup>16</sup>.

Alternative IS reactors such as the impinging stream jet loop reactor (ISJLR) could also be tested. The ISJLR has three impingement zones: one head-on impingement zone and two perpendicular impingement zones as shown in

Fig. 17. The mass transfer coefficients in the impingement zone and the main reactor tube are 4 and 2.5 times higher, respectively, than the remainder of the reactor at high power dissipation<sup>9</sup>.

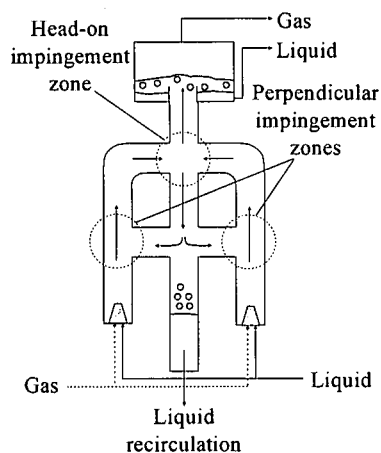


**Figure 17** Schematic of an impinging stream jet loop reactor

The IS reactor system is ideal for providing intimate mixing conditions as compared to, for example, a conventional stirred tank reactor. These reactors have no moving parts or expensive packing material, are of simple construction, of small geometric size and high throughput<sup>17</sup>. The reactors should have as few sharp angles as possible with nozzle inlets positioned such that turbulent conditions in the reactor can be produced and sustained. A smooth reactor surface may also prevent the adhesion of reagents (especially in the case of gaseous reagents). The nozzles used in such systems are supplied with certain pressure-flow rate characteristics. They need to be inert, readily available, affordable and should possess sufficient mechanical strength to withstand high pressure operation.

Disadvantages of using such reactors include the potential blocking, fouling or degradation of nozzles with time as a result of the high pressure feed. They may also be associated with relatively high energy consumption rates but would be of great advantage where feed is already pressurised and where space and stability constraints are important<sup>17</sup>.

The reactors as used in these tests could theoretically produce 8 – 12 nm diameter magnetite precipitate particles at rates of between 30 g min<sup>-1</sup> at 200 kPa and 50 g min<sup>-1</sup> at 500 kPa, using the experimental setup described here. It would be relatively easy to scale-up to higher throughputs using larger capacity nozzles or increased pressures. In addition, commercially available dosing pumps could be used for continuous reagent feed. It has therefore been shown that the IS reactor system can be used for the large-scale continuous precipitation of nanosized magnetite particles for which results have recently been accepted for publication (Vatta, L. L.; Sanderson, R. D.; Koch, K. R., An investigation into the potential large-scale continuous magnetite nanoparticle synthesis by high pressure impinging stream reactors. *Journal of Magnetism and Magnetic Materials* 2007.)

## References

1. Willard, M. A.; Kurihara, L. K.; Carpenter, E. E.; Calvin, S.; Harris, V. G., *Encycl. Nanosci. Nanotech.* 2004, **1**, 815.
2. Bönemann, H.; Nagabhushana, K. S., *Chemical synthesis of nanoparticles, Encycl. Nanosci. Nanotech.* 2004, **1**, 777.
3. Buske, N.; Sonntag, H.; Götze, T., *Colloids Surf.* 1984, **12**, 195.
4. Häfeli, U. O., *Int. J. Pharm.* 2004, **277**, 19.
5. Feltin, N.; Pileni, M. P., *Langmuir* 1997, **13**, 3927.
6. Farkas, J., *Sep. Sci. Technol.* 1983, **18**, 787.
7. Cornell, R. M.; Schwertmann, U., *The iron oxides* VCH Publishers, New York, 1996.
8. Gribanov, N. M.; Bibik, E. E.; Buzunov, O. V.; Naumov, V. N., *J. Magn. Magn. Mater.* 1990, **85**, 7.
9. Kleingeld, A. W., MSc dissertation, University of Stellenbosch, 1999.
10. Tamir, A., *Impinging-stream reactors: fundamentals and applications* Elsevier, Amsterdam, 1994.
11. Botes, F. G., MSc dissertation, University of Stellenbosch, 1995.
12. Mare, P. W., MSc dissertation, University of Stellenbosch, 1999.
13. Tamir, A.; Herskowitz, D., *Chem. Eng. Sci.* 1985, **40**, 2149.
14. Ramshaw, C.; Cook, S., *The Chemical Engineer* 2006, **775**, 42.
15. Loftus, B. M., MSc dissertation, University of Stellenbosch, 1999.
16. Botes, F. G.; Lorenzen, L.; van Deventer, J. S. J., *Chem. Eng. Commun.* 1998, **170**, 217.
17. Lorenzen, L.; Kleingeld, A. W., *Miner. Eng.* 2000, **13**, 1107.
18. Rasband, W. ImageJ: Image processing and analysis in Java <http://rsb.info.nih.gov/ij/>.
19. Chantrell, R. W.; Popplewell, J.; Charles, S. W., *IEEE Transactions on Magnetics* 1978, **Mag-14**, 975.
20. Cullity, B. D., *Elements of X-ray diffraction* Addison-Wesley, California, 1978.
21. Ismat Shah, S., *Encycl. Nanosci. Nanotech.* 2004, **5**, 449.
22. Khalafalla, S. E.; Reimers, G. W.; Rholl, S. A., US Patent 4 208 294, 1980.
23. Krishnan, K. M.; Pakhomov, A. B.; Bao, Y.; Blomqvist, P.; Chun, Y.; Gonzales, M.; Griffin, K.; Ji, X.; Roberts, B. K., *J. Mater. Sci.* 2006, **41**, 793.
24. Leslie-Pelecky, D. L.; Rieke, R. D., *Chem. Mater.* 1996, **8**, 1770.
25. Lefebure, S. e. a.; Dubois, E.; Cabuil, V.; Neveu, S.; Massart, R., *J. Mater. Res.* 1998, **13**, 2975.
26. Charles, S. W.; Popplewell, J., *IEEE Transactions on Magnetics* 1980, **Mag-16** **2**, 172.
27. Kaiser, R.; Miskolczy, G., *J. Appl. Phys.* 1970, **41**, 1064.
28. Petipas, C., *Thermomechanics of magnetic fluids* Hemisphere, Washington DC, 1980.
29. Hilgendorff, M., *Encycl. Nanosci. Nanotech.* 2004, **1**, 213.
30. Kim, D. K.; Zhang, Y.; Voit, W.; Rao, K. V.; Kehr, J.; Bjelke, B.; Muhammed, M., *Scr. Mater.* 2001, **44**, 1713.
31. Reimers, G. W.; Khalafalla, S. E. Technical progress report 56, U. S. Department of the Interior, Twin Cities Metallurgy Research Centre, 1972, 1.

## Chapter 4\*

### Magnetic liquids, magnetic liquid/Aliquat 336 and magnetic liquid/methyl isobutyl ketone mixtures for the extraction of $[\text{Co}(\text{SCN})_4]^{2-}$ from an aqueous solution by solvent extraction

---

#### Abstract

Investigations have been performed into the extraction of  $[\text{Co}(\text{SCN})_4]^{2-}$  from an aqueous phase onto the surface of bare magnetite and into a magnetic organic phase (magnetic liquid or Aliquat 336/methyl isobutyl ketone (MIBK) in magnetic liquid) by ion pair formation  $[\text{Co}(\text{SCN})_4]^{2-}\text{R}_2^{2+}$  ( $\text{R}^+$  is the Aliquat 336 or the solvated oxonium ion in MIBK). The results were compared to the extraction into a conventional non-magnetic organic phase (Aliquat 336/MIBK in kerosene). The percentage extraction of the cobalt complex was found to increase with an increase in volume of magnetite, magnetic liquid or percentage Aliquat 336 in magnetic liquid. Although initial investigations using MIBK showed poor  $[\text{Co}(\text{SCN})_4]^{2-}$  extraction and liquid instability, a suitable extraction system using the MIBK for preliminary extraction followed by the use of the magnetic liquid as an MIBK scavenger was developed. Owing to its magnetic properties, the magnetic liquid system may allow for a more rapid organic phase separation from the aqueous phase than is possible with conventional liquid extractants.

#### 1. Magnetic supports for extraction

Magnetic supports are magnetic materials that can selectively attach themselves to non-magnetic materials. The supports thereby confer magnetic properties to the target and enable the non-magnetic material to be separated by magnetic means<sup>1</sup>. The concept of magnetic supports originated in the 1940s when magnetite was used in the removal of organic impurities from effluent streams. Since the 1970s, work has been performed in the use of magnetic supports in effluent processing and metal ion removal, in the biological and pharmaceutical fields, in mineral separation and in food processing<sup>1-5</sup>.

Magnetic supports may be broadly classified as magnetic carriers or magnetic tags<sup>1</sup>. Magnetic carriers are usually 10 to 1 000 times larger than the target which can become entrapped on the carrier surface or within the carrier particle (Fig. 1 (a)). Magnetic tags are usually smaller than the particles to be separated and coat or cluster around the target (Fig. 1 (b)).

---

\* Based in part on the papers, Vatta, L. L.; Sanderson, R. D.; Koch, K. R., *Magnetic nanoparticles: Properties and potential applications*. *Pure Appl. Chem.* 2006, 78, (9), 1791-1799 and Vatta, L. L.; Koch, K. R., *The extraction of  $[\text{Co}(\text{SCN})_4]^{2-}$  from an aqueous solution by solvent extraction using a magnetic liquid and a magnetic liquid/Aliquat 336 mixture*. Manuscript in preparation 2007.

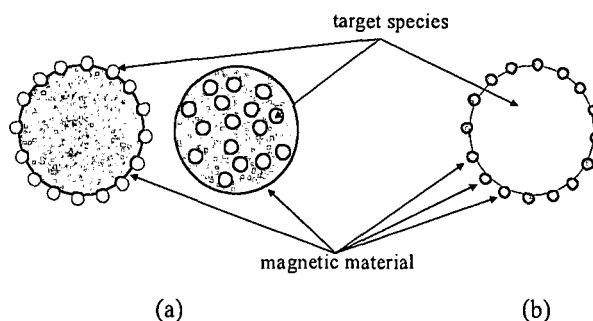


**Figure 1** Schematic representation of (a) magnetic carriers which are usually 10 to 1000 times larger than the target and (b) magnetic tags which are usually smaller than and cluster around the target species

### 1.1 Bare magnetic supports

Initial work in the fields of effluent processing and metal ion recovery showed that the main factor controlling the attachment of bare magnetic carriers to target species is an electrostatic interaction and that by the judicious addition of pH modifiers and electrolytes, the surface charge of particles and targets could be controlled<sup>1, 6</sup>. Fundamental work was performed by de Latour in the 1970s where he investigated the precipitation of Al(III), Fe(III) and Cu(II) upon the addition of a magnetite seed<sup>7</sup>. In his work, de Latour demonstrated that the mechanism of species removal was electrostatic adsorption onto the magnetite surface and was highly dependent on the surface charge of the magnetite particles. Terashima *et al.* in their work on the removal of dissolved heavy metals by chemical coagulation, magnetic seeding and high gradient magnetic filtration<sup>8</sup> also confirmed that the attachment of the target to the magnetic seed was predominantly as a result of surface charge and the resultant electrostatic interactions. Parsonage<sup>9</sup> corroborated the importance of the surface charge and found that the attachment of surfactants to the particle surface caused a change in the magnetite point of zero charge (PZC) which could, for example, be adjusted from approximately 6.5 to 4.5 when magnetite particles were coated with sodium oleate. Such investigations led to a commercial process which exploits these findings, namely, the Sirofloc™ process, developed by the CSIRO research group<sup>10</sup>. In this application, micron-sized magnetite particles in media of pH 4 – 6 have protonated surfaces for the adsorption of negatively charged colloids or suspended solids.

### 1.2 Other applications of magnetic supports

Besides the use of bare magnetic particles for species extraction, magnetic supports have also been used in the following types of applications:

- Ferrihydrite or ferric hydroxide gel-coated magnetite was used for the removal of Cr(IV) and Zn(II) and colour and turbidity from wastewater by Chen *et al.*<sup>11</sup> and Anderson *et al.*<sup>12</sup>, respectively. The aim of the gel coating was to increase the carrier's specific surface area, but the coatings showed poor long-term stability.

- Bolto<sup>13</sup> performed work on magnetic polymer beads (magnetic resins) for use in conventional ion exchange processes in order to increase the reaction and sedimentation rates.
- Homogenous as well as heterogeneous resins have been tested in wastewater treatment processes<sup>14</sup>. In homogenous resins, the magnetic material is uniformly distributed within the cross-linked ion exchange resin or inert cross-linked polymer<sup>15</sup>. In heterogeneous resins, homogeneous magnetic polymer particles are functionalised by the attachment of selected polymeric chains<sup>15</sup>.
- Surface-functionalised magnetic carriers (such as through attachment of a bolamphiphilic surfactant) have also been developed. Gélinas *et al.* synthesised diethylenetriamine-terminated maghemite carriers for the complexation of copper ions<sup>16</sup>.

## 2. Magnetic liquids

### 2.1 Composition and properties of magnetic liquids

Significant developments in various scientific fields in the last 50 years have seen the increased interest of scientists in the field of condensed matter science with a particular focus on soft materials whose properties and behaviour differ from solid matter<sup>17</sup>. Soft materials include fluids, liquid crystals, polymers, emulsions and colloids, and are characterised, for example, by the fact that they are easily deformed by external stresses and electromagnetic and gravitational fields<sup>17</sup>.

Magnetic particles in the nanosize range suspended in an appropriate fluid may be used in magnetic liquids (also known as ferromagnetic liquids or ferrofluids when containing iron) which are a typical hybrid of the nanoparticle and a soft material<sup>17</sup>. Magnetic liquids consist of a stable colloidal dispersion or suspension of single domain ferro- or ferrimagnetic particles in a carrier liquid<sup>18</sup>. The stability imparted to the particles comes about as a result not only of the size of the particles but also through stabilisation of the suspended particle by a surfactant (see magnetic liquid components in Fig. 2). The magnetic particles in the magnetic liquid could be, for example, magnetite ( $\text{Fe}_3\text{O}_4$ ), maghemite ( $\gamma\text{-Fe}_2\text{O}_3$ ), iron, cobalt, nickel, gadolinium, dysprosium, manganese, magnesium or copper<sup>19, 20</sup>. Carrier liquids could be, for example, different types of oils, fluorocarbons or even water. (Water-based fluids usually exhibit a lower saturation magnetisation than hydrocarbon-based fluids as they are more difficult to stabilise.)

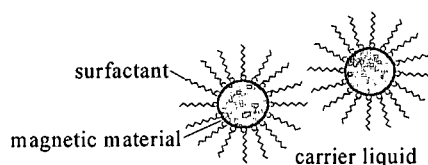


**Figure 2** Schematic representation of the three components of a magnetic liquid: surfactant, carrier liquid and magnetic material

Fig. 3 (a) shows a magnetic fluid suspended in an aqueous solution and exposed to a magnetic field. The fluid forms spikes as the nanosized magnetic particles align themselves with the external magnetic field lines. Upon removal of the magnet (Fig. 3 (b)), the superparamagnetic fluid relaxes and settles completely.

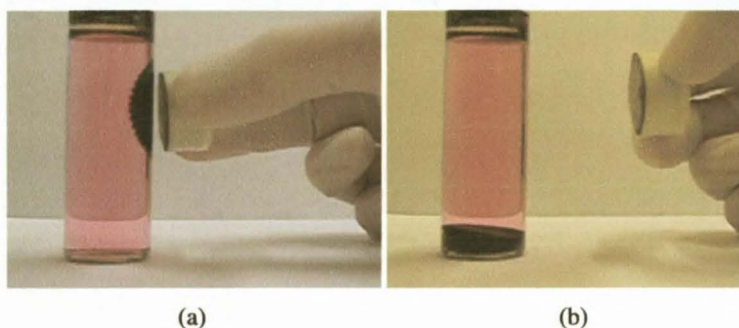


**Figure 3** Magnetic liquid (suspended in an aqueous solution) (a) forming spikes when exposed to a magnetic field as coated magnetite nanoparticles align with the external magnetic field lines and (b) relaxing completely upon removal of the magnet

The magnetite particle size required to ensure stability of the fluid (to maintain the stable colloidal suspension) is approximately 10 nm. This particle size is small enough such that the kinetic energy imparted to the particle by the motion of solvent molecules (Brownian motion) is sufficient to maintain stability in a magnetic field, in a gravitational field and against the magnetic attraction of particles to one another in the absence of a magnetic field thereby preventing particle agglomeration and settling<sup>18, 21-23</sup>. However, attractive London-type van der Waals forces that arise from induced dipole-dipole interactions and the tendency of particles to minimise their total surface or interfacial energy cannot be overcome by thermal agitation and may result in agglomeration<sup>20, 24</sup>.

Coalescence of nanoparticles can be minimised through two main methods. In electrostatic stabilisation, a double layer is formed by the ions adsorbed at the particle surface and their corresponding counter ions. The resultant Coulombic repulsion between particles ensures that they remain suspended<sup>25</sup>. Anionic and non-ionic surfactants have been used to produce a surface double layer<sup>24</sup>. Alternatively, a surfactant molecule on the surface of the nanoparticles may provide steric repulsion between particles thereby preventing agglomeration<sup>4, 25, 26</sup>.

Magnetic suspensions were first used to detect microscopic magnetic patterns on ferromagnetic tools (through deposition of the fluid on the surface and evaporation of the carrier liquid) and later for the identification of flux change on magnetic tapes. The National Aeronautical and Space Administration (NASA) manufactured magnetic liquid for investigations into its use as a pumpable rocket propellant in microgravity conditions (controlling fuel flow under conditions of weightlessness)<sup>22, 23</sup>. Magnetic liquids can be manipulated to flow or remain immobilized via application of an external magnetic field and have therefore been used in the voice coils of loudspeakers, to form

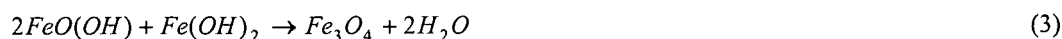
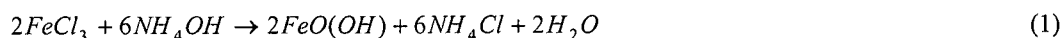
airtight seals in rotating machinery, as a variable density fluid for the separation of scrap metals, in magnetic paints and in the fields of biology and medicine, e.g., in targeted drug delivery<sup>3,20,22,23</sup>.

## 2.2 Synthesis of magnetic liquids

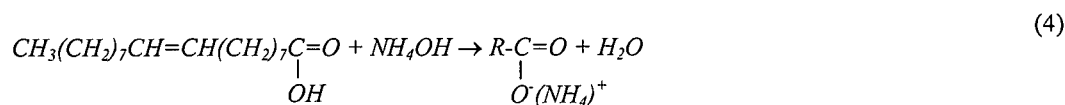
Magnetic fluids were first synthesised in the 1960s by the milling of a magnetic powder to 5 to 10 nm in a ball mill for more than 1000 hours at a time<sup>19</sup>. Interparticle magnetic flocculation and interparticle attraction caused by van der Waals forces made this preparation method rather unattractive. In the 1970s, a simpler method of chemical precipitation was developed which led to an increased interest in applications of magnetic nanoparticles<sup>17</sup>.

A simple method for the precipitation of magnetite is by the addition of ammonium hydroxide solution to a solution of ferric and ferrous ions as described in Chapter 2. The magnetite is coated with oleic acid as a surfactant (which allows for dispersion in a hydrocarbon carrier liquid) and is suspended in kerosene as the carrier liquid. The oleic acid coating is approximately 2 nm thick<sup>27,28</sup>.

Fig. 1 in Chapter 2 illustrated the complexity of the formation of magnetite but a very simplified representation of a possible synthesis route<sup>23</sup> is given by eqs 1 to 3.



Excess ammonium hydroxide then reacts with oleic acid to form an ammonium oleate soap:



The ammonium oleate soap can bond covalently to the magnetite particle through the iron ions on the surface which results in a coated particle that still retains an affinity for water due to the polar nature of the oleate coating<sup>29</sup>. The ammonium oleate coating is transformed upon heating into oleic acid with possible modes of coordination of the carboxylic acid group to the iron oxide surface<sup>30</sup> shown in Fig. 4. (The monodentate complex, Fig. 4 (b) is most likely formed.) Depending on the pH of the solution, one could also envisage an electrostatic interaction of the carboxylic acid with the magnetite surface taking place as a result of the magnetite surface charge.

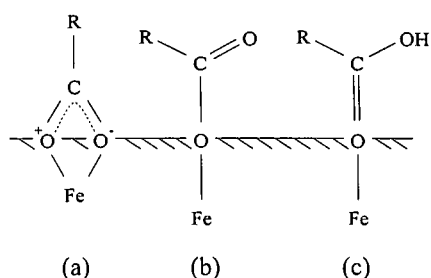


**Figure 4** Possible modes of coordination of COOH groups to the iron oxide surface: (a) bidentate, (b) monodentate (most likely) and (c) monodentate (least likely)

The ammonium ion redissolves in water (eq. 5) but as the temperature increases, the equilibrium of eq. 6 is driven to the right liberating ammonia gas from solution and further promoting the peptisation reaction.



The oleic acid-coated magnetite particles are now reasonably non-polar and would be more stable in a non-polar liquid such as kerosene. A migration of particles therefore takes place to the kerosene phase where they form a stable colloidal suspension.

### 3. Solvent extraction using a magnetic liquid or a magnetic liquid/extractant mixture

Liquid-liquid extraction is used for the extraction and isolation of a wide range of components, e.g., metals or impurities from a variety of feed streams. The component is removed from an aqueous phase by partition into an organic phase using an organic extractant, such as tricaprylyl methyl ammonium chloride (with commercial name Aliquat 336) or methyl isobutyl ketone (MIBK) and is then recovered from the organic phase usually by back extraction (stripping) of the component into a second aqueous phase<sup>31, 32</sup>. In commercial processes, it is unlikely that metals will form a non-polar species, thereby rendering them soluble in an organic solvent. It is more likely that the metals would exist as hydrated species thereby making them incompatible with non-polar organic liquids. There are a variety of methods<sup>31, 33</sup> whereby the hydrophilic metals could be converted into hydrophobic species by complexation with suitable ligands for extraction (extractants) by a non-polar diluent:

- the metallic cation can be complexed with an anion to form a neutral species (using an acidic extractant),
- an ion-pair complex can be formed (using an ion-pair extractant) or
- hydrated water molecules can be replaced with a solvating extractant (using a solvating extractant).

The aqueous-phase chemistry of the metal is a critical factor in determining the extent of extraction and selectivity, and is affected by<sup>31</sup>:

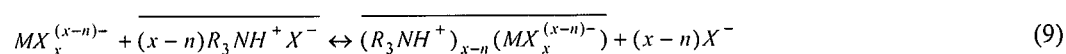
- the nature and concentration of the complexing ion,
- the degree of hydration of the aqueous-phase complexes and
- the relative strength of metal-water and metal-extractant bonds

Stripping of the extracted metal from the organic phase is usually achieved by contacting with an aqueous phase of low concentration of complexing ion, by using a high concentration of an alternate ion that forms a stronger aqueous-phase complex and is more easily extracted or by pH manipulation<sup>31,32</sup>.

### 3.1 Ion-pair extractant: Aliquat 336

The quaternary amine salts  $R^1R^2R^3N^+(CH_3)Cl^-$  (where  $R^1 = R^2 = R^3 = (C_8H_{17} - C_{10}H_{21})$ ), are classified as ion-pair extractants<sup>31</sup>. Aliquat 336 (mixture of octyl and decyl amines, of average molar mass  $442 \text{ g mol}^{-1}$  and density  $0.88 \text{ g cm}^{-3}$ ) is a water-insoluble quaternary ammonium salt supplied predominantly for commercial use in acidic to slightly alkaline conditions<sup>32</sup>. It is used in solvent extraction for the recovery or purification of anionic complexes of cadmium, cobalt, iron, molybdenum, rare earth metals, tungsten, uranium and zinc. Amongst others, Aliquat 336 has been used in waste treatment, as an anti-static agent and for the decolourisation and deodorisation of fermentation broths<sup>32</sup>.

Protonated amines (shown for a tertiary amine in eq. 7) can form an ion pair (eq. 9) with a negatively charged metal species (see eq. 8 where  $M$  is the metal and  $X$  is the anionic species with which the metal complexes) such as a chloride, nitrate, carbonate, thiocyanate, carboxylate or phosphate complex. Loaded organic phases can be stripped by reversing eqs 7 and 9 ( $R$  denotes the hydrocarbon moiety and the overbar represents the species in the organic phase)<sup>31</sup>.

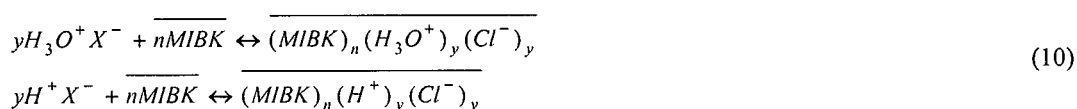


Because of the permanent positive charge on the quaternary ammonium ion, Aliquat 336 can form salts with anions over a wider range of pH than the primary, secondary and tertiary amines and therefore finds application across a

wider range of pH<sup>32</sup>. It has also been shown that, in general, quaternary ammonium reagents are stronger extractants of anionic thiocyanate complexes than primary amines for certain metals<sup>31</sup>. A disadvantage, however, of Aliquat 336 is that it is more difficult to strip than many other amines.

### 3.2 Solvating 'oxonium' extractant: Methyl isobutyl ketone

In solvating extraction, neutral inorganic molecules or complexes are extracted by organic compounds containing electron-donor groups through replacement of the hydrated water molecules with the solvating extractant. The extraction using MIBK, a solvating extractant, is based on the fact that MIBK, as a ketone, is an oxygen donor solvent which can form or stabilise cationic oxonium ions<sup>31</sup>. MIBK in the presence of acid in the aqueous phase ( $H^+X^-$  or  $H_3O^+X^-$ , where  $X^-$  is the anionic species to be extracted) is known to extract the  $H^+X^-$  or  $H_3O^+X^-$  in the form of solvated oxonium and/or hydronium ions:



### 3.3 Application of magnetic fluids for solvent extraction

Conventional practice for the extraction of metal ions from solution using liquid-liquid extraction and an extractant such as Aliquat 336 generally involves the dissolution of the extractant in a suitable hydrocarbon solvent<sup>31, 32, 34</sup>. Although it would be advantageous to use the metal extractant alone (as is usually the case for MIBK), dissolution of the extractant in a solvent may be necessary as the extractants are often highly viscous in a pure state<sup>31</sup> and the diluent may improve the solubility of the extracted complex, reduce the viscosity of the organic phase, minimise solubility and entrainment losses and improve phase separation<sup>34</sup>. Depending on the system, however, the use of a diluent may also result in unfavourable rates of mass transfer or may cause extracted metal complexes to precipitate or separate as a 'third phase'<sup>31</sup>. (Diluent modifiers are often used to prevent this third-phase formation and to prevent the formation of precipitates or emulsions<sup>34</sup>.)

The mass of extractant required is determined by the stoichiometry of the extraction reaction. This extractant is dispersed in a certain volume of diluent with the concentration of the extractant in the diluent possibly limited by certain physical effects such as viscosity, solubility, etc. According to this concentration, the required ratio of the aqueous to the organic phase (phase ratio) can then be established. After extraction, the aqueous phase and organic phase (containing extractant and possibly a diluent) separate by means of gravity. It would be advantageous if this process could be modified to provide a more rapid phase separation.

As mentioned previously, bare magnetic particles have been used in the extraction of various species from wastewater and effluents. It was decided to investigate whether extraction from an aqueous solution would be possible using magnetic particles incorporated into a magnetic liquid. Because of the superparamagnetic property of the magnetic liquid, it was envisaged that it could behave as a liquid during extraction but would be responsive when exposed to a magnetic field allowing for efficient removal of the magnetic liquid phase. In addition, mixing of two liquid phases during extraction should allow for good phase contact and it should be possible to use conventional liquid-liquid extraction equipment or equipment modified such as to utilize the magnetic characteristics of the fluid. As proof of concept, it was decided to investigate the extraction of the cobalt thiocyanate complex from an aqueous solution using a magnetic liquid.

In addition to the extraction by the magnetic liquid itself, it was decided to investigate whether a magnetic liquid could be used as the diluent in a liquid-liquid extraction system using Aliquat 336 and MIBK as the extractants. Aliquat 336 is soluble in kerosene (the magnetic fluid carrier liquid) in the temperature range of interest and kerosene as diluent is ideal because it is commonly used as the carrier liquid in magnetic liquid technology and has also been used traditionally in liquid-liquid extraction<sup>31, 32</sup>. It was envisaged that the magnetic properties of the resultant system could be manipulated for more rapid phase separation after extraction.

Although a magnetic solvent extraction process has been patented, to our knowledge, only preliminary investigations into the extraction of  $\text{Cu}^{2+}$  and  $\text{UO}_2^{2+}$  have been studied thus far using this technique<sup>35, 36</sup>. The patent<sup>35</sup> describes the possible principal of using a magnetic liquid containing an extractant for more rapid phase separation in solvent extraction. Examples are provided of magnetic solvent extractant mixtures prepared using LIX 64N (hydroxy-5-nonylbenzo-phenoneoxime and 5,8-diethyl-7-hydroxydodecan-6-oxime) and LIX-54 (tri-octylphosphine oxide, tri-( $\text{C}_n$ )methylaluminium chloride and tri-( $\text{C}_n$ )amine,  $n = 8 - 10$ ). The case of using the LIX 64N extractant to extract 90 % of the  $\text{Cu}^{2+}$  from a  $9.83 \text{ g l}^{-1} \text{ CuSO}_4 \cdot 5\text{H}_2\text{O}$  solution is discussed. No further references could be found in literature relating to work done in this regard by the inventor (Hwang) or assignee of this patent (Michigan Technological University).

Palyska and Chmielewski<sup>36</sup> investigated the extraction of  $\text{Cu}^{2+}$  from a  $\text{CuSO}_4$  solution ( $10.3 \text{ mg Cu cm}^{-3}$ , pH 4.05) using an 11 % solution of di(2-ethylhexyl) phosphoric acid (D2EHPA) in kerosene and a magnetic liquid consisting of 15 % magnetite and an organic to aqueous phase ratio in the range of 1:1 to 1:2.5. They also investigated the extraction of  $\text{UO}_2^{2+}$  from a  $\text{UO}_2(\text{NO}_3)_2$  solution ( $1.025 \text{ mg U cm}^{-3}$ ) using 8 % tributylphosphate (TBP) in kerosene or magnetic liquid. Little information is given in this paper regarding percentage extraction of the metal ions while an increased magnetic phase separation rate of between 60 and 120 times higher than gravitational separation in the presence of a permanent magnet was observed.

In our application it was proposed that after addition of the Aliquat 336 or MIBK to the magnetic liquid, the extractant would be soluble in the kerosene carrier liquid of the magnetic liquid and the oleic acid surfactant on the

surface of the magnetic particles. It was also envisaged that the oxygen of the MIBK could potentially partition into the hydrophobic shell of the magnetic particle. This concept is illustrated schematically in Fig. 5.

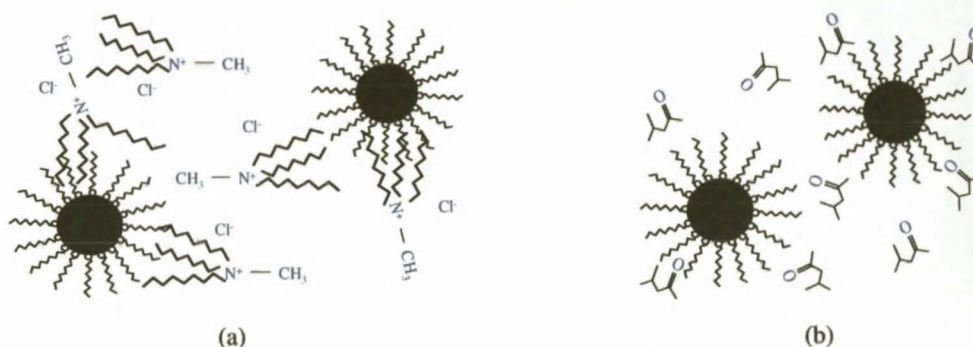


**Figure 5** Envisaged schematic incorporation of the (a) Aliquat 336 and (b) MIBK extractants in a magnetic liquid

An aqueous solution of cobalt sulphate and potassium thiocyanate is pink in colour as a result of the pink octahedral  $[\text{Co}(\text{SCN})_4(\text{H}_2\text{O})_2]^{2-}$  complex which is formed (Fig. 6 (a)). Vogel reported the cobalt (II)-thiocyanate analytical test, in which a bluish colour is obtained upon the addition of acetone to an aqueous solution of cobalt thiocyanate<sup>37</sup>. This colour is accepted to be the tetrahedral species,  $[\text{Co}(\text{SCN})_4]^{2-}$ , which forms as the activity of the water is reduced<sup>38-40</sup> (Fig. 6 (b)). This property lends itself to convenient studies using UV-visible absorbance<sup>41</sup>: measurement of the absorbance spectra before and after addition of the magnetic liquid to an aqueous solution of  $\text{K}_2[\text{Co}(\text{SCN})_4(\text{H}_2\text{O})_2]$  can be used to determine whether adsorption of the  $[\text{Co}(\text{SCN})_4(\text{H}_2\text{O})_2]^{2-}$  has taken place.

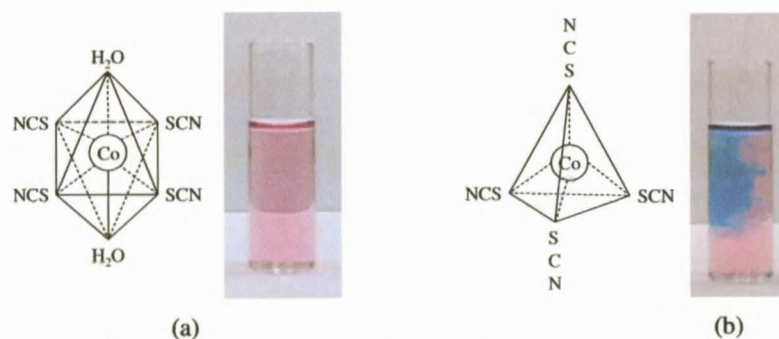


**Figure 6** The structure of the (a) pink octahedral  $[\text{Co}(\text{SCN})_4(\text{H}_2\text{O})_2]^{2-}$  complex in the aqueous phase and (b) blue tetrahedral species  $[\text{Co}(\text{SCN})_4]^{2-}$  in the organic phase (the colour change in the photograph occurs upon addition of acetone to the aqueous  $\text{K}_2[\text{Co}(\text{SCN})_4(\text{H}_2\text{O})_2]$  solution)

Extraction of the cobalt thiocyanate complex was performed using magnetite alone and with magnetic liquid on its own as well as in the presence of Aliquat 336 and MIBK. The extraction by these magnetic organic extractants was compared to that of Aliquat 336 and MIBK in kerosene. The effects of the percentage magnetite, magnetic liquid,

Aliquat 336 and MIBK, the ratio of the organic to aqueous phase during extraction and the kinetics of extraction were investigated in this chapter.

## 4. Experimental

### 4.1 Reagents

All reagents and solvents were purchased from commercial sources and were used without further purification.  $\text{FeCl}_3 \cdot 6\text{H}_2\text{O}$ ,  $\text{FeSO}_4 \cdot 7\text{H}_2\text{O}$  and 25 %  $\text{NH}_4\text{OH}$  (Merck) were used for the precipitation of magnetite. Oleic acid and kerosene were purchased from Fluka and BP, respectively. Kerosene is a mixture of  $\text{C}_{10}$  –  $\text{C}_{16}$  petroleum hydrocarbons, with a density of  $0.78 \text{ g cm}^{-3}$ , boiling range of  $190 - 260 \text{ }^\circ\text{C}$  and containing approximately 60 % n-branched alkanes and up to 35% (but usually  $< 5 \%$ ) aromatics with the remainder consisting of cycloalkanes and alkenes.  $\text{CoSO}_4 \cdot 7\text{H}_2\text{O}$  and KSCN were from B. Owen Jones and Merck, respectively. Ultrapure Milli-Q water ( $\text{MQ} > 18 \text{ M}\Omega$ ) was used for the preparation of aqueous solutions. Aliquat 336 in the chloride form and MIBK were obtained from Aldrich and Merck, respectively.

### 4.2 Synthesis of magnetic liquid

For a typical preparation of approximately 100 ml magnetic liquid, 84 g  $\text{FeCl}_3 \cdot 6\text{H}_2\text{O}$  and 43.2 g  $\text{FeSO}_4 \cdot 7\text{H}_2\text{O}$  were added to 600 ml water. The resultant solution was heated to  $\sim 35 \text{ }^\circ\text{C}$ . 220 ml 25 %  $\text{NH}_4\text{OH}$  was added to the iron solution with rapid agitation. The resultant precipitate was washed via magnetic decantation three times with 600 ml water to remove relics from precipitation such as chlorides that may result in a low quality magnetic fluid with increased viscosity<sup>19</sup>. 600 ml water and 10 ml 25 %  $\text{NH}_4\text{OH}$  were added to the precipitate, followed by a 10 ml oleic acid/80 ml kerosene mixture. The mixture was stirred and heated to  $90 \text{ }^\circ\text{C}$ . The final organic magnetic liquid was separated by magnetic decantation from the aqueous phase and washed with water to a pH of 7 – 8. A final wash with distilled water was performed. The volumetric packing fraction of the magnetite in the concentrated fluid was 0.1, i.e., 10 % magnetite by volume or  $0.52 \text{ g magnetite cm}^{-3}$  concentrated fluid. The magnetic liquid was centrifuged at 4200 rpm for 30 minutes for the removal of agglomerates and diluted from the original density ( $\sim 1.3 \text{ g cm}^{-3}$ ) to  $0.9 \text{ g cm}^{-3}$  by the addition of kerosene except where otherwise stated.

Magnetic liquid samples consisting of 0, 17, 33, 50, 67, 83 and 100 % concentrated magnetic liquid were prepared by the addition of kerosene to the synthesised concentrated magnetic liquid (density  $\sim 1.3 \text{ g cm}^{-3}$ ).

#### 4.3 Preparation of Aliquat 336 extractant mixtures

Stock solutions of 1, 3, 5, 8, 10, 14, 18 and 25 % (by volume) kerosene-Aliquat 336 (**KA**) and magnetic liquid-Aliquat 336 (**MA**) mixtures were prepared by the addition and mixing of the required mass of Aliquat 336 to the required volume of kerosene or magnetic liquid, respectively. (Owing to the viscosity of the Aliquat 336, the required amounts of Aliquat 336 were measured out by mass.) The magnetic liquid was diluted to  $0.9 \text{ g cm}^{-3}$  by the addition of kerosene to more closely approximate the Aliquat 336 density ( $0.884 \text{ g cm}^{-3}$ ).

#### 4.4 Preparation of MIBK extractant mixtures

Concentrations of greater than 50 % MIBK in magnetic liquid (by volume) resulted in the magnetic liquid becoming unstable as shown by the precipitation of magnetite and phase separation of the MIBK and magnetic liquid. For the extraction test work, mixtures of MIBK in magnetic liquid in concentrations of 1, 2, 3, 4, 5, 6, 7, 8, 9, 10, 20, 30, 40 and 50 % (by volume) were prepared.

#### 4.5 Experimental procedure and analytical methods

A solution of  $\text{CoSO}_4 \cdot 7\text{H}_2\text{O}$  (Co(II) concentration of  $17 \text{ mmol l}^{-1}$ ) and 20 times excess KSCN was prepared in deionised water. Triplicates were prepared for all extraction test samples. After addition of the organic phase, samples were sealed and agitated on a Labcon horizontal shaker. The aqueous phase was removed using Pasteur pipettes for measurement of the UV-visible absorbance spectra using a GBC UV-visible Cintra 10e Spectrometer. A wavelength scan from 400 to 700 nm at  $200 \text{ nm min}^{-1}$  ( $0.4 \text{ nm}$  step size and  $1.5 \text{ nm}$  slit width) was performed. The maximum absorbance at 512.3 nm was used to calculate the percentage extraction. The average absorbance and unbiased standard deviation of the triplicates was calculated and the percentage extraction determined as a function of the original  $\text{K}_2[\text{Co}(\text{SCN})_4(\text{H}_2\text{O})_2]$  concentration. A NdFeB magnet was used to separate the magnetic phase (when present) from the aqueous phase.

To determine the extraction of the  $[\text{Co}(\text{SCN})_4]^{2-}$  by magnetite, 0 to 1.5 g magnetite in increments of 0.3 g were added to 10 ml of the  $\text{K}_2[\text{Co}(\text{SCN})_4(\text{H}_2\text{O})_2]$  solution in a glass polytop. The samples were agitated overnight at 110 rpm before measuring the UV-visible absorbance spectra. Extractions were remeasured at day 5, 20 and 44. Agitation was discontinued after 5 days.

For the extraction by different concentrations of magnetic liquid, 3 ml of 0 – 100 % concentrated magnetic liquid was added to 10 ml of the  $\text{K}_2[\text{Co}(\text{SCN})_4(\text{H}_2\text{O})_2]$  solution in a glass polytop. The agitation time (at 80 rpm) was 5 hours. The samples remained standing for 48 hours before measurements were made. For kinetics studies, 3 ml magnetic liquid was added to 10 ml aqueous solution and the extraction determined at 30 min, 1 h, 2 h, 5 h, 22.5 h and 120 h and at 80 and 110 rpm shaker speeds.

To determine the effect of the percentage Aliquat 336 on the extraction of the  $[\text{Co}(\text{SCN})_4]^{2-}$ , 3 ml of 1 – 25 % kerosene-Aliquat 336 (KA) and magnetic liquid-Aliquat 336 (MA) were added to 15 ml of the  $\text{CoSO}_4 \cdot 7\text{H}_2\text{O}/\text{KSCN}$  solution in a glass polytop. The agitation time (at 110 rpm) was 10 minutes. The extraction of the  $[\text{Co}(\text{SCN})_4]^{2-}$  by the magnetic liquid/MIBK mixture was determined by adding 3 ml of the MIBK-magnetic liquid mixture in a range of concentrations from 0 to 50 % MIBK in magnetic liquid to 10 ml of the  $\text{CoSO}_4 \cdot 7\text{H}_2\text{O}/\text{KSCN}$  solution in a glass polytop. For the initial extraction experiments, single samples were prepared. The agitation time (at 80 rpm) was 15 hours.

## 5. Results and discussion

### 5.1 Extraction of $[\text{Co}(\text{SCN})_4]^{2-}$ by magnetite

The extent of extraction of  $[\text{Co}(\text{SCN})_4]^{2-}$  from the  $17 \text{ mmol l}^{-1}$  Co(II) aqueous solution as a function of the mass of bare magnetite over 44 days is shown in Figure 7. There does not appear to be a significant increase in percentage extraction with an increase in time.

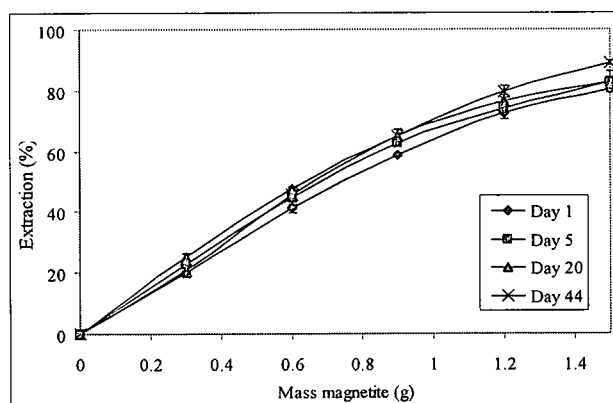


**Figure 7** Percentage extraction of  $[\text{Co}(\text{SCN})_4]^{2-}$  by bare magnetite as a function of the mass of magnetite

The percentage Co(II) extraction increases with mass of magnetite and is thought to result from interaction of the anionic species with the magnetite surface hydroxyl groups. In an aqueous environment, magnetite surface hydroxyl groups that arise from adsorption of water may be coordinated to between one and three surface iron atoms or may be attached geminally<sup>30</sup> as shown in Fig. 8. It is claimed that magnetite has a density of 5 hydroxyl groups per square nanometre<sup>30</sup>.

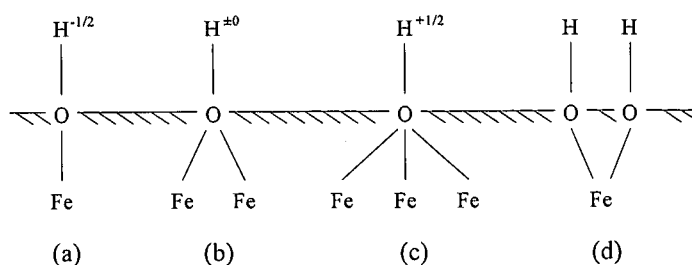


**Figure 8** (a) Singly, (b) doubly, (c) triply coordinated and (d) geminal surface hydroxyl groups proposed on iron oxides<sup>30</sup>

The hydroxyl group electron lone pairs and dissociable hydrogen atom allows it to act amphoterically<sup>30</sup>. The charge on the oxide surface is established by the dissociation or ionisation of surface hydroxyl groups. This corresponds to the adsorption or desorption of protons depending on the pH of the solution and can be represented by the following dissociation reactions<sup>1,30</sup>:

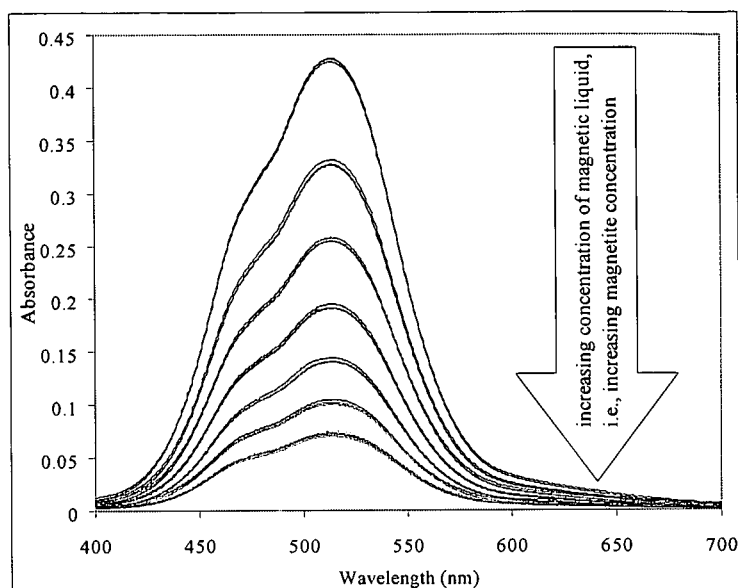


A range of PZC values varying from 6 to 8.2 has been reported for magnetite<sup>42-46</sup>. At a pH lower than the magnetite PZC, the  $\text{FeOH}_2^+$  groups predominate. At a pH greater than the PZC, the  $\text{FeO}^-$  groups predominate. When the pH equals the PZC, the number of  $\text{FeOH}_2^+$  groups equals the number of  $\text{FeO}^-$  groups<sup>30</sup>. The pH of the  $\text{CoSO}_4 \cdot 7\text{H}_2\text{O}/\text{KSCN}$  solution used here was approximately 6. At this pH, it is suspected that the magnetite surface is protonated to a certain extent and the  $\text{FeOH}_2^+$  groups should predominate<sup>30</sup> allowing for extraction of the anionic  $[\text{Co}(\text{SCN})_4]^{2-}$  by simple ion pairing.

Theoretically it would be expected that the extraction would increase with the increase in mass of magnetite. It is proposed that hindered mixing with increase in magnetite mass and possible agglomeration of particles may occur thereby limiting the exposed surface area and decreasing the  $[\text{Co}(\text{SCN})_4]^{2-}$  extraction.

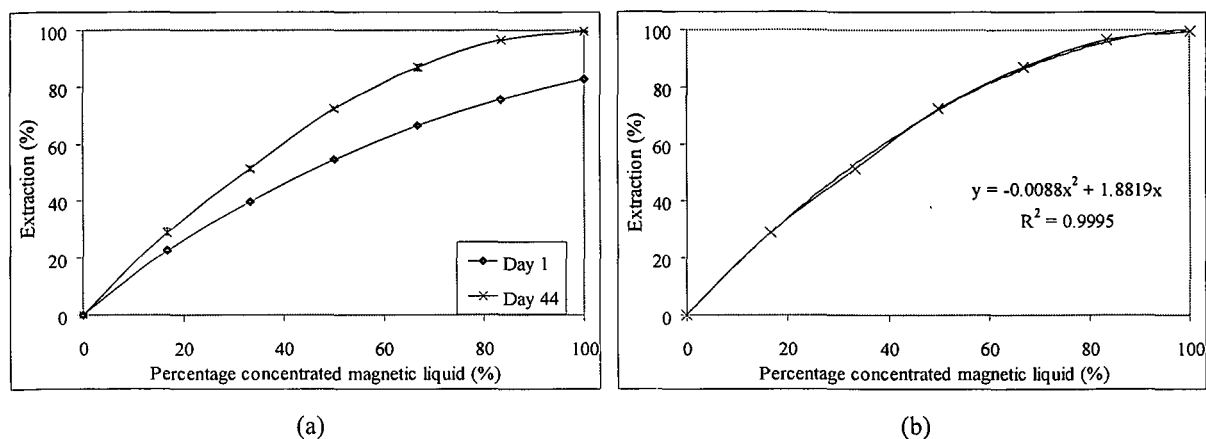
### 5.2 Extraction of $[\text{Co}(\text{SCN})_4]^{2-}$ by magnetic liquid

Fig. 9 gives an example of the absorbance spectra measured for increasing magnetic liquid concentrations for the magnetic liquid extraction tests with super-imposed lines indicating replicate tests. The change in absorbance with change in magnetite concentration allows for the calculation of percentage extraction of  $[\text{Co}(\text{SCN})_4]^{2-}$ . During test work, it was observed that the magnetic phase is immediately attracted towards the magnet allowing for rapid phase separation and easy removal of the underlying aqueous phase for absorbance measurements.



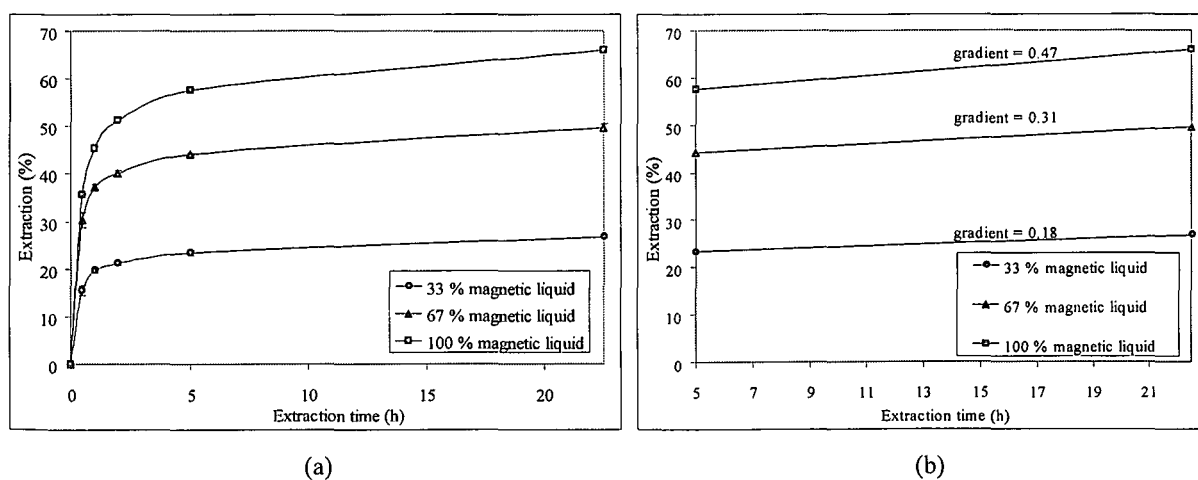
**Figure 9** Example of typical absorbance spectra obtained for the magnetic liquid extraction tests

Fig. 10 (a) shows the percentage extraction of  $[\text{Co}(\text{SCN})_4]^{2-}$  on day 1 and that after 44 days as a function of the percentage concentrated magnetic liquid (where the concentrated magnetic liquid has a volumetric packing fraction of 10 % magnetite in organic carrier liquid). Fig. 10 (b) shows a second-order polynomial regression curve fitted to the 44-day extraction data. The extraction per gram of magnetite decreases as the percentage concentrated magnetic liquid increases. It is suspected that the higher packing fraction in the more concentrated fluids may hinder contact between the magnetite and the  $[\text{Co}(\text{SCN})_4]^{2-}$  in the aqueous phase as compared to the more dilute fluids: the magnetic particles in the more concentrated magnetic liquid may not all be exposed equally to the anions in solution during phase contact. A ratio of approximately 40 times molar excess magnetite to cobalt is required for 100 % extraction (approximately 155 g magnetite/g Co). It must be noted that the oleic acid surfactant which coordinates to the iron oxide surface results in a lowering<sup>9</sup> of the PZC to approximately 4.5 (as compared to the bare magnetite PZC which varies from 6 to 8.2<sup>42-46</sup>). This implies that the  $\text{FeO}^-$  groups should dominate. However, even with a dominance of  $\text{FeO}^-$  groups, there are still very likely  $\text{FeOH}_2^+$  groups available for adsorption of the  $[\text{Co}(\text{SCN})_4]^{2-}$  anions<sup>30</sup> (and in fact it is seen that this is so as the magnetic liquid is still capable of anion extraction). (pH conditions lower than the  $\text{K}_2[\text{Co}(\text{SCN})_4(\text{H}_2\text{O})_2]$  solution pH (~6) were not investigated owing to the magnetite's poor resistance to acidic media<sup>47</sup>.)



**Figure 10** (a) Percentage extraction of  $[\text{Co}(\text{SCN})_4]^{2-}$  as a function of percentage concentrated magnetic liquid in the organic extractant volume and (b) with regression curve fitted to the extraction data after 44 days

Relative extraction kinetics determined using magnetic liquids of concentrations 33, 67 and 100 % concentrated magnetic liquid diluted with kerosene (densities 0.9, 1.1 and 1.3 g cm<sup>-3</sup>, respectively), showed that the higher the concentration of magnetic liquid, the higher the percentage  $[\text{Co}(\text{SCN})_4]^{2-}$  extraction (Fig. 11 (a)). Adsorption of anions onto iron oxides is usually thought to be a two-step process. In the first stage, there is rapid attachment of the species to the surface limited mainly by the diffusion to the surface. The second stage is limited by diffusion into particle aggregates or crystal nanopores and structural rearrangement of the surface complexes<sup>30</sup>. This possibly explains the rapid initial extraction by the magnetic liquid followed by a further slow and gradual adsorption of species and therefore slightly increased extraction percentage with time. There is an increase of only 5 % extraction over the next 10 days. (Desorption of anions from the surface with a change of anion concentration in solution may be slow for two reasons: multidentate surface complexes which desorb less easily may form and adsorbed ions may diffuse slowly out of the nanopores<sup>30</sup>.)



**Figure 11** (a) Extraction kinetics for the extraction of  $[\text{Co}(\text{SCN})_4]^{2-}$  using magnetic liquids of different concentrations and (b) gradients (determined between 5 and 22.5 hours) of extraction kinetics curves

It appears from the gradients for the extraction kinetics curves (Fig. 11 (b), determined between 5 and 22.5 hours) that the lower the concentration of magnetic liquid, the lower the gradient of extraction. This may imply that maximum extraction is reached soonest by the magnetic liquids of lower magnetite concentrations (although the final percentage extraction is lower owing to the lower amount of magnetite present). Again it is suspected that the magnetite in the more concentrated hydrocarbon fluids may not come into contact as easily with the cobalt thiocyanate anions in the aqueous phase as may occur for the more dilute fluids (where magnetite is more dispersed in the hydrocarbon phase and may more easily come into contact with the anions in the aqueous phase). Although the extraction by the 33, 67 and 100 % concentrated magnetic liquid in Fig. 10 is slightly higher as compared to that in Fig. 11, this reflects a difference of  $[\text{Co}(\text{SCN})_4]^{2-}$  extraction of less than  $\sim 0.04$  mmol and is most likely caused by slight variations in dilutions of the magnetic liquid.

A higher shaker speed appears to provide for an improved phase contact between the aqueous cobalt solution and the magnetic liquid, resulting in a higher overall percentage  $[\text{Co}(\text{SCN})_4]^{2-}$  extraction (Fig. 12) within the time investigated. An increase in shaker speed from 80 to 110 rpm led to an 8 % increase in extraction after 30 minutes and remained at 4 – 5 % higher extraction for the duration of the measuring period.

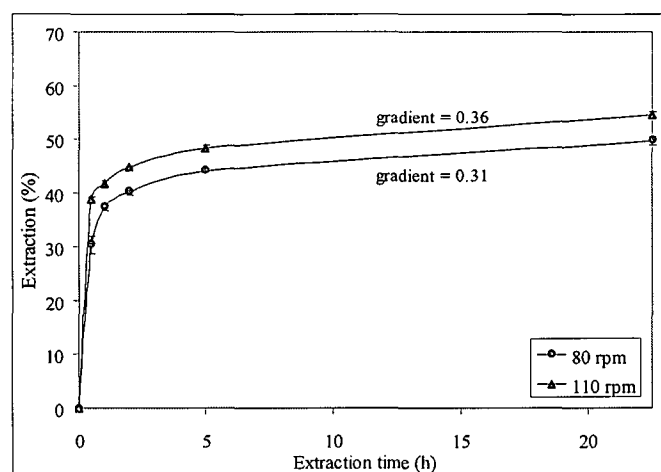


**Figure 12** Percentage extraction of  $[\text{Co}(\text{SCN})_4]^{2-}$  by 25 % concentrated magnetic liquid as a function of shaker speed

### 5.3 Extraction of $[\text{Co}(\text{SCN})_4]^{2-}$ by a mixture of Aliquat 336 in magnetic liquid or kerosene

Because of its permanent positive charge, the quaternary ammonium ion of Aliquat 336 does not have to undergo the protonation reaction as discussed for basic or ion-exchange extractants (eq. 8). During extraction, the anionic cobalt thiocyanate species and the cationic Aliquat 336 species would react as follows where  $R$  is  $\text{C}_8\text{H}_{17} - \text{C}_{10}\text{H}_{21}$  (the overbar again indicates species in the organic phase):

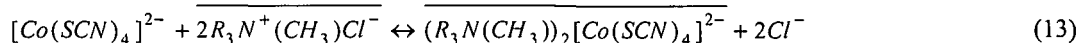
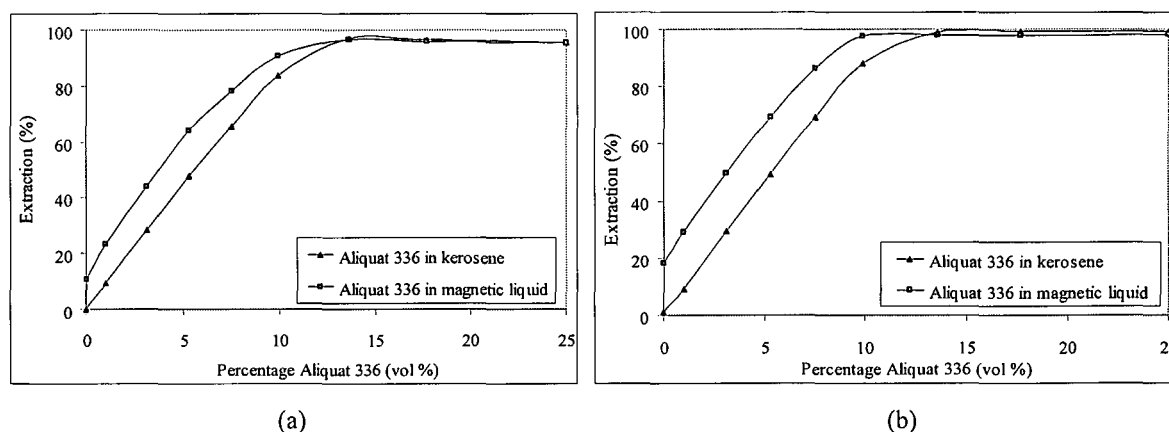
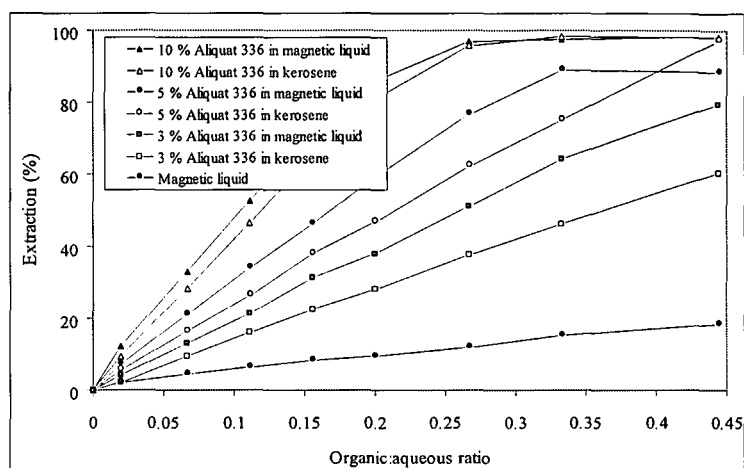


Fig. 13 (a) shows the percentage extraction of  $[\text{Co}(\text{SCN})_4]^{2-}$  after 10 minutes and that after 50 days (Fig. 13 (b)) as a function of the increasing percentage Aliquat 336 in the kerosene-Aliquat 336 (KA) and magnetic liquid-Aliquat 336 (MA) mixtures. There was no mixing of the samples after the initial extractions were determined and the samples were kept in the dark. (Error bars have been excluded for clarity. The maximum unbiased standard deviation obtained for the experiments was 2 %.) The percentage extraction of  $[\text{Co}(\text{SCN})_4]^{2-}$  increases with an increase in the percentage Aliquat 336 for both the KA and MA mixtures. The MA mixture exhibits a consistently higher extraction (of approximately 8 %) than the KA mixtures for the same percentage Aliquat 336 up to ~14 % Aliquat 336. From this point onwards, the extraction is approximately equal. The higher extraction by the magnetic liquid is as a result of the extraction of the  $[\text{Co}(\text{SCN})_4]^{2-}$  by the magnetite by simple ion pairing. (It can be seen that at 0 % Aliquat 336, between 8 to 19 %  $[\text{Co}(\text{SCN})_4]^{2-}$ , see Figs 13 (a) and (b), respectively, is extracted by the MA mixture.) The molar excess for the MA mixture according to the reaction stoichiometry (eq. 13) is 2.5 as compared to 3.5 required for the KA mixture. There is a slight increase in  $[\text{Co}(\text{SCN})_4]^{2-}$  extraction after 50 days owing to additional adsorption of  $[\text{Co}(\text{SCN})_4]^{2-}$  onto the magnetite surface.



**Figure 13** (a) Percentage extraction of  $[\text{Co}(\text{SCN})_4]^{2-}$  after 10 minutes and (b) extraction after 50 days as a function of percentage Aliquat 336 in kerosene (KA) or magnetic liquid (MA)

The effect of the ratio of organic extractant to the aqueous phase was investigated by varying the volume of organic extractant used relative to the aqueous fraction. Fig. 14 shows the percentage extraction as a function of the total volume of organic extractant using 3, 5 and 10 % (by volume) Aliquat 336 KA and MA mixtures. (For clarity, error bars are again not indicated on the graphs. The maximum unbiased standard deviation obtained for the experiments was 5 %.)



**Figure 14** Percentage extraction of  $[\text{Co}(\text{SCN})_4]^{2-}$  as a function of the total volume of organic extractant for the 3, 5 and 10 % KA and MA mixtures and bare magnetic liquid

As seen previously and as expected, the percentage extraction of  $[\text{Co}(\text{SCN})_4]^{2-}$  increases as the percentage Aliquat 336 (and total organic volume) in the mixture increases. However, for 50 %  $[\text{Co}(\text{SCN})_4]^{2-}$  extraction after 10 minutes, approximately one times molar excess of Aliquat 336 relative to  $[\text{Co}(\text{SCN})_4]^{2-}$  is required for the 3, 5 and 10 % MA samples. This is in comparison to an approximate molar excess of 1.5 required for the equivalent KA samples. A lower volume of Aliquat 336 would therefore be required to effect the same extent of extraction when incorporated into a magnetic liquid as opposed to a diluent such as kerosene. The UV absorbance of these samples remeasured after 50 days (with no mixing of the samples over this period of time and with the samples kept in the dark) showed an increase in extraction of  $[\text{Co}(\text{SCN})_4]^{2-}$  by up to 11 %. Again, this is probably as a result of kinetic effects owing to the diffusion of species into nanopores<sup>30</sup>. The slight variation in percentage  $[\text{Co}(\text{SCN})_4]^{2-}$  extraction in Figs 13 and 14 is most likely caused by small variations in composition of the KA and MA mixtures prepared for these studies.

A 1 and 5 % MA mixture and bare magnetic liquid used to determine extraction kinetics showed that  $[\text{Co}(\text{SCN})_4]^{2-}$  extraction is rapid with an increase of only 5 % extraction over a further 12 days (Fig. 15).

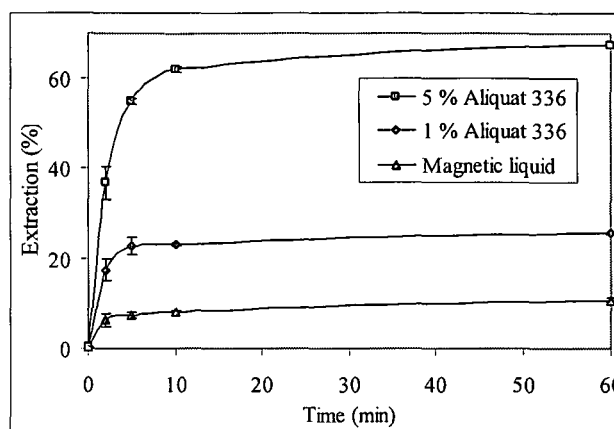


**Figure 15** Extraction kinetics for the extraction of  $[\text{Co}(\text{SCN})_4]^{2-}$  by 1 and 5 % MA mixture and by magnetic liquid without Aliquat 336

Over a 20-day period tested and over the range of percentages of Aliquat 336 in magnetic liquid tested (2, 5, 10, 15, 20 to 50 %), with the exception of the 50 % Aliquat 336 mixture, it was found that the fluids were stable under the influence of gravity. No precipitation of agglomerates of magnetic particles or phase separation of the Aliquat 336 and magnetic liquid was observed. It is important, however, to be aware of the potential effect of a magnetic field on an MA mixture. On occasion it was observed that after extraction and under the influence of a magnetic field, some of the blue-coloured cobalt-Aliquat 336 complex leached out of the magnetic liquids. This was usually observed for the liquids with higher volumes of Aliquat 336. (This blue third-phase was also observed in the KA mixtures after extraction and has been reported to occur in industry<sup>31</sup>.) The apparent density of the magnetic liquid is varied by changing the magnetic field gradient to which the fluid is exposed<sup>48</sup>. This in turn could cause the separation, as a result of the density differential, of the Aliquat 336 and magnetic liquid phases (although it is more likely that the third-phase formation is an intrinsic property of the system owing to the comparative stabilisation of the extracted species in both the organic and aqueous phases as it was observed for the KA extractions as well). An advantage of the resultant separation of the loaded Aliquat 336 extractant (third-phase) and the magnetic liquid is that it offers the potential for the removal of the loaded Aliquat 336 and reuse of the magnetic liquid. There would, however, still be a need to strip the magnetic liquid.

#### 5.4 Extraction of $[\text{Co}(\text{SCN})_4]^{2-}$ by a mixture of methyl isobutyl ketone in magnetic liquid or kerosene

The extraction by magnetic liquid and by MIBK alone compared to that by the MIBK in magnetic liquid or kerosene is shown in Fig. 16. (When MIBK was incorporated into the kerosene or magnetic liquid, the total organic volume was 3 ml. The curve for the magnetic liquid was obtained using 3 ml of the magnetic liquid with no MIBK and is included on the graph for comparison with the results obtained using MIBK.)

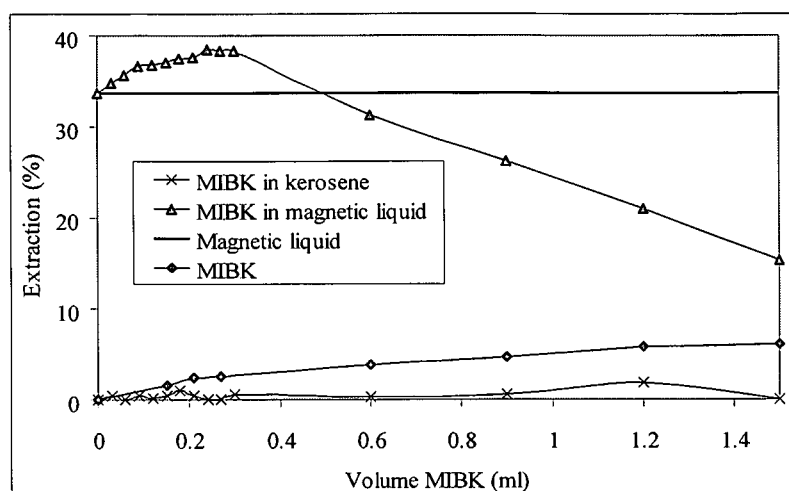
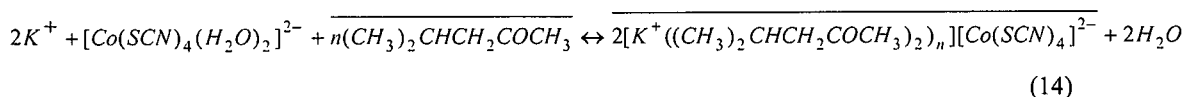


**Figure 16** Percentage extraction of  $[\text{Co}(\text{SCN})_4]^{2-}$  as a function of percentage MIBK in kerosene and magnetic liquid as compared to the extraction by pure MIBK and magnetic liquid

Although it is possible to extract  $[\text{Co}(\text{SCN})_4]^{2-}$  using pure MIBK<sup>39</sup>, it can be seen from Fig. 16 that MIBK would not be the ideal extractant for this system with relatively high aqueous solution pH (~6). Under these conditions, very little  $[\text{Co}(\text{SCN})_4]^{2-}$  is extracted, probably because of the lack of an appropriately solvatable cation ( $\text{K}^+$  is present as opposed to, for example, having  $\text{H}^+$  or  $\text{H}_3\text{O}^+$  ions available in acidic media). In the absence of acid, MIBK presumably forms solvated cations, e.g.,  $[\text{K}^+(\text{CH}_3)_2\text{CHCH}_2\text{COCH}_3]_n$  which in turn form stable ion pairs with the tetrahedral blue  $[\text{Co}(\text{SCN})_4]^{2-}$  and the extraction of the anionic cobalt thiocyanate species by MIBK is therefore thought to proceed according to:



More than 70 times molar excess of MIBK to Co(II) results in a percentage extraction of  $[\text{Co}(\text{SCN})_4]^{2-}$  of only 6%. Furthermore, it was also found that the miscibility of the relatively polar MIBK and the non-polar kerosene was poor. The MIBK in magnetic liquid yielded significantly improved extraction with no evidence of the third phase formation as experienced with the Aliquat 336/magnetic liquid system. (The polarity of the kerosene phase is increased in the magnetic fluid as a result of the polar oleic acid thereby improving the MIBK/magnetic liquid miscibility.) It is likely, however, that the total observed  $[\text{Co}(\text{SCN})_4]^{2-}$  extraction is due mainly to the extraction by the magnetic liquid itself. An increase in percentage  $[\text{Co}(\text{SCN})_4]^{2-}$  extraction is observed as the MIBK is increased to approximately 10% in magnetic liquid. At higher percentages, a decrease in the extraction is observed. It is possible that at higher percentages of MIBK, the polar MIBK interacts with the magnetite particle surface thereby limiting the extraction of the  $[\text{Co}(\text{SCN})_4]^{2-}$  and destabilising the magnetic liquid.

As a result of the poor extractability of  $[\text{Co}(\text{SCN})_4]^{2-}$  by this system, it was decided to test a different approach in the extraction setup and to use the MIBK as extractant without first mixing it in the magnetic liquid as diluent. The magnetic liquid would then be added as a scavenger for removal of any cobalt-loaded MIBK from the aqueous solution. The volume of magnetic liquid added was such that the concentration of MIBK in the final total organic phase was 8 %. (This value was selected because maximum extraction was obtained with 8 % MIBK in magnetic liquid, see Fig. 16.)

Using this new approach, it was found that the extraction after 15 hours by the pure MIBK was less than 10 %  $[\text{Co}(\text{SCN})_4]^{2-}$ . (Again, this low percentage extraction is most likely as a result of the lack of solvatable  $\text{H}^+$  ions available in the relatively high pH solution.) The magnetic liquid was then added for the removal of the MIBK using a magnetic field. The magnetic liquid was also able to remove some of the anionic  $[\text{Co}(\text{SCN})_4]^{2-}$  complex via the protonated magnetite surface sites resulting in an increase in extraction to over 70 % (see Fig. 17 showing the extraction of  $[\text{Co}(\text{SCN})_4]^{2-}$  as a function of the total organic volume (MIBK and magnetic liquid) added).

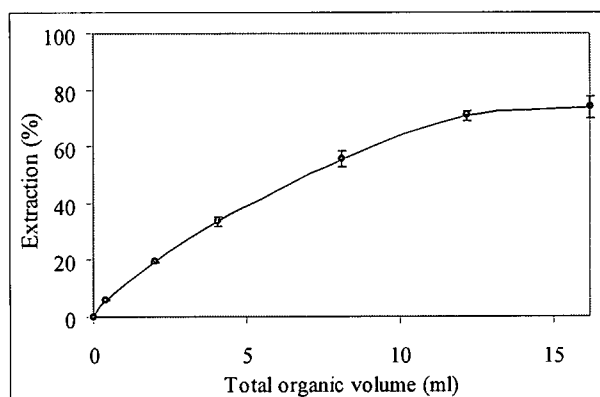


**Figure 17** Percentage extraction of  $[\text{Co}(\text{SCN})_4]^{2-}$  using the extractant-scavenger approach where magnetic liquid is used to remove the MIBK extractant after preliminary extraction by the MIBK alone

## 6. Conclusions

It has been shown as proof of principle that essentially quantitative rapid extraction of the  $[\text{Co}(\text{SCN})_4]^{2-}$  complex (from an aqueous  $[\text{Co}(\text{SCN})_4(\text{H}_2\text{O})_2]^{2-}$  solution) into the organic phase is possible using three systems consisting of magnetite, magnetic liquid and an Aliquat 336/magnetic liquid mixture. The percentage  $[\text{Co}(\text{SCN})_4]^{2-}$  extraction increases with an increase in volume of magnetite, magnetic liquid or percentage Aliquat 336 in magnetic liquid. Forty times molar excess of magnetite (in magnetic liquid) to cobalt is required for 100 % extraction of  $[\text{Co}(\text{SCN})_4]^{2-}$ . From the extraction studies, a 1 – 2.5 times molar excess of Aliquat 336 to cobalt is required for extraction of the  $[\text{Co}(\text{SCN})_4]^{2-}$  by the magnetic liquid system as compared to the 1.5 – 3.5 times molar excess

required by the conventional extractant systems. The lower volume of Aliquat 336 required for the magnetic system is as a result of the extraction of the  $[\text{Co}(\text{SCN})_4]^{2-}$  by the magnetite in the magnetic liquid by simple ion pairing. This could be advantageous in an industrial application where, for example, the extraction of 100 kg of Co(II) would require 740 litres less Aliquat 336 in a magnetic liquid than in kerosene. [For laboratory applications, the synthesis cost of magnetic liquid at  $\sim \$1.50 - 7 \text{ l}^{-1}$  (depending on raw material source) is lower than the cost price of Aliquat 336 at  $\sim \$115 \text{ l}^{-1}$ . However, the cost of these products would have to be evaluated on a commercial scale where raw materials could be purchased in bulk.]

Preliminary extraction tests comparing MIBK in kerosene and magnetic liquid showed poor extraction and liquid instabilities, respectively. The extent of extraction may have been limited owing to the lack of an easily solvatable cation and poor miscibility of the MIBK in the non-polar kerosene. The method of extraction was modified such that preliminary extraction took place by pure MIBK without addition of a diluent. The magnetic liquid was then added as an MIBK scavenger and  $[\text{Co}(\text{SCN})_4]^{2-}$  extractant. Although it is unlikely that such a system would be used in practice, the MIBK investigations highlight the potential for use of a magnetic liquid as a scavenger of solvent extractants or other hydrocarbons.

Results from these preliminary model systems allow for further work using magnetic liquids in solvent extraction in Chapter 5.

## References

1. Broomberg, J.; Gélinas, S.; Finch, J. A.; Xu, Z., *Magnetic and Electrical Separation* 1999, **9**, 169.
2. Bolto, B. A.; Pawlowski, L., *Wastewater treatment by ion-exchange* E. & F. N. Spon Ltd, London, 1987.
3. Häfeli, U. O., *Int. J. Pharm.* 2004, **277**, 19.
4. Willard, M. A.; Kurihara, L. K.; Carpenter, E. E.; Calvin, S.; Harris, V. G., *Encycl. Nanosci. Nanotech.* 2004, **1**, 815.
5. Leslie-Pelecky, D. L.; Rieke, R. D., *Chem. Mater.* 1996, **8**, 1770.
6. Sjögren, C. E.; Johansson, C.; Naevestad, A.; Sontum, P. C.; Briley-Saebo, K.; Fahlvik, A. K., *Magnetic Resonance Imaging* 1997, **15**, 55.
7. de Latour, C., *J. Am. Water Works Assoc.* 1976, **68**, 443.
8. Terashima, Y.; Ozaki, H.; Sekine, M., *Wat. Res.* 1986, **20**, 537.
9. Parsonage, P., *Trans. Inst. Min. Metall. Sect. C: Mineral Process. Extr. Metal.* 1984, **93**, C37.
10. Kolarik, L. O., *Wat. Res.* 1982, **17**, 141.
11. Chen, W. Y.; Anderson, P. R.; Holsen, T. M., *Research Journal WPCF* 1991, **63**, 958.
12. Anderson, N. J.; Bolto, B. A.; Eldridge, R. J.; Kolarik, L. O.; Swinton, E. A., *Wat. Res.* 1982, **20**, 537.
13. Bolto, B. A.; Dixon, D. R.; Swinton, E. A.; Weiss, D. E., *J. Chem. Tech. Biotechnol.* 1979, **29**, 325.
14. Anderson, N. J.; Kolarik, L. O.; Swinton, E. A.; Weiss, D., *Wat. Res.* 1980, **14**, 967.
15. Bolto, B. A., *J. Macromol. Sci. Chem. A* 1980, **14**, 107.
16. Gélinas, S.; Finch, J. A.; Vreugdenhill, A. J., *Int. J. Miner. Process* 2000, **59**, 1.
17. Homg, H. E., *J. Phys. Chem. Solids* 2001, **62**, 1749.
18. Rosensweig, R. E., *Ferrohydrodynamics*. Cambridge University Press, Cambridge, 1985.
19. Khalafalla, S. E.; Reimers, G. W.; Rholl, S. A., US Patent 4 208 294, 1980.
20. Buske, N.; Sonntag, H.; Götze, T., *Colloids Surf.* 1984, **12**, 195.
21. Chantrell, R. W.; Popplewell, J.; Charles, S. W., *IEEE Transactions on Magnetics* 1978, **Mag-14**, 975.

22. Charles, S. W.; Popplewell, J., *Ferromagnetic liquids, ferromagnetic materials: a handbook on the properties of magnetically ordered substances* North-Holland Publishing Company, Amsterdam, 1980.
23. Farkas, J., *Sep. Sci. Technol.* 1983, **18**, 787.
24. Charles, S. W.; Popplewell, J., *IEEE Transactions on Magnetics* 1980, **Mag-16**, 172.
25. Bönnemann, H.; Nagabhushana, K. S., *Encycl. Nanosci. Nanotech.* 2004, **1**, 777.
26. Hilgendorff, M., *Encycl. Nanosci. Nanotech.* 2004, **1**, 213.
27. Lefebure, S.; Dubois, E.; Cabuil, V.; Neveu, S.; Massart, R., 1998, **13**, 2975.
28. Matusevich, N. P.; Orlov, L. P.; Samoilov, V. B.; Fertman, V. E., *Heat Transfer - Soviet Research* 1987, **19**, 25.
29. Reimers, G. W.; Khalafalla, S. E., US Patent 3 843 540, 1973.
30. Cornell, R. M.; Schwertmann, U., *The iron oxides* VCH Publishers, New York, 1996.
31. Cox, M., *Liquid-liquid extraction* Ullmann's Encyclopedia of Industrial Chemistry 1988, **B3**, 6-43.
32. Cognis Corporation, Ion Transfer Technology Aliquat@336, [www.cognis.com](http://www.cognis.com).
33. Cognis Corporation Mining Chemicals Technology Division, *MCT Redbook, Solvent extraction using Cognis Corporation liquid ion exchange reagents*.
34. Kunin, R.; Winger, A. G., *Angew. Chem. Internat. Edit* 1962, **1**, 149.
35. Hwang, J. Y., US Patent 5 043 070, 1991.
36. Palyska, W.; Chmielewski, A. G., *Sep. Sci. Technol.* 1993, **28**, 127.
37. Vogel, H. W., *Ber.* 1979, **12**, 2313.
38. Velloso, N. C. F.; Neves, E. A. G., I. G. R., *Polyhedron* 1985, **4**, 2043.
39. Pyatnitskii, I. V., *Analytical chemistry of cobalt*. Academy of Sciences of the USSR, Vernadskii Institute of Geochemistry and Analytical Chemistry, Israel, 1966.
40. Brackenbury, K. F. G., MSc dissertation, University of Cape Town, 1987.
41. Irving, H. M. N. H.; Al-Jarrah, R. H., *Anal. Chim. Acta* 1973, **63**, 79.
42. Milonjic, S. K.; Kopenci, M. M.; Ilic, Z. E., *J. Radioanal. Chem.* 1983, **78**, 15.
43. Kosmulski, M., *J. Colloid Interface Sci.* 2004, **275**, 214.
44. Ito, S.; Sumi, S., *Tohoku Kogyo Gijutsu Shikensho Hokoku* 1985, **18**, 1.
45. Sun, Z.-X.; Su, F.-W.; Forsling, W.; Samskog, P.-O., *J. Colloid Interface Sci.* 1998, **197**, 151.
46. Wesolowski, D. J.; Machesky, M. L.; Palmer, D. A.; Anovitz, L. M., *Chem. Geol.* 2000, **167**, 193.
47. Pourbaix, M., *Atlas of electrochemical equilibria in aqueous solutions* Pergamon Press Ltd., Oxford, 1966.
48. Svoboda, J., *Magnetic Techniques for the Treatment of Materials* Kluwer Academic Publishers, Dordrecht, 2004.

## Chapter 5\*

### Sterically stabilised magnetic nanoparticle liquids for magnetically assisted base metal solvent extraction

---

#### Abstract

In solvent extraction, the rate of separation of the organic/aqueous phase after phase contact directly affects throughput time in a system especially on a large commercial scale. We here investigate the use of magnetic particles to improve the rate of phase separation after solvent extraction by comparison of a conventional solvent extraction system with a system, in which a commercially available liquid organic extractant (Cyanex 272, D2EHPA and LIX 984N) is incorporated into the magnetic liquid, thereby conferring magnetic properties to the organic phase. Prior to determining rates of phase separations, the extraction performance of the magnetic liquid system was compared to that of the conventional solvent extraction system. The selective extraction of Co(II) by Cyanex 272, Zn(II) by D2EHPA and Cu(II) by LIX 984N through incorporation of the extractant into a commercial hydrocarbon Shellsol 2325 diluent (non-magnetic system) and a synthesised magnetic liquid diluent (magnetic system) was compared. It was found that the magnetic and non-magnetic extraction systems showed similar percentage metal ion extractions with the magnetite in the magnetic liquid sometimes promoting a greater extent of metal ion extraction by neutralisation of liberated  $H^+$  ions. Rates of phase separation were compared through conventional mixer-settler, UV-visible absorbance and inductance studies. Use of the magnetic liquid system improves the rate of phase separation by up to 86 % in a mixer-settler system without a decrease in percentage primary metal ion extracted or loss of selectivity. Disadvantages of this technique would be the potential suspension of magnetite in the aqueous phase and possible limitations as to its chemical compatibility with various process streams because of the magnetite solubility at a pH lower than approximately 4.

#### 1. Introduction

As shown in Chapter 4, single domain nanosized magnetite particles which have been stabilised sterically by means of coating with a surfactant may be incorporated into a carrier liquid, such as kerosene, to form a stable colloidal suspension or dispersion known as a magnetic liquid (ML)<sup>1</sup>. These liquids exhibit superparamagnetic behaviour and show no hysteresis in their magnetization curve<sup>2</sup>. The principle of solvent extraction for a wide range of valuable

---

\* Based in part on the paper, Vatta, L. L.; Sole, K. C.; Koch, K. R., *Sterically stabilised nanoparticle magnetic liquids for magnetically assisted base metal solvent extraction. Manuscript in preparation 2007.*

components, e.g., metal ions or impurities from a variety of feed streams was also discussed: in solvent extraction, the selected component is removed from an aqueous phase by partitioning into an organic phase by vigorous mixing with an organic extractant (dissolved in a hydrocarbon diluent). After separation of the organic/aqueous phases, the extracted component may be recovered from the organic phase usually by back extraction of the component into a second aqueous phase<sup>3,4</sup>.

Important characteristics for liquid ion exchangers are (1) low solubility, (2) good miscibility with low-cost diluents, (3) low cost, (4) low likelihood of emulsion-forming tendencies, (5) rapid and easy phase separation after extraction, (6) high selectivity, (7) their ability to be stripped or regenerated with common reagents in cyclic processes and (8) their stability towards common reagents under normal conditions<sup>5</sup>. It appears that the magnetic liquid may comply with the first three criteria in terms of its:

- low solubility (kerosene, the carrier liquid for magnetic liquids, is insoluble in water<sup>6</sup>),
- miscibility with other hydrocarbon diluents if required,
- low cost (the cost per litre of magnetic liquid varies from approximately \$1.50 – 7 l<sup>-1</sup> depending on the source of the raw materials).

The fourth and fifth criteria (low likelihood of emulsion-forming tendencies and rapidity and ease of phase separation after extraction), are critical in that they directly affect the retention time in a system<sup>5</sup>. Ease of phase separation and the low likelihood of emulsion formation depend on the relative densities and viscosities of the two phases and on the extent of emulsion formation which may lead to the excessive consumption or loss of reagent and product. The use of a magnetic liquid for more rapid phase separation (and its potential ability to reduce emulsion-forming tendencies via magnetic separation) may be extremely advantageous. The magnetic properties of such an extractant may allow for rapid and more complete phase separation than conventional liquid extractants. In addition, the magnetic liquid may be used as a diluent for other extractants.

In Chapter 4, the extraction of  $[\text{Co}(\text{SCN})_4]^{2-}$  from an aqueous phase by magnetite, by a magnetic liquid and by an extractant incorporated into the magnetic liquid was investigated and the magnetically modified systems were found to perform as well as, if not better, for the extraction of  $[\text{Co}(\text{SCN})_4]^{2-}$  than the conventional non-magnetic system.

In this chapter, we investigate the actual rate of phase separation after solvent extraction by comparison of a conventional solvent extraction system with a system in which the liquid organic extractant is incorporated into a magnetic liquid, thereby conferring magnetic properties to the organic phase or solvent. As mentioned previously, although a magnetic solvent extraction process has been patented<sup>7, 8</sup>, to our knowledge, only preliminary investigations into the extraction of  $\text{Cu}^{2+}$  and  $\text{UO}_2^{2+}$  have been studied thus far using this principle. We compare the percentage metal cation (Co(II), Zn(II) and Cu(II)) extraction, selectivity, kinetics and rate of phase separation by three extraction agents (Cyanex 272, D2EHPA and LIX 984N) using a conventional, commercial hydrocarbon

Shellsol 2325 (SS) and a magnetic liquid diluent. The rate of phase separation was determined using a conventional mixer-settler system, as well as by UV-visible absorbance and inductance studies.

The three extraction agents investigated in this chapter, namely Cyanex 272, D2EHPA and LIX 984N, are used commercially on a wide scale for metal ion separation and production:

- Cyanex 272 (bis(2,4,4-trimethylpentyl)phosphinic acid,  $R_2POOH$ , Fig. 1) is an organic acidic extractant which possesses properties similar to both the chelating extractants and the neutral or solvating extractants where hydrated water molecules are replaced by the extractant<sup>3</sup>. Cyanex 272 can be used for the selective extraction of Co(II) at relatively high pH (~5) thus requiring neutralisation of the solution by the addition of a base for pH control<sup>9</sup>. The Cyanex 272 molecules release protons and solvate the metal ion during extraction as shown by<sup>9,10</sup> (where  $M$  is the metal,  $R$  is the hydrocarbon moiety and the overbar represents the species in the organic phase)<sup>3</sup>:

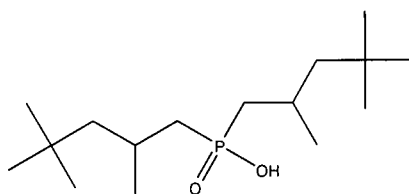
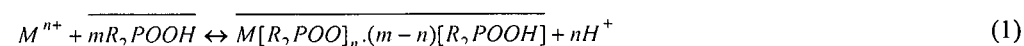


Figure 1 Cyanex 272

- D2EHPA (di(2-ethylhexyl)phosphoric acid,  $(RO)_2POOH$ , Fig. 2) is an organic acidic extractant used in commercial applications often for the selective extraction of Zn(II) at low pH (~2 – 4 depending on the secondary metal ions present)<sup>9</sup> but also for uranium, beryllium, yttrium and cobalt recovery. Zn(II) extraction by D2EHPA requires little to no pH adjustment during extraction which proceeds via a loss of protons and the solvation of the metal ion as shown by (when  $n$  is equal to 2,  $m = 2$  to 4)<sup>3,9,10</sup>:

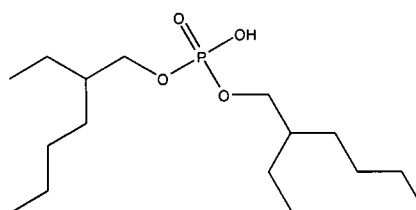
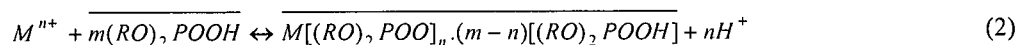


Figure 2 D2EHPA

- LIX 984N (Fig. 3) which is a mixture of LIX 860N-I (5-nonylsalicylaldoxime) and LIX 84-I (2-hydroxy-5-nonylacetophenone oxime) can be used for the selective extraction of Cu(II) at pH ~2 – 4 (depending on the secondary metal ions present). As an acidic chelating extractant<sup>3</sup>, it releases the equivalent number of hydrogen ions upon extraction of a metal ion ( $X$  is the anion<sup>10</sup>), but requires no pH control when used for extraction in media of relatively low pH:

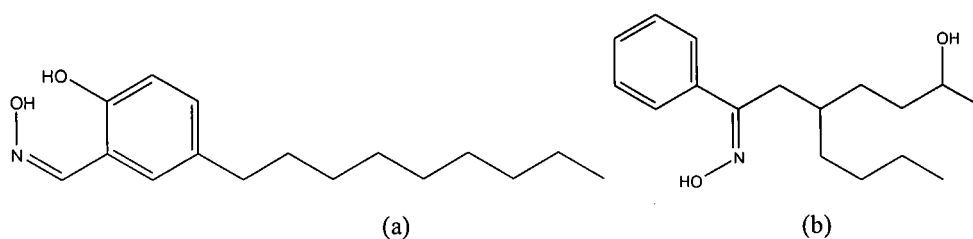
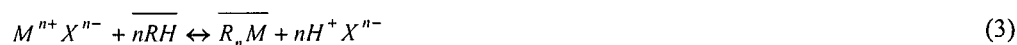


Figure 3 (a) LIX 860N-I and (b) LIX 84-I

The different extractants exhibit different  $pK_a$  values and show different affinities for various metals<sup>3, 9</sup>. Separation of metal ions and selectivities of extraction are highly pH dependent with extraction and stripping isotherms for individual metal ions differing significantly. The extraction sequences (from the pH isotherms) for Cyanex 272, D2EHPA and LIX 984N are:

- Fe(III)>Zn(II)>Cu(II)>Mn(II)>Co(II)>Mg(II)>Ca(II)>Ni(II),
- Fe(III)>Zn(II)>Cd(II)>Ca(II)>Mn(II)>Cu(II)>Mg(II)>Co(II)>Ni(II) and
- Cu(II)>Fe(III)>Ni(II)>Co(II)>Zn(II), respectively.

## 2. Experimental

### 2.1 Reagents and analytical methods

All reagents and solvents were purchased from commercial sources and were used without further purification.  $FeCl_3 \cdot 6H_2O$ ,  $FeSO_4 \cdot 7H_2O$  and 25 %  $NH_4OH$  (from Merck) were used for the precipitation of magnetite. Oleic acid and kerosene were purchased from Fluka and BP, respectively.

Cyanex 272, D2EHPA and LIX 984N were supplied by Cytec, Rhodia and Cognis Corporation, respectively. Various properties of the diluents used in this study are given in Table 1.

**Table 1** Properties of diluents, Shellsol 2325 and kerosene used in this study

Diluent	Supplier	Density (g cm <sup>-3</sup> )	Flash point (°C)	Aromatic content (vol. %)
Shellsol 2325	Shell Chemicals	0.81	87	18
Prepared as magnetic liquid using kerosene as the carrier liquid	BP	0.78	38	up to 35% (but usually < 5 %)

The compositions of the aqueous solutions used in the studies are given in Tables 2 to 4. Deionised water and a 0.6 M NaOAc/HOAc buffer matrix (pH 4, 5 and 6) were used for the preparation of aqueous solutions from sulphate salts with the exception of Ca(II) which was prepared from the chloride salt. The solutions will be referred to as **C1**, **C2**, **C3**, **L1**, **L2**, **L3**, **L4**, **D1**, **D2**, **D3**, **D4** and **D5** in subsequent sections. The letters **C**, **L** and **D** are used to indicate the extractants Cyanex 272, LIX 984N and D2EHPA, respectively, that were used for metal ion extraction from these solutions. The primary metal ion to be extracted from each solution is indicated by the shaded cells in Tables 2 to 4.

**Table 2** Composition of aqueous solutions used in investigations into the selective extraction of Co(II) using Cyanex 272 as extractant

Solution name	C1	C2	C3
Aqueous phase	MQ water	pH 5 acetate buffer	pH 6 acetate buffer
Concentration (g l <sup>-1</sup> )			
Co(II)	5.4	6.1	5.3
Ni(II)	1.1	1.2	1.1

**Table 3** Composition of aqueous solutions used in investigations into the selective extraction of Zn(II) using D2EHPA as extractant

Solution name	D1	D2	D3 (i-iv) <sup>a</sup>	D4	D5 (i-iv) <sup>a</sup>
Aqueous phase	MQ water			pH4 acetate buffer	
Concentration (g l <sup>-1</sup> )					
Ca(II)	0.9	0.6	0.8	0.6	0.8
Co(II)	1.1	1.1	1.1	1.1	1.1
Cu(II)	1.0	1.1	1.1	1.0	1.1
Ni(II)	1.1	1.2	1.2	1.2	1.2
Zn(II)	5.2	5.4	5.5	5.4	5.7

<sup>a</sup>Solutions **D3** and **D5** consisted of five separate solutions (**i-iv**) of single elements Ca(II), Co(II), Cu(II), Ni(II) and Zn(II)

**Table 4** Composition of aqueous solutions used in investigations into the selective extraction of Cu(II) using LIX 984N as extractant

Solution name	L1	L2	L3	L4
Aqueous phase	MQ water		pH 4 acetate buffer	
<b>Concentration (g l<sup>-1</sup>)</b>				
Co(II)	1.1	1.1	1.1	1.0
Cu(II)	4.8	4.5	4.6	4.7
Mn(II)	1.0			
Zn(II)	1.1			

Metal ion analysis was performed using an Inductively Coupled Plasma-Atomic Emission Spectrometer (Varian Liberty II ICP-AES) and a linear calibration method. Alternatively, UV-visible absorbance spectra for metal ion extraction calculations were obtained using a GBC UV-visible Cintra 10e Spectrometer. A wavelength scan from 400 to 700 nm at 200 nm min<sup>-1</sup> (0.4 nm step size and 1.5 nm slit width) was performed and the percentage extractions determined using the maximum absorbances for the selected metal. An Agilent 8453E single beam diode array UV-visible spectrophotometer was used for phase separation measurements. Inductance measurements (also for phase separation determination) were performed with an inductance measuring device (procured on loan from De Beers Consolidated Mines where it was manufactured in-house), of which the principle of operation is discussed in the appendix of this chapter. A Labcon horizontal shaker or Gemmy VM-300 vortex mixer was used for sample agitation.

### 2.2 Synthesis of magnetic liquid

For a typical preparation of approximately 100 ml magnetic liquid, 84 g FeCl<sub>3</sub>·6H<sub>2</sub>O and 43.2 g FeSO<sub>4</sub>·7H<sub>2</sub>O were added to 600 ml water. The resultant solution was heated to ~35 °C. 220 ml 25 % NH<sub>4</sub>OH was added to the iron solution with rapid agitation. The resultant precipitate was washed via magnetic decantation three times with 600 ml water. 600 ml water and 10 ml 25 % NH<sub>4</sub>OH, followed by a 10 ml oleic acid/80 ml kerosene mixture were added to the precipitate. The mixture was stirred and heated to 90 °C. The final organic magnetic liquid was separated by magnetic decantation from the aqueous phase and washed with distilled water to a pH of 7 – 8. The magnetic liquid was centrifuged at 4200 rpm for 30 minutes for the removal of agglomerates and diluted to 0.84 g cm<sup>-3</sup> by the addition of kerosene.

### 2.3 Procedure for solvent extraction and phase separation studies

Three **solvent extraction procedures** were followed in which the:

- percentage extraction, selectivity, kinetics and rate of phase separation were investigated using ICP-AES for analysis (Procedure 1),

- the effect of buffering and percentage metal ion extraction were investigated using ICP-AES for analysis (Procedure 2) and
- the percentage extraction and selectivity were investigated using UV-visible absorbance for analysis (Procedure 3).

The **rate of phase separation** was determined not only by a conventional method (determination of phase interface height with time in the mixer-settler system, Procedure 1) but also by two alternative methods (Procedures 4 and 5) which made use of UV-visible absorbance and inductance measurements.

A summary of the experimental extraction procedures followed is given in Fig. 4. All extraction studies were performed in triplicate unless otherwise stated and were carried out at room temperature.

Procedure 1		
Determined:	Mixing by:	Analysis by:
% Extraction	Mixer-settler system	ICP-AES
Selectivity		
Kinetics		
Phase separation		
Procedure 2		
Determined:	Mixing by:	Analysis by:
Buffering effect	Horizontal shaker	ICP-AES
Loading capacity		
Procedure 3		
Determined:	Mixing by:	Analysis by:
% Extraction	Horizontal shaker	UV-vis absorbance
Selectivity		
Kinetics		
Buffering effect		
Loading capacity		
Procedure 4		
Determined:	Mixing by:	Analysis by:
Phase separation	Vortex mixer	UV-vis absorbance
Procedure 5		
Determined:	Mixing by:	Analysis by:
Phase separation	Vortex mixer	Inductance

**Figure 4** Summary of experimental extraction and phase separation determination procedures followed

### 2.3.1 Procedure 1: Mixer-settler system/ICP-AES

50 ml each of the aqueous and organic phases were contacted in a baffled vessel stirred by means of an overhead stirrer (mixer-settler system with dimensions as shown in Fig. 5) for 15 minutes. Unbuffered aqueous solutions **C1**, **D1** and **L1** (see Tables 2 to 4) and 10 % Cyanex 272, LIX 984N and D2EHPA in Shellsol 2325 or magnetic liquid

were used in the study. Two millilitre samples were taken at 2, 5 and 10 minutes. The phases were allowed to separate (under the influence of an external magnetic field provided by a NdFeB permanent magnet for those samples containing magnetic liquid) and the aqueous fraction used for metal ion concentration analysis by ICP-AES. Extraction studies were performed under aqueous-continuous (organic droplets suspended in aqueous phase) and organic-continuous (aqueous droplets suspended in organic phase) mixing conditions illustrated conceptually in Fig. 6. The formation of an aqueous- or organic-continuous phase depends on the phase in which the agitator impeller is located when the mixing starts. Phase continuity was determined by measuring conductivity. For the Cyanex 272 extraction studies, pH was controlled by the addition of a concentrated NaOH solution.

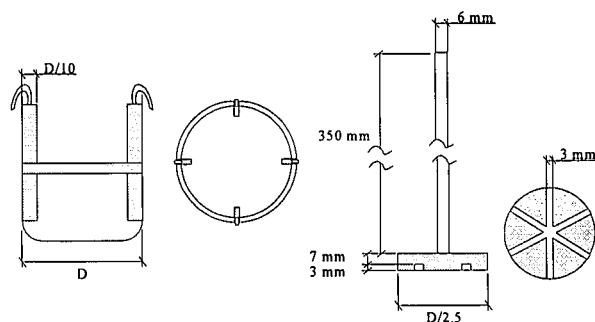


**Figure 5** Dimensions of impellers and baffles used in the mixer-settler system

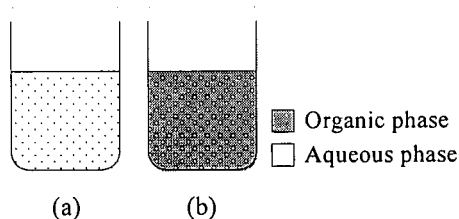


**Figure 6** Schematic representation of (a) aqueous- and (b) organic-continuous phases as used for mixer-settler tests

The rate of phase separation was determined (after 15 minutes stirring and once the stirrer had been stopped) by monitoring the time required to achieve clarity of the aqueous phase and was recorded as a function of the interface height between the aqueous and organic phases. After a 5 minute interval, the phases were mixed for 3 minutes and the rate of phase separation remeasured. This was repeated 4 times to obtain 6 readings in total. A final sample was taken from the aqueous phase for metal ion concentration analysis by ICP-AES. (This procedure is illustrated in the text below, see Fig. 13.)

### 2.3.2 Procedure 2: Horizontal shaker/ICP-AES

5 ml each of the aqueous and organic phases were contacted in sealed vessels and agitated overnight on a horizontal shaker at 110 rpm. The phases were allowed to separate and the aqueous fraction used for metal ion concentration analysis by ICP-AES. Aqueous buffered and unbuffered solutions C2, C3, D2-5, L2 and L3 (see Tables 2 to 4) and 10 % Cyanex 272, LIX 984N and D2EHPA in Shellsol 2325 or magnetic liquid were used in the study. For the

percentage extraction studies, only LIX 984N was used as extractant. The organic volume was varied from 1 to 7 ml (in increments of 1 ml) while the aqueous volume was maintained at 5 ml.

### 2.3.3 Procedure 3: Horizontal shaker/UV-visible absorbance

A 2.5 ml aqueous solution was contacted for 5 hours in a sealed vessel on a horizontal shaker at 110 rpm with a volume of organic solution such that the ratio of organic to aqueous phase was 6:4, 4:4, 3:4, 2:4 and 1:4. Buffered and unbuffered solutions **C1**, **C2**, **C3**, **L1**, **L2** and **L4** (see Tables 2 and 4) and 10 % Cyanex 272 and LIX 984N in Shellsol 2325 or magnetic liquid were used in the study. Sample triplicates were used for solutions **C1** and **L1** (but not for **C2**, **C3**, **L2** and **L4**). The phases were allowed to separate and the aqueous fraction metal ion concentration analysed using a UV-visible spectrophotometer. The absorbances at 512.89, 647.72 and 809.85 nm were used for the determination of the percentage extraction of the Co(II), Ni(II) and Cu(II), respectively, (relative to the absorbance of the original aqueous solution at the required wavelength).

### 2.3.4 Procedure 4: Vortex mixer/UV-visible absorbance

The rate of phase separation of the organic and aqueous phases after solvent extraction was also quantified by UV-visible absorbance studies on the diode array UV-visible spectrometer. The organic (1 ml) and aqueous (2 ml) phases were agitated in plastic ICP tubes for 10 s using a vortex mixer. (The variance on the UV-visible absorbance measurements for different ICP tubes was found to be 0.1 absorbance units.) UV-visible absorbance measurements of four replicates (repeated five times each) were recorded during phase separation. The combination of liquid phases as indicated by the shaded areas in Table 5 were contacted with and without the influence of an external magnetic field.

**Table 5** Combination of organic and aqueous phases contacted for Procedure 4 (illustrated by the shaded areas in the table). Compositions of solutions **C1** and **L1** are given in Tables 2 and 4, respectively.

		Organic phase					
		SS	ML	10 % Cyanex 272 in SS	10 % Cyanex 272 in ML	10 % LIX 984N in SS	10 % LIX 984N in ML
Aq. phase	Water	a	a	b	b	b	b
	Solution <b>C1</b> (MQ water)			b	b		
	Solution <b>L1</b> (MQ water)					b	b

<sup>a</sup>Five replicates

<sup>b</sup>Three replicates

The 850, 600 and 800 nm traces were used for the plot of absorbance vs time when the aqueous phase was water, LIX 984N metal ion solution **L1** and Cyanex 272 metal ion solution **C1**, respectively, as these wavelengths showed

the least interference from the metal ions contained in solution. (This procedure is illustrated in the text below, see Fig. 17.)

### 2.3.5 Procedure 5: Vortex mixer/Inductance

A second alternative to the conventional phase separation method was the determination of the rate of phase separation by inductance measurements. 0.5 ml each of the organic and aqueous phases (as indicated by the shaded areas in Table 6) were added to four different glass vials and agitated for 20 s using a vortex mixer. Inductance measurements were taken at a fixed sample height after agitation with (five replicates) and without (no replicates, one sample only) the influence of an external magnetic field. (This procedure is illustrated in the text below, see Fig. 23.)

**Table 6** Combination of magnetic liquid and aqueous phases contacted for Procedure 5 (illustrated by the shaded areas in the table). Compositions of solutions **C1** and **L1** are given in Tables 2 and 4, respectively.

		Organic phase		
		ML	10 % Cyanex 272 in ML	10 % LIX 984N in ML
Aq. phase	Water			
	Solution <b>C1</b> (MQ water)			
	Solution <b>L1</b> (MQ water)			

As a comparison, the rate of phase separation of the identical systems with the extractant in Shellsol 2325 was measured using the diode array spectrophotometer after agitation (20 s). The 850, 600 and 800 nm traces for all UV-visible absorbance measurements were used for the plot of absorbance vs time when the aqueous phase was water, LIX 984N metal ion solution **L1** and Cyanex 272 metal ion solution **C1**, respectively. (These wavelengths showed the least interference from the metal ions contained in solution.)

## 3. Results and discussion

### 3.1 Comparison of the percentage extraction of the primary metal ion, selectivity and buffering effect determined during solvent extraction tests using the magnetic liquid and Shellsol 2325 systems

#### 3.1.1 Metal ion extraction by Procedure 1: Mixer-settler system/ICP-AES

Table 7 gives the comparative results of the metal ion extractions by Cyanex 272, LIX 984N and D2EHPA in magnetic liquid or Shellsol 2325 from MQ water solutions **C1**, **L1** and **D1**, respectively, using the mixer-settler system, Procedure 1 (the primary metal ion to be extracted is highlighted in Table 7). Where possible, the separation

coefficient ( $\alpha_{M_2}$ , (eq. 4) which provides an indication of the selectivity of the extraction of the primary metal ion,  $M_1$  over the secondary metal ion,  $M_2$ ) is given in parentheses in Table 7. The higher the value of the separation coefficient, the lower the percentage impurity being extracted from the aqueous phase<sup>11</sup>. If the percentage extraction of the secondary metal is negligible (tending to zero), the separation coefficient cannot be determined and is therefore not indicated in Table 7.

$$\alpha_{M_2} = \frac{([M_2]/[M_1])_{in\ aqueous\ fraction}}{([M_2]/[M_1])_{in\ organic\ fraction}} \quad (4)$$

**Table 7** Extraction of metal ions by Cyanex 272 (solution C1, initial pH = 5.7, maintained at pH ~5.1), LIX 984N (solution L1, pH = 4.0) and D2EHPA (solution D1, pH = 4.2). The compositions of solutions C1, D1 and L1 are given in Tables 2, 3 and 4, respectively. The separation coefficients ( $\alpha_{M_2}$ ,  $M_2$  is the secondary metal ion) are indicated in italics in parentheses where possible.

Extractant	Metal	Extraction in SS (%)		Extraction with ML (%)	
		Aqueous-continuous	Organic-continuous	Aqueous-continuous	Organic-continuous
Cyanex 272	Co(II)	74 ± 3	76 ± 5	60 ± 4	62 ± 4
	Ni(II)	<2 (82) <sup>a</sup>	<6 (17) <sup>a</sup>	<1	<1
D2EHPA	Zn(II)	42 ± 1	43 ± 4	50 ± 4	56 ± 2
	Co(II)	<1	<4 (14) <sup>b</sup>	<1	17 ± 7 (3) <sup>b</sup>
	Ca(II)	6 ± 7 (7) <sup>c</sup>	8 ± 6 (6) <sup>c</sup>	<12	9 ± 6 (7) <sup>c</sup>
	Cu(II)	<1	<1	<1	9 ± 6 (2) <sup>d</sup>
	Ni(II)	<1	<1	<1	25 ± 8
LIX 984N	Cu(II)	78 ± 0.2	78 ± 0.1	68 ± 1	69 ± 0.2
	Co(II)	<1	<1	<1	<1
	Zn(II)	<1 (3915) <sup>e</sup>	<2 (390) <sup>e</sup>	<1	<1
	Mn(II)	<3 (172) <sup>f</sup>	<3 (171) <sup>f</sup>	<1	<1

<sup>a</sup> $\alpha_{Ni}$ , <sup>b</sup> $\alpha_{Co}$ , <sup>c</sup> $\alpha_{Ca}$ , <sup>d</sup> $\alpha_{Cu}$ , <sup>e</sup> $\alpha_{Zn}$ , <sup>f</sup> $\alpha_{Mn}$

It can be seen from Table 7 that the Cyanex 272 extracts Co(II) selectively over Ni(II) while the metal ion extraction by D2EHPA and LIX 984N is according to the following selective extraction sequences, respectively: Zn(II)>Ca(II)> Cu(II)~Co(II)~Ni(II) and Cu(II)>Mn(II)~Co(II)~Zn(II). This is in accordance with data obtained in literature<sup>3, 9</sup>. The percentage extraction of the primary metal ions Co(II), Zn(II) and Cu(II) by the extractants in Shellisol 2325 as compared to the magnetic liquid differ by a maximum absolute value of ~14 % while the behaviour

of the aqueous- and organic-continuous systems do not differ significantly within the Shellsol 2325 and magnetic liquid systems. Selectivities are similar for the extractions with, in general, 0 to approximately 10 % of the secondary metal ion being extracted over the primary metal ion. The highest extraction of secondary metal ion is in the case of the 25 % extraction of Ni(II) by D2EHPA in magnetic liquid. Although the Cyanex 272 and LIX 984N in magnetic liquid show a slightly lower percentage primary metal ion extraction (Co(II) and Cu(II) extractions of ~60 and 70 %, respectively) than the Shellsol 2325 system (Co(II) and Cu(II) extractions of ~75 and 78 %, respectively), the magnetic liquid system appears to be slightly more selective (less secondary metal ion extracted) than the Shellsol 2325 system. The D2EHPA in magnetic liquid shows a higher percentage Zn(II) extraction than the extractant in Shellsol 2325 (~50 versus 40 %) but displays a lower selectivity with, in general, a greater extraction of the secondary metal ions.

The slight variation in metal ion extraction ability by the magnetic and non-magnetic systems may be as a result of interaction of the extractant molecules with the magnetite surface. In fact, it has been found that Fe(III) forms stable complexes with extractants such as Cyanex 272 and D2EHPA<sup>9</sup>. Although coordination of the extractants to the magnetite may be detrimental in that the extractant loading capacity may be reduced, the addition of a surfactant to the magnetite surface may result in the modification of the point of zero charge (PZC)<sup>12</sup> which may be favourable, depending on the pH of the solution from which metal ions are to be extracted. Above, below and at the magnetite PZC (6 to 8.2)<sup>12-16</sup>, the magnetite surface should be negatively charged ( $\text{FeO}^-$ ), positively charged ( $\text{FeOH}_2^+$ ) and neutral ( $\text{FeOH}_2^+$  groups equals the number of  $\text{FeO}^-$  groups), respectively<sup>12</sup>. Reduction of the PZC by surfactant addition would therefore allow for the removal of more cationic metal species by the extractants than by the uncoated magnetite. For example, addition of oleic acid<sup>17</sup> to the magnetite surface lowers the PZC to approximately 4.5, thereby potentially allowing for the extraction of more cationic metal species at the pH of extractions that we have investigated.

### 3.1.2 Metal ion extraction by Procedure 2: Horizontal shaker/ICP-AES

After the solvent extraction mixer-settler tests, it was decided that, because the aqueous solution chemistry could potentially affect the magnetite surface charge which in turn could influence extraction, buffered solutions (Procedure 2, horizontal shaker, analysis by ICP-AES) should be used to eliminate or at least reduce potential charge effects due to variable pH.

Fig. 7 gives the metal ion extraction from unbuffered MQ water solution **D2** and pH 4 buffered solution **D4 (mixed metal ion solutions** of which the compositions are given in Table 3) by D2EHPA in magnetic liquid or Shellsol 2325. In general, the trends in extraction by D2EHPA in both the magnetic liquid and Shellsol 2325 mixture are comparable with Zn(II) being extracted selectively (44 – 49 % extraction) over Ca(II), Co(II), Cu(II) and Ni(II) (0 – 13 % extraction). The selectivity for the magnetic liquid and Shellsol 2325 systems improves slightly when the buffered solutions are used but it was found that the use of buffered solutions in this case does not significantly affect the extent of extraction. The D2EHPA extraction sequence reported in literature<sup>3</sup> is followed

with Zn(II) being selectively extracted over Cu(II), Co(II), Ca(II) and Ni(II). (Error bars are determined as the unbiased standard deviation from the results of three triplicate experiments.)

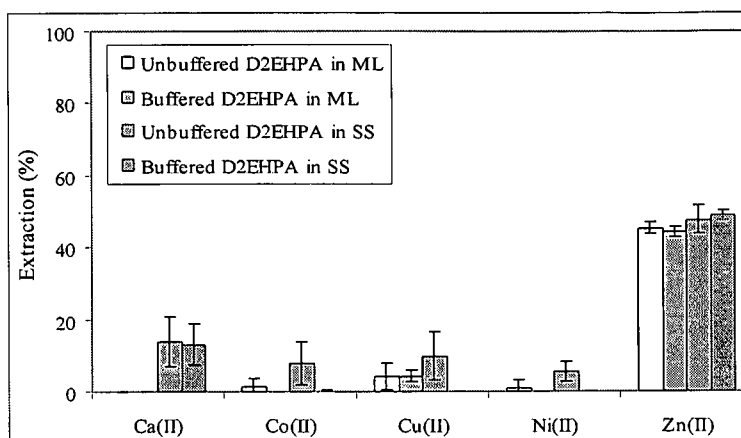


**Figure 7** Percentage extraction of metal ions from unbuffered and pH 4 buffered mixed metal ion solutions **D2** and **D4**, respectively, (see solution composition in Table 3) by 10 % D2EHPA in magnetic liquid or Shellsol 2325

The extent of extraction of the metal ions from the **individual metal ion solutions** (unbuffered **D3 (i-iv)** and pH 4 buffered **D5 (i-iv)**, see Table 3) by the D2EHPA in magnetic liquid or Shellsol 2325 presents a different picture (Fig. 8). For the unbuffered magnetic liquid system, there is greater than 50 % extraction of all metal ions while the extractions decrease for the buffered system (in some cases significantly, see for example, Ca(II), Co(II) and Ni(II)). This variation in extraction behaviour may possibly be explained by the interaction of charged species with the magnetite surface. Extraction by D2EHPA proceeds with the liberation of  $H^+$  ions (see eq. 2). In the unbuffered system, the magnetite surface may take up these liberated  $H^+$  ions (or the metal cations themselves), become protonated and thereby promote continued extraction. In the buffered system, however, the  $Na^+$  or  $H^+$  ions from the buffer itself may saturate the magnetite surface. This could reduce the potential for additional extraction of  $H^+$  ions liberated by the D2EHPA. (In the mixed metal ion solution, the loading capacity of the magnetic liquid and extractant may be approached because of the higher total ionic strength thereby more clearly illustrating the selectivity of the extractant towards the metal ions.)

In the Shellsol 2325 system, the extraction of metal ions increases for the buffered conditions as compared to the unbuffered solution (significantly in the case of Co(II), Cu(II) and Ni(II) where no extraction is observed for the unbuffered solution). In the unbuffered system, it is likely that as the concentration of liberated  $H^+$  ions increases, the solution pH drops and the ability to extract metal ions decreases. In the buffered system, the pH is maintained relatively constant and an increased extent of extraction is observed. The percentage extraction by the buffered magnetic liquid and Shellsol 2325 systems are closer in value than the unbuffered solutions in most cases.

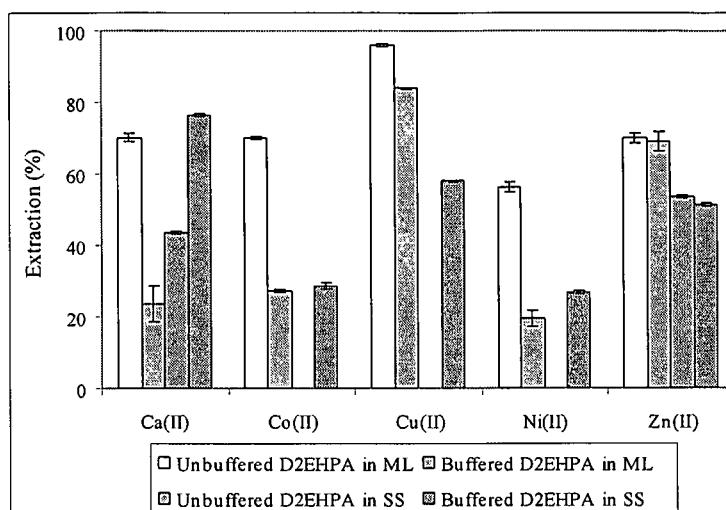


**Figure 8** Percentage extraction of metal ions from unbuffered and buffered **single metal ion solutions D3 (i-iv)** and **D4 (i-iv)**, respectively, (see solution composition in Table 3) by 10 % D2EHPA in magnetic liquid or Shellsol 2325

A comparison of the extraction of Co(II) by Cyanex 272 from two buffered solutions pH 5 to 6 (solutions **C2** and **C3**, respectively, see Table 2) and Cu(II) by LIX 984N from water and pH 4 (solutions **L2** and **L3**, respectively, see Table 4) is now presented.

The percentage extraction of Co(II) as shown in Table 8 increases by approximately 20 % as the pH increases from 5 to 6 for both the Shellsol 2325 and magnetic liquid systems. There is also a slight increase in selectivity of Co(II) over Ni(II) ( $\alpha_{Ni}$ ) for both systems (5 to 19 for the Shellsol 2325 and 6 to 12 for the magnetic liquid system). Extraction of Co(II) by Cyanex 272 proceeds with the liberation of  $H^+$  ions (eq. 1), so that a higher pH buffer medium allows for the neutralisation of more  $H^+$  ions and therefore higher metal ion extraction percentages. The percentage extraction of Cu(II) by LIX 984N does not change significantly (variation of 2 – 3 %) in a buffered solution as compared to water because the extraction is not pH sensitive as is the case for Cyanex 272. The overall extent of extraction by the magnetic liquid systems (for both Cyanex 272 and LIX 984N) is approximately 10 % lower than that by the Shellsol 2325 as observed previously and was suggested to be as a result of coordination of the extractant to the magnetite surface with a resulting loss in ability to extract metal ions.

**Table 8** Percentage extraction of Co(II) and Ni(II) by Cyanex 272 from solutions C2 and C3 (see solution compositions in Table 2) and Cu(II) and Co(II) by LIX 984N from solutions L2 and L3 (see solution compositions in Table 4) under different buffering conditions. The separation coefficient ( $\alpha_{Ni}$  and  $\alpha_{Co}$ , indicating selectivity of Co(II) to Ni(II) and Cu(II) to Co(II), respectively) is indicated in italics in parentheses where possible.

Extractant	Metal	Extraction in SS (%)		Extraction in ML (%)	
		pH 5 acetate buffer (C2)	pH 6 acetate buffer (C3)	pH 5 acetate buffer (C2)	pH 6 acetate buffer (C3)
Cyanex 272	Co(II)	44 ± 3	65 ± 3	34 ± 2	52 ± 5
	Ni(II)	10 ± 6 (5) <sup>a</sup>	3 ± 5 (19) <sup>a</sup>	6 ± 4 (6) <sup>a</sup>	4 ± 8 (12) <sup>a</sup>
LIX 984N	Cu(II)	78 ± 1	81 ± 1	68 ± 0.3	69 ± 1.0
	Co(II)	0 ± 0.4	4 ± 1 (19) <sup>b</sup>	0 ± 0.4	0 ± 3

<sup>a</sup> $\alpha_{Ni}$ , <sup>b</sup> $\alpha_{Co}$

### 3.1.3 Metal ion extraction by Procedure 3: Horizontal shaker/UV-visible absorbance

Fig. 9 gives an indication of the percentage metal ion extraction by the Cyanex 272, where the percentage extraction of Co(II) and Ni(II) by Cyanex 272 (determined using solutions C1, C2 and C3 by Procedure 3 making use of the horizontal shaker and with analysis by UV-visible absorbance) is given as a function of the ratio of the organic to aqueous phase (O/A). (Error bars are included for the extraction from solution C1 (three replicates used) but the error is small and is therefore not visible in Fig. 9. Single samples were used for solutions C2 and C3 and no confidence interval is reported for these data.)

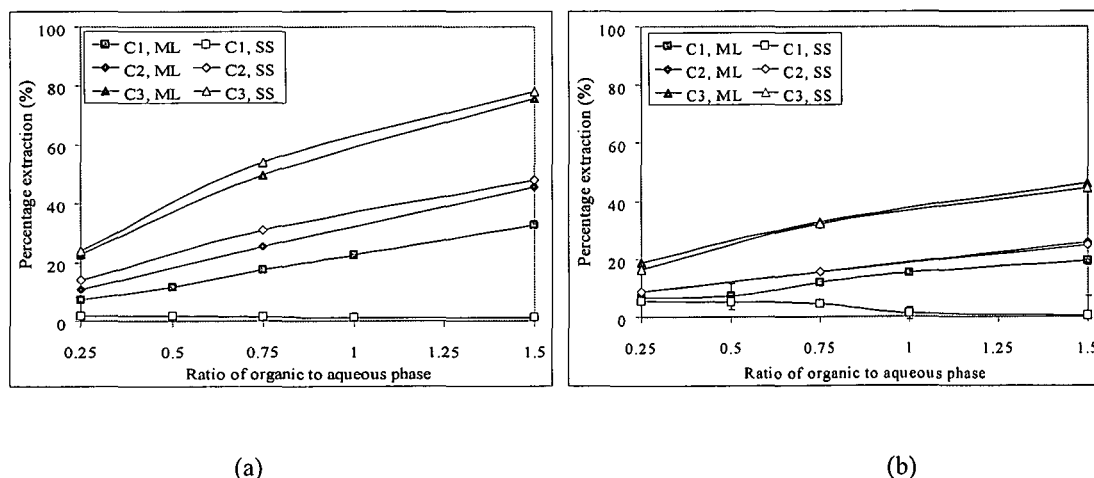


**Figure 9** Percentage extraction of (a) Co(II) and (b) Ni(II) from water solution C1, pH 5 acetate buffer C2 and pH 6 acetate buffer C3 (see solution compositions in Table 2) by Cyanex 272 in the Shellsol 2325 (SS) or magnetic liquid (ML) system

The magnetic and non-magnetic systems show similar extent of extraction percentages of Co(II) and Ni(II) for the buffered solutions (pH 5, C2 and pH 6, C3) as the organic/aqueous (O/A) ratio increases. The extraction increases with increase in pH from 5 to 6 as was also observed in Table 8 (with analysis by ICP-AES).

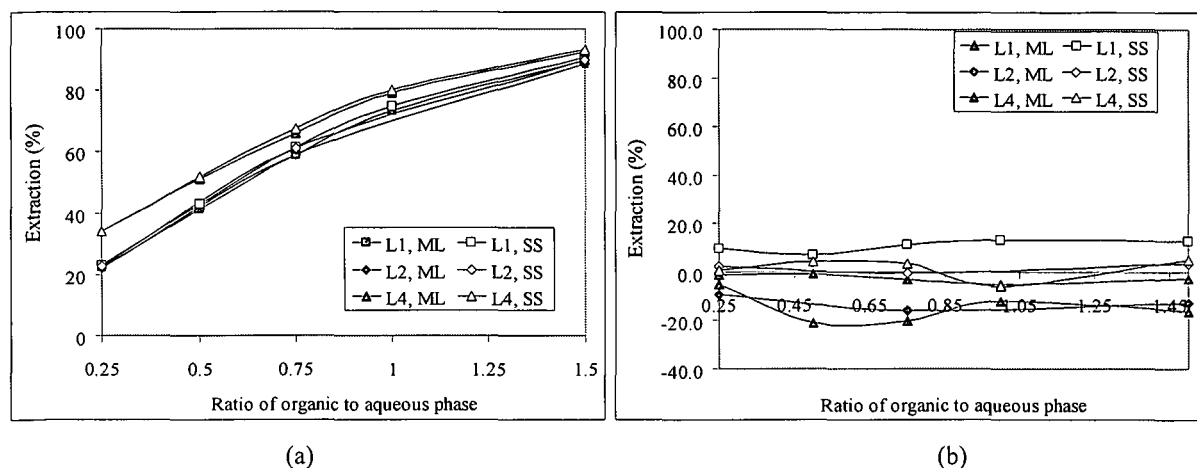
Although the buffered Shellsol 2325 and all the magnetic liquid systems showed an increase in extraction of both Co(II) and Ni(II) with an increase in O/A ratio, the unbuffered Shellsol 2325 system (C1) showed an almost constant extraction of Co(II) (~1 – 2 %) and Ni(II) (~0.5 – 5.5 %) with an increase in O/A ratio. For the Shellsol 2325 and water matrix (C1), the liberation of H<sup>+</sup> ions according to eq. 1 may have resulted in a decrease of the solution pH. This in turn may have limited further extraction of Co(II) and Ni(II) by the Cyanex 272. As mentioned previously, in the case of the magnetite, it is possible that the magnetite surface itself may act as a buffer, becoming protonated by the H<sup>+</sup> ions released by the Cyanex 272 (see eq. 1). This may allow for further deprotonation of Cyanex 272 and additional Co(II) and Ni(II) extraction.

Table 9 gives the separation coefficients (for the extractions as shown in Fig. 9) which indicate the selectivity of extraction of Co(II) relative to Ni(II) for the magnetic liquid and Shellsol 2325 systems. With the exception of the extraction by the Cyanex 272 in Shellsol 2325 for the unbuffered C1 solution, separation coefficients are relatively similar (~2) for an increase in O/A ratio. The extraction by the Cyanex 272 in Shellsol 2325 for the unbuffered C1 solution was poor resulting in low selectivities (~0.3 – 3) of Co(II) to Ni(II).

**Table 9** Separation coefficient ( $\alpha_{Ni}$ ) indicating the selectivity of Co(II) to Ni(II) for the extraction of Co(II) and Ni(II) from solutions C1, C2 and C3 (see solution compositions in Table 2) by Cyanex 272 in Shellsol 2325 (SS) or magnetic liquid (ML) with increasing ratio of organic to aqueous phase

Solution matrix	Water (C1)					pH 5 acetate buffer (C2)			pH 6 acetate buffer (C3)			
	O/A	1:4	2:4	3:4	4:4	6:4	1:4	3:4	6:4	1:4	3:4	6:4
$\alpha_{Ni}$ (SS)	0.3	0.4	0.3	1	3	1.6	2	2	2	2	2	2
$\alpha_{Ni}$ (ML)	1	2	2	2	2	1	2	2	1	2	2	2

Figs 10 (a) and (b), respectively, give the percentage extraction of Cu(II) and Co(II) by LIX 984N as a function of the O/A ratio (determined using solutions L1, L2 and L4 by Procedure 3 using a horizontal shaker and with metal ion analysis by UV-visible absorbance). Solution L1 contained Co(II), Cu(II), Mn(II) and Zn(II) while L2 and L4 contained only Co(II) and Cu(II). (No data are reported for Mn(II) and Zn(II). Unbiased standard deviation error bars are included for the extraction from solution L1 (three replicates used) but the error is small and is therefore not visible in Fig. 10. Single samples were used for solutions L2 and L4 and no confidence interval is therefore reported for these data.)



**Figure 10** Percentage extraction of (a) Cu(II) and (b) Co(II) from water solution **L1**, water solution **L2** and pH 4 acetate buffer solution **L4** (see solution compositions in Table 4) by LIX 984N in the Shellsol 2325 (SS) or magnetic liquid (ML) system

The extent of extraction of Cu(II) from the water solutions (**L1** and **L2**) by LIX 984N compares to the extraction from the pH 4 acetate buffer (**L4**) for both the Shellsol 2325 and magnetic liquid systems. This is in contrast to what was observed for the Cyanex 272 extraction system, where the extraction from the water solution **C1** by the Shellsol 2325 system was lower than that for the magnetic liquid system. Unlike for the Cyanex 272 extraction system where pH control is required (and is believed to take place by adsorption of the  $H^+$  ions onto the magnetite surface), the neutralisation of liberated  $H^+$  ions is not required for LIX 984N extraction. Cu(II) extraction for the unbuffered (**L1** and **L2**) as well as the buffered (**L4**) solutions therefore increases with an increase in O/A ratio. An O/A ratio of approximately 1.5 is required for greater than 90 % extraction. (This compares with the results obtained using ICP-AES for analysis where a 1.4 times O/A ratio with 10 % Cyanex 272 extractant appears to be sufficient for 100 % removal of the Cu(II) ions.)

The percentage extraction of Cu(II) and Co(II) by LIX 984N as a function of the O/A ratio as determined using UV-visible absorbance spectra (Procedure 3) after 20 days is given in Figs 11 (a) and (b), respectively. (Single samples were used for solutions **L2** and **L4** and no confidence interval is therefore reported for these data.) A 'negative extent of Co(II) extraction' is observed after the extended contact period. The negative percentage extraction reported for the Co(II) at higher magnetic liquid concentrations is very likely as a result of leaching of magnetite from the magnetic liquid into the aqueous phases thereby forming a dilute aqueous magnetite suspension. Absorbances for the iron oxides goethite, lepidocrocite, akagnéite, ferrihydrite, haematite and maghemite are 492, 489, 502, 504, 542 and 495/512 nm, respectively (run on thin samples in transmission mode)<sup>12</sup>. Magnetite very likely also absorbs at a wavelength close to these iron oxides and most likely very close to the absorbance of maghemite (495/512 nm). The extent of Co(II) extraction is determined according to:

$$\text{Co(II) extraction (\%)} = \frac{[\text{Co(II)}]_{\text{in initial sample}} - [\text{Co(II)}]_{\text{in final sample}}}{[\text{Co(II)}]_{\text{in initial sample}}} * 100 \quad (5)$$

Co(II) absorbs at a similar wavelength (512 nm) to magnetite or maghemite and the resultant absorbance as determined in these studies may be a sum of the absorbance of both the Co(II) and the iron oxide. The concentration of Co(II) in the final sample may therefore be calculated to be higher than the initial concentration, resulting in the determination of a negative extent of Co(II) extraction. The determination of Co(II) extraction using UV-visible spectra is therefore not optimal especially when larger volumes of magnetic liquid or extended contact times are used. However, more importantly, this phenomenon highlights the fact that some unwanted magnetite may become suspended in the aqueous phase during processing.

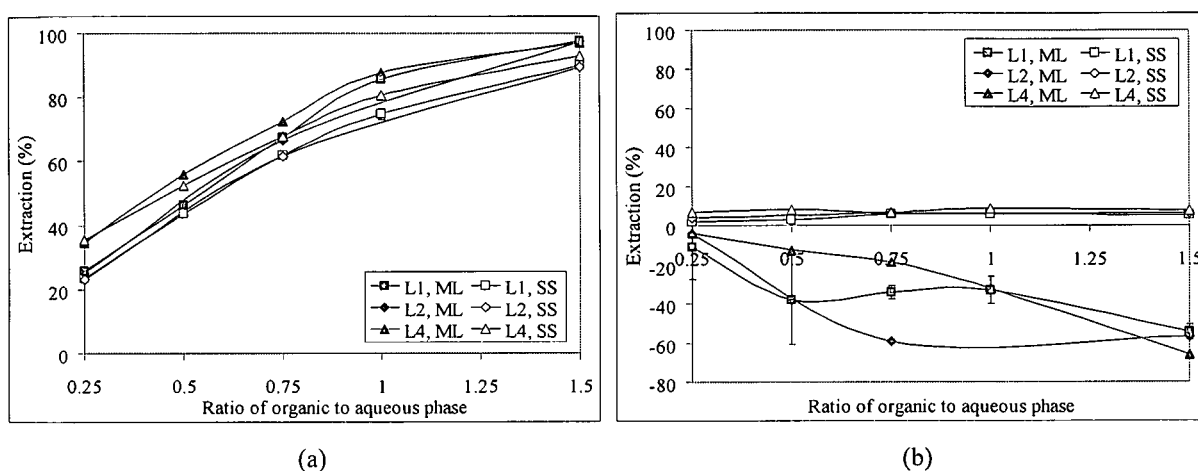


**Figure 11** Percentage extraction after 20 days of (a) Cu(II) and (b) Co(II) from water solution L1, water solution L2 and pH 4 acetate buffer solution L4 (see solution compositions in Table 4) by LIX 984N in the Shellsol 2325 (SS) or magnetic liquid (ML) system

Table 10 compares the initial separation coefficient and that after 20 days indicating the selectivity of extraction of Cu(II) relative to Co(II) for the Shellsol 2325 system. No separation coefficients could be determined for the magnetic liquid system, because of the negative extent of Co(II) extraction observed. Separation coefficients are relatively similar for an increase in O/A ratio in the Shellsol 2325 system.

**Table 10** Initial separation coefficient ( $\alpha_{Co,0}$ ) and separation coefficient after 20 days ( $\alpha_{Co,20}$ ) indicating the selectivity of Cu(II) relative to Co(II) for the extraction of Cu(II) and Co(II) from solutions **L1**, **L2** and **L4** (see solution compositions in Table 4) by LIX 984N in Shellsol 2325 (SS) with increasing ratio of organic to aqueous phase

Solution matrix	Water (L1)					Water (L2)			pH 4 acetate buffer (L4)				
	1:4	2:4	3:4	4:4	6:4	1:4	3:4	6:4	1:4	2:4	3:4	4:4	6:4
<b>Metal</b>	<b>Extraction in Shellsol 2325 (%)</b>												
$\alpha_{Co,0}$ (SS)	2	6	5	6	7	10	NE	26	43	43	19	NE	18
$\alpha_{Co,20}$ (SS)	13	14	11	13	17	6	10	14	5	5	10	9	12

NE: No extraction of  $M_2$  (Co(II))

### 3.2 Comparison of the kinetics of metal ion distribution from the aqueous to the organic phase determined during extraction tests using the magnetic liquid and Shellsol 2325 systems

Figs 12 (a) to (c) give the percentage extraction of Co(II), Zn(II) and Cu(II) by Cyanex 272, D2EHPA and LIX 984N, respectively, as a function of time determined by Procedure 1 (from solutions **C1**, **D1** and **L1** in Tables 2 to 4, using the mixer-settler system and under aqueous-continuous and organic-continuous conditions as described in Section 2.3.1). Extraction was found to be rapid with maximum extraction occurring within 10 minutes for all systems.

The LIX 984N samples were kept unstirred in the dark for 20 days and the metal ion concentrations remeasured. In all cases, the percentage extraction of Cu(II) by the LIX 984N in Shellsol 2325 increased by a maximum of 0.5 % while that in magnetic liquid increased by up to 9 %. The percentage Co(II) extraction increased by 11 and 30 % for the non-magnetic and magnetic systems, respectively. The greater percentage extraction after 20 days contact time of both the Cu(II) and the Co(II) by the magnetic liquid system is probably as a result of the diffusion of metal ions into particle aggregates or crystal nanopores<sup>12</sup>.

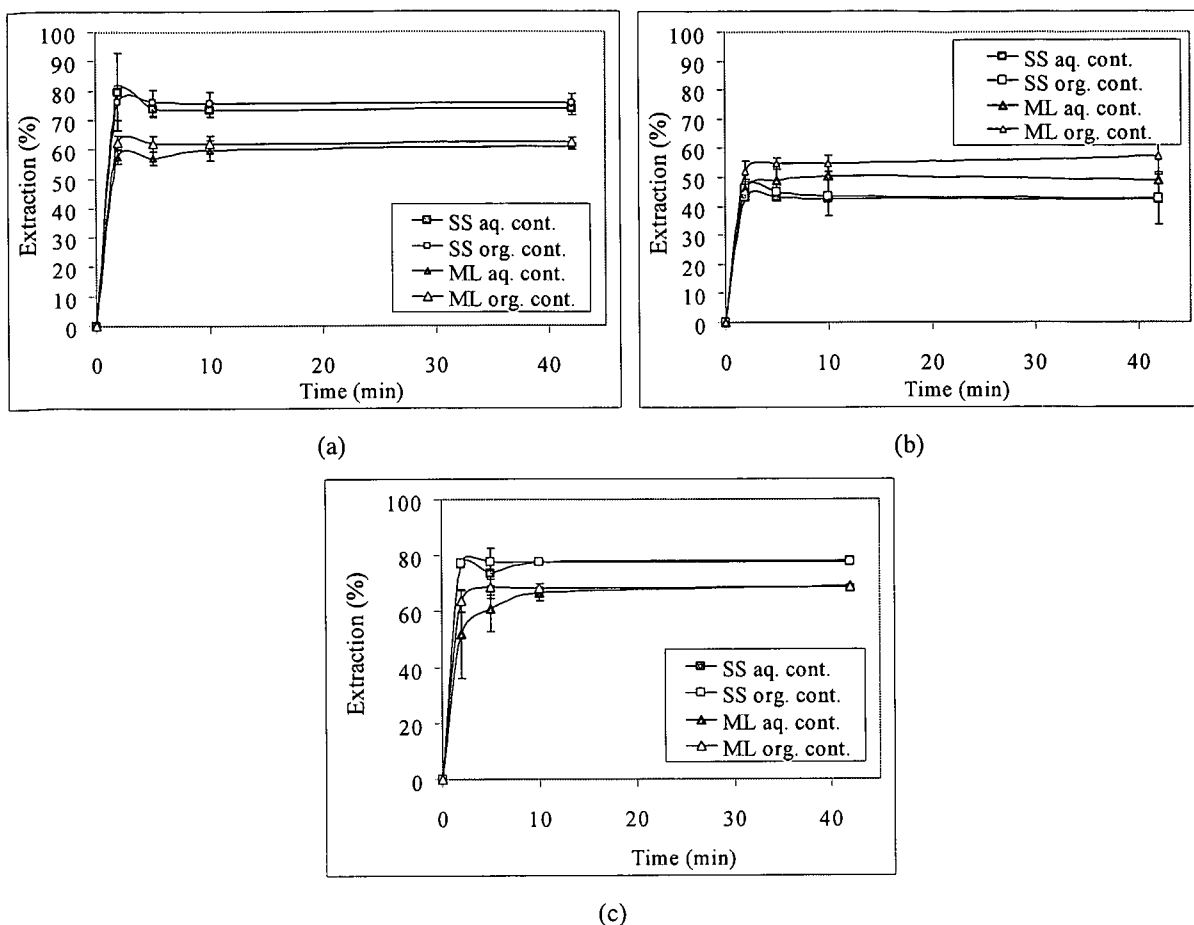


**Figure 12** Kinetics of metal ion distribution for the extraction of (a) Co(II) using Cyanex 272, (b) Zn(II) using D2EHPA and (c) Cu(II) using LIX 984N in a mixer-settler system (see Procedure 1, Section 2.3.1) with Shellsol 2325 (SS) or magnetic liquid (ML) under aqueous-continuous and organic-continuous conditions

In summary then, a comparison of the percentage extraction of the primary metal ion, selectivity of extraction of the primary metal ion over secondary metal ions in solution and kinetics of metal ion extraction as determined using the magnetic liquid and Shellsol 2325 systems (Sections 3.1 and 3.2) show similar results. A noticeable ‘buffering effect’ was observed in some cases for the magnetic liquid system where it appears that the magnetite surface may provide for the neutralisation of  $H^+$  ions released during extraction. Based on these preliminary positive results, investigations were then extended to compare the kinetics of organic/aqueous phase separation for the magnetic liquid and Shellsol 2325 systems.

### 3.3 Comparison of the kinetics of organic/aqueous phase separation using the magnetic liquid and Shellsol 2325 systems

A variety of factors, such as interfacial tension, relative densities and viscosities of the two phases, degree of agitation, temperature, etc., affect the rate of phase separation of the organic and aqueous phases after mass transfer

of the metal ion has taken place from the aqueous to the organic phase<sup>3</sup>. In this section, the relative rates of phase separation of the organic and aqueous phases are compared using three evaluation techniques: the mixer-settler system, UV-visible absorbance measurements and inductance measurements.

### 3.3.1 Rate of phase separation using the mixer-settler system (Procedure 1)

The rate of phase separation using the mixer-settler system was determined by agitation of the organic and aqueous phases to form an emulsion and then recording, as a function of time, the phase interface height (emulsified organic/aqueous layer) of the organic/aqueous emulsion. The experimental method is illustrated in Fig. 13. After stirring, the initial phase interface height ( $h_{ti}$ ) is recorded at time  $t_i$  (initial time). The successive decrease in interface height ( $h_{ti+1} \dots h_{ti+n}$ ) is recorded with time ( $t_{i+1} \dots t_{i+n}$ ) until the phases have separated ( $h_{tf}$ ) at time  $t_f$  (final time). The change in phase interface height as a function of time can then be plotted. The interface height is measured with a ruler and relies on a visual determination by the investigator.

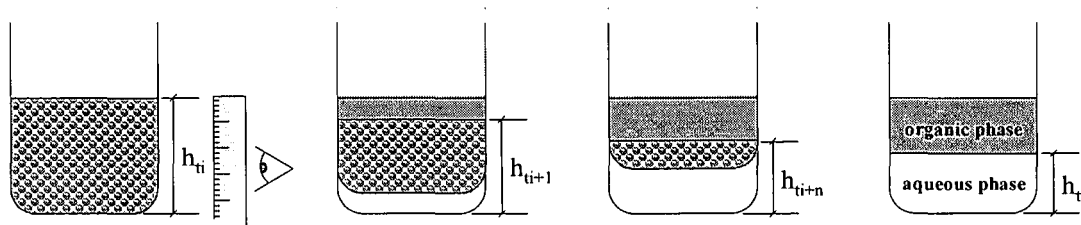


**Figure 13** Schematic illustration of the method of measurement of phase separation in the mixer-settler system: the emulsified layer is measured visually using a ruler. The initial interface height ( $h_{ti}$ ), subsequent heights ( $h_{ti+1} \dots h_{ti+n}$ ) and final height ( $h_{tf}$ ) are recorded and plotted as a function of time

Figs 14 to 16 indicate the rate of phase separation as a function of the interface height for the conventional and magnetic liquid systems in the mixer-settler system (Procedure 1). (The phases were contacted with real metal ion solutions **C1**, **D1** and **L1**, see compositions in Tables 2, 3 and 4, respectively.) Phase separation for the Shellsol 2325 system is indicated as an S-shaped curve showing the decrease in phase interface height with time. In the magnetic liquid system, the externally applied magnetic field pulls the magnetic liquid towards the base of the beaker without a clear phase interface during phase separation. The time required for phase separation for the magnetic liquid systems is therefore represented as a single dashed line at the time at which phase separation had been achieved, e.g., in Fig. 14 (a), phase separation for the aqueous-continuous system for Cyanex 272 in Shellsol 2325 took approximately 60 s while phase separation for the Cyanex 272 in magnetic liquid system was achieved in just over 30 s.

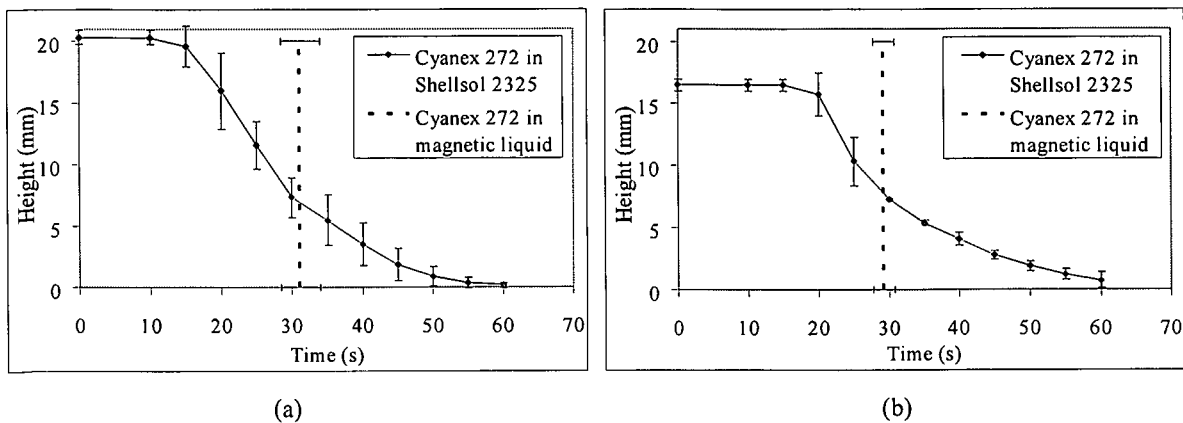


**Figure 14** Phase separation rate for Shellsol 2325 (indicated by an S-shaped curve) and magnetic liquid system (indicated by a single dashed line) for the (a) aqueous- and (b) organic-continuous extraction in the mixer-settler system (see description in Section 2.3.1) using Cyanex 272 as the extractant

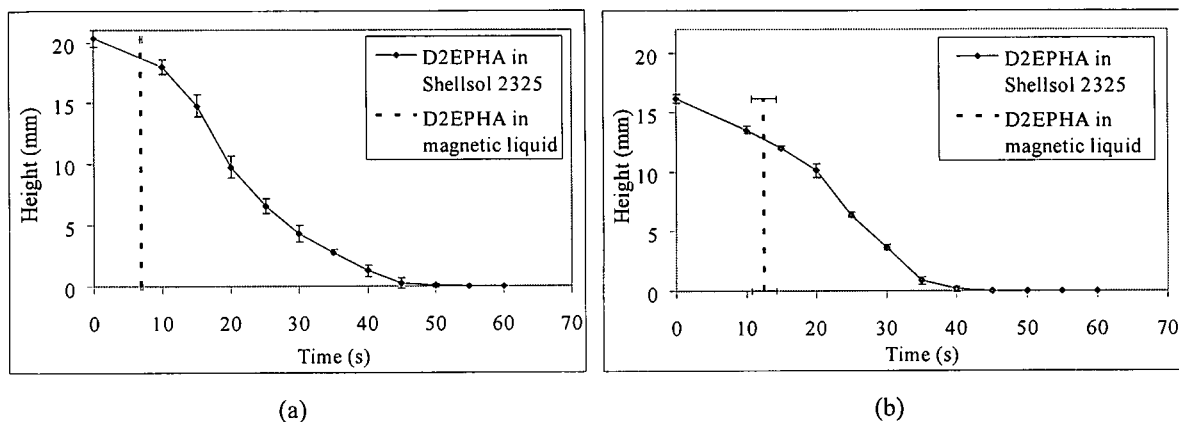


**Figure 15** Phase separation rate for Shellsol 2325 (indicated by an S-shaped curve) and magnetic liquid system (indicated by a single dashed line) for the (a) aqueous- and (b) organic-continuous extraction in the mixer-settler system (see description in Section 2.3.1) using D2EHPA as the extractant

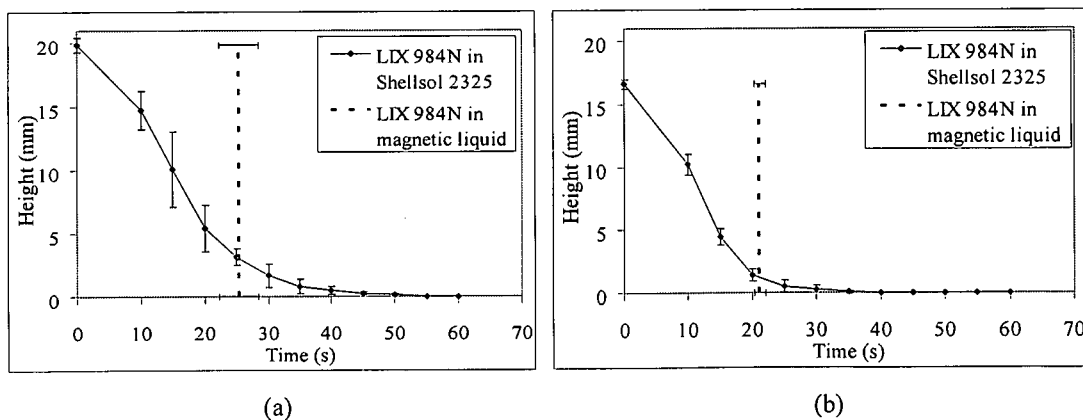


**Figure 16** Phase separation rate for Shellsol 2325 (indicated by an S-shaped curve) and magnetic liquid system (indicated by a single dashed line) for the (a) aqueous- and (b) organic-continuous extraction in the mixer-settler system (see description in Section 2.3.1) using LIX 984N as the extractant

The difference in rate of phase separation between the Shellsol 2325 and the magnetic liquid systems was calculated as follows:

$$\begin{aligned} & \text{Difference in rate of extraction between Shellsol 2325 and magnetic liquid system (\%)} \\ & = \frac{\text{Phase separation time}_{\text{Shellsol 2325 system}} - \text{Phase separation time}_{\text{magnetic liquid system}}}{\text{Phase separation time}_{\text{Shellsol 2325 system}}} * 100 \end{aligned} \quad (6)$$

The phase separations for the magnetic liquid system under aqueous-continuous conditions with Cyanex 272, D2EHPA and LIX 984N were found to be 48, 86 and 49 % faster, respectively, than the Shellsol 2325 system. For the organic-continuous phases with Cyanex 272, D2EHPA and LIX 984N, the magnetic liquid phase separations were found to be 51, 68 and 39 % faster, respectively, than the Shellsol 2325 system.

### 3.3.2 Rate of phase separation using UV-visible absorbance measurements (Procedure 4)

The rate of phase separation as determined using the mixer-settler system relies on an optical determination of phase interface height as a function of time (Procedure 1). Because of errors in parallax and possible bias, the rate of phase separation was also determined by UV-visible absorbance measurements in order to obtain a more objective assessment of phase separation. Fig. 17 provides a schematic illustration of the experimental measurement method. A sample consisting of the organic and aqueous phase was agitated in an ICP tube in a vortex mixer. The sample was then placed into a single beam diode array UV-visible spectrophotometer where the UV-visible absorbance was measured at set intervals over a period of time. The absorbance decreases with time as the phases separate and the UV-light is transmitted through the aqueous phase rather than through the emulsified interface layer. The absorbance at a specific wavelength was then plotted as a function of time. Firstly, the phase separation rate of the Shellsol 2325 or magnetic liquid as contacted with water was determined. Tests were then extended to samples consisting of Shellsol 2325 or magnetic liquid with extractant contacted with water and then with the metal ion solutions.

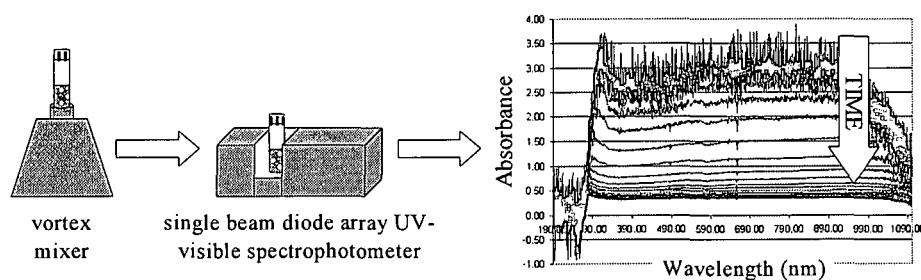


**Figure 17** Schematic illustration of method of determining phase separation using the single beam diode array UV-visible spectrophotometer: after mixing, the decrease in sample absorbance as the organic and aqueous phases separate is measured as a function of time

In order to allow for comparison of phase separation times, three settling time parameters were defined:

1. Time  $t_{50}$ , was defined to be where the absorbance is 50 % of the initial absorbance, i.e.:

$$absorbance_{t_{50}} = \frac{50}{100} absorbance_{initial} \quad (7)$$

2. In some cases, the magnetic liquid coated the sides of the ICP tube and although phase separation had occurred, the final absorbance was not zero. A time  $t_{p50}$ , was therefore defined where the absorbance is 50 % of the average of the initial and final absorbances, i.e.:

$$absorbance_{t_{p50}} = \left( \frac{absorbance_{initial} + absorbance_{final}}{2} \right) \quad (8)$$

3. To determine whether phase separation had occurred, a time  $t_{0.5}$ , was defined where the change of absorbance between two consecutive times  $t_i$  and  $t_{i+1}$  was less than 0.5 % of the initial absorbance, i.e.:

$$\Delta absorbance_{t_{0.5}} = absorbance_{t_{i+1}} - absorbance_{t_i} = \frac{0.5}{100} absorbance_{initial} \quad (9)$$

If a sample failed to satisfy condition 3, it was assumed that phase separation was still taking place.

If the condition  $t_{50}$ ,  $t_{p50}$  or  $t_{0.5}$  was not reached, i.e., the absorbance did not drop to 50 % of the initial absorbance, the absorbance did not drop to 50 % of the average of the initial and final absorbances or the change of absorbance between two consecutive times was not less than 0.5 % of the initial absorbance, respectively, the statement '*not reached*' is reported in the Tables 11 – 14. In some cases, all three of the settling time parameters were not reached and this is reported in the Tables 11 – 14 as '*no separation observed over the measurement time*'.

A one-way analysis of variance (ANOVA) was used to determine whether mean settling times between different samples were statistically significantly different from one another. The p-value reported for these data indicates the statistical significance of the result and represents the probability of error that is involved in accepting the observed result as valid, e.g., a p-value of 0.05 indicates that there is a 5 % probability that the relation between the variables found in the sample is coincidental. For these studies, a p-value of 0.05 was treated as an acceptable error level.

### 3.3.2.1 Rate of phase separation using UV-visible absorbance measurements for Shellsol 2325 or magnetic liquid contacted with water

Table 11 gives the settling times as defined by eqs 7 to 9 and p-values for the phase separation times of the Shellsol 2325 or magnetic liquid contacted with water. The  $t_{50}$ ,  $t_{p50}$  and  $t_{0.5}$  conditions were determined for the four replicates (runs 1-4, 5-8, 9-12, 13-16 and 17-20) of the five different samples tested.

**Table 11** Mean settling times,  $t_{50}$ ,  $t_{p50}$  and  $t_{0.5}$  as given by eqs 7 to 9 for the contact of Shellsol 2325 or magnetic liquid with water (time in s)

Condition	Run	$t_{50}$	$t_{p50}$	$t_{0.5}$
Shellsol 2325 (no magnet)	1-4	55	53	109
	5-8	35	33	85
	9-12	53	49	109
	13-16	71	69	125
	17-20	31	31	89
Shellsol 2325 (with magnet)	1-4	63	61	153
	5-8	35	35	91
	9-12	31	27	111
	13-16	81	79	141
	17-20	45	43	99
Magnetic liquid (no magnet)	1-4	No separation observed over the measurement time		
	5-8			
	9-12			
	13-16			
	17-20			
Magnetic liquid (with magnet)	1-4	9	9	37
	5-8	9	7	37
	9-12	7	7	47
	13-16	11	11	51
	17-20	5	5	31
p-value		0.0012 <sup>a</sup>	0.00149 <sup>a</sup>	0.0006 <sup>a</sup>

<sup>a</sup> excluding magnetic liquid without magnet

The p-values as determined in Table 11 exclude the magnetic liquid system with no magnetic field as no  $t_{50}$  and  $t_{p50}$  values were obtained and condition 3 is violated (see also Fig. 18). It is therefore assumed that the phases have not separated completely. The p-values obtained for the  $t_{50}$ ,  $t_{p50}$  and  $t_{0.5}$  conditions were 0.0012, 0.00149 and 0.0006, respectively, indicating that there is a difference in phase separation between the different conditions (Shellsol 2325 setup vs. magnetic liquid setup). There is approximately an 86 % percentage improvement in settling rate (determined using the average of the means) for the magnetic liquid system under the influence of an external magnetic field as compared to the Shellsol 2325 system.

The change in absorbance with time determined for these measurements is shown in Fig. 18 (a) with the error bars (95 % confidence interval) excluded in Fig. 18 (b) for clarity. There is a relatively large variation in absorbance measurements between 20 and 60 seconds. This is as a result of the variation in mixing and the variation in sample properties with time. (With each consecutive agitation, a more emulsified mixture may form leading to a slightly different phase separation time. It was for this reason that five new samples were used and phase separation was performed four consecutive times for each of these samples.) Despite the variation in absorbance readings, the overall trends show that the separation of the magnetic liquid from water under the influence of a magnetic field is the most rapid as was confirmed by the p-values (Table 11).

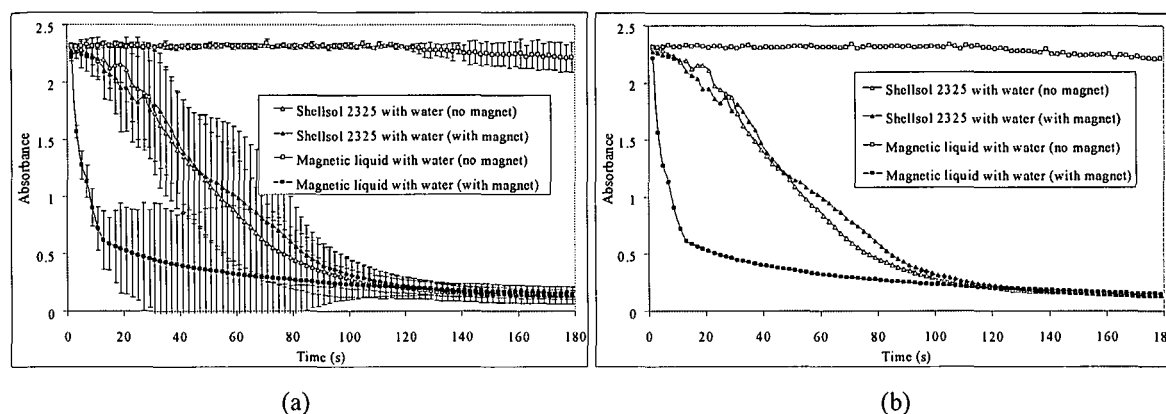


**Figure 18** Change in absorbance versus time for Shellsol 2325 and magnetic liquid contacted with water (a) with the 95 % confidence intervals and (b) without the error bars for clarity

### 3.3.2.2 Rate of phase separation using UV-visible absorbance measurements for Shellsol 2325 or magnetic liquid containing Cyanex 272 or LIX 984N and contacted with water

With the addition of an extractant to the Shellsol 2325 or to the magnetic liquid, the time required for phase separation increases significantly as shown in Figs 19 (a) and (b) for Cyanex 272 and LIX 984N, respectively.

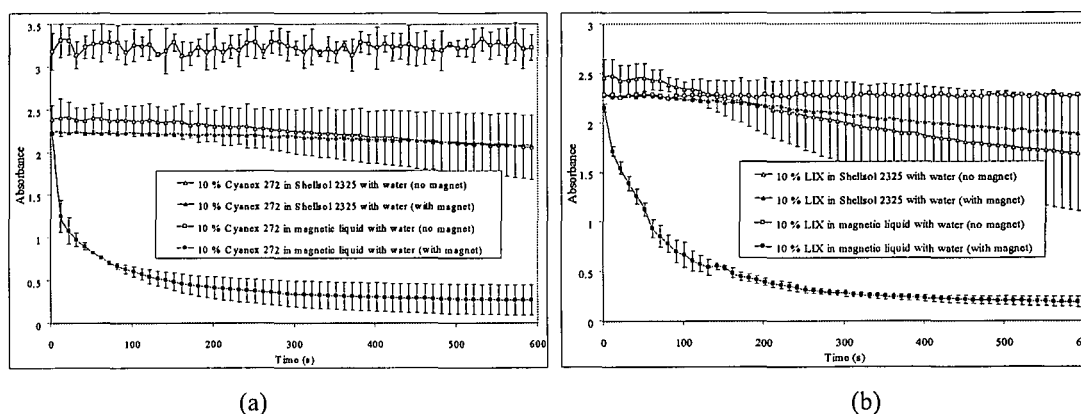


**Figure 19** Change in absorbance versus time for (a) 10 % Cyanex 272 and (b) 10 % LIX 984N in Shellsol 2325 and magnetic liquid contacted with water

It is likely that the slightly polar extractants in the non-polar hydrocarbon Shellsol 2325 and magnetic liquid interact with the water phase thereby increasing the time required for phase separation. For example, depending on solution conditions such as pH and salt concentration<sup>11</sup>, Cyanex 272 may exhibit some solubility in aqueous solutions: as the salt concentration decreases and the pH increases, the solubility of the Cyanex 272 increases as a result of its acidic nature. The viscosity, relative densities and interfacial tension, however, are most likely the more important effects.

An ANOVA performed to test for significant differences between the means of the various settling conditions for the organic phase with Cyanex 272 or LIX 984N in Shellsol 2325 or magnetic liquid and water yielded the p-values as given in Table 12.

The p-values (Table 12) for the conditions  $t_{p50}$  and  $t_{0.5}$  (0.00065 and 0.00006) for Cyanex 272 show that the differences in terms of phase separation times for the different conditions can be accepted. According to parameter 3 (time  $t_{0.5}$  where the change of absorbance is less than 0.5 % of the original absorbance), it appears that only the magnetic liquid with magnet system achieved phase separation. There is a percentage improvement of approximately 94 % in settling rate (determined using the average of the means) for the magnetic liquid with magnet as compared to the Shellsol 2325 system. No p-value for the condition  $t_{50}$  was calculated as only the magnetic liquid with magnet complied with this criterion.

The p-values (Table 12) for the conditions  $t_{p50}$  and  $t_{0.5}$  (0.00218 and 0.00013) for LIX 984N show that the differences in terms of phase separation times for the different conditions can be accepted. There is a percentage improvement of approximately 84 % in settling rate (based on  $t_{p50}$  and determined using the average of the means) for the magnetic liquid with magnet as compared to the Shellsol 2325 system. Again, no p-value for the condition  $t_{50}$  was calculated as only the magnetic liquid with magnet complied with this criterion.

**Table 12** Mean settling times,  $t_{50}$ ,  $t_{p50}$  and  $t_{0.5}$  as given by eqs 7 to 9 for the contact of Shellsol 2325 or magnetic liquid containing Cyanex 272 or LIX 984N with water (time in s)

Condition	Run	$t_{50}$	$t_{p50}$	$t_{0.5}$	$t_{50}$	$t_{p50}$	$t_{0.5}$
		Cyanex 272			LIX 984N		
Shellsol 2325 (no magnet)	1-4	Not reached	392	592	372.1	222	572
	5-8		292	Not reached	Not reached	362	582
	9-12		412	Not reached		422	582
Shellsol 2325 (with magnet)	1-4		392	592		322	Not reached
	5-8		312	572		372	Not reached
	9-12		492	542		302	592
Magnetic liquid (no magnet)	1-4		Not reached	Not reached		572	582
	5-8		Not reached	592		Not reached	Not reached
	9-12		592	Not reached		Not reached	592
Magnetic liquid (with magnet)	1-4	22.2	22	212		62.1	52
	5-8	12.1	12	172	52.1	52	262
	9-12	32.1	32	222	62.1	52	322
p-value		-	0.00065 <sup>a</sup>	0.00006 <sup>b</sup>	-	0.00218 <sup>a</sup>	0.00013 <sup>c</sup>

<sup>a</sup> excluding magnetic liquid without magnet

<sup>b</sup> excluding Shellsol 2325 without magnet and magnetic liquid without magnet

<sup>c</sup> excluding Shellsol 2325 with magnet and magnetic liquid without magnet

### 3.3.2.3 Rate of phase separation using UV-visible absorbance measurements for Shellsol 2325 or magnetic liquid containing Cyanex 272 or LIX 984N and contacted with a metal ion solution **C1** or **L1**

When the extractant in Shellsol 2325 or magnetic liquid is added to the metal ion solution, **C1** or **L1**, the time required for phase separation decreases as compared to that when the organic phases are contacted with pure water. This is shown in Figs 20 and 21 for Cyanex 272 and LIX 984N, respectively. After extraction, the neutral, less polar metal extractant complex may be more stable in the organic carrier diluent which promotes more rapid phase separation.

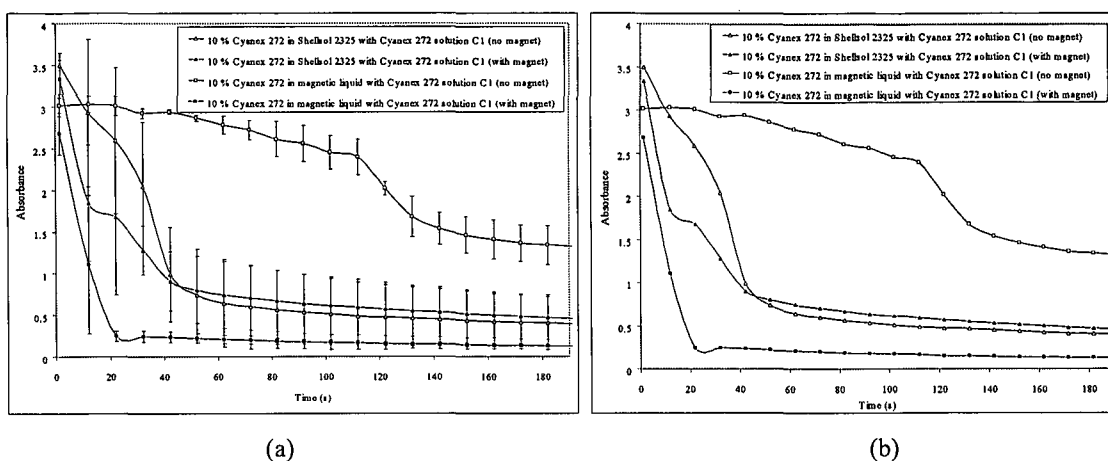


**Figure 20** Mean settling times for 10 % Cyanex 272 in Shellsol 2325 and magnetic liquid contacted with solution C1 (see solution composition in Table 2) (a) with the 95 % confidence intervals and (b) without the error bars for clarity

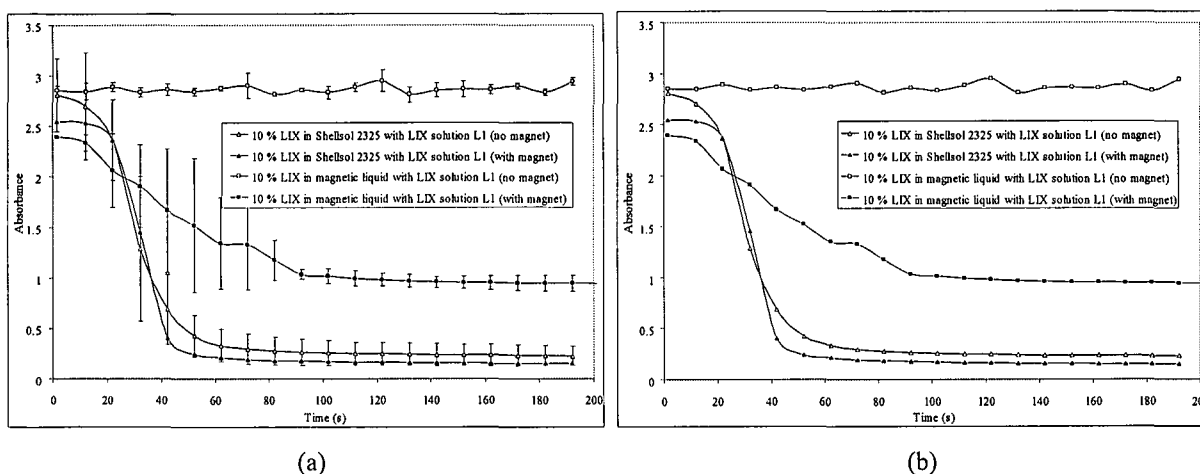


**Figure 21** Mean settling times for 10 % LIX 984N in Shellsol 2325 and magnetic liquid contacted with solution L1 (see solution composition in Table 4) (a) with the 95 % confidence intervals and (b) without the error bars for clarity

Various p-values were determined for Shellsol 2325 and the magnetic liquid with extractant (with and without the magnet). These data are reported in Table 13. Visually it appears from Figs 20 and 21 that the Shellsol 2325 system exhibits faster phase separation. However, the variety of p-values determined for the different conditions (with the exception of the two values highlighted in Table 13) did not show a statistically significant difference in data. It was noticed, during these last tests that the mixing in this system resulted in bubble formation. (The magnetic liquid also coats the sides of the plastic ICP tube but this contributes to a lesser extent.) As a result of the bubble formation, although the bulk of the phase has separated, the UV-visible spectra may report inflated absorbances. An alternative method, namely, the inductance measuring device used in Procedure 5 is not influenced by these factors and it was decided to repeat these studies using this device. The results will be discussed in the subsequent section.

**Table 13** Mean settling times,  $t_{50}$ ,  $t_{p50}$  and  $t_{0.5}$  as given by eqs 7 to 9 for the contact of Shellsol 2325 or magnetic liquid containing Cyanex 272 or LIX 984N with metal ion solutions C1 and L1, respectively (solution compositions are given in Tables 2 and 4 and time is in s)

Condition	Run	$t_{50}$	$t_{p50}$	$t_{0.5}$	$t_{50}$	$t_{p50}$	$t_{0.5}$
		Cyanex 272			LIX 984N		
Shellsol 2325 (no magnet)	1-4	22	12	182	32	32	122
	5-8	42	32	102	42	32	102
	9-12	42	42	122	42	32	82
Shellsol 2325 (with magnet)	1-4	12	12	Not reached	42	42	92
	5-8	32	32		32	32	82
	9-12	22	12		42	42	82
Magnetic liquid (no magnet)	1-4	172	112	182	No separation observed over the measurement time		
	5-8	142	122	Not reached			
	9-12	182	112	Not reached			
Magnetic liquid (with magnet)	1-4	22	22	32.075	92	82	142
	5-8	12	12	72.1	52	42	152
	9-12	12	12	92.05	52	32	112
p-value		0.09891 <sup>a</sup>	0.39730 <sup>a</sup>	0.07867 <sup>b</sup>	0.09540 <sup>a</sup>	0.34561 <sup>a</sup>	<b>0.02926<sup>a</sup></b>
		0.05534 <sup>b</sup>	0.23056 <sup>b</sup>		0.12397 <sup>b</sup>	0.26034 <sup>b</sup>	0.11606 <sup>b</sup>
		0.37404 <sup>c</sup>	0.67854 <sup>c</sup>		0.12392 <sup>d</sup>	0.44094 <sup>d</sup>	<b>0.01594<sup>d</sup></b>

<sup>a</sup> excluding magnetic liquid without magnet

<sup>b</sup> excluding Shellsol 2325 with magnet and magnetic liquid without magnet

<sup>c</sup> excluding Shellsol 2325 without magnet and magnetic liquid without magnet

<sup>d</sup> excluding Shellsol 2325 and magnetic liquid without magnet

### 3.3.3 Rate of phase separation using inductance measurements (Procedure 5)

The device manufactured for the measurement of inductance and used to obtain a comparative estimate of phase separation to that obtained using UV-visible measurements is shown in Fig. 22. A schematic illustration of this measurement method is given in Fig. 23 while the details of the principle of operation are described in the appendix. After agitation, the emulsified organic/aqueous sample for measurement is placed concentric to a coil through which an electric current flows thus generating a magnetic field. As the phases separate, the current induced in the coil by the magnetic phase decreases as it settles out of range of the coil and in this way it can be determined once the phases have separated. Although the formation of bubbles after mixing may affect the inductance measurement slightly, the measurements will not be affected as significantly as for the UV-visible measurements because the magnetic component in the bubble is small. Therefore, the contribution to the flux density will be negligible.

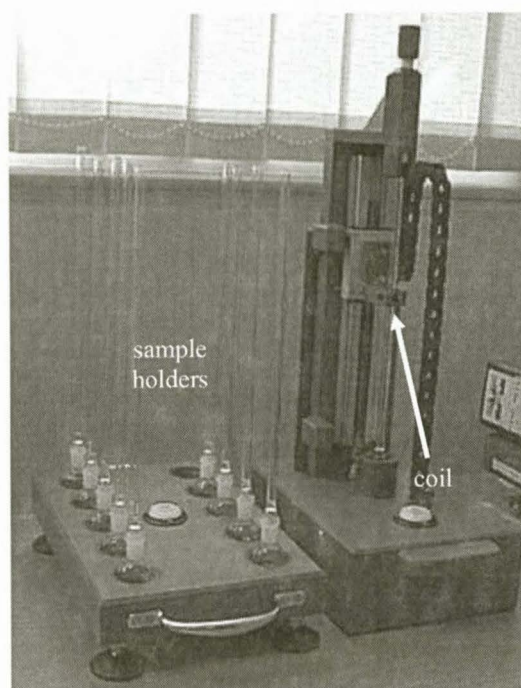


**Figure 22** Inductance unit used for the determination of relative rates of organic/aqueous phase separation

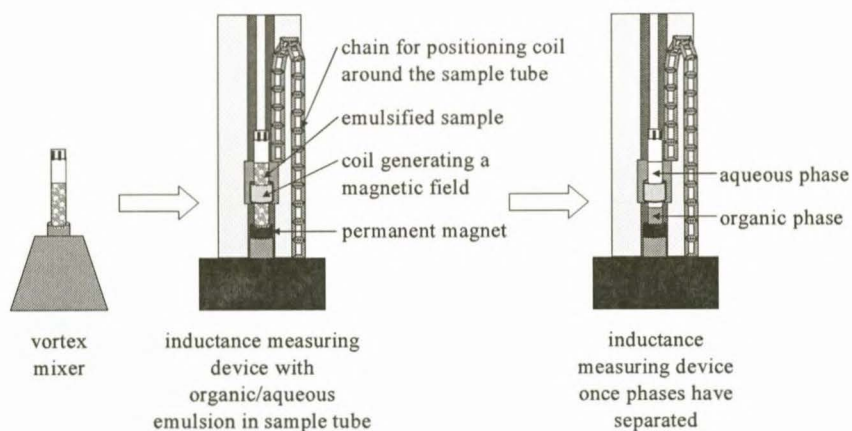
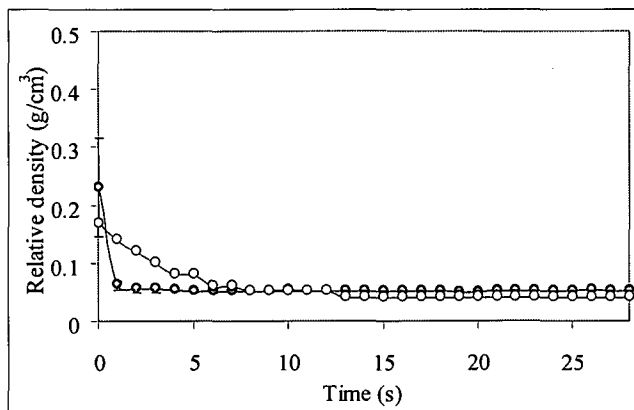


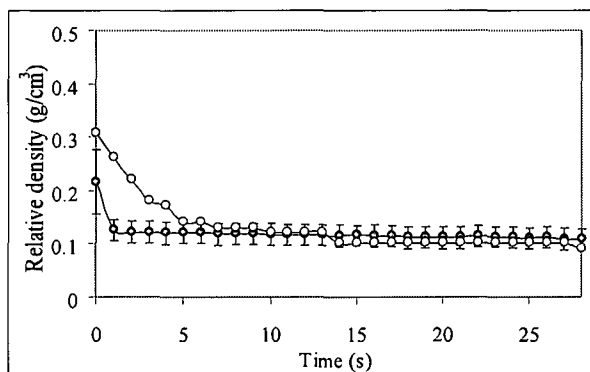
**Figure 23** Schematic illustration of method of determining phase separation using the inductance measuring device: after mixing, the emulsified sample is placed concentric to a coil through which a current flows thereby generating a magnetic field. As the phases separate, the current induced in the coil by the magnetic phase decreases as the magnetic phase settles out of range of the coil.

A magnetic liquid sample both with and without Cyanex 272 or LIX 984N extractants was contacted with various aqueous phases with or without the influence of a magnetic field (the permanent magnet in the setup in Fig. 23 can be removed as required). The inductance device measured the change in relative density with time of the magnetic liquid mixture (corresponding to the rate of phase separation) and the data are given in Figs 24 (a) to (g). It can be seen that the relative density decreases more rapidly when a magnetic field is applied to the magnetic liquid than

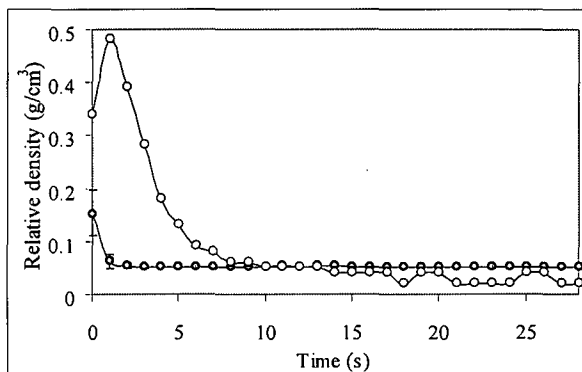
when no field is applied. Confidence intervals are indicated for the phase separation with the magnet as four replicates (repeated five times each) were used. Only single measurements were performed for the phase separation without the influence of the external magnetic field and no confidence intervals are indicated for these data.



(a)

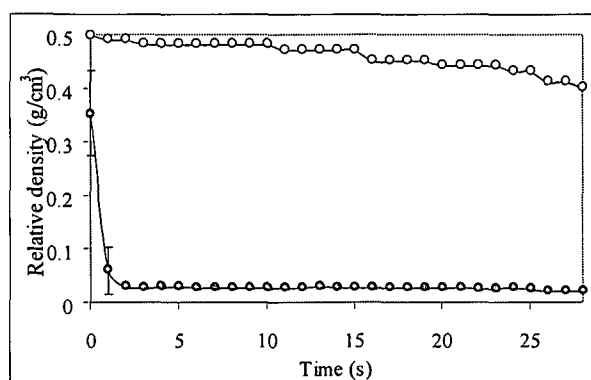


(b)

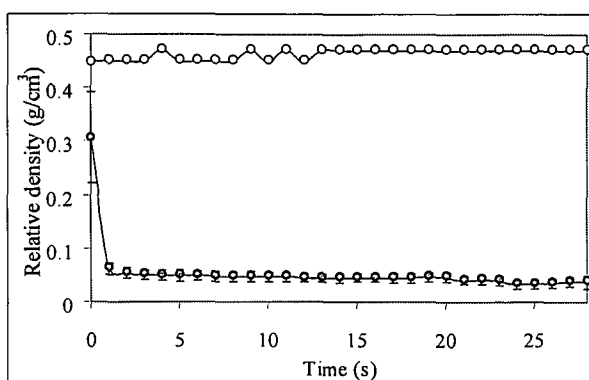


(c)

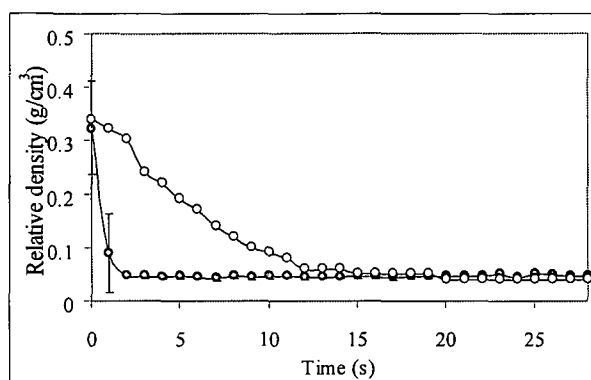
**Figure 24** Phase separation indicated by change in relative density for magnetic liquid with (a) water, (b) Cyanex 272 metal ion solution C1 and (c) LIX 984N metal ion solution L1 with the application of a magnetic field (◐) and without the magnetic field (◑). C1 and L1 solution compositions are given in Tables 2 and 4.



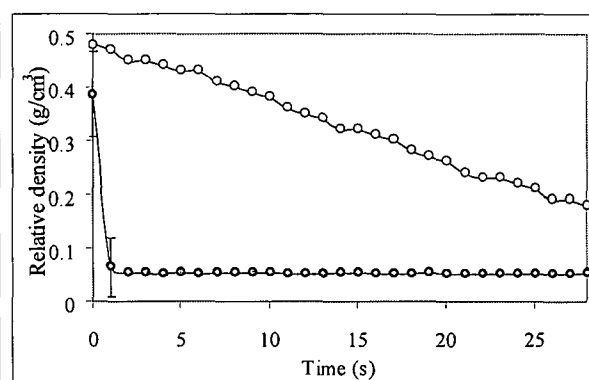
(d)



(e)



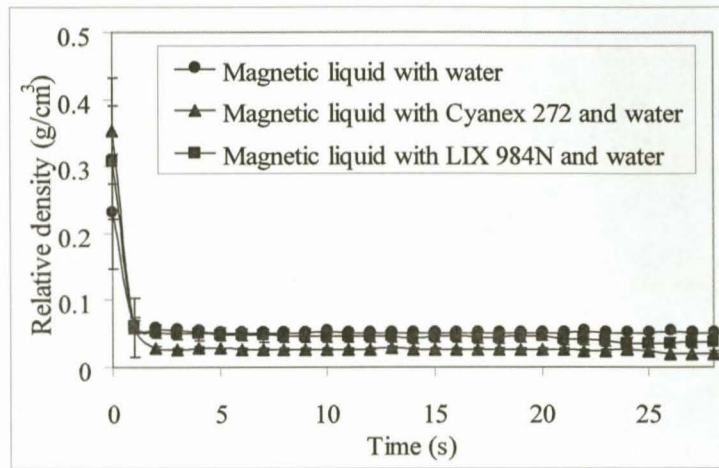
(f)



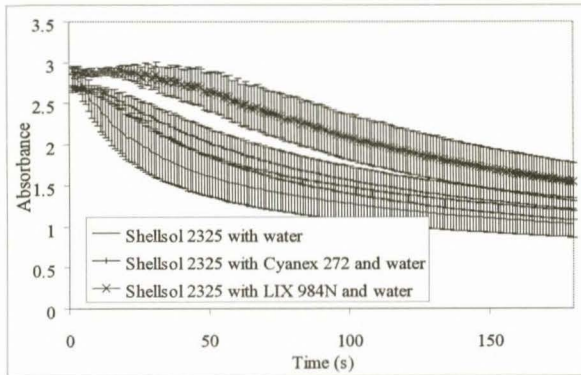
(g)

**Figure 24 (cont.)** Phase separation indicated by change in relative density for magnetic liquid with (d) Cyanex 272 extractant and water, (e) LIX 984N extractant and water, (f) Cyanex 272 extractant and Cyanex 272 metal ion solution C1 and (g) LIX 984N extractant and LIX 984N metal ion solution L1 with the application of a magnetic field ( $\bullet$ ) and without the magnetic field ( $\circ$ ). C1 and L1 solution compositions are given in Tables 2 and 4.

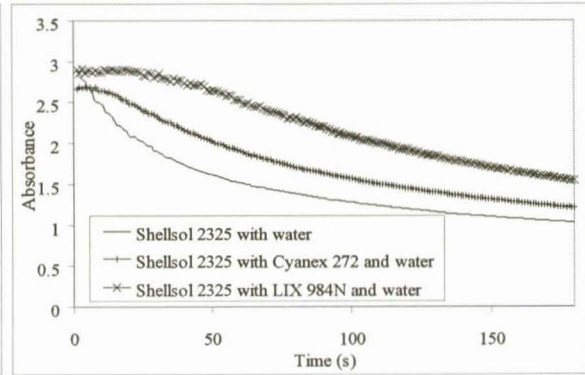
Figs 25 to 27 (a) give the settling rates (relative densities from inductance measurements) for the magnetic liquid system and 25 to 27 (b) and (c) give the settling rates (comparative absorbances from UV-visible spectra) for the Shellsol 2325 system under the same conditions, i.e., same volumes of liquids, agitation times, etc.



(a)

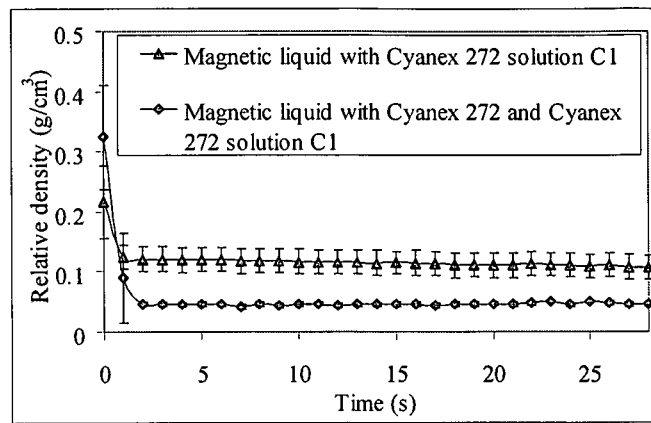


(b)

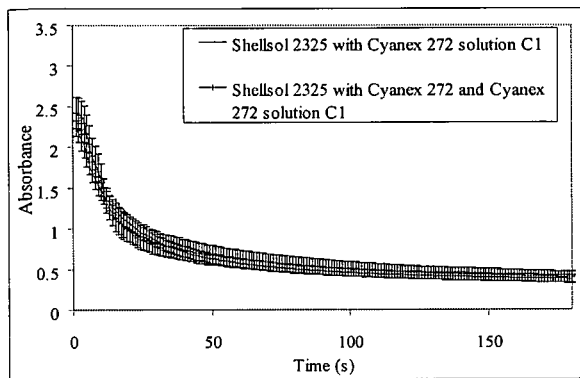


(c)

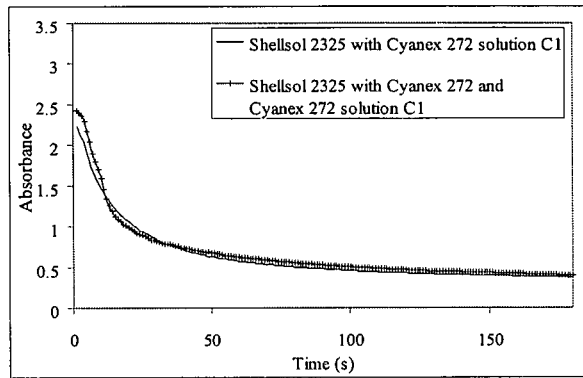
**Figure 25** Settling rates in terms of (a) relative densities for the magnetic liquid system and (b) absorbances for the Shellsol 2325 system with water, Cyanex 272 extractant and water and LIX 984N and water and (c) excluding confidence intervals for clarity



(a)

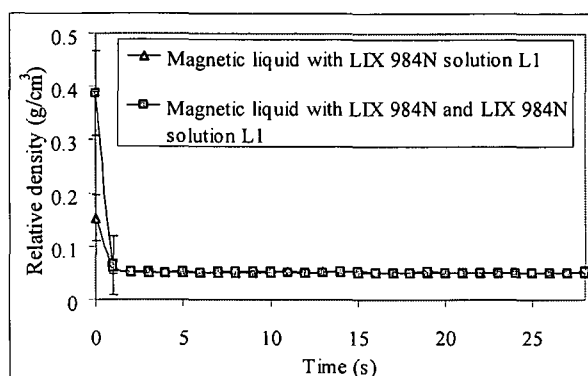


(b)

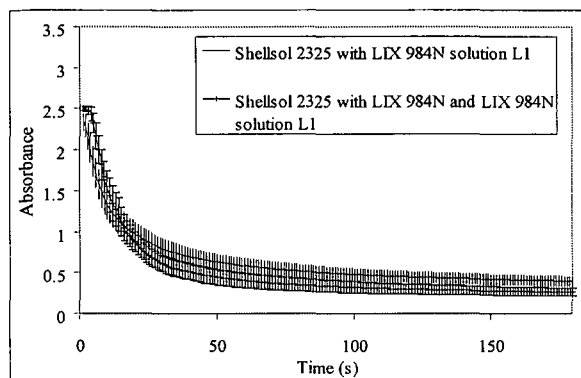


(c)

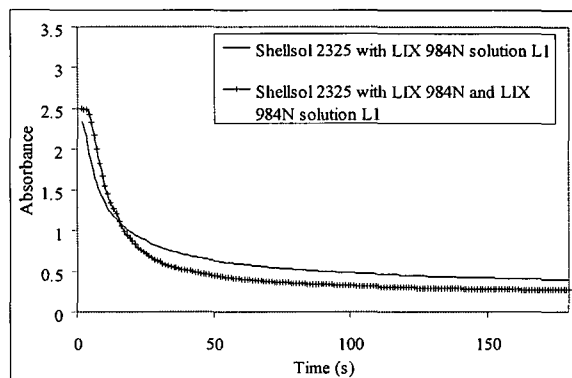
**Figure 26** Settling rates in terms of (a) relative densities for the magnetic liquid system and (b) absorbances for the Shellsol 2325 system with Cyanex 272 metal ion solution C1 (see solution composition in Table 2) and Cyanex 272 extractant and Cyanex 272 metal ion solution C1 and (c) excluding confidence intervals for clarity



(a)



(b)



(c)

**Figure 27** Settling rates in terms of (a) relative densities for the magnetic liquid system and (b) absorbances for the Shellsol 2325 system with LIX 984N metal ion solution L1 (see solution composition in Table 4) and LIX 984N extractant and LIX 984N metal ion solution L1 and (c) excluding confidence intervals for clarity

It can be seen from Table 14, which compares the time conditions for phase separation from the data in Figs 25 to 27 ( $t_{50}$ ,  $t_{p50}$  and  $t_{0.5}$  for the extractants and aqueous phases in different combinations using inductance for the magnetic systems and UV-visible absorbance for the non-magnetic systems), that the separation is fastest for the system of the magnetic liquid with magnet by up to 99 % (based on the  $t_{0.5}$  values). The  $t_{50}$  values indicate that, in general, the rate of phase separation decreases when the extractant is added to the organic phase in contact with water but increases again once the metal ion solution is used. As mentioned previously, this is most likely as a result of the interaction of the slightly polar organic extractants in the organic phase with water. However, after contact with the metal ion solutions, the less polar metal organic complex is stabilised more in the organic phase than in the more polar aqueous phase allowing for more rapid phase separation.

**Table 14** Mean separation times for organic phase with extractants and aqueous phases in various combinations

Condition	$t_{50}$	$t_{p50}$	$t_{0.5}$	$t_{50}$	$t_{p50}$	$t_{0.5}$	$t_{50}$	$t_{p50}$	$t_{0.5}$	% change in separation <sup>a</sup>
	Magnetic liquid (with magnet)			Magnetic liquid (without magnet)			Shellsol 2325 (without magnet)			
Water	1	1	2	44	4	7	74	13	56	96
Cyanex 272 metal ion solution C1	28	1	2	14	3	6	19	9	43	95
LIX 984N metal ion solution L1	1	1	2	6	5	9	7	8	39	95
Cyanex 272 extractant and water	1	1	3	63	51	568	145	2	105	97
LIX 984N extractant and water	1	1	2	NR	163	164	NR	29	159	99
Cyanex 272 extractant and Cyanex 272 metal ion solution C1	1	1	3	9	6	44	14	10	1	-67 <sup>b</sup>
LIX 984N extractant and LIX 984N metal ion solution L1	1	1	3	28	21	574	1	10	33	91

NR: Not reached

<sup>a</sup> Based on the  $t_{0.5}$  values, for the magnetic liquid with magnet and the Shellsol 2325 without magnet<sup>b</sup> Negative percentage occurs because the difference in phase separation times,  $t_{0.5}$ , is only 2 seconds.

#### 4. General discussion and conclusions

##### 4.1 Metal ion extraction

The magnetic and non-magnetic extraction systems showed similar percentage metal ion extractions throughout. In the mixer-settler system, the extraction of Co(II) by the Cyanex 272 was in the range of 60 – 75 %, Zn(II) by D2EHPA 42 – 56 % and Cu(II) by LIX 984N 68 – 78 %, with the magnetic liquid Cyanex 272 and LIX 984N systems showing a lower extraction and the D2EHPA showing a higher percentage extraction than the Shellsol 2325 system. The difference in extraction observed when using the different extractants could be as a result of the interaction of the extractant molecules with the magnetite surface or the coating in a complex, and, as yet not understood, mechanism. Extraction selectivities were similar for these tests.

Extractions by D2EHPA from the buffered mixed metal ion solutions were similar for the magnetic and non-magnetic systems. The individual metal ion solutions, Ca(II), Co(II), Cu(II), Ni(II) and Zn(II), however, showed a variation for the buffered and unbuffered systems. In the magnetic liquid system this is expected to occur as a result of the magnetite which may neutralise the  $H^+$  ions liberated during extraction thereby promoting further extraction. The Shellsol 2325 system shows an increase in metal ion extraction for the buffered system where liberated  $H^+$  can be neutralised thereby increasing the percentage metal ion extracted. In the unbuffered solutions, the pH decreases upon liberation of  $H^+$  ions by the D2EHPA thereby limiting further extraction.

In the Cyanex 272 buffered system, extraction and selectivity increase by 10 – 20 % with an increase in pH from 5 – 6. The higher pH solutions allow for increased neutralisation of liberated  $H^+$  thereby increasing extraction. An increased O/A ratio results in an increased extraction of the primary and secondary metal ions with no change in selectivity. In an unbuffered solution (water), the magnetite surface becomes protonated with liberated  $H^+$  and is able to act as a type of buffer while the Shellsol 2325 system shows no increase in extraction with increased O/A ratio as liberated  $H^+$  ions cannot be neutralised.

The LIX 984N buffered solution shows no change in extraction between a buffered pH 4 and water solution indicating that the extraction is not pH sensitive. With an increase in O/A ratio, there appears to be an increased extraction of both primary and secondary metal ions, however, in this system, leached magnetite affected absorbance readings and the results are inconclusive. The use of UV-visible absorbance is therefore not recommended for extraction studies involving Co(II) and ICP-AES analysis would be a more accurate analysis tool.

Close to maximum metal ion extraction into the organic phase for all three extractants and magnetic and non-magnetic systems occurs within approximately 10 minutes. With a further 20 days contact time, the magnetic LIX 984N system showed an increased extraction of all metal ions, very possibly as a result of adsorption of the ions into magnetite pores.

#### *4.2 Rate of phase separation*

Investigations into the rate of phase separation using the magnetic liquid systems showed very promising results with an improved rate of phase separation being exhibited for the magnetic liquid system:

- In the conventional mixer-settler system, phase separation was found to improve by 48 – 86 % for the magnetic liquid system.
- Using UV-visible absorbance measurements, it was found that there is a greater than 80 % increase in phase separation for the magnetic liquid in contact with water and the magnetic liquid containing Cyanex 272 or LIX 984N in contact with water when an externally applied magnetic field is used to effect separation. There was no statistically significant difference in extractions when the extractants in organic carriers were contacted with solutions containing metal ions for extraction. This could be as a result of the experimental setup and owing to the fact that bubble formation occurs in the magnetic liquid system which influences the UV-visible absorbances. Inductance measurements were therefore used to further investigate the phase separation rate.
- The inductance measuring device (for the measurement of phase separation of the magnetic liquid systems) as compared to the phase separation by the non-magnetic system using the diode array UV-visible spectrometer showed an increased phase separation by the magnetic liquid systems by up to 99 % with only

one case where the phase separation time was slower by 2 s (magnetic liquid with Cyanex 272 extractant and Cyanex 272 metal ion solution C1).

In the conditions investigated here, the use of the magnetic liquid system promotes rapid phase separation without loss of extraction ability or selectivity. Its use in an extraction processes would have to be carefully determined depending on the requirements and bearing in mind that the system may behave differently from conventional solvent extractant diluents as a result of the amphoteric magnetite surface charge (as was observed especially in the buffered systems). Consideration of the optimal use of a magnetic liquid as a diluent would not be unlike the considerations that must be borne in mind when using diluents containing aromatics. Such diluents have shown to associate the extractant itself or influence selectivity through interaction with the metal-extractant complex in the organic phase<sup>3</sup>.

A disadvantage of the magnetic solvent extraction system as seen from the UV-visible absorbance studies is that there is a possibility that the magnetic liquid will be unstable over time and magnetite may become suspended in the aqueous phase. In addition, in certain preliminary investigations, the formation of a relatively stable emulsion was observed if the O/A ratio was too low (this emulsion could be broken up by increasing the aqueous phase volume). Finally, because magnetite is soluble at pHs lower than approximately 4<sup>18</sup>, there is a limitation as to its chemical compatibility with various process streams which operate at a pH outside the stability region for magnetite. Cyanex 272 and LIX 984N which operate under higher pH conditions may therefore be more favourable for magnetic liquid solvent extraction processes. The resistance of the magnetite and magnetic liquid, however, to various common reagents, e.g., acids, may be limited<sup>18</sup>, particularly in view of the fact that strong acids, e.g. 1800 g l<sup>-1</sup> H<sub>2</sub>SO<sub>4</sub>, are used for stripping of the organic phases. In Chapters 6 and 7, steps have been taken to improve the resistance of the magnetite to acidic media.

## Appendix

### *Principle of operation of inductance measuring device*

The principle of operation of the inductance measuring device as used to determine relative rates of phase separation (Section 3.3.3) is described here. An electric current ( $I$ ) flowing through a coil generates a magnetic field in the area enclosed by the coil. The inductance of the coil ( $L$ ), is dependent on the flux density ( $B$ ), the number of turns per unit length ( $n$ ) and the volume enclosed by the coil ( $V$ ):

$$L = \frac{BnV}{I} \quad (10)$$

The total flux density when a magnetic liquid is placed inside such a coil is the sum of the flux densities of the magnetic component of the magnetic liquid magnetite (of volume fraction  $m$ ), the carrier fluid in which the magnetic particles (of volume fraction  $c$ ) are suspended and the air between the sample and the coil (of volume fraction  $a$ ):

$$B_{total} = B_{magnetite} + B_{carrier\ fluid} + B_{air} \quad (11)$$

$B = \mu nI$  (where  $\mu$  is the magnetic permeability) and eq. 11 can therefore be written as:

$$B_{total} = nI(m\mu_{magnetite} + c\mu_{carrier\ fluid} + a\mu_{air}) \quad (12)$$

The magnetic permeability of air and kerosene is approximately  $1.26 \times 10^{-6} \text{ H m}^{-1}$  as compared to approximately  $1.26 \times 10^{-4} \text{ H m}^{-1}$  for magnetite and the last two terms can therefore be disregarded. Eq. 12 reduces to:

$$B_{total} \cong nI(m\mu_{magnetite}) \quad (13)$$

By combination of eqs 10 and 13,

$$L = n^2 V m \mu_{magnetite} \quad (14)$$

$n$ ,  $V$  and  $\mu_{magnetite}$  are constants and only  $m$  contributes to the inductance, i.e.,  $L \propto m$ .

Variations in the inductance of a coil,  $L$ , (induced by variations in the volume of magnetic material in a sample internal to the coil,  $m$ ) will result in a resonance frequency shift in an oscillator circuit. This allows one to obtain an indication of the change of magnetic material over the length of a tube and can be related to the density of a sample. Calibration could be performed to obtain absolute densities, but, for example in the application of interest which is to determine phase separation, the determination of the presence or lack of magnetic material at a specific point in the tube will be sufficient to determine whether or not phase separation has taken place. Densities are therefore reported as relative densities, i.e., the density relative to the original density at time  $t = 0$  s is plotted.

## References

1. Rosensweig, R. E., *Ferrohydrodynamics*. Cambridge University Press, Cambridge, 1985.
2. Buske, N.; Sonntag, H.; Götze, T., *Colloids Surf.* 1984, **12**, 195.
3. Cox, M., *Liquid-liquid extraction* Ullmann's Encyclopedia of Industrial Chemistry 1988, **B3**, 6-43.
4. Cognis Corporation, Ion Transfer Technology Aliquat@336, [www.cognis.com](http://www.cognis.com).
5. Kunin, R.; Winger, A. G., *Angew. Chem., Int. Ed.* 1962, **1**, 149 - 155.
6. Mallinckrodt Baker Inc, Kerosene (low odor) material safety data sheet MSDS number K2175, 2003.
7. Hwang, J. Y., US Patent 5 043 070, 1991.
8. Palyska, W.; Chmielewski, A. G., *Sep. Sci. Technol.* 1993, **28**, 127.
9. Cole, P. M.; Sole, K. C., *Mineral Processing and Extractive Metall. Rev.* 2003, **24**, 91.
10. Cognis Corporation Mining Chemicals Technology Division, *MCT Redbook, Solvent extraction using Cognis Corporation liquid ion exchange reagents*.
11. Cytec Industries Inc., *Cyanex 272 Extractant* West Paterson, NJ, USA, 2005.
12. Cornell, R. M.; Schwertmann, U., *The iron oxides* VCH Publishers, New York, 1996.
13. Milonjic, S. K.; Kopenci, M. M.; Ilic, Z. E., *J. Radioanal. Chem.* 1983, **78**, 15.
14. Kosmulski, M., *J. Colloid Interface Sci.* 2004, **275**, 214.
15. Sun, Z.-X.; Su, F.-W.; Forsling, W.; Samskog, P.-O., *J. Colloid Interface Sci.* 1998, **197**, 151.
16. Wesolowski, D. J.; Machesky, M. L.; Palmer, D. A.; Anovitz, L. M., *Chem. Geol.* 2000, **167**, 193.
17. Parsonage, P., *Trans. Inst. Min. Metall. Sect. C: Mineral Process. Extr. Metal.* 1984, **93**, C37.
18. Pourbaix, M., *Atlas of electrochemical equilibria in aqueous solutions* Pergamon Press Ltd., Oxford, 1966.

## Chapter 6

### The preparation of silica-coated, diethylenetriamine functionalized magnetic nanoparticle ion exchangers

---

#### Abstract

Various methods of coating magnetite nanoparticles with silica were investigated in order to provide an acid-resistant shell around the magnetic core particles (which are otherwise soluble in acidic media) for their subsequent use in metal ion extraction. Stabilisation of particles with citric acid followed by two wet-method silica coatings using tetraethoxysilane improved the particles' acid resistance by 80 % compared to the bare magnetite. Attempts were made to further improve acid resistance through providing multiple silica coatings and through silica sintering, however, these techniques did not provide any significant improvement in terms of acid resistance. Silica-coated particles were functionalised with diethylenetriamine for use in metal ion extraction. Finally, a recommendation and preliminary calculations are made for an alternative method for dry coating of the magnetite which could lend itself more readily to scale-up of the magnetic ion exchanger synthesis.

#### 1. Introduction

Magnetite particles are soluble in slightly acidic aqueous solutions<sup>1</sup> at a pH < 4. This limits the operating window for use of magnetic liquids in solvent extraction as discussed in Chapter 5. In addition to improving the chemical stability and resistance of magnetite particles to acid attack, a coating of silica or other inert material may also prevent their aggregation in suspension. The silanol group on the surface may be useful for the covalent attachment of ligands to the surface of the coated nanoparticles providing functionalised silica-coated particles.

There are a number of examples where the properties of silica and magnetic particles have been combined for a specific application:

- Silica particles in which iron oxide was captured into the pores and onto which amino acid groups were introduced have been used for radionuclide separation from liquid wastes<sup>2</sup>.
- Magnetic silica particles have been used for the binding of proteins<sup>3</sup> or enzymes<sup>4</sup>, for DNA extraction<sup>5</sup> and as biocatalysts<sup>6</sup>.
- Magnetic particles have also been enclosed in a silica-gel matrix for high gradient magnetic separation processes<sup>7</sup>.

The aim of the work in this chapter is to provide the magnetite with a protective silica coating. This coating could be functionalised with an anion exchange ligand and the final particle used as an ion exchanger. Coated nanomagnetic

ion exchanger particles would be capable of providing a larger surface area compared to micron-sized ion exchanger particles typically used in applications such as metal ion extraction. This could allow for a modified approach to chemical processing. For example, the particles could extract metal ions in a stirred tank and be removed from suspension using a magnet, as opposed to the conventional packed column processing route where even micron-sized particles may yield large pressure drops across columns<sup>8,9</sup>.

Silica coating of the magnetite particles may proceed via a number of different routes, such as laser-induced pyrolysis of ferrocene and tetraethoxysilane (TEOS) aerosols<sup>10</sup>, through microemulsion systems in which micelles or inverse micelles are used to confine and control the coating of particles<sup>11</sup> and via a popular synthesis method, the Stöber process, where silica is formed via hydrolysis and condensation from a sol-gel precursor<sup>12</sup>. Processes such as pyrolysis are relatively complex and it may be difficult to separate the surfactant from a microemulsion system. For ease and simplicity, the liquid-based sol-gel process was selected for investigation.

Stöber *et al.*<sup>12</sup> investigated the synthesis of monodisperse suspensions of silica spheres in the colloidal size range via the hydrolysis (eq. 1) and condensation (eq. 2) of TEOS under alkaline conditions in ethanol<sup>13,14</sup>:



With overall stoichiometric reaction:



Recent models explain the chemical and physical growth of silica via two steps of nucleation and growth. Two models: that of monomer addition and controlled aggregation have been proposed. In monomer addition, there is an initial phase where nucleation takes place<sup>15-17</sup> followed by the addition of hydrolysed monomer to the silica surface. In controlled aggregation, nucleation occurs throughout the reaction<sup>14,17,18</sup> and a narrow size distribution is prepared by the aggregation of primary particles or nuclei with one another or with larger aggregates<sup>19</sup>. Chen *et al.* have proposed that the  $\text{Si}(\text{OH})_4$  does not actually take part in the silica growth or form silica particles directly, (according to eq. 2) but that an intermediate species  $\text{Si}_x\text{O}_y(\text{OH})_z$  deposits on the surface of silica particles or forms new particles depending on its concentration as indicated schematically<sup>15</sup> in Fig. 1.

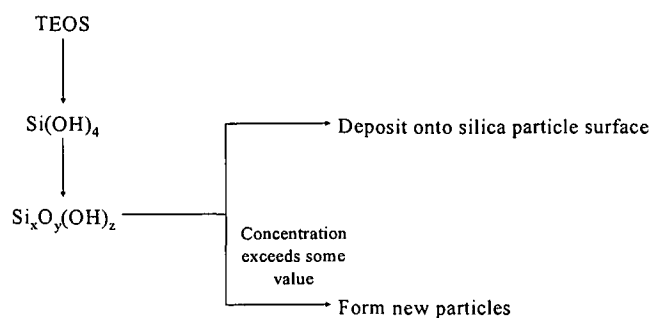


**Figure 1** Schematic<sup>15</sup> of proposed deposition of silica on existing particle surfaces or formation of new silica particles from  $\text{Si}_x\text{O}_y(\text{OH})_z$

Hydrolysis (eq. 1) with water alone is very slow and the reaction is therefore usually acid or base catalysed<sup>13</sup>. In acid-catalysed reactions, the condensation of silane groups produces chain-like or open-branched polymers which are considered to be gel phases and not particles. In base-catalysed reactions, a morphological catalyst results in internal condensation and cross-linking, producing spherical particles with an interior consisting of four silicon-oxygen bonds with hydroxyl groups attached to the surface of the particles<sup>13</sup>. We were interested in the precipitation of spherical particles and therefore selected the base-catalysed ammonium hydroxide solution system for the synthesis of the coated magnetite particles, which also helped protect the magnetite particles.

A variety of discussions have originated on the reaction mechanism and effect of various solution chemistry factors (such as concentration of TEOS, nature of alcohol solvent, initial water concentration and amount of ammonia catalyst present) that control the reaction kinetics and silica sphere diameter<sup>15, 20, 21</sup>. These parameters are important in determining the time before the initial nucleation of silica particles takes place and the subsequent particle growth rate<sup>13, 19</sup>.

In this chapter,

- Five methods (**Methods 1a-c, 2, 3, 4 and 5**, see Sections 2.2.1 to 2.2.5) for coating magnetite with silica (referred to as FeSi) were investigated and evaluated such that a simple, reproducible and most cost effective synthesis method can be established.
- Two of the more promising methods (**Methods 4 and 5**) were selected to further investigate the influence on FeSi synthesis of experimental parameters such as increased magnetite and varying volumes of ammonium hydroxide solution or ethanol.
- The FeSi resistance to dissolution in acid was determined and compared to potential improvements in terms of acid resistance through providing multiple silica coatings and through silica sintering.
- Finally, the functionalising of the FeSi particles with an anion exchange ligand, diethylenetriamine, and the resistance of this functionalised coated material (referred to as FeSiDETA) to acid dissolution are discussed.

## 2. Experimental

### 2.1 Reagents and analytical methods

All reagents and solvents were purchased from commercial sources and were used without further purification.  $\text{FeCl}_3 \cdot 6\text{H}_2\text{O}$ ,  $\text{FeSO}_4 \cdot 7\text{H}_2\text{O}$  and 25 %  $\text{NH}_4\text{OH}$  (all obtained from Merck) were used for the precipitation of magnetite. Ultrapure Milli-Q water ( $\text{MQ} > 18 \text{ M}\Omega$ ) was used for the preparation of aqueous solutions. Sodium silicate, tetraethoxysilane (TEOS), tetramethyl ammonium hydroxide (TMA), N'-(3-trimethoxysilylpropyl)diethylenetriamine (DETA) (all Aldrich) and citric acid (from Merck) were used for the coating and functionalising of the magnetite particles.

Transmission electron micrographs (TEM) were obtained using a JEOL 200CX and LEO EM912 electron microscope. Magnetic measurements were obtained on a SQUID magnetometer. Elemental compositions were determined by scanning electron microscopy energy dispersive spectrometry (SEM-EDS) using back scatter detection and an INCA Analyser. Fourier Transform Infrared (FTIR) spectra were recorded on a Nexus Nicolet Fourier Transform Infrared Spectrometer using dried powder dispersed in a KBr matrix and compacted as thin pellets or on a Nicolet Avator 330 FTIR using a ZnSe sample holder. Elemental analyses (Fe, C, H and N) were carried out by the Microanalytical Laboratory of the University College Dublin. Two replicates were obtained per sample. Thermogravimetric analysis (TGA) was performed using a Perkin Elmer TGA 7 unit. The chamber was purged with nitrogen at  $20 \text{ ml min}^{-1}$ . Fe concentrations in aqueous solutions were determined using an Inductively Coupled Plasma-Atomic Emission Spectrometer (Varian Liberty II ICP-AES) and a linear calibration method.

### 2.2 Coating of magnetite with silica

For a typical preparation of approximately 0.45 g magnetite, 1.05 g  $\text{FeCl}_3 \cdot 6\text{H}_2\text{O}$  and 0.54 g  $\text{FeSO}_4 \cdot 7\text{H}_2\text{O}$  were added to 25 ml water and the resultant solution heated to  $35 \text{ }^\circ\text{C}$ . 5 ml 25 %  $\text{NH}_4\text{OH}$  was added to the iron solution with rapid agitation. The resultant precipitate was stirred for 10 minutes and washed via magnetic decantation four times with 100 ml MQ water. This will be termed the 'standard magnetite procedure' (SMP).

Various different procedures have been reported for the coating of magnetite particles with silica<sup>4, 20, 22-26</sup>. Five types of methods have been grouped as follows:

- **Method 1a-c:** coating with sodium silicate alone (based on the methods of Atarashi<sup>22</sup>, Bruce<sup>23</sup> and Liu<sup>4</sup>),
- **Method 2:** coating with TEOS alone (based on the method of Taylor<sup>24</sup>),
- **Method 3:** coating with sodium silicate and TEOS (based on the method of Philipse<sup>20</sup>),
- **Method 4:** coating with TEOS after stabilising with citric acid (based on the method of van Ewijk<sup>25</sup>) and
- **Method 5:** coating with sodium silicate and TEOS after stabilising with citric acid (based on the method of Sun<sup>26</sup>).

### 2.2.1 Coating with sodium silicate alone

#### 2.2.1.1 Coating based on the method of Atarashi<sup>22</sup> (Method 1a)

Magnetite was prepared using two times the SMP and diluted to 1.4 g l<sup>-1</sup> with MQ water. Sodium silicate solution (1.5 mass %) was added dropwise to 169 ml of the suspension whilst controlling the pH between 8 and 11 (pH<sub>initial</sub> = 9.2, pH<sub>final</sub> = 10.3). The suspension was heated to 80 °C and washed with ethanol by magnetic decantation.

#### 2.2.1.2 Coating based on the method of Bruce<sup>23</sup> (Method 1b)

After magnetite preparation using two times the SMP, the pH was raised to 13 by the addition of TMA and diluted to 1.5 g l<sup>-1</sup> with MQ water (total volume 1.2 l). A Duolite C-26 ion exchange resin (Aldrich) was regenerated with 500 ml hot MQ water, 500 ml 3 M HCl and 500 ml MQ water at room temperature. 200 ml sodium silicate solution (1.12 mass % SiO<sub>2</sub>) was passed through the ion exchange resin and the first 20 and last 47 ml discarded. The pH of the retained solution was raised to 9.5 by the addition of a few drops of the original sodium silicate solution. 133 ml of this solution was added to the precipitate and stirred. The resulting mixture was titrated to pH 10 by the addition of 0.5 M HCl over 1 hour and then stirred for 2 hours. The suspension was stable and could not be separated on a magnet and so could not be washed with a mixture of TMA and ammonia solution.

#### 2.2.1.3 Coating based on the method of Liu<sup>4</sup> (Method 1c)

Magnetite was prepared using two times the SMP and diluted with MQ water to 600 ml after washing. Sodium silicate (1.17 mass % SiO<sub>2</sub>) was added to the magnetite which was ultrasonicated for 30 min before being heated to 80 °C. 0.5 M HCl was added dropwise to reduce the pH to 6.6. The mixture was washed with MQ water by magnetic decantation and dispersed in 50 ml methanol. Sample preparation for TEM analysis involved washing by magnetic decantation and resuspension in ethanol.

### 2.2.2 Coating with tetraethoxysilane based on the method of Taylor<sup>24</sup> (Method 2)

Two times the SMP was used to precipitate approximately 0.9 g Fe<sub>3</sub>O<sub>4</sub>. After washing, the supernatant of the suspension was removed by magnetic decantation and the magnetite added to 230 ml of a 10 % v/v TEOS solution and 200 ml ethanol. The pH was lowered to 4.6 by the addition of glacial acetic acid. The mixture was stirred and heated at 90 °C for 2 h under nitrogen. After cooling, the precipitate was washed two times each with 500 ml MQ water, 300 ml methanol and 500 ml MQ water.

### 2.2.3 Coating with sodium silicate and tetraethoxysilane, based on the method by Philippe<sup>20</sup> (Method 3)

Magnetite was prepared using two times the SMP, diluted to 1.4 g l<sup>-1</sup> by addition of 643 ml MQ water and the pH raised to 12.8 by the addition of TMA. A Duolite C-26 ion exchange resin was regenerated as described previously. 300 ml sodium silicate solution was passed through the ion exchange resin and the first 150 and last 20 ml discarded. The pH of the retained solution was raised to 9.5 by the addition of a few drops of the original sodium silicate solution. 31 ml of this solution was then added to 170 ml of the precipitate. The resulting mixture was

titrated to pH 10 by the addition of 0.5 M HCl over 1 hour and stirred for 2 hours. The sample was dialysed with TMA for 2 days. The solution was refreshed after 1 day. Owing to the expense of the TMA, the TMA was diluted approximately 50 % with 25 % ammonia solution. 11.5 ml of the suspension was added to 42 ml ammonia solution (25 %), 1 l ethanol and 1 ml TEOS and stirred for 1 day. 4, 8, 16 and 32  $\mu\text{l}$  TEOS were then added to four 10 ml samples.

#### *2.2.4 Coating with tetraethoxysilane after stabilising with citric acid, based on the method by van Ewijk<sup>25</sup> (Method 4)*

Twice the SMP was used to precipitate approximately 0.9 g  $\text{Fe}_3\text{O}_4$ . After washing, 500 ml 0.01 M citric acid solution was added to the magnetite suspension and TMA added to raise the pH to 7. The magnetite suspension concentration was approximately 1.8 g  $\text{l}^{-1}$ . 160 ml of the magnetite suspension was added to 268 ml ethanol, 72 ml MQ water and 18 ml ammonia solution (25 %). One day later, 0.4 ml TEOS and 0.7 ml TEOS were added to the suspension.

#### *2.2.5 Coating with sodium silicate and tetraethoxysilane after stabilising with citric acid, based on the method by Sun<sup>26</sup> (Method 5)*

The SMP was used to prepare a 2 g  $\text{l}^{-1}$  suspension of  $\text{Fe}_3\text{O}_4$  in water. After washing, the pH was adjusted to 3.2 by the addition of 0.1 M HCl. Citric acid (2.0 g in 250 ml MQ water) was added to the precipitate, while stirring, over 4 h. The final precipitate was washed by magnetic decantation 3 times and the final volume made up to 200 ml. 2 ml of this suspension was dispersed in 200 ml ethanol and 120  $\mu\text{l}$   $\text{Na}_2\text{O}\cdot\text{SiO}_2$  (0.22 wt %  $\text{SiO}_2$ ) was added to the ethanol under vigorous mechanical stirring. After 2 h, 4 ml MQ water, 1.4 ml 25 % ammonia solution and 50  $\mu\text{l}$  TEOS were added to the mixture. After 30 minutes, a further 250  $\mu\text{l}$  TEOS was added to the mixture. The mixture was stirred for 14 h before the precipitate was separated and washed by magnetic decantation four times.

TEM micrographs for a visual indication of the morphology and effectiveness of coating and FTIR spectra for information regarding particle composition were obtained for all syntheses.

### *2.3 Investigation into the effect of various experimental parameters on the silica coating of magnetite*

After preliminary investigations into the various different syntheses methods, a number of parameters were investigated in terms of their effect on the synthesis of FeSi particles using the citric acid stabilised methods (Methods 4 and 5). Decreased volumes of the initial sodium silicate solution, initial TEOS and water, ethanol and ammonia solution (decreased catalyst) as well as increased volumes of initial TEOS, citric acid stabilised magnetite and water, ethanol and ammonia solution (increased catalyst) were investigated using Methods 4 and 5 (summarised in Table 1).

For Method 4, magnetite prepared by the SMP was diluted to a final volume of 80 ml ( $5.6 \text{ g Fe}_3\text{O}_4 \text{ l}^{-1}$ ) with MQ water. To this volume, 320 ml 0.02 M citric acid solution was added. The pH was increased from pH 3 to pH 7 by addition of TMA to redisperse the precipitate. The final magnetite concentration was approximately  $1.1 \text{ g l}^{-1}$ . 4 ml volumes of this dispersion ( $\sim 4.5 \text{ g Fe}_3\text{O}_4$ ) were used for the parametric investigation.

For Method 5, the precipitate was diluted to  $\sim 2.3 \text{ g l}^{-1}$  with MQ water up to a final volume of 200 ml. The pH was adjusted to 3 by the addition of 0.5 M HCl. 250 ml of a 0.04 M citric acid solution was added to the magnetite suspension. After 2 h, the suspension was washed by magnetic decantation 3 times and made up to 200 ml with MQ water ( $\sim 2.3 \text{ g l}^{-1}$ ). 2 ml volumes of this dispersion ( $\sim 4.5 \text{ mg Fe}_3\text{O}_4$ ) were used for the parametric investigation (except for runs P1d and P2d where a 20 and 10 ml magnetite dispersion, respectively, i.e.,  $\sim 22.5 \text{ mg Fe}_3\text{O}_4$  was used for the tests).

Magnetite volumes were added to the ethanol and water and ultrasonicated before the ammonia solution and sodium silicate solution or TEOS addition. In the case where sodium silicate (0.27 mass %) was added, the first TEOS volume was added 4 hours after the sodium silicate was added. In all cases, the second TEOS volume was added a day after the first TEOS volume.

**Table 1** Volumes used to investigate the effect of various parameters on the silica coating with magnetite

	Run	Change	Fe <sub>3</sub> O <sub>4</sub> (ml)	EtOH (ml)	H <sub>2</sub> O (ml)	NH <sub>4</sub> OH soln (ml)	Sodium silicate ( $\mu\text{l}$ )	First TEOS coating (ml)	Second TEOS coating (ml)
Method 4	P1a	None	4	270	72	18	N/A	0.35	0.7
	P1b	TEOS X 3	4	270	72	18	N/A	1.07	2.1
	P1c	TEOS/3	4	270	72	18	N/A	0.12	0.2
	P1d	Fe <sub>3</sub> O <sub>4</sub> X 5	20	270	72	18	N/A	0.35	0.7
	P1e	H <sub>2</sub> O, NH <sub>4</sub> OH soln X 3	4	270	216	54	N/A	0.35	0.7
	P1f	H <sub>2</sub> O, NH <sub>4</sub> OH soln/3	4	270	24	6	N/A	0.35	0.7
Method 5	P2a	Increased EtOH	2	333	4	1.4	120	0.05	0.25
	P2b	TEOS X 3, increased EtOH	2	333	4	1.4	120	0.15	0.75
	P2c	TEOS/3, increased EtOH	2	333	4	1.4	120	0.045	0.08
	P2d	Fe <sub>3</sub> O <sub>4</sub> X 5, increased EtOH	10	333	4	1.4	120	0.05	0.25
	P2e	EtOH/1.5	2	200	4	1.4	120	0.05	0.25
	P2f	H <sub>2</sub> O, NH <sub>4</sub> OH soln X 3, increased EtOH	2	333	12	4.2	120	0.05	0.25
	P2g	H <sub>2</sub> O, NH <sub>4</sub> OH soln /3, increased EtOH	2	333	1.3	0.5	120	0.05	0.25

#### 2.4 Functionalisation of silica-coated magnetite particles with diethylenetriamine and 'medium' and 'large' scale synthesis

After results were obtained from the base case scale parametric studies for the functionalisation of the silica-magnetite particles, the scale on which the particles had originally been produced was tripled and the mass of magnetite added to the ethanol increased fivefold. Magnetite produced by the standard procedure was diluted to  $5.6 \text{ g Fe}_3\text{O}_4 \text{ l}^{-1}$  and 80 ml final volume. 1.05 g citric acid was dissolved in 320 ml water and added to the magnetite precipitate whilst stirring. The initial pH of 2.8 was raised to 7.5 by the addition of TMA to redisperse the precipitate. The final volume of 400 ml had a magnetite concentration of  $\sim 1.1 \text{ g l}^{-1}$ .

To determine whether the FeSiDETA synthesis could be scaled up (only approximately 15 mg FeSiDETA was produced using the preliminary syntheses methods), a 'medium' and 'large' scale synthesis of FeSiDETA was attempted for the synthesis of approximately 70 and 170 mg FeSiDETA, respectively. For FeSiDETA synthesis on a 'medium' scale, 60 ml of the magnetite suspension ( $\sim 70 \text{ mg magnetite}$ ) was added to 810 ml ethanol, 216 ml water and 54 ml ammonia solution (25 %) and stirred. 1.1 ml TEOS followed by 2.15 ml TEOS one day later was added to the suspension. After washing and drying at room temperature through evaporation of the solvent, 10.2 mg FeSi particles were resuspended in 105  $\mu\text{l}$  ethanol (5 – 10 ml solvent/g FeSi) before 5  $\mu\text{l}$  DETA was added to the FeSi particles (approximately 1.7 mmol DETA/g FeSi)<sup>27, 28</sup>. After 2 days the samples were washed by magnetic decantation and dried. For FeSiDETA synthesis on a 'large' scale, 150 ml of this magnetite suspension ( $\sim 170 \text{ mg magnetite}$ ) was added to 2.025 l ethanol, 540 ml water and 135 ml ammonia solution (25 %) and stirred. 2.65 ml TEOS followed by 5.35 ml TEOS one day later were added to the suspension. After washing and drying at room temperature through evaporation of the solvent, 60 mg FeSi particles were resuspended in 600  $\mu\text{l}$  ethanol (5 – 10 ml solvent/g FeSi) before 15  $\mu\text{l}$  DETA was added to the FeSi particles (approximately 1.7 mmol DETA/g FeSi)<sup>27, 28</sup>. After 2 days the samples were washed by magnetic decantation and dried. In general, for DETA functionalising, 10 ml solvent (ethanol) and 1.7 mmol DETA were added per gram of FeSi. Samples were left to stand in excess of 24 hours before magnetic washing with 80 % ethanol in MQ water.

#### 2.5 Multiple tetraethoxysilane coatings

In order to potentially improve the acid resistance of the FeSi particles, particles were coated with multiple silica layers. Magnetite prepared by the SMP was made up to  $5.6 \text{ g l}^{-1}$  by dilution to 80 ml. To this was added, whilst stirring, 1.05 g citric acid dissolved in 320 ml water. The pH (2.6) was raised to 7.0 to redisperse the precipitate by addition of TMA. The final volume (400 ml) contained  $\sim 1.1 \text{ g l}^{-1}$  magnetite.

20 ml magnetite suspension was added to 270 ml ethanol and 72 ml MQ water. The mixture was ultrasonicated before the addition of 18 ml ammonia solution (25 %). 0.36 ml TEOS was added with rapid stirring. One day later, 0.72 ml TEOS was added to the suspension. After 1 day, the FeSi suspension was washed with 150 ml ethanol by

magnetic decantation, dried and resuspended in 270 ml ethanol and 72 ml water using an ultrasonic bath. 18 ml ammonia solution (25 %) and 0.72 ml TEOS were added to the mixture. This was repeated two more times (5 TEOS coats in total).

### 2.6 *Silica-coated magnetite particle sintering*

Besides the multiple TEOS coatings, a second method was attempted to improve the acid resistance of the FeSi particles: that of sintering the silica coating on the magnetite surface. Sintering was performed in a TGA unit where a 7.0 mg sample was heated at 20 °C per minute from 45 °C to 920 °C in a chamber purged with nitrogen at 20 ml min<sup>-1</sup>. Mass loss was determined as a function of temperature, the sample was analysed by TEM and FTIR and its resistance to acid determined. TGA mass loss profiles were then used to estimate appropriate conditions for sintering in a vertical tube furnace. Sintering in the vertical tube furnace was performed at 800 and 1100 °C for 30 minutes after purging the furnace with argon.

### 2.7 *Resistance of silica-coated magnetite particles to acid*

The resistance of the silica-coated particles to acid was investigated by addition of 25 mg each of magnetite, FeSi and FeSiDETA to 10 ml of 0.5, 1, 2 and 3 M HCl for 30 minutes; 25 mg portions of multiply-coated and sintered FeSi (from the TGA and vertical tube furnace) was also added to 10 ml of the 0.5 M HCl solution. The supernatant was collected for Fe concentration determination by ICP-AES for estimation of the percentage magnetite dissolution.

## 3. Results and discussion

### 3.1 *Coating of magnetite particles with silica*

The selection of a method for the coating of the magnetite with silica was based on the following criteria:

- Morphology and extent of coating of particles from TEM micrographs
- Material composition from FTIR spectra
- Ease and cost of synthesis

#### 3.1.1 *Coating with sodium silicate or tetraethoxysilane alone (Methods 1a-c and Method 2)*

Methods 1a-c and 2 (no prior stabilisation of the magnetite) yielded magnetite particles approximately 10 nm in size embedded in an amorphous mass of silica (see Fig. 2). Isolated particles were not visible and the silica coating was very thin. The point of zero charge (PZC) of magnetite<sup>29-33</sup> is in the range of 6 to 8.5. If no stabilisation of the

magnetite occurs through coating with a surfactant, agglomeration of particles is possible. Silica will then coat the agglomerated magnetite core, which is believed to have happened in these cases, as shown by the TEM images (Fig.2).

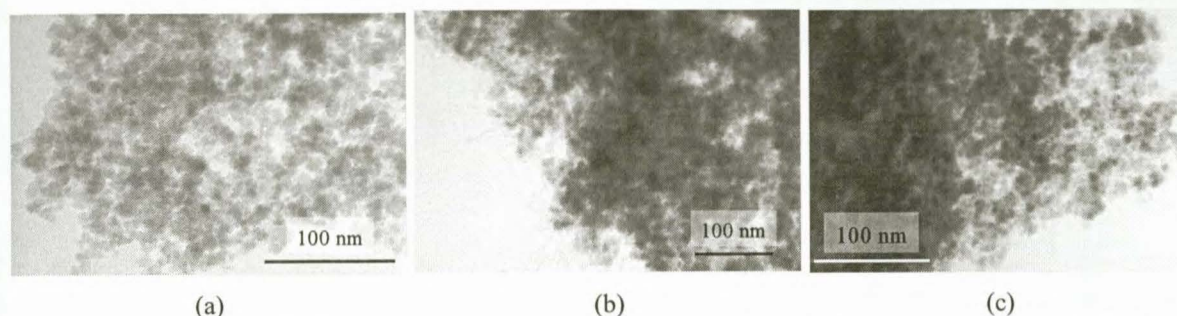


**Figure 2** FeSi particles produced by (a) Method 1a, (b) Method 1c and (c) Method 2 (where magnetite particles were coated with sodium silicate only)

### 3.1.2 Coating with sodium silicate and tetraethoxysilane alone (Method 3)

The coating of magnetite with sodium silicate followed by TEOS (Method 3) also appeared to result in the embedding of magnetite particles in a silica mass (Fig. 3 (a)) with isolated silica particles forming (Fig. 3 (b)). The PZC of silica<sup>31</sup> is 2.0 and providing the magnetite particles with an initial silica layer through coating with sodium silicate should result in a reduction in zeta potential. This corresponds to an increase in the coulombic repulsion between particles which should stabilise the particles before the second coating with TEOS. Dialysing with TMA should also provide repulsion between particles. Conditions were satisfactory for silica particle production as indicated by Fig. 3 (b) and it is therefore possible that insufficient tetramethyl ammonium hydroxide (TMA) was used during dialysis resulting in particle agglomeration before coating.

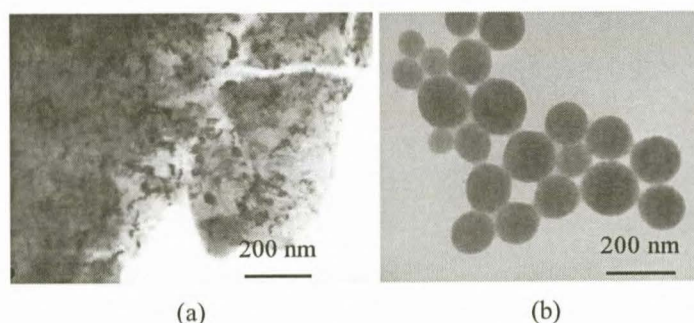


**Figure 3** (a) FeSi particles and (b) free silica produced by Method 3 (where magnetite particles were coated with sodium silicate and TEOS )

### 3.1.3 Coating with tetraethoxysilane after stabilising with citric acid (Method 4)

Method 4, which involved stabilising the magnetite with citric acid (which is believed to attach to the oxide surface by association to the surface hydroxyl groups of the citrate ions) before coating with TEOS, yielded more defined,

but still irregularly-shaped silica-coated particles, containing multiple magnetite particles at their centre. Adjacent particles appeared to have agglomerated in some cases. Two clear regions of different electron densities can be identified in the TEM micrographs (Fig. 4). The electron dense core corresponds to the magnetite particles while the less dense shell region is the silica coating.

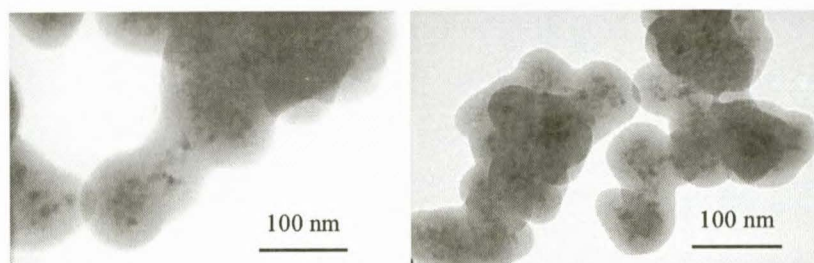


**Figure 4** FeSi particles produced by Method 4 (where magnetite particles were coated with TEOS after stabilising with citric acid)

The hydrolysis of TEOS and polymerisation of silica on the magnetite surface takes place in an alkaline ethanol/water system. At this pH, the PZC of the magnetite (6 to 8.5) is such that the uncharged magnetite surface is unlikely to provide an electrostatic repulsive force allowing the particles to be dispersed in the reaction mixture. Coating the particles with citric acid is expected to lower the solution pH and the coated magnetite PZC to approximately 3<sup>25</sup>. In this acidic suspension (pH = 2 - 3), the two free carboxyl groups of the citric acid (assuming just one citric acid carboxyl group is attached to the magnetite surface) are uncharged (pK = 4.30, 5.65) and since the coated magnetite particles bear no charge, flocculation may result. The addition of TMA raised the suspension pH to 7 so that the electrostatic repulsion of the now anionic citrate ions allowed for a stable suspension of magnetite coated particles<sup>34</sup>. These stable, isolated particles are clearly seen in the TEM micrograph (Fig. 5) of the citric acid-coated magnetite produced prior to silica coating. The citrate ion coating should inhibit nucleation, particle growth and agglomeration and assist in the formation of isolated FeSi particles upon further coating with silica, which appears to have happened using Method 4.

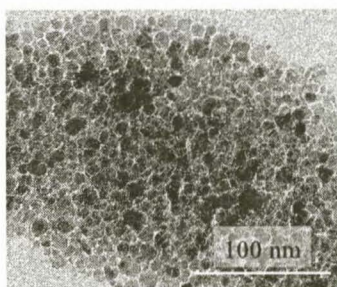


**Figure 5** Citric acid-coated magnetite prior to silica coating

The irregularly-shaped FeSi material in Fig. 4 appears to contain more than one magnetite particle at the core. According to van Blaaderen, particles grow via a reaction-limiting mechanism<sup>14</sup> with particle size increasing at the

same rate regardless of initial size. Therefore, if the magnetite particles used as initial seeds have a narrow size distribution and are not agglomerated, the resultant silica-coated particles should be monodisperse<sup>35</sup>. Coating with a preliminary surfactant, such as by coating with a silicic acid layer, is considered a necessary, but insufficient, condition for maintaining colloidal stability<sup>20</sup>. So, although the citric acid coating assists in providing stability to the magnetite, the magnetite may still agglomerate if the surface coating is incomplete (as may also occur if the magnetite particle concentration in suspension is too high). The resultant magnetite core seed may thus consist of more than one magnetite particle and grow to a final irregular shape<sup>20</sup> as is likely to have occurred in the sample in Fig. 4. For our application, a core containing several magnetic particles is no less desirable and in fact may be more beneficial than a single magnetic core as a lower magnetic field may be required for attraction of the particles.

It is assumed that the silica attaches itself to the magnetite surface in areas where no citric acid is present<sup>25</sup> as there are still surface hydroxyl groups available with which the alkoxy silanes condense to form Si-O-Si bonds. It is suspected that some agglomeration of the particles in Fig. 4 may have occurred as a result of oligomerisation of the silanol groups on adjacent particles. This reaction may occur as a competing reaction to the covalent binding of the silica to the magnetite surface.

#### 3.1.4 Coating with sodium silicate and tetraethoxysilane after stabilising with citric acid (Method 5)

Method 5, which involved the coating of citric acid stabilised magnetite particles with sodium silicate followed by TEOS, yielded particles similar in appearance (see Fig. 6), but of less uniform shape than those citric acid stabilised particles coated only with TEOS (Fig. 4).

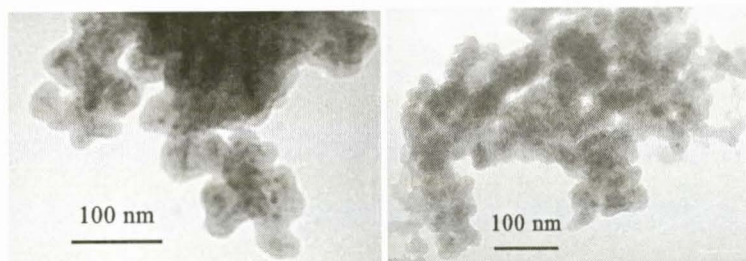


**Figure 6** FeSi particles produced by Method 5 (coating magnetite particles with sodium silicate and TEOS after stabilising with citric acid)

In summary then,

- Coating with sodium silicate or TEOS alone without prior stabilisation of the magnetite (Methods 1a-c and 2, respectively) tended to yield an unacceptably thin silica layer on the magnetite surface.
- Coating the magnetite with sodium silicate followed by TEOS also without prior stabilisation of the magnetite (Method 3) resulted in a magnetite-silica agglomeration.

- Citric acid stabilised magnetite that was coated with TEOS alone (Method 4) and that coated with both sodium silicate and TEOS (Method 5) yielded the most defined particles although the particles were irregularly-shaped. As a further advantage, this method was one of the simplest and most cost effective. Methods involving preparation of silicic acid by ion exchange and using TMA require greater amounts of preparation time and are more expensive.

It was therefore decided to continue investigations using Methods 4 and 5.

### 3.2 Parametric study for silica coating of magnetite using Methods 4 and 5 (stabilising with citric acid prior to coating with silica)

As mentioned previously, the reaction kinetics of silica deposition and the silica sphere diameter are controlled by the solution chemistry<sup>13, 19</sup>. A study was conducted to determine the effect of some of the reaction conditions (volumes of sodium silicate solution, TEOS, water, ethanol, ammonia solution and citric acid stabilised magnetite) on the synthesis of FeSi by Methods 4 and 5. Table 2 summarises the observed effects of the various parameters investigated on the formation of FeSi.

**Table 2** Effect of various parameters on the silica coating of magnetite

Run	Change	Observation
<b>Coating with TEOS after stabilising with citric acid (based on Method 4)</b>		
P1a	No change	Magnetite encapsulated in silica. Particles agglomerated extensively.
P1b	TEOS X 3	Magnetite not easily visible, large amorphous masses of silica visible.
P1c	TEOS/3	Encapsulated magnetite with less silica clustering visible (Fig. 7 (a)).
P1d	Fe <sub>3</sub> O <sub>4</sub> X 5	Easily visible magnetite enclosed in silica (Fig. 7 (b)).
P1e	Water, ammonia solution X3	Magnetite encapsulated in silica. Agglomeration of particles (Fig. 7 (c)).
P1f	Water, ammonia solution/3	Magnetite encapsulated in silica. Agglomeration of particles (Fig. 7 (d)).
<b>Coating with sodium silicate and TEOS after stabilising with citric acid (based on Method 5)</b>		
P2a	Increased EtOH	Magnetite particles with very thin silica coating.
P2b	TEOS X 3, increased EtOH	Magnetite particles with very thin silica coating. Empty silica particles formed.
P2c	TEOS/3, increased EtOH	Magnetite particles with very thin silica coating. Empty silica particles formed.
P2d	Fe <sub>3</sub> O <sub>4</sub> X 5, increased EtOH	Magnetite particles with very thin silica coating. Empty silica particles formed.
P2e	Ethanol/1.5	Magnetite encapsulated amorphous material. Similar in appearance to P1f (Fig. 8 (a)).
P2f	Water, ammonia solution X 3, increased EtOH	Empty amorphous silica formed (Fig. 8 (b)).
P2g	Water, ammonia solution/3, increased EtOH	Isolated silica particles and magnetite coated with a thin layer of silica (Fig. 8 (c)).

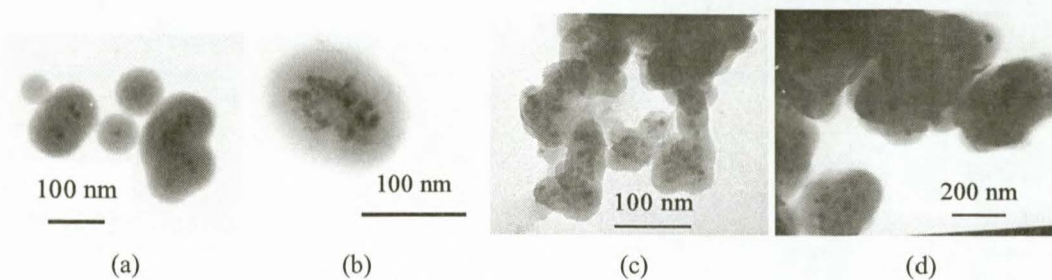


**Figure 7** FeSi particles from run (a) P1c, (b) P1d, (c) P1e and (d) P1f (see run descriptions in Tables 1 and 2)

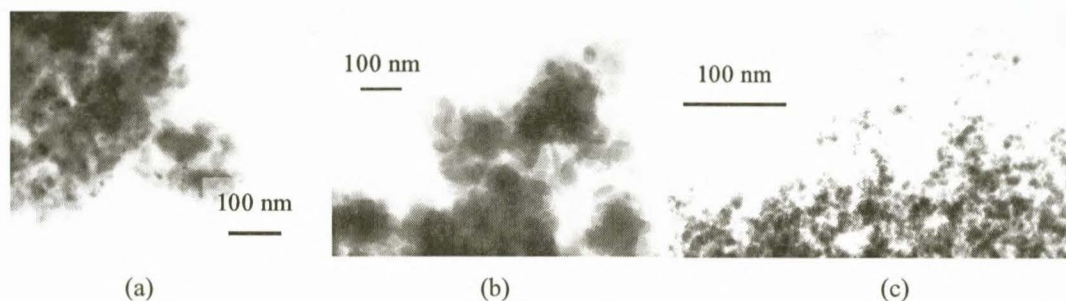


**Figure 8** FeSi particle from run (a) P2e, (b) P2f and (c) P2g (see run descriptions in Tables 1 and 2)

Although silica is not clearly identifiable in all TEM micrographs, FTIR confirmed the presence of a silica coating by characteristic IR absorbances for all particles prepared (see data in Table 3). The spectral region from 400 to 1300  $\text{cm}^{-1}$  usually corresponds to the absorption bands associated with iron oxide and silicon oxide networks<sup>36</sup>. All samples P1a-f and P2a-g (see descriptions in Tables 1 and 2) contain Si-O-Si as observed especially from the absorbance at  $\sim 1080 - 1090 \text{ cm}^{-1}$ .

**Table 3** FTIR data from parametric study indicating the presence of siloxane structures for runs P1a-f and P2a-g (see descriptions in Tables 1 and 2)

Max absorbances ( $\text{cm}^{-1}$ )						Assignment
P1a	P1b	P1c	P1d	P1e	P1f	
464	465	465	462	466	465	Bending of siloxane bridges Si-O-Si <sup>36,37</sup> and Fe-O <sup>37-39</sup>
1086	1089	1085	1080	1086	1082	Si-O-Si asym stretch <sup>36,38,40</sup> , Si-O <sup>40</sup> , Si-O-CH <sub>3</sub> or Si-O-R <sup>33,41</sup>
1637	1637	1637	1637	1637	1636	Si-OH, Fe-OH and water <sup>37-39,42</sup>
P2a	P2c	P2d	P2e	P2f	P2g	
451	451	450	452	466	452	Bending of siloxane bridges Si-O-Si <sup>36,37</sup> and Fe-O <sup>37-39</sup>
1079	1080	1082	1090	1089	1073	Si-O-Si asym stretch <sup>36,38,40</sup> , Si-O <sup>40</sup> , Si-O-CH <sub>3</sub> or Si-O-R <sup>33,41</sup>
1631	1634	1631	1631	1632	1631	Si-OH, Fe-OH and water <sup>37-39,42</sup>

From the experimental studies, an increase in initial TEOS added results in a large amorphous silica mass forming (run P1b), while a decrease in the initial TEOS added appears to result in more uniform particle formation (run P1c, Fig 7 (c)). Stöber *et al.* observed that smaller particles can be produced by decreasing the volume of TEOS<sup>12</sup> while Chen *et al.*<sup>43</sup> observed that the growth of monodisperse silica particles is controlled by the reaction of soluble condensed silica precursor species on the surface of existing silica particles: if the concentration of silica particles is low, particles of different size grow at the same rate. Thus, limiting the TEOS volume may limit the formation of new silica nuclei so offering greater control of particle morphology, i.e., silica will condense on the initial magnetite cluster that is present, with the cluster size and morphology determining the final FeSi particle size and morphology. With limited TEOS, the silica thickness of the final particle will be similar, regardless of the size of the nucleus.

It appears that an increase in magnetite concentration (run P1d, Fig 7 (b)) was beneficial to the formation of isolated and more uniformly sized FeSi particles. The larger volume of magnetite may have provided more nuclei centres or seeds for silica condensation. There appears to have been some magnetite agglomeration prior to condensation as the FeSi nuclei contain more than one magnetite particle.

Runs P1e and P1f (Figs 7 (c) and (d)) with varying water and ammonia solution volumes did not yield well-defined FeSi particles. Final particle size and size distribution is influenced by the silica surface potential and by the reaction medium ionic strength during growth<sup>14, 17</sup>, factors that are directly related to the concentration of ammonia and water. Ammonia affects the particle surface charge and resulting electrostatic particle interaction which affects intermediate particle colloidal stability<sup>14</sup> thereby influencing the particle morphology, size and size distribution. (In the absence of ammonia, irregularly-shaped flocs of silica form in the conventional Stöber synthesis.) For run P1e with the higher initial concentration of water and ammonia solution, smaller FeSi particles with a thin silica coating were formed. Increasing the ammonia concentration may provide the particles with a negative surface stabilising charge<sup>14</sup> through dissociation of silanol groups:



Because these particles (run P1e) are more stable, a smaller number of particles grow to a larger final size and the surface is smoother because more TEOS is available per particle<sup>14</sup>. For run P1f, with the decreased initial ammonia concentration, relatively large masses of amorphous silica were formed. At low water and ammonia concentrations, smaller particles are produced<sup>12</sup>, as is observed when comparing the TEM micrographs of runs P1e and f (Figs 7 (c) and (d)). The particles are stable and a larger number of particles therefore grow to a smaller final size with a rough surface because only a thin layer of TEOS is deposited on the particle<sup>14</sup>.

For runs P2a-g (with the exception of run P2e) where the ethanol volume was increased, the magnetite concentration as compared to the preliminary experiments was reduced from 20 to 13.5 mg l<sup>-1</sup> (with a volumetric ratio of magnetite to ethanol of 0.02 and 0.015, respectively). It is believed that reduced silica deposition occurs because

there are now fewer magnetite nuclei seeds in the more dilute suspension upon which initial silica deposition can take place. Silica particles were formed instead as silica condensed on silica seeds instead of on magnetite nuclei. Runs P2f and P2g (Figs 8 (b) and (c)) with increased and decreased ammonia solution, respectively, yielded amorphous silica alongside magnetite with a very thin silica coating partly as a result of the increased ethanol volume and reduced initial concentration of magnetite in the reaction mixture.

The initial water and catalyst concentrations have the largest influence on the rate of hydrolysis of the TEOS<sup>12</sup> with the reaction being first order with respect to the ammonia concentration and between first and second order with respect to the water concentration<sup>13</sup>. Increasing the water concentration relative to the ammonia concentration would promote a faster hydrolysis of TEOS<sup>19</sup>. Increasing the ammonia concentration relative to the water concentration would increase the initial nucleation rate<sup>19</sup> because the anion of the TEOS monomers hydrolysed by the ammonia and the ammonium cation itself are less soluble resulting in nucleation of silica particles (see eq. 4). In cases P1e, P1f, P2f and P2g, both the water and ammonia volumes were increased by the same ratio. The reaction rate should therefore not have been affected as significantly as the particle morphology and size would have been.

From results of the above experimental study, it was decided to increase the initial magnetite concentration fivefold (as this appeared to result in a greater concentration of magnetite particles in the silica core) whilst maintaining the water, ammonia and ethanol concentrations unchanged. A volume ratio of 1:67:250 was used for the total TEOS:water:alcohol. It was also decided to continue with the coating of the particles using the TEOS alone as this method was the simplest and yielded positive results.

To confirm the optimum conditions selected, additional batches of FeSi were prepared and particles examined for consistency. A modification was also introduced for the TEM sample preparation in that previously, samples had been suspended in ethanol until measurements were made whilst in the modified TEM sample method, samples were dried at room temperature after synthesis and then resuspended in ethanol for TEM measurements. The latter method of sample preparation limited particle agglomeration during storage as can be seen in Fig. 9. The TEM micrographs again indicate that the silica forms a relatively homogeneous layer on the magnetite surface and the particles appear to adopt the shape of the original magnetite core. Particles have an average diameter of  $63 \pm 13$  nm. The number of magnetite particles (each of approximately 10 nm diameter) in the magnetite core varies such that the mean FeSi core diameter is  $28 \pm 10$  nm while the silica shell is  $35 \pm 3$  nm thick. Nanoparticles are generally termed 'monodisperse' where the particle size deviates by less than 15 % from the average value<sup>44</sup> and are said to have a 'narrow size distribution' when the standard deviation from the mean particle size is approximately 20 %. By definition therefore, the FeSi particles are not monodisperse but do exhibit a narrow size distribution (see inset of Fig. 9), acceptable for the purposes of this study.

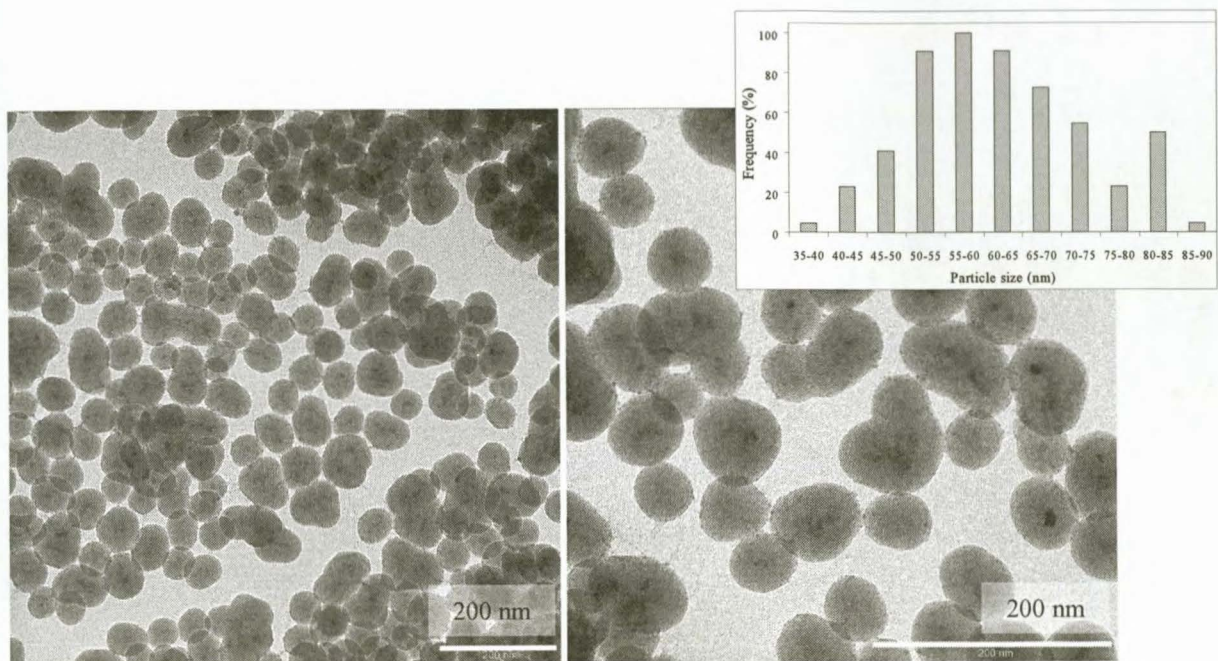


**Figure 9** FeSi samples produced by Method 4 and with modified TEM sample preparation with inset of particle size distribution

The magnetisation curve (Fig. 10) indicates that the FeSi is superparamagnetic<sup>45</sup>. At zero applied field, the remanent magnetisation is very small at a value of  $\sim 0.5 \text{ emu g}^{-1}$ , i.e., the material will exhibit almost no magnetisation when the external applied field is removed.

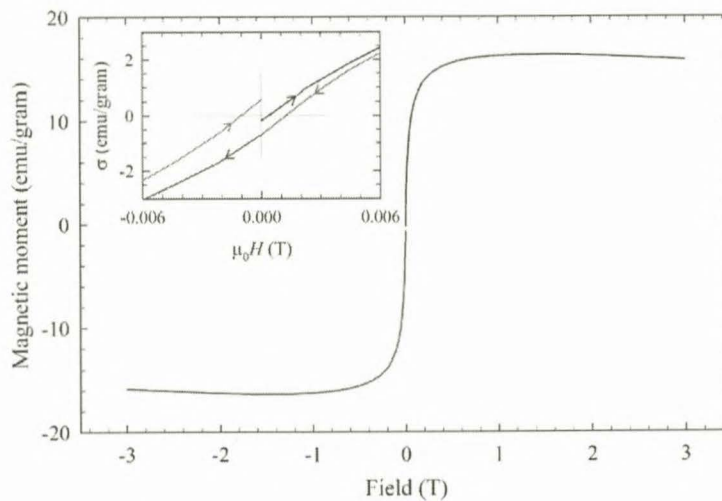


**Figure 10** Magnetisation curve of FeSi sample

### 3.3 Functionalisation of silica-coated magnetite particles with diethylenetriamine

The coating of magnetite occurs via condensation of the hydroxyl silanes that react with the iron hydroxyl groups to form a siloxane linkage<sup>46</sup> and is illustrated schematically in Fig. 11 with the overall reaction described by:

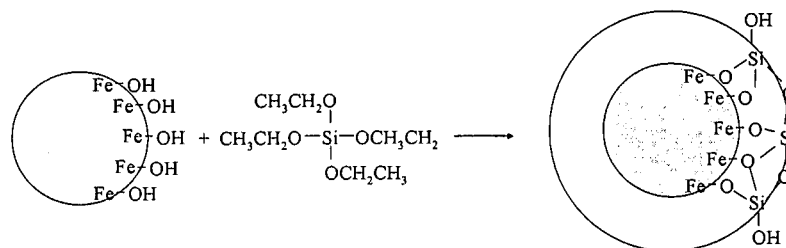
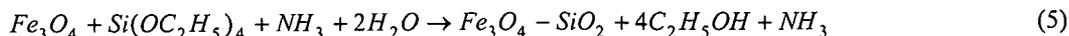


**Figure 11** Coating of magnetite particles with silica by the Stober sol-gel process using citric acid to stabilise magnetite particles

(Interestingly, the condensation reaction can be observed to be occurring after the addition of the second volume of TEOS by the increasing bluish-white opalescence of the mixture which indicates the presence of silica.)

A typical silane coupling agent has the structure  $X_3-Si-(CH_2)_n-Y$ . The  $Si-X_3$  group (where X is the alkoxy or halide group) hydrolyses readily to form silanol groups in the presence of water and a catalyst. Y, the organic functional group can be chosen specifically to determine the chemical character of the surface and may include amines, thiols, hydroxide, carboxylic and phosphate groups<sup>33, 47</sup>. The FeSi particles prepared as discussed in Section 3.2 were functionalised with the silane coupling agent, diethylenetriamine (DETA). The available hydroxyl groups on the silica surface couple to DETA via siloxane bonds. DETA could have been bound directly to the magnetite surface, M: upon dehydration, the trialkoxy group of the organosilane could bind covalently to the free hydroxyl group on the surface to form a  $Si-O-M$  bond thereby providing the functional Y group on the surface. However, it was decided to use an additional preliminary TEOS coating to provide protection to the magnetite core against harsh chemical environments. The overall reaction, illustrated schematically in Fig. 12, can be described by:

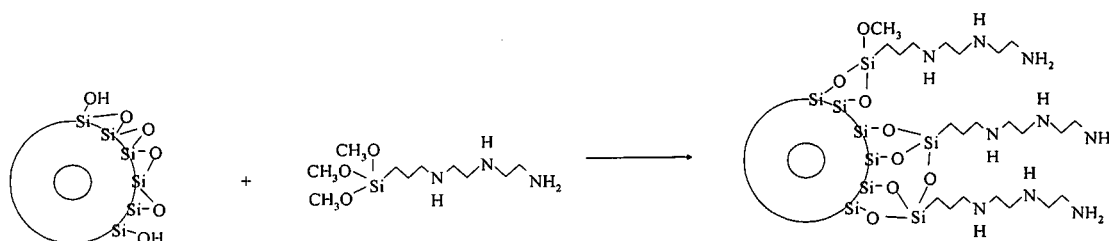
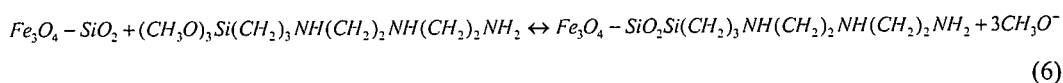


**Figure 12** Functionalisation of FeSi particles with DETA

The extent of DETA bound to the FeSi particles as determined by elemental analysis performed on two separate sets of FeSi and FeSiDETA samples indicated a ligand concentration of 0.05 – 0.07 mmol g<sup>-1</sup> ion exchanger (Table 4). (Sample 2 was used for subsequent extraction studies in Chapter 7.) The percentage carbon and nitrogen determined from elemental analysis provide an indication of the amount of DETA on the FeSi particles, from which the ligand concentration can be estimated.

**Table 4** Elemental analysis for two FeSi and FeSiDETA samples

		Fe (%)	C (%)	H (%)	N (%)	Ligand concentration (mmol g <sup>-1</sup> ) <sup>a</sup>
Sample 1	FeSi	12.6-12.8	4.1	1.4	0.7-0.8 <sup>b</sup>	-
	FeSiDETA	12.3	5.8-5.9	1.7-1.8	1.0	0.07
Sample 2	FeSi	16.5-17.0	3.6	1.4	0.9 <sup>b</sup>	-
	FeSiDETA	16.4-16.5	3.7-3.8	1.4-1.5	1.0-1.1	0.05

<sup>a</sup>based on the difference in nitrogen percentage between the FeSi and FeSiDETA

<sup>b</sup>N present in the FeSi is believed to originate from the ammonia solution used in the FeSi synthesis

FTIR data confirm the silica coating of magnetite by silica in the synthesis of FeSi (see Table 5), however, because the Si functional group absorbances may overlap with the amino functional group absorbances, FTIR is inconclusive for determining whether the particle surfaces have been functionalised by DETA.

**Table 5** FTIR data for bare magnetite, citric acid-coated magnetite, FeSi and FeSiDETA

Max absorbances (cm <sup>-1</sup> )				Assignment
Fe <sub>3</sub> O <sub>4</sub>	Citric acid-coated Fe <sub>3</sub> O <sub>4</sub>	FeSi	FeSiDETA	
451		466	466	Bending of siloxane bridges Si-O-Si <sup>36, 37</sup> and Fe-O <sup>37-39</sup>
573	578			Fe-O <sup>36, 39, 40</sup>
		1085	1083	Si-O-Si asym stretch <sup>36, 38, 40</sup> , Si-O <sup>40</sup> , Si-O-CH <sub>3</sub> or Si-O-R <sup>33, 41</sup>
1631	1620	1637	1637	Si-OH, Fe-OH and water <sup>37-39, 42</sup>
2849	2849	2849	2850	CH <sub>3</sub> sym stretch (OCH <sub>2</sub> CH <sub>3</sub> ) <sup>33, 42</sup> , N-CH <sub>3</sub> <sup>42</sup> , CH <sub>2</sub> sym stretch <sup>33</sup>
2917	2918	2918	2918	CH <sub>2</sub> asym <sup>42</sup>

The attempt to increase the mass of FeSiDETA synthesised in the laboratory from ~15 mg (base case) to ~70 mg on a 'medium' scale (see Section 2.4) was successful, as indicated by the particles in the TEM micrograph (Fig. 13 (a)),

the agitation provided in the large scale FeSiDETA synthesis was insufficient, leading to condensation of silica on adjacent particles and subsequent agglomeration of particles.

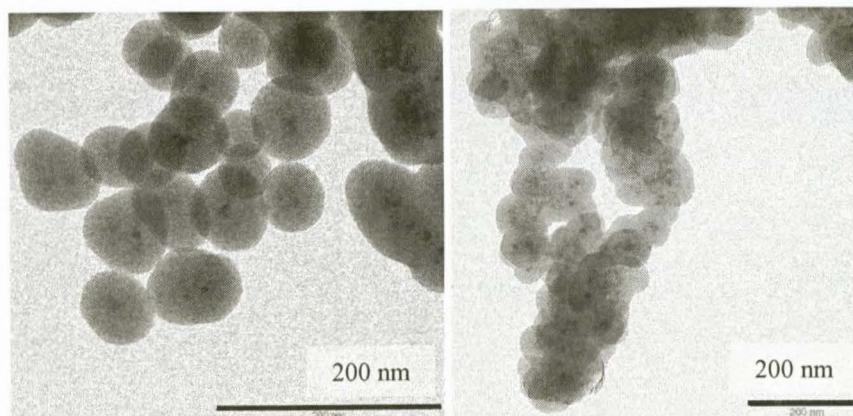


**Figure 13** TEM images from the (a) 'medium' and (b) 'large' scale synthesis of FeSiDETA (see Section 2.4)

#### 3.4 Multiple tetraethoxysilane coatings

SEM-EDS analysis of material produced from the multiple coatings of the magnetite with TEOS gives the element abundances in mass percent (normalised to 100 mass %) as compared to laboratory-synthesised bare magnetite, 5  $\mu\text{m}$  magnetite as purchased from Sigma-Aldrich and FeSi with two TEOS coatings as shown in Table 6.

**Table 6** Comparison of the composition of multiply-coated FeSi as obtained by SEM-EDS to bare magnetite and FeSi with two TEOS coatings

Sample	Percentage mass (%)				
	C	Si	Mn	Fe	O
Laboratory synthesised magnetite	10.6	-	-	47.6	41.9
5 $\mu\text{m}$ magnetite purchased from Sigma-Aldrich	9.7	-	0.7	49.4	40.2
FeSi (two TEOS coatings)	10.1	19.5	-	16.5	53.9
Multiply-coated FeSi	8.5	25.1	-	11.7	54.7

The nanosized magnetite synthesised in the laboratory and the 5  $\mu\text{m}$  magnetite as supplied by Sigma-Aldrich have relatively similar compositions (unusually, the Sigma-Aldrich sample appears to contain traces of Mn). Although, in general, samples were relatively homogeneous, the magnetite did not completely cover the tape on which the sample was mounted, resulting in a recorded C percentage. The FeSi samples show an increase in the Si and O compositions with a corresponding decrease in Fe percentage. The multiply-coated FeSi shows the greatest increase in Si and decrease in Fe percentage masses, indicating that a thicker coating of silica is present on the magnetite surface.

### 3.5 Silica-coated magnetite particle sintering

The decrease in mass percent FeSi versus temperature, as determined by TGA and shown in Fig. 14, can be explained as follows<sup>48</sup>: up to 200 °C, there is a removal of hydrogen bonded and absorbed water; up to 500 °C, all vicinal silanol groups (Si-OH) are completely condensed and above 600 °C, isolated Si-OH groups are removed and the silica surface is fully dehydrated. This material was tested for acid resistance (see Section 3.6) to determine whether the resistance had improved as a result of the sintering through reduction of the porosity in the outer silica coating.

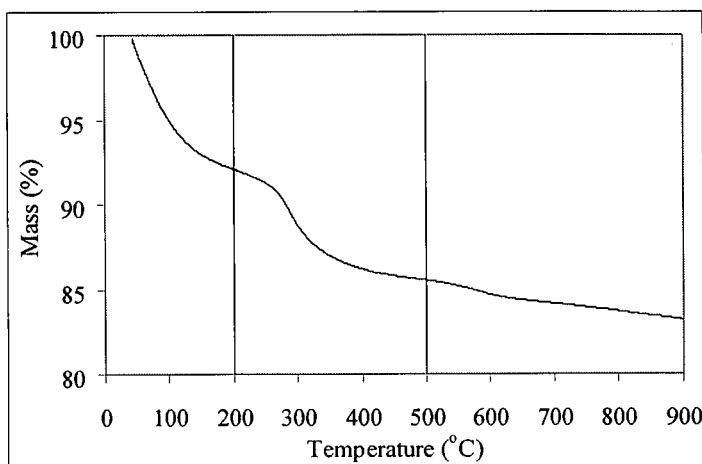


**Figure 14** TGA plot for FeSi sample with two silica coats

A TEM micrograph of the sintered FeSi sample is shown in Fig. 15 (a). It appears that sintering may have resulted in the fusion of adjacent particles as compared to unsintered particles in Fig. 9. During sintering, adjacent particles may be bridged by the formation of a neck between particles but this may not necessarily reduce the porosity of the silica matrix itself to a significant extent<sup>49</sup>. This is illustrated schematically in Fig. 15 (b). In addition, sintering may be detrimental in that the high temperatures used may result in oxidation of the magnetite and removal of the surface hydroxyl groups which are required for further functionalisation. In fact, despite repeated flushing of the vertical tube furnace with argon (which was tested in addition to sintering using TGA), sintering yielded a material with a slightly reddish colour as compared to the original FeSi. It is possible that oxidation of the magnetite took place to yield haematite. Because of the potential variation in material properties, the method of sintering using a vertical tube furnace was not investigated further.

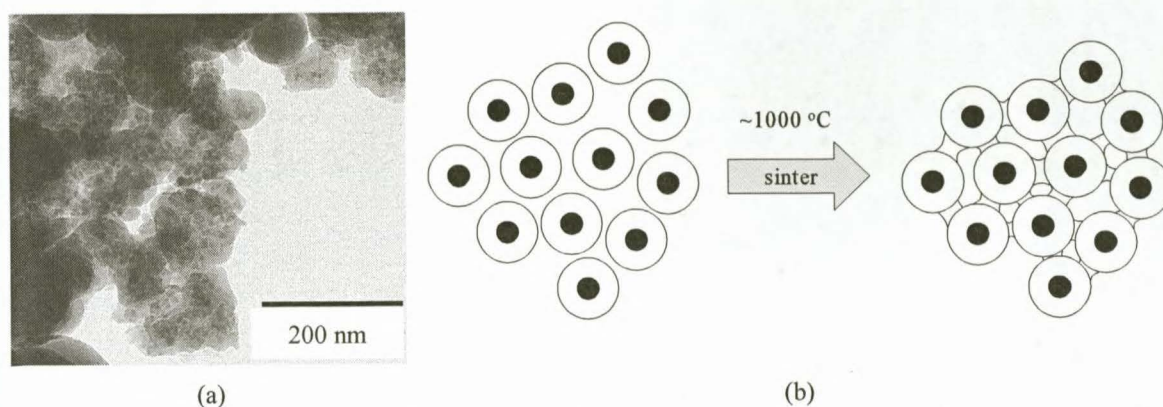


**Figure 15** (a) TEM micrograph of sintered FeSi sample and (b) schematic of potential effect of sintering on the porosity of the FeSi material

### 3.6 Resistance of silica-coated particles to acid

The solubility of magnetite in aqueous solutions<sup>1</sup> at low pHs (less than approximately 4) is clearly illustrated in Fig. 16 (a) where the magnetite resistance to acid decreases as the acid molar strength increases from 0.5, 1, 2 up to 3 M HCl. The FeSi and FeSiDETA show a highly improved resistance to the acid with, for example, the Fe dissolution decreasing from above 80 % down to approximately 1 % in the 3 M HCl solution (shown in Fig. 16 (b)). The acid resistance of the multiply-coated and sintered FeSi samples (Fig. 16 (b)) determined using only the 0.5 M HCl) do not appear to possess a significantly greater ability to resist acid attack although the resistance appears to have improved over that of the FeSi with two silica coatings. The acid resistance is approximately the same as that of the FeSiDETA.

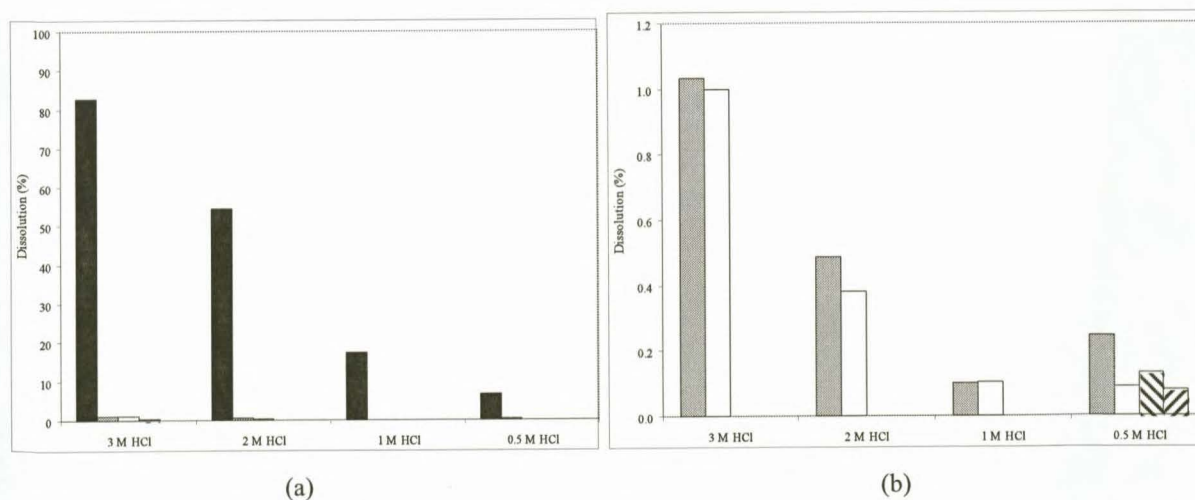


**Figure 16** (a) Resistance to 0.5, 1, 2 and 3 M HCl of magnetite (in black ■), FeSi (in grey □) and FeSiDETA (no colour □) with (b) enlarged area below 1.2 % dissolution showing in particular the multiply-coated FeSi (downward diagonal ▨) and sintered FeSi (upward diagonal ▩). Note the different scale on the y-axis in (a) and (b).

#### 4. Conclusions

A variety of synthesis methods and experimental conditions were investigated for the silica coating of magnetite nanoparticles. The relatively simple citric acid stabilisation of magnetite nanoparticles and subsequent coating by the Stöber process using a TEOS sol-gel precursor was chosen for FeSi synthesis with subsequent functionalising of the particles using diethylenetriamine. Optimum reagent volumetric ratios for FeSi synthesis were determined to be ~1:17:67:250 for TEOS:NH<sub>4</sub>OH solution: water: ethanol, with the magnetite concentration being relatively low at ~60 mg l<sup>-1</sup> total solution in order to prevent the agglomeration of particles during coating.

When comparing the resistance to dissolution of the iron in the uncoated magnetite as well as the FeSi and FeSiDETA in a variety of concentrations of acidic media, it was found that the FeSi and FeSiDETA offer a significant improvement (> 80 %) in resistance to acid attack while attempts to improve acid resistance through routes such as multiple silica coatings and sintering did not offer any distinct advantage. These coated and functionalised FeSiDETA particles will be used in the extraction of metal ions from aqueous solutions (discussed in Chapter 7).

#### 5. Recommendation for the preparation of silica-coated magnetite via a dry synthesis route

A drawback of the wet Stöber synthesis route is that large solution volumes are required to prevent agglomeration of the magnetite in suspension, resulting in the synthesis of small masses of FeSi (at most ~70 mg FeSi was produced per laboratory synthesis). Although, on a laboratory scale, FeSi synthesis is relatively simple and cost-effective, scale-up of such a process would be difficult and expensive. Preliminary calculations are provided here for the tetramethylsilane (TMS) dry coating of magnetite which would lend itself more easily to scale-up. No experimental test work was performed in this regard as it was beyond the scope of this work but it is recommended that this preliminary design be used for further investigations into dry FeSi synthesis.

Silica coatings are commonly deposited using plasma enhanced chemical vapour deposition (CVD) at high temperatures (> 250 °C) with TEOS or silanes as reagents<sup>50</sup>. Silanes are easily metered using mass flow controllers, but the deposition can be potentially hazardous as silanes are toxic and pyrophoric. TEOS has a low vapour pressure (0.3 Pa), cannot be metered out with conventional mass flow controllers and requires heated delivery lines and chambers to prevent TEOS deposition. Magnetite is rapidly oxidised to maghemite<sup>51</sup> at temperatures greater than approximately 60 °C and high temperature CVD would therefore be unsuitable for silica coating of magnetite unless an inert atmosphere were used. TMS allows for the lower temperature deposition of silica. In addition, TMS is non-toxic, non-pyrophoric and has a higher vapour pressure (77 Pa) which allows for metering using conventional mass flow controllers.

A setup as shown in Fig. 17 was proposed. Tetramethylsilane as transported by argon gas and magnetite can be injected into a vertical perspex tube using a mass flow controller with coated magnetite particles collected at the outlet by means of magnets.

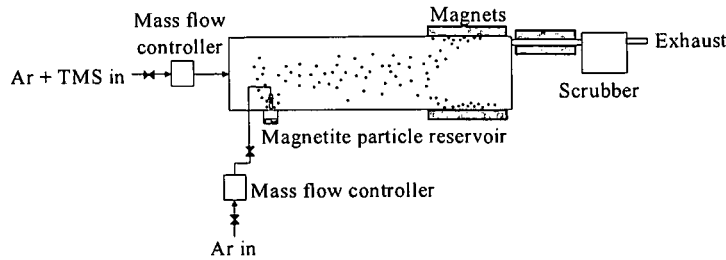


**Figure 17** Deposition setup for coating of magnetite with TMS

The minimum velocity required for turbulent flow of argon and TMS for transport of the magnetite along the length of the reactor is calculated from:

$$Re_{turbulent\ flow} = \frac{\rho_{transport\ gas} D v_{transport\ gas}}{\mu} > 30 \quad (7)$$

With a 100 mm diameter tube, the velocity of the argon transport gas is calculated to be  $\sim 4.65\text{ mm s}^{-1}$ .

The minimum fluidisation velocity  $u_{mf}$  for fluidisation of the magnetite in the magnetite particle reservoir by argon is calculated in two manners<sup>52</sup>. The first is using the following equation which holds if  $Re_{p,mf} < 20$ :

$$u_{mf} = \frac{d_p^2 (\rho_{Fe_3O_4} - \rho_{transport\ gas}) g}{150\mu} \left( \frac{\varepsilon^3 \Phi_s^2}{(1-\varepsilon)} \right) \quad (8)$$

using  $\rho_{transport\ gas} = \rho_{air} = 1.29 \frac{kg}{m^3}$ ,  $\varepsilon = 0.4 - 0.45$ ,  $\Phi_s = 1$  and  $d_p = 1\ \mu m$ ,  $u_{mf}$  is calculated to be equal to  $0.0028\text{ mm s}^{-1}$ . This value of  $u_{mf}$  gives a  $Re_{p,mf}$  of  $1.8 \times 10^{-7}$  and the equation is therefore valid.

A second method of calculating the minimum fluidisation velocity is from:

$$(\rho_{Fe_3O_4} - \rho_{transport\ gas}) g = \frac{\rho_{transport\ gas} u_{mf}^2}{\Phi_s d_p \varepsilon^3} \left[ \frac{150(1-\varepsilon)\mu}{\Phi_s d_p u_{mf} \rho_f} + 1.75 \right] \quad (9)$$

Again,  $u_{mf}$  is found to be equal to  $0.0028 \text{ mm s}^{-1}$ .

Thermodynamic calculations performed using HSC Chemistry software and the parameters as given in Table 7 (with 1000 mol  $(\text{CH}_3)_4\text{Si}(\text{l})$  and  $\text{O}_2(\text{g})$  added initially) indicated that  $\text{SiO}_2$  should form at equilibrium (Fig. 18) from the chosen starting materials. However, from preliminary tests using TMS (with analysis by SEM-EDS), it is believed that owing to kinetic constraints,  $\text{SiO}_2$  does not form. It is possible that higher temperature conditions are required for silica deposition on the magnetite surface and it is recommended that this premise be tested using a heated deposition reactor.

**Table 7** Input parameters for HSC Chemistry software design

Parameter		Value	
Temperature range		25 – 1025 °C	
Initial temperature		298.15 K	
Pressure		1 bar	
Number of steps		501 steps	
<b>Possible reagents or products</b>			
$(\text{CH}_3)_2\text{SiH}_2(\text{g})$	$\text{CH}_2\text{O}(\text{g})$	$\text{H}_2\text{O}(\text{g})$	$\text{SiC}(\text{g})$
$(\text{CH}_3)_4\text{Si}(\text{l})$	$\text{CH}_3\text{OH}(\text{g})$	$\text{HCOOH}(\text{g})$	$\text{SiC}_2(\text{g})$
$\text{C}_2\text{H}_2(\text{g})$	$\text{CH}_4(\text{g})$	$\text{O}(\text{g})$	$\text{SiH}_4(\text{g})$
$\text{C}_2\text{H}_4(\text{g})$	$\text{CH}_6\text{Si}(\text{g})$	$\text{O}_2(\text{g})$	$\text{SiO}(\text{g})$
$\text{C}_2\text{H}_4\text{O}_2(\text{ACA}(\text{g}))$	$\text{CO}(\text{g})$	$\text{Si}(\text{g})$	$\text{SiO}_2$
$\text{C}_2\text{H}_6(\text{g})$	$\text{CO}_2(\text{g})$	$\text{Si}_2\text{H}_6$	$\text{SiO}_2(\text{g})$
$\text{C}_3\text{H}_{10}\text{Si}(\text{TMS}(\text{g}))$	$\text{H}_2(\text{g})$	$\text{Si}_2\text{H}_6(\text{g})$	$\text{SiO}_2 \cdot \text{H}_2\text{O}$
$\text{C}_6\text{H}_{18}\text{OSi}_2(\text{HMS}(\text{g}))$	$\text{H}_2\text{O}$		
<b>Additional potential reaction products that are not available in the HSC database list</b>			
$\text{Si}_2(\text{CH}_3)\text{H}_5$	$\text{Si}_2(\text{CH}_3)_2\text{H}_4$	$\text{Si}_2(\text{CH}_3)_3\text{H}_3$	$\text{Si}_2(\text{CH}_3)_4\text{H}_2$
$\text{Si}_2(\text{CH}_3)_5\text{H}$	$\text{Si}_2(\text{CH}_3)_6$	$\text{Si}_2\text{O}(\text{CH}_3)\text{H}_5$	$\text{Si}_2\text{O}(\text{CH}_3)_2\text{H}_4$
$\text{Si}_2\text{O}(\text{CH}_3)_3\text{H}_3$	$\text{Si}_2\text{O}(\text{CH}_3)_4\text{H}_2$	$\text{Si}_2\text{O}(\text{CH}_3)_5\text{H}_1$	

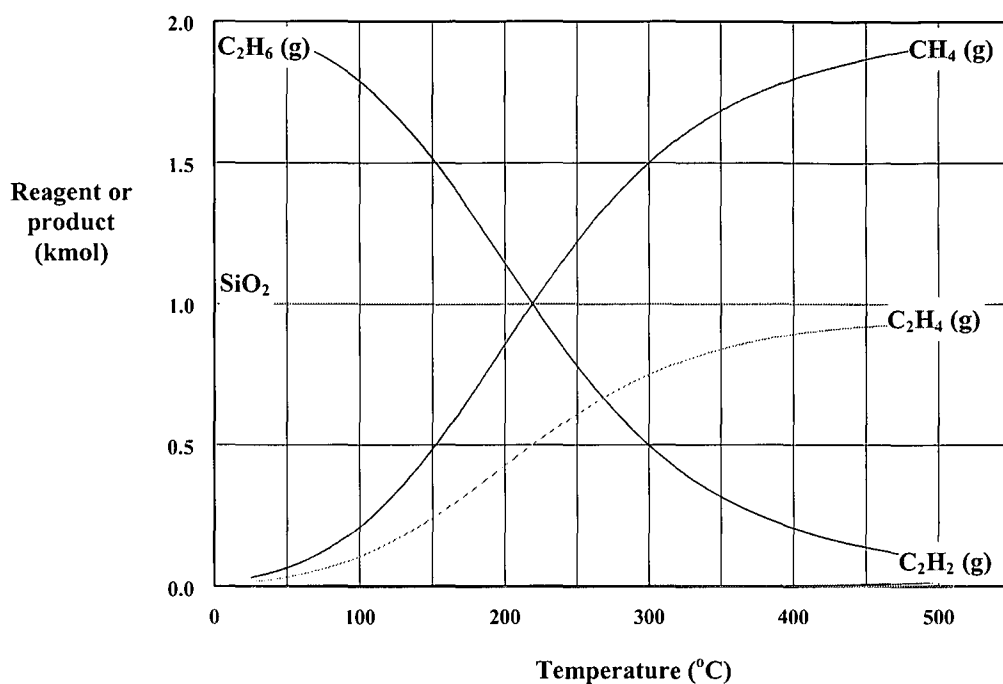


Figure 18 Equilibrium amount of potential products formed

## References

1. Pourbaix, M., *Atlas of electrochemical equilibria in aqueous solutions* Pergamon Press Ltd., Oxford, 1966.
2. Grüttner, C.; Rudershausen, S.; Teller, J., *J. Magn. Magn. Mater.* 2005, **293**, 559.
3. Grüttner, C.; Rudershausen, S.; Teller, J., *J. Magn. Magn. Mater.* 2001, **225**, 1.
4. Liu, X.; Ma, Z.; Xhing, J.; Huizhou, L., *J. Magn. Magn. Mater.* 2004, **270**, 1.
5. Nagy, M.; Otremba, P.; Krüger, C.; Bergner-Greiner, S.; Anders, P.; Henske, B.; Prinz, M.; Roewer, L., *Forensic Science International* 2005, **152**, 13.
6. Reetz, M. T.; Zonta, A.; Vijayakrishnan, V.; Schimossek, K., *J. Mol. Catal. A: Chem.* 1998, **134**, 251.
7. Shen, J.; Ebner, A. D.; Ritter, J. A., *J. Colloid Interface Sci.* 1999, **214**, 333.
8. Dorfner, K., *Ion exchangers: properties and applications* Ann Arbor Science Publishers Inc., Michigan, 1973.
9. De Dardel, F.; Arden, T. V., *Ion exchangers* VCH Verlagsgesellschaft mbH, Weinheim, 1989.
10. Bomati-Miguel, O.; Leconte, Y.; Morales, M. P.; Herlin-Boime, N.; Veintemillas-Verdaguer, S., *J. Magn. Magn. Mater.* 2005, **290 - 291**, 272.
11. Santra, S.; Tapeç, R.; Theodoropoulou, N.; Dobson, J.; Hebard, A.; Tan, W., *Langmuir* 2001, **17**, 2900.
12. Stöber, W.; Fink, A.; Bohn, E., *J. Colloid Interface Sci.* 1968, **26**, 62.
13. Byers, C. H.; Harris, M. T.; Williams, D. F., *Ind. Eng. Chem. Res.* 1987, **26**, 1916.
14. van Blaaderen, A.; van Geest, J.; Vrij, A., *J. Colloid Interface Sci.* 1992, **154**, 481.
15. Chen, S.-L.; Dong, P.; Yang, G.-H.; Yang, J.-J., *J. Coll. Int. Sci.* 1996, **180**, 237.
16. Matsoukas, T.; Gulari, E., *J. Colloid Interface Sci.* 1988, **124**, 252.
17. Nagao, D.; Osuzu, H.; Yamada, A.; Mine, E.; Kobayashi, Y.; Konno, M., *J. Colloid Interface Sci.* 2004, **279**, 143.
18. Bogush, G. H.; Zukoski, C. F., *J. Colloid Interface Sci.* 1991, **142**, 19.
19. Green, D. L.; Lin, J. S.; Lam, Y.-F.; Hu, M. Z.-C.; Schaefer, D. W.; Harris, M. T., *J. Colloid Interface Sci.* 2003, **266**, 346.
20. Philipse, A. P.; Bruggen, M. P. B. v.; Pathmamanoharan, C., *Langmuir* 1994, **10**, 92.
21. van Helden, A. K.; Jansen, J. W.; Vrij, A., *J. Colloid Interface Sci.* 1981, **81**, 354.
22. Atarashi, T.; Kim, Y. S.; Fujita, T.; Nakatsuka, K., *J. Magn. Magn. Mater.* 1999, **201**, 7.

23. Bruce, I. J.; Taylor, J.; Todd, M.; Davies, M. J.; Borioni, E.; Sangregorio, C.; Sen, T., *J. Magn. Magn. Mater.* 2004, **284**, 145.
24. Taylor, J. I.; Hurst, C. D.; Davies, M. J.; Sachsinger, N.; Bruce, I. J., *J. Chromatogr., A* 2000, **890**, 159.
25. van Ewijk, G. A.; Vroege, G. J.; Philipse, A. P., *J. Magn. Magn. Mater.* 1999, **201**, 31.
26. Sun, Y.; Duan, L.; Guo, Z.; DuanMu, Y.; Ma, M.; Xu, L.; Zhang, Y.; Gu, N., *J. Magn. Magn. Mater.* 2005, **285**, 65.
27. Kramer, J.; Driessen, W. L.; Koch, K. R.; Reedijk, J., *Hydrometallurgy* 2002, **64**, 59.
28. Kramer, J.; Garcia, A. R.; Driessen, W. L.; Reedijk, J., *Chem. Commun.* 2001, **23**, 2420.
29. Milonjic, S. K.; Kopenci, M. M.; Ilic, Z. E., *J. Radioanal. Chem.* 1983, **78**, 15.
30. Kosmulski, M., *J. Colloid Interface Sci.* 2004, **275**, 214.
31. Sun, Z.-X.; Su, F.-W.; Forsling, W.; Samskog, P.-O., *J. Colloid Interface Sci.* 1998, **197**, 151.
32. Wesolowski, D. J.; Machesky, M. L.; Palmer, D. A.; Anovitz, L. M., *Chem. Geol.* 2000, **167**, 193.
33. Xu, Z.; Liu, Q.; Finch, J. A., *Appl. Surf. Sci.* 1997, **120**, 269.
34. Bee, A.; Massart, R.; Neveu, S., *J. Magn. Magn. Mater.* 1995, **149**, 6.
35. Satoh, T.; Akitaya, M.; Konno, M.; Saito, S., *J. Chem. Eng. Jpn.* 1997, **30**, 759.
36. Klotz, M.; Ayrál, A.; Guizard, C.; Ménager, C.; Cabuil, V., *J. Coll. Int. Sci.* 1999, **220**, 357.
37. García Cerda, L. A.; Montemayor, S. M., *J. Magn. Magn. Mater.* 2005, **294**, 43.
38. Barrado, E.; Rodríguez, J. A.; Prieto, F.; Medina, J., *J. Non-Cryst. Solids* 2005, **351**, 906.
39. Ma, M.; Zhang, Y.; Yu, W.; Shen, H.-Y.; Zhang, H.-Q.; Gu, N., *Colloids Surf., A* 2003, **212**, 219 - 226.
40. Woo, K.; Hong, J.; Ahn, J.-P., *J. Magn. Magn. Mater.* 2005, **293**, 177.
41. Socrates, G., *Infrared characteristic group frequencies* John Wiley & Sons Ltd, Chichester, 1994.
42. Pathmanoharan, C.; Wijkens, P.; Grove, D. M.; Philipse, A. P., *Langmuir* 1996, **12**, 4372.
43. Chen, S.-L.; Dong, P.; Yang, G.-H., *J. Coll. Int. Sci.* 1997, **189**, 268 - 272.
44. Bönnemann, H.; Nagabhushana, K. S., *Encycl. Nanosci. Nanotech.* 2004, **1**, 777.
45. Craik, D., *Magnetism: principles and applications* John Wiley and Sons Ltd, Chichester, 1995.
46. Butterworth, M. D.; Illum, L.; Davies, S. S., *Colloids Surf.* 2001, **179**, 93.
47. del Campo, A.; Sen, T.; Lellouche, J.-P.; Bruce, I. J., *J. Magn. Magn. Mater.* 2005, **293**, 33.
48. Biernat, J. F.; Konieczka, P.; Tarbot, B. J.; Bradshaw, J. S.; Izatt, R. M., *Sep. Purif. Methods* 1994, **23**, 77.
49. Alcock, C. B., *Thermochemical processes: principles and models* Butterworth-Heinemann, Oxford, 2001.
50. Reber, D. M.; Fonash, S., International patent 6 159 559, 2000.
51. Cornell, R. M.; Schwertmann, U., *The iron oxides* VCH Publishers, New York, 1996.
52. Kunii, D.; Levenspiel, O., *Fluidization engineering* Wiley, New York, 1969.
53. Hwang, J. Y., US Patent 5 043 070, 1991.

## Chapter 7\*

### Diethylenetriamine-functionalised silica-coated magnetite nanoparticles for selective palladium (II) ion extraction from chloride-rich aqueous solutions

---

#### Abstract

The extraction of Pd(II) and Cu(II) from Pd(II), Cu(II) and mixed Pd(II)/Cu(II) solutions was investigated using a nanosized (~70 nm diameter) superparamagnetic ion exchanger material consisting of particles with magnetite core modified by diethylenetriamine-functionalised silica (FeSiDETA). The extent of extraction, selectivity and acid resistance of the FeSiDETA was compared to that of unmodified magnetite and silica-coated magnetite (FeSi), showing very promising results. FeSiDETA was found to quantitatively extract Pd metal ions as compared to the extraction by the magnetite and FeSi with high selectivity towards Pd(II) over Cu(II) at relatively low pH (pH < 4). Moreover, the FeSiDETA resistance to iron dissolution for single-stage extractions is up to 87 % higher than that of unmodified magnetite in 3 M HCl. The material robustness is improved considerably, since complete dissolution was observed for the uncoated magnetite particles. Nevertheless, up to 55 % iron dissolution occurs during four successive recovery cycles as a result of the harsh conditions used for desorption (2 M HCl). We are confident that degradation may be further reduced if less acidic desorbents or a more impenetrable silica coating is used. FeSiDETA particles could potentially provide ion exchanger surface areas orders of magnitude greater than conventional ion exchangers and offer alternative novel magnetic processing techniques.

#### 1. Introduction

Packed columns are often used in industrial ion exchange processes<sup>1</sup>. The diameters of commercial ion exchanger particles used in the packed columns generally range from 0.3 to 1.2 mm<sup>2,3</sup>. A compromise in ion exchanger particle size is usually required as small particles display faster ion exchange rates and are less susceptible to abrasion and fragmentation during processing while coarser particles may be required to minimise head loss at high flow rates<sup>1,2</sup>.

Superparamagnetic nanoparticles are becoming increasingly important in a variety of different applications such as magnetic storage media<sup>4</sup>, catalysis<sup>5</sup> and medical applications<sup>4,6,7</sup>. A nanosized ion exchanger with superparamagnetic properties could provide particles with surface areas orders of magnitude greater than

---

\* Based in part on the papers, Vatta, L. L.; Kramer, J., Koch, K. R., Diethylenetriamine functionalised silica coated magnetite nanoparticles for selective palladium ion extraction from aqueous solutions. *In press. Separation Science and Technology* 2007 and Vatta, L. L.; Sanderson, R. D.; Koch, K. R., *Magnetic nanoparticles: Properties and potential applications. Pure Appl. Chem.* 2006, 78, (9), 1791-1799.

conventional ion exchanger materials. In addition, the magnetic nature of the ion exchanger could allow for the use of novel processing technologies, e.g., magnetic fields could be used for the mixing and extraction of ion exchange particles from solutions. This could eliminate problems associated with pressure drops across packed columns, blockages and potential scale-up issues as experienced when larger diameter commercial ion exchangers are used<sup>3</sup>.

Platinum, palladium and the other platinum group metals (PGMs) are highly valuable, rare precious metals and are used in a number of industrial applications, such as auto-catalyst manufacture and jewellery fabrication<sup>8-10</sup>. PGM recoveries involve difficult mining conditions and laborious refining processes<sup>11</sup>. The major PGM deposits are the Bushveld igneous complex (South Africa) and the Ni-Cu-PGM sulphide deposits in the Russian Arctic, with smaller deposits found in the Ural mountains (Russia), Sudbury (Canada), the Hartley mine (Zimbabwe), the Stillwater complex (USA), the Northern Territory (Australia) and the Zechstein copper deposit (Poland)<sup>9</sup>. Increased amounts of costly PGMs are required annually to replace material lost in processing, for increased capacity in industry and for new applications<sup>9</sup>. It is for this reason that we have become interested in the improved recovery of PGMs from process streams and effluents. In addition, the high value of PGMs would justify the cost of making nanosized magnetic ion exchanger materials if these could be recycled.

A variety of unmodified and functionalised micron- and nanosized-magnetic particles have been used, for example, in turbidity and colour removal<sup>3, 12-14</sup> and cadmium<sup>15</sup>, mercury<sup>15</sup>, chromium<sup>16</sup>, zinc<sup>16</sup>, aluminium<sup>17</sup>, iron<sup>17</sup>, copper<sup>17-19</sup>, nickel<sup>20</sup>, cobalt<sup>20</sup> and silver<sup>18, 19, 21</sup> extraction through chelating and electrostatic interactions. Although very recently some work has been performed on the extraction of PGMs using nonylthiourea-coated magnetite nanoparticles<sup>22</sup>, to our knowledge, no investigation into PGM extraction using diethylenetriamine-functionalised silica-coated nanosized superparamagnetic ion exchange materials has yet been attempted.

In this chapter, a preliminary assessment is performed as to the use of a silica-coated, diethylenetriamine-functionalised nanosized magnetite ion exchanger for, amongst others, PGM extraction. Since PGM extraction using (poly)amines generally takes place under acidic conditions<sup>11</sup> and as magnetite particles are soluble<sup>23</sup> in aqueous solutions at pHs less than approximately 4, it was necessary to provide the magnetite with a protective silica coating. We have investigated the extraction efficiency, selectivity, resistance to various aqueous solution matrices and longer term performance of the functionalised magnetite ion exchanger compared to that of unmodified magnetite and silica-coated magnetite through the extraction of Cu(II) and Pd(II) from Cu(II), Pd(II) and a mixed Cu(II)/Pd(II) solutions.

## 2. Experimental

### 2.1 Reagents and analytical methods

All reagents and solvents were purchased from commercial sources and were used without further purification.  $\text{FeCl}_3 \cdot 6\text{H}_2\text{O}$ ,  $\text{FeSO}_4 \cdot 7\text{H}_2\text{O}$  and 25 %  $\text{NH}_4\text{OH}$  (Merck) were used for the precipitation of magnetite. Sodium silicate, tetraethoxysilane (TEOS), tetramethyl ammonium hydroxide (TMA), N'-(3-trimethoxysilylpropyl)diethylenetriamine (DETA) (Aldrich) and citric acid (Merck) were used for the coating and functionalising of the magnetite particles. Ultrapure Milli-Q water ( $\text{MQ} > 18 \text{ M}\Omega$ ) was used for the preparation of aqueous solutions.

Transmission electron microscopy (TEM) micrographs were obtained using a LEO EM912 electron microscope. Particle size was determined using the TEM micrographs and ImageJ, a public domain image processing program<sup>24</sup>. Fourier Transform Infrared (FTIR) spectra were recorded on a Nexus Nicolet Fourier Transform Infrared Spectrometer using dried powder dispersed in a KBr matrix. Thermogravimetric analysis (TGA) was performed on a 7 mg FeSi sample heated at 20 °C per minute from 45 °C to 920 °C in a Perkin Elmer TGA 7 unit. The chamber was purged with nitrogen at 20 ml min<sup>-1</sup>. Magnetic measurements were obtained on a SQUID magnetometer. Elemental analyses (Fe, C, H and N) were carried out by the Microanalytical Laboratory of the University College Dublin. Two replicates were obtained per sample.

### 2.2 Ion exchanger synthesis: immobilisation of diethylenetriamine on silica-coated magnetite

The selected preparation method for the DETA-functionalised silica-magnetite material as discussed in Chapter 6 is summarised here. Nanosized magnetite ( $\text{Fe}_3\text{O}_4$ ) particles were prepared by the method of Massart<sup>25</sup> as follows: for a typical preparation of approximately 0.9 g  $\text{Fe}_3\text{O}_4$ , 2.1 g  $\text{FeCl}_3 \cdot 6\text{H}_2\text{O}$  and 1.1 g  $\text{FeSO}_4 \cdot 7\text{H}_2\text{O}$  were added to 50 ml water. The resultant solution was heated to 35 °C. 10 ml 25 %  $\text{NH}_4\text{OH}$  was added to the iron solution with rapid agitation. The resultant  $\text{Fe}_3\text{O}_4$  precipitate was stirred for 10 minutes and washed via magnetic decantation four times with 200 ml water. The magnetite particles were then coated with silica by the sol-gel method<sup>26</sup> modified as follows: after washing the precipitate, the magnetite was diluted to 5.6 g  $\text{Fe}_3\text{O}_4 \text{ l}^{-1}$  (80 ml total volume). 1.1 g citric acid was dissolved in 320 ml water and added to the magnetite precipitate whilst stirring. The initial pH of ~2.8 was raised to ~7 by the addition of TMA to redisperse the precipitate. The final volume of 400 ml had a magnetite concentration of ca. 1.1 g l<sup>-1</sup>. 150 ml of this magnetite suspension (approximately 0.17 g magnetite) was added to 2.025 l ethanol, 540 ml water and 135 ml ammonia solution (25 %) and stirred. 2.7 ml TEOS was added to the mixture and after approximately 24 h, a further volume of 5.4 ml TEOS was added to the suspension. The silica-coated magnetite will be referred to as FeSi. The FeSi was washed with an 80 % ethanol in water solution and excess liquid removed by magnetic decantation. The FeSi was dried by evaporation of the solvent at room temperature.

For immobilisation of diethylenetriamine (DETA) onto the silica surface, 60 mg FeSi particles were resuspended in 600  $\mu\text{l}$  ethanol (5 – 10 ml solvent/g FeSi) before 15  $\mu\text{l}$  DETA was added to the FeSi particles (approximately 1.7 mmol DETA/g FeSi)<sup>27, 28</sup>. After 2 days the samples were washed with an 80 % ethanol in water solution by magnetic decantation and dried by evaporation of the solvent at room temperature. The functionalised silica-coated magnetite will be referred to as FeSiDETA.

### 2.3 Extraction using FeSiDETA particles

To determine extraction potentials, 50 mg of Fe<sub>3</sub>O<sub>4</sub>, FeSi and FeSiDETA particles were added to 20 ml of the following solutions (prepared using 1000 mg l<sup>-1</sup> Cu(II) and Pd(II) solution standards in 4 % HNO<sub>3</sub> and 10 % HCl, respectively):

- 20 mg l<sup>-1</sup> Cu(II) solution in a 0.6 M NaOAc/HOAc buffer matrix (pH 4 and pH 6) (solution **I**),
- 7.5 mg l<sup>-1</sup> Pd(II) in a 0.5, 1, 2 and 3 M HCl, 0.6 M NaCl/HCl (pH 2) and 0.6 M NaOAc/HOAc buffer solution (pH 3 – 6) (solution **II**) and
- 7.5 mg l<sup>-1</sup> Pd(II)/7.5 mg l<sup>-1</sup> Cu(II) solution in a 0.5, 1, 2 and 3 M HCl, 0.6 M NaCl/HCl (pH2) and 0.6 M NaOAc/HOAc buffer solution (pH 3 – 6) (solution **III**).

The ligand:total metal ion molar ratios for solutions **I**, **II** and **III** were 0.5, 1.7 and 0.6, respectively.

The effect of pH (solution matrix type) on the extraction efficiency, the selectivity and the Fe dissolution during extraction and from materials handling were investigated. Samples were agitated in sealed polytops at 110 rpm on a Labcon horizontal shaker for approximately 24 hours to attain equilibrium. Samples were then placed on a ferrite magnet for approximately 2 minutes to allow for magnetic sedimentation. 5 ml of the supernatant was added to 5 ml 1.8 M H<sub>2</sub>SO<sub>4</sub> solution and analysed for Cu(II), Pd(II) and Fe using an Inductively Coupled Plasma-Atomic Emission Spectrometer (Varian Liberty II ICP-AES) and a linear calibration method. Calibration standards were prepared in 0.9 M H<sub>2</sub>SO<sub>4</sub>.

### 2.4 Successive recovery extraction studies

All FeSiDETA samples from the extraction studies were used for successive extraction and desorption studies for solutions **I** to **III** (excluding the 2 and 3 M HCl solutions). Four successive extraction studies (E1 to E4) were performed with the conditions and analyses as described previously with the exception of a shorter contact time of one hour for extraction. Samples were desorbed (after each extraction cycle, i.e., desorption cycles 1 to 4: D1 to D4) using a 2 M HCl solution (5 ml) by agitation on the horizontal shaker for one hour. Supernatant samples were used for metal analysis by ICP-AES as described in Section 2.3. An average relative standard deviation in all the

extraction samples of approximately 10 % is determined, based on a comparison of different spectral lines for each element and the measurement of four replicates<sup>29</sup>.

The percentage extraction and desorption of metal ions was calculated from the initial and final concentrations of metal ions in the supernatants. The percentage iron dissolution from the magnetite (unmodified or coated) was calculated as a percentage of the Fe in the supernatant compared to the initial Fe mass present using values obtained from ICP-AES analysis. Final samples were weighed to obtain an overall Fe mass balance.

### 3. Results and discussion

#### 3.1 *FeSiDETA synthesis*

Characterisation of the FeSi and FeSiDETA was performed by TEM microscopy, TGA, SQUID magnetometry, elemental analysis and FTIR. These data have been reported in Chapter 6, Figs. 9, 10, 13 and 14 and Tables 4 and 5.

#### 3.2 *Single-stage extraction from the Cu(II), Pd(II) and mixed metal ion solutions*

##### 3.2.1 *Extraction of Cu(II) from solution I*

The percentage Cu(II) extraction for Fe<sub>3</sub>O<sub>4</sub>, FeSi and FeSiDETA from the Cu(II) solution I (0.6 M NaOAc/HOAc pH 4 and 6 buffer) is illustrated in Fig. 1. Since a 0.5 ligand:Cu(II) ion molar ratio was used for the extraction experiments, a maximum extraction of only 50 % of the Cu(II) initially present in solution can be attained, assuming maximum binding of one metal ion per ligand molecule.

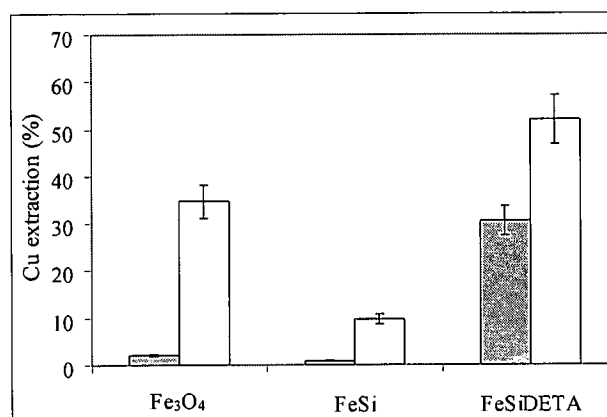


**Figure 1** Percentage Cu(II) extraction by Fe<sub>3</sub>O<sub>4</sub>, FeSi and FeSiDETA from buffered solution I at pH 4 (in grey  $\square$ ) and pH 6 (no colour  $\square$ ). A ligand to Cu metal ion molar ratio of 1 to 2 has been applied.

As discussed in Chapter 4, the magnetite surface charge is established by the dissociation or ionisation of surface hydroxyl groups corresponding to the adsorption or desorption of protons depending on the pH of the solution<sup>30</sup>. The point of zero charge (PZC) for magnetite<sup>30-34</sup> has been reported to be in the range of 6 to 8.2. At a pH less than the PZC, the  $\text{FeOH}_2^+$  groups predominate. At a pH greater than the PZC, the  $\text{FeO}^-$  groups predominate. When the pH equals the PZC, the number of  $\text{FeOH}_2^+$  groups equals the number of  $\text{FeO}^-$  groups<sup>30</sup>.

It is likely that the blue-green cationic aqua ion  $[\text{Cu}(\text{H}_2\text{O})_6]^{2+}$  would be present in solution<sup>8, 11, 35</sup> and the percentage Cu(II) extraction by the magnetite most likely increases with an increase of pH from 4 to 6 as illustrated in Fig. 1 as more  $\text{FeO}^-$  groups become available on the unmodified magnetite surface for cation extraction.

The FeSi particles show a lower percentage Cu(II) extraction at both pH 4 and 6 than the unmodified magnetite and FeSiDETA as a result of their silica surface covering. It is unlikely that the silica coating provides complete shielding of the iron oxide from the Cu(II) solution and the higher percentage extraction occurring at pH 6 compared to that at pH 4 for the FeSi particles is probably as a result of ion pairing with exposed or uncoated  $\text{FeO}^-$  groups and non-specific surface adsorption of Cu(II) complex species by the silica coating. Alternatively, Sjöberg reports that at a pH higher than the PZC of silica ( $\sim$ pH 2), cation adsorption by an electrostatic interaction with negatively charged  $\text{SiO}^-$  may take place<sup>36</sup> with Cu(II) adsorption increasing significantly above pH 6. The increased extraction of Cu(II) by the FeSi at pH 6 could therefore possibly also be as a result of the electrostatic interaction of the Cu(II) ions with the surface  $\text{SiO}^-$ . A third possibility is that, at higher pH,  $\text{Cu}(\text{OH})_2$  precipitates form thereby reducing the dissolved Cu(II) in solution.

On the other hand, the FeSiDETA shows the highest overall extraction compared to the unmodified magnetite and FeSi particles at these pHs. Extraction at this pH 4 – 6 is believed to occur through a complexing or chelating mechanism where coordination to the cationic Cu(II) readily takes place via the lone pairs of the amine groups<sup>37</sup> rather than through an anion ion pairing mechanism since the DETA amine groups are unlikely to be fully protonated. Extraction therefore increases with an increase in pH as the amino groups become increasingly less protonated.

### 3.2.2 Extraction of Pd(II) from solution II

The percentage Pd(II) extraction from the Pd(II) solution II (0.5, 1, 2 and 3 M HCl and pH 2 to 6 buffer solution) is illustrated in Fig. 2. Theoretically, the 1.7 ligand: Pd(II) ion molar ratio should allow for complete extraction of the Pd(II) ions by the DETA-containing extractant.

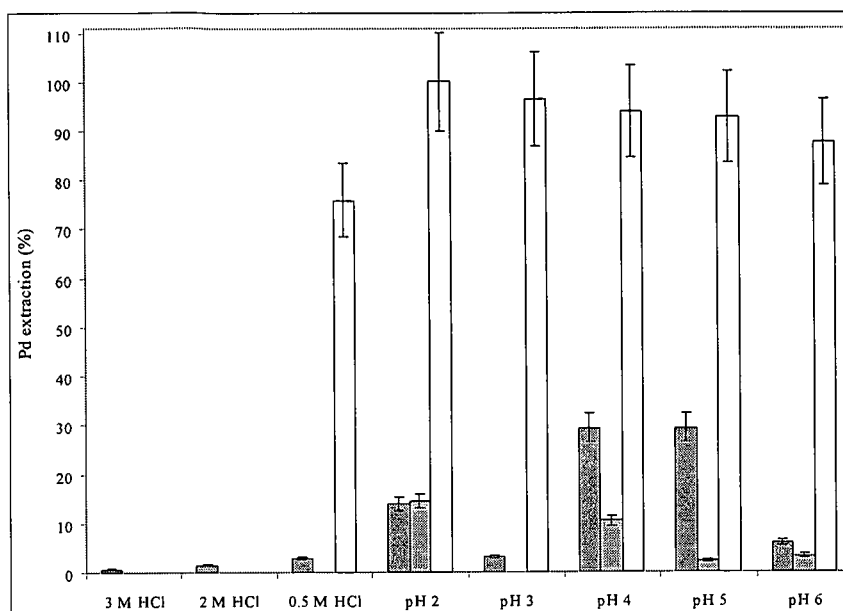


**Figure 2** Percentage Pd(II) extraction by magnetite (in black  $\blacksquare$ ), FeSi (in grey  $\blacksquare$ ) and FeSiDETA (no colour  $\square$ ) from solution II

Pd(II) readily forms  $[\text{PdCl}_4]^{2-}$  anionic complexes in acidic chloride media<sup>8</sup>. In the acidic solutions, it is believed that the positively charged amine groups of the FeSiDETA extract the  $[\text{PdCl}_4]^{2-}$  from solution via an anion exchange mechanism between the anionic Pd(II) chlorocomplex and the chloride or acetate counterion (as illustrated schematically in Fig. 3). In the 2 and 3 M HCl solutions, no extraction occurs as the high concentration of chloride ions compete with the  $[\text{PdCl}_4]^{2-}$  for binding to the ion exchanger by mass action<sup>35, 37, 38</sup>. Nevertheless using FeSiDETA, up to quantitative Pd(II) removal could be effected at pH 2 and 3. The percentage extraction decreases somewhat at higher pH, where it is possible that the increasing anionic acetate ions may compete for extraction or extraction may occur increasingly through a chelating ion exchange mechanism and the  $[\text{PdCl}_4]^{2-}$  tends to dissociate to  $[\text{Pd}(\text{H}_2\text{O})_n\text{Cl}_{4-n}]^{(2+n)+}$ . Furthermore coordination of the amine groups to cationic Pd(II) ions may take place via the lone pairs of the amine groups, as the pH increases<sup>37</sup>.

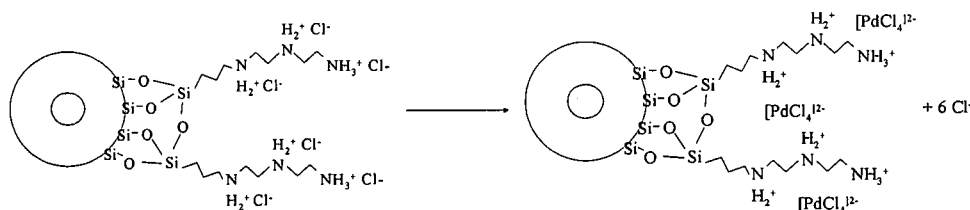


**Figure 3** Schematic illustration of extraction of  $[\text{PdCl}_4]^{2-}$  by the positively charged FeSiDETA amine groups

### 3.2.3 Extraction of Pd(II) and Cu(II) from solution III

The percentage Pd(II) and Cu(II) extraction from mixed metal ion solution III (0.5, 1, 2 and 3 M HCl and pH 2 to 6 buffer solution) is illustrated in Figs 4 (a) and (b), respectively. (Data for the Cu(II) extraction at pH 2 are excluded from Fig. 4 (b) owing to unreliable results obtained from the ICP-AES measurements.)

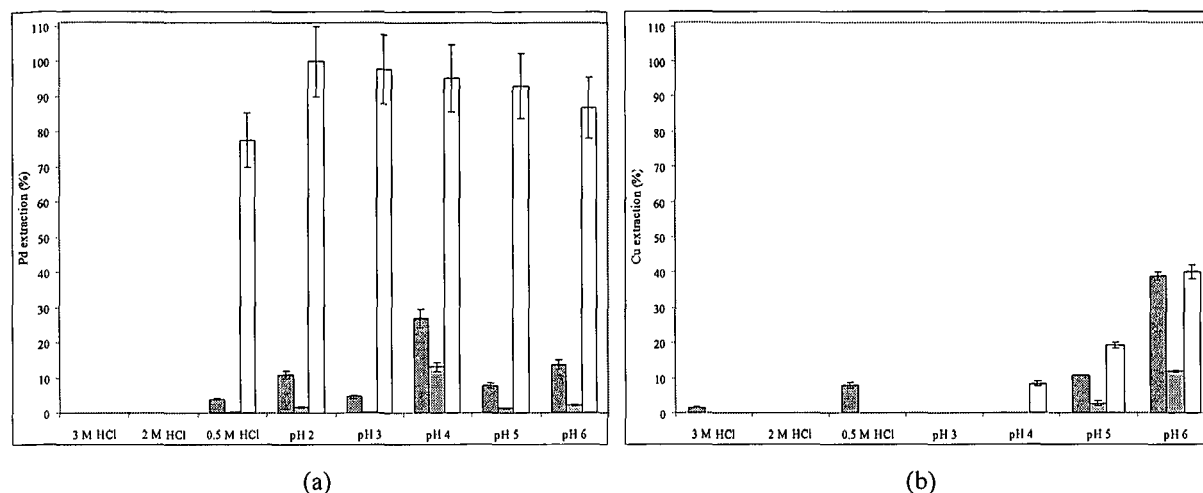


**Figure 4** pH-dependent competitive (a) Pd(II) and (b) Cu(II) extraction from mixed solution III for magnetite (in black □), FeSi (in grey □) and FeSiDETA (no colour □)

A ligand:total metal ion (Cu(II) + Pd(II)) molar ratio of 0.6 was used and some degree of selectivity of the DETA towards one of the metal ions might be expected. It was found that the FeSiDETA preferentially extracts Pd(II) (Fig. 4 (a)) with a higher binding constant<sup>8</sup> under these conditions as compared to Cu(II) (Fig. 4 (b)) from solution III. With increasing pH and decreasing protonation of the amine groups, there is an increased Cu(II) extraction<sup>37</sup>, presumably as a result of Cu(II) binding by coordination of amine groups. The Pd(II) to Cu(II) selectivity is greatest in acidic media, where the DETA is sufficiently protonated to form ion pairs, with the anionic Pd(II) chlorocomplex being favoured, whilst Cu(II) tends to form aquated cationic species mainly, which are not significantly extracted by FeSiDETA under these conditions. (Cu(II) ions form weak anionic complexes,  $[\text{CuCl}_4]^{2-}$ , in acidic chloride solutions<sup>8</sup>.) The observations are consistent with the extraction patterns observed for the single metal solutions I and II.

In general, the FeSi shows low Pd(II) extraction (< 15 %, Fig. 4 (a)) with some Cu(II) extraction at pH 5 and 6 (Fig. 4 (b)). As in the case of the magnetite, extraction probably takes place via electrostatic interaction with uncoated magnetite at the FeSi centre ( $\text{FeOH}_2^+$  or  $\text{FeO}^-$  depending on the pH) or via electrostatic adsorption by negatively charged  $\text{SiO}^-$  at higher pH<sup>36</sup>.

The unmodified magnetite shows some extraction of Pd(II) in most solutions (< 30 %, Fig. 4 (a)) except from chloride-rich solutions containing 2 and 3 M HCl. Depending on the magnetite surface charge, Pd(II) would be

extracted as either anionic  $[\text{PdCl}_4]^{2-}$  or cationic  $\text{Pd}^{2+}$ . Increased cationic Cu(II) extraction by the increasing magnetite surface  $\text{FeO}^-$  groups is observed above pH 4<sup>30</sup> (Fig. 4 (b)).

Because an almost quantitative percentage of Pd(II) is extracted using the 50 mg FeSiDETA sample, no significant additional Pd(II) is extracted when the FeSiDETA mass is increased to 100 mg at pH 4 for solution III. Instead, the additional DETA results in an increased degree of Cu(II) extraction, up to 24 % with a corresponding decrease in selectivity,  $k_{\text{Pd/Cu}}$ , from 7.4 to 2.1 where the selectivity is defined as:

$$k_{\text{Pd/Cu}} = \frac{[\text{Pd}]_{\text{IX}} [\text{Cu}]_{\text{sol}}}{[\text{Pd}]_{\text{sol}} [\text{Cu}]_{\text{IX}}} \quad (1)$$

with ion-exchanger concentrations,  $[\text{metal ion}]_{\text{IX}}$ , in  $\text{mmol g}^{-1}$  and solution phase concentrations,  $[\text{metal ion}]_{\text{sol}}$ , in  $\text{mg l}^{-1}$ <sup>39</sup>.

With double the extractant mass, the percentage Pd(II) extraction increases by approximately 15 % for the magnetite and FeSi, probably as a result of the additional magnetite surface available for extraction. There is no further uptake of Cu(II) by the magnetite or FeSi. At pH 4 with the  $\text{FeOH}_2^+$  predominating, the anionic  $[\text{PdCl}_4]^{2-}$  will most likely be extracted in preference to the cationic  $[\text{Cu}(\text{H}_2\text{O})_6]_2^+$ .

In summary then, it is possible with careful choice of conditions to selectively and quantitatively extract Pd(II) from a Pd(II)/Cu(II) mixed metal ion solution at relatively low pH ( $\text{pH} < 4$ ) using the FeSiDETA ion exchanger material.

### 3.3 Extraction from the Cu(II), Pd(II) and mixed metal ion solutions during successive recovery studies

In practice, ion exchanger materials would be used for the extraction of a metal ion species, followed by desorption or stripping of the extracted metal ion and reuse of the ion exchanger. Four successive extraction-desorption cycles (E1-D1, E2-D2, E3-D3 and E4-D4, described in Section 2.4) were therefore used to obtain an idea as to the robustness of the FeSiDETA for reuse as an ion exchanger extractant.

The successive percentages of extraction (cycles E1 to E4) and desorption (cycles D1 to D4) of Pd(II) and Cu(II) from solution III in four successive recovery cycles are illustrated in Figs 5 (a), (b), (c) and (d).

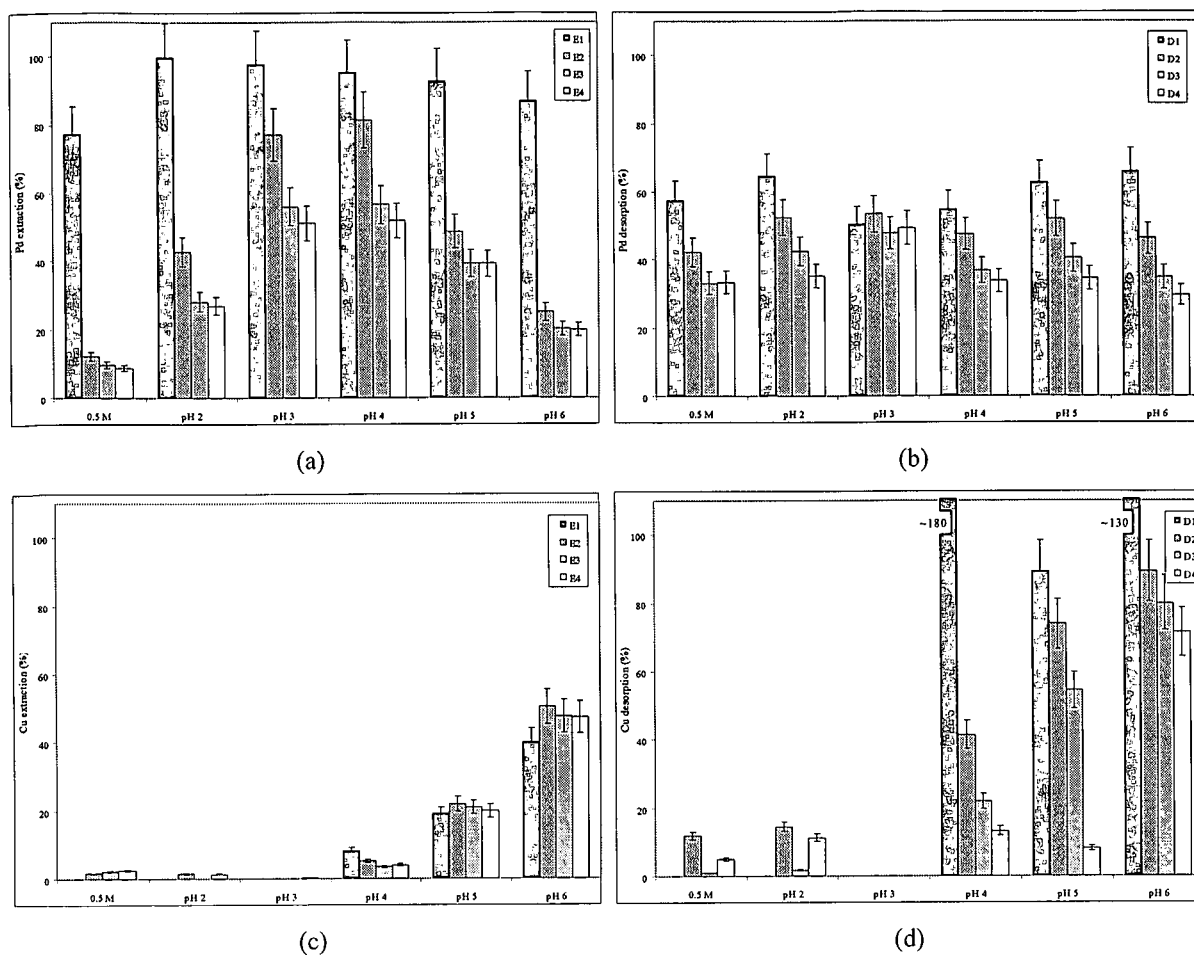


**Figure 5** pH dependent successive percentage (a) Pd(II) extraction, (b) Pd(II) desorption, (c) Cu(II) extraction and (d) Cu(II) desorption by FeSiDETA from solution **III** with ligand:total metal ion ratio of 0.6

A high (> 75 %) to quantitative extraction of Pd(II) is achieved in extraction cycle E1 (Fig 5 (a)), with the percentage extraction decreasing over successive cycles. The possible reasons for this decrease in extraction are threefold:

- The desorption takes place using 2 M HCl which provides large quantities of competing  $\text{Cl}^-$  anions to strip the Pd(II)<sup>35</sup>. However, some dissolution of the Fe in the FeSiDETA may occur, resulting in a deterioration of the FeSiDETA over an extended period of time. DETA-functionalised silica no longer possessing a magnetic core may be lost in the magnetic decantation washing process resulting in a decreased extraction potential in successive cycles. (Fe losses are discussed in Section 3.4.)
- A second possible reason for the decrease in extraction with successive cycles is that the ion exchanger may become saturated with extracted Pd(II). As can be seen from the first desorption cycle D1 (Fig 5 (b)) and for all solution matrices, less than ~70 % of the extracted Pd(II) is desorbed from the surface of the

material. There are therefore, not as many available sites on the ion exchanger in the subsequent extraction cycle E2 ((Fig 5 (a)), for Pd(II) extraction.

- Finally, the decrease in Pd(II) extraction at higher pH (Fig 5 (a)) may occur as a result of competition from Cu(II) for binding sites. In fact, this decrease in Pd(II) extraction above pH 5 is slower in solution **II** containing only Pd(II) and no Cu(II) (data not presented here) as compared to solution **III** very likely owing to the lack of competing metal ions.

The initial percentage Pd(II) desorption (D1, Fig 5 (b)) is less than ~70 % for most cases and shows a decrease in extent of desorption with time. This could occur for two reasons:

- The percentage desorption in the second desorption cycle, D2 (Fig 5 (b)), is calculated as a function of the mass of Pd(II) extracted in the previous cycle E2 plus any Pd(II) remaining on the extractant after desorption in cycle D1. It is possible that some Pd(II) binds irreversibly to the FeSiDETA through more stable chelated complexes which are difficult to desorb, thereby impairing the capacity of the material for extraction during subsequent cycles. (Desorption of anions from the surface with a change of anion concentration in solution may be slow because of the high energy of required to desorb multidentate surface complexes and because adsorbed ions may diffuse slowly out of the nanopores<sup>30</sup>.)
- An additional possibility is that FeSiDETA loaded with Pd(II) is lost during materials handling, since up to 10 % Fe is lost from materials handling (losses from materials handling are discussed in Section 3.4). The removal of this Pd(II) from the system via FeSiDETA losses is not taken into account in desorption calculations (based on a Pd(II) mass balance and assuming the mass of ion exchanger substrate is constant) and may therefore result in an under-reported desorption percentage.

The percentage Cu(II) extraction is low for most extraction cycles (Fig. 5 (c)) with Pd(II) being selectively extracted from solution over Cu(II) with a decrease in pH. As for the percentage Pd(II) desorption (Fig. 5 (b)), the percentage Cu(II) desorption (Fig. 5 (d)) also decreases with time possibly owing to the buildup of Cu(II) on the extractant surface. The percentage desorption at pH 4 and 6 for the first desorption cycle (D1) is greater than 100 %. A potential experimental error may have arisen in these calculations owing to the relatively low mass of Cu(II) extracted in cycles E1 (< ~10 % for pH 4). Because low masses of Cu(II) are extracted originally, the liberation of even small quantities of Cu(II) could inflate desorption percentages. In addition, the deterioration of FeSiDETA under the harsh desorption conditions may result in the liberation of extracted Cu(II) into the supernatant which is then reported as being desorbed material.

Similar trends are observed for subsequent extraction and desorption cycles (E3 to E4 and D3 to D4) across all solution matrices. The percentage successive Pd(II) and Cu(II) extraction and desorption from solutions **I** and **II** was also determined. The data are not presented here because these results indicated similar trends as for the mixed metal ion solution.

### 3.4 Fe dissolution and losses during extraction, desorption and materials handling

During the Pd(II)/Cu(II) extraction from the mixed metal ion solution **III**, a significant amount (75 – 88 %) of iron dissolution from the  $\text{Fe}_3\text{O}_4$  is observed in the lower pH solutions (0.5, 2 and 3 M HCl solutions, see Fig. 6 (a)), while in comparison, the Fe dissolution from the FeSi and FeSiDETA material is greatly reduced for these solutions (< 3 % iron dissolution, see Fig. 6 (b)). This translates to an improvement in resistance to Fe dissolution offered by the silica coating of up to 87 %. The fact that some Fe dissolution does still take place indicates that the FeSiDETA is slightly porous and magnetite could be leached out from the core depending on the contact time and nature of the contact solution. In this case, the contact time of 24 hours during extraction in specifically the 0.5, 1, 2 and 3 M HCl media and pH 2 and 3 buffer solutions resulted in dissolution of the unmodified magnetite within approximately 1 hour (also noticeable from the solution which became yellowish in colour). (Similar Fe dissolution patterns were observed for the Pd(II) solution **II** and the data are therefore not presented here. For the Cu(II) solution **I** (pH 4 and 6 buffers), the Fe dissolution from the magnetite, FeSi and FeSiDETA particles is less than ~1 % owing to the low magnetite solubility<sup>23</sup> at and above pH 4.)

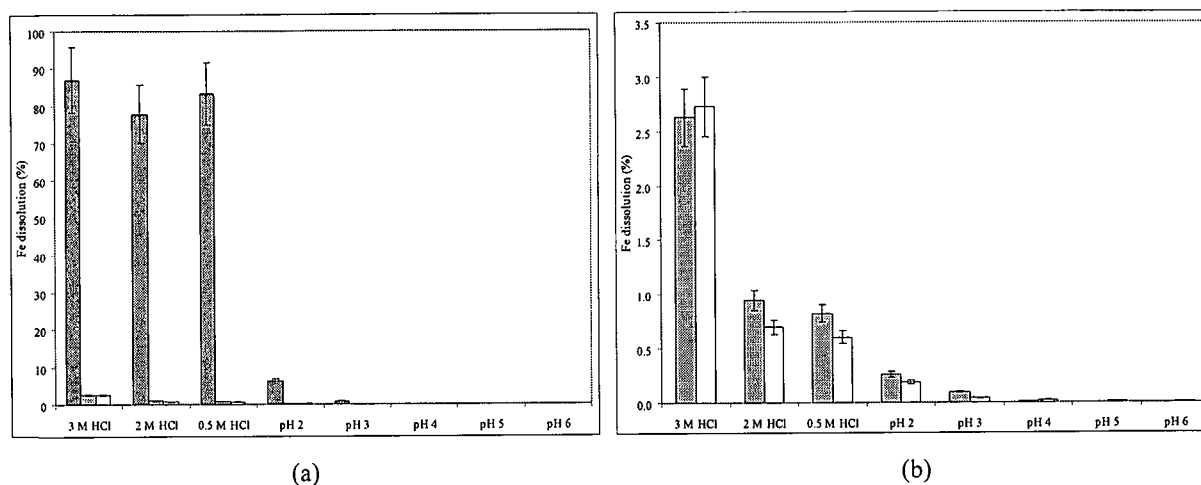


**Figure 6** (a) Percentage Fe dissolution during extraction studies for magnetite (in black  $\blacksquare$ ), FeSi (in grey  $\square$ ) and FeSiDETA (no colour  $\square$ ) from solution **III** with the Fe dissolution below 3 % enlarged in (b). Note the different scale on the x and y axes.

Table 1 gives the cumulative percentage Fe dissolution from FeSiDETA after successive cycles of extraction at varying pH and with desorption using 2 M HCl for solutions **I** to **III**. In general, the cumulative Fe dissolution (after cycle 4) is approximately 40 % with the 0.5 M HCl solution matrix showing the greatest Fe dissolution (> 60 %).

**Table 1** Cumulative Fe dissolution of FeSiDETA from solutions **I** to **III** after each recovery cycle (one recovery cycle consists of one extraction cycle at varying acidity and one desorption cycle using 2 M HCl)

Cycle	Cumulative Fe dissolution (%)					
	0.5 M HCl	pH 2	pH 3	pH 4	pH 5	pH 6
Solution <b>I</b> (Cu(II), pH 4 and pH 6 buffer solutions)						
1	-	-	-	4	-	6
2	-	-	-	8	-	16
3	-	-	-	14	-	29
4	-	-	-	25	-	44
Solution <b>II</b> (Pd(II), 0.5, 1, 2 and 3 M HCl and pH 2–6 buffer solutions)						
1	7	5	5	5	4	4
2	22	14	14	14	11	13
3	43	28	27	29	21	27
4	63	44	43	48	34	43
Solution <b>III</b> (Pd(II) and Cu(II), 0.5, 1, 2 and 3 M HCl and pH 2–6 buffer solutions)						
1	7	6	5	7	5	5
2	22	16	13	19	13	14
3	44	32	26	36	26	28
4	65	48	43	53	43	44

The dissolution of iron from magnetite, FeSi or from FeSiDETA (as given in Table 1) takes place during the three stages of ion exchange: during an extraction or desorption cycle and during materials handling (washing, magnetic decantation, etc.). It is, however, the desorption stage that gives rise to the highest percentage Fe dissolution. For example, the dissolution of Fe from FeSiDETA that occurred during the Pd(II)/Cu(II) extraction and desorption cycles (solution **III**) is shown in Fig. 7. During the extraction cycles (Fig. 7 (a)), the maximum overall Fe dissolution is less than 4 % with the percentage dissolved Fe from the FeSiDETA being highest in the 0.5 M HCl and pH 2 and 3 solutions, lowest in the higher pH buffers (< 0.1 %), and in general, increasing with successive extraction cycles. By comparison, the Fe dissolution in successive desorption cycles (Fig. 7 (b)) rises up to ~20 % with a steady increase in dissolution per cycle and the sum of the Fe losses from the four desorption cycles being as high as 50 %. The increase in dissolution is very likely the result of successive attack and entry of the relatively strong acidic desorbent solution (2 M HCl) into the pores of the FeSiDETA extractant and could be minimised by implementing one or more of the following options:

- An alternative less acidic solution with high anion counterion concentration or less acidic desorbent such as thiourea, thiourea/HCl, HNO<sub>3</sub> or NaClO<sub>4</sub> could be used<sup>22</sup>.

- The desorption time could be decreased to minimise diffusion of acid desorbents into FeSiDETA pores. In addition, the extractant could be washed more thoroughly to remove the acid desorbent from the pores (although this could potentially lead to increased materials handling and an increased possibility of additional material loss).
- The acid resistance of the magnetite particles could be improved by increasing the silica coating thickness on the magnetite particles. There is, however, a limitation as to the thickness of silica that can be applied to particles as this has an influence on the magnetic response of the particles in a magnetic field. (Preliminary attempts at sintering particles in a vertical tube furnace were discussed in Chapter 6, but sintered material did not yield FeSiDETA with a greatly improved acid resistance and caused material agglomeration.)
- Finally, the magnetite could be coated with a more resistant polymeric material before being functionalised with DETA.

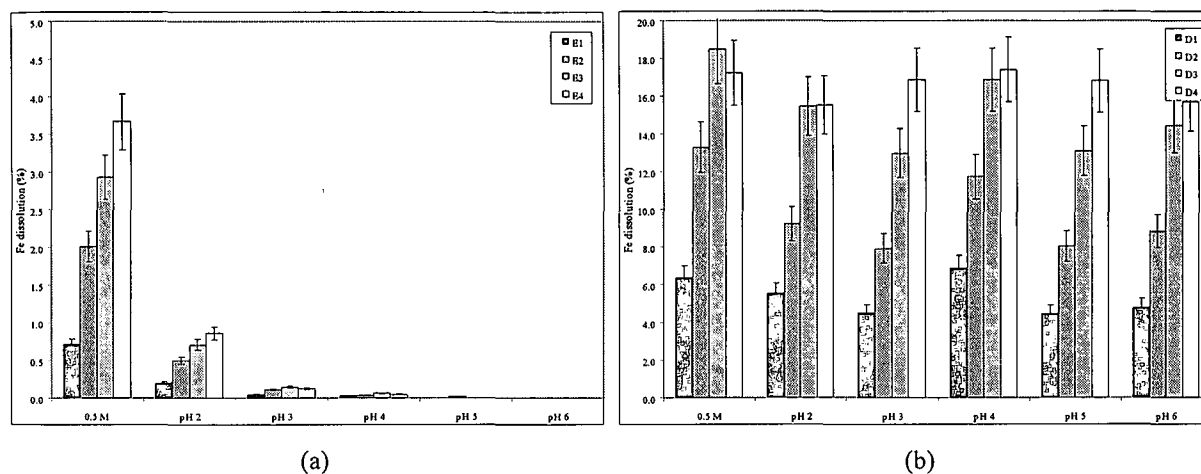


**Figure 7** Successive percentage Fe dissolution of FeSiDETA during (a) extraction and (b) desorption (note different scales on y-axis) of Pd(II) and Cu(II) from the mixed metal ion solution **III**

The third factor causing Fe losses, that of material losses from handling, could be minimised by modifying the experimental method used, e.g., through the use of stronger rare earth magnets as opposed to ferrite magnets for better retention of magnetic FeSiDETA extractants or through the use of a column setup as opposed to batch magnetic decantation of samples.

The degradation as observed for the FeSiDETA material also occurs in commercial resins which are subject to chemical degradation (oxidation, reaction of the resins with organic material present in the process solution or thermal instability) and physical degradation (expansion and contraction by variation in osmotic pressure, attrition during transportation such as in a moving-bed system, precipitation of inorganic solids inside or outside the bead)<sup>3</sup>. To obtain additional information as to the longer-term performance of the FeSiDETA, the extent and rate of deterioration of the nanomagnetic resin could be evaluated against that of a commercial resin with both resins under similar operating conditions.

#### 4. Conclusions

Nanosized, DETA-functionalised silica-coated magnetite ion exchange particles synthesised as described in Chapter 6 were used successfully for extraction studies. These studies have shown that more Pd(II) is extracted consistently by the FeSiDETA as compared to the unmodified magnetite and FeSi. In very acidic media (2 and 3 M HCl solutions), no extraction occurs as the chlorides compete with the anionic  $[\text{PdCl}_4]^{2-}$  for binding to the ion exchanger whereas under slightly less acidic conditions up to quantitative extractions could be achieved. In addition, Pd(II) is extracted selectively to Cu(II) with the greatest selectivity occurring in more acidic media. Increasing the molar ratio of ligand:total metal ion in a solution of Pd(II) and Cu(II) ions still results in the quantitative extraction of Pd(II) and an increased extraction of Cu(II) as compared to the case where stoichiometric ligand:Pd(II) ion is used. To further improve extraction efficiency, the FeSi ligand loading could be increased, i.e., increase functional group density.

In general, for the successive recovery extraction/desorption tests, good (> 80 %) to quantitative Pd(II) extraction is observed, decreasing with successive cycles. This decrease may occur as a result of deterioration or loss of the FeSiDETA ion exchanger with time thereby decreasing the capacity for successive extraction. Secondly, the ion exchanger may become saturated with the extracted metal ion due to incomplete desorption. The selective extraction of Pd(II) to Cu(II) is again observed in the successive recovery studies. The selectivity is greatest in acidic media where the DETA is sufficiently protonated to bind through ion pairing with the  $[\text{PdCl}_4]^{2-}$  whilst the Cu(II) forms non-extractable cationic  $[\text{Cu}(\text{H}_2\text{O})_6]^{2+}$  complexes under these conditions.

Fe dissolution for the silica-coated magnetite particles is reduced from up to 88 % to below 3 % for a single-stage extraction. Fe dissolution during the successive recovery studies is greatest during desorption (maximum of 55 %) followed by materials handling (maximum of 18 %) and extraction (maximum of 10 % in 0.5 M HCl) across all solution matrices. Fe dissolution may pose a problem for continuous or long-term processing in acidic media. However, a less acidic desorbent, shorter desorption time, thicker silica coating or more resistant polymeric coating material could be investigated to reduce FeSiDETA deterioration.

With the judicious selection of operating parameters, the FeSiDETA particles could, in future, potentially provide an ion exchanger surface area orders of magnitude greater than conventional ion exchangers and, with their unique magnetic properties, offer alternative novel processing techniques as compared to, for example, packed columns.

#### References

1. Dorfner, K., *Ion exchangers: properties and applications* Ann Arbor Science Publishers Inc., Michigan, 1973.
2. De Dardel, F.; Arden, T. V., *Ion exchangers* VCH Verlagsgesellschaft mbH, Weinheim, 1989.
3. Bolto, B. A.; Pawlowski, L., *Wastewater treatment by ion-exchange* E. & F. N. Spon Ltd, London, 1987.

4. Willard, M. A.; Kurihara, L. K.; Carpenter, E. E.; Calvin, S.; Harris, V. G., *Encycl. Nanosci. Nanotech.* 2004, **1**, 815.
5. Bönemann, H.; Nagabhushana, K. S., *Encycl. Nanosci. Nanotech.* 2004, **1**, 777.
6. Buske, N.; Sonntag, H.; Götze, T., *Colloids Surf.* 1984, **12**, 195.
7. Häfeli, U. O., *Int. J. Pharm.* 2004, **277**, 19.
8. Warshawsky, A., *Hydrometallurgical processes for the separation of platinum group metals (PGM) in chloride media in Ion exchange technology* Ellis Horwood Ltd, Chichester, 1984.
9. Rao, C. R. M.; Reddi, G. S., *Trends Anal. Chem.* 2000, **19**, 565.
10. Venter, I., *Mining Weekly* 2006, **12**, 7.
11. Warshawsky, A., *Extraction of platinum group metal ions by ion exchange resins in Ion exchange and sorption processes in hydrometallurgy* John Wiley & Sons, Chichester, 1987.
12. Anderson, N. J.; Kolarik, L. O.; Swinton, E. A.; Weiss, D., *Wat. Res.* 1980, **14**, 967.
13. Anderson, N. J.; Bolto, B. A.; Eldridge, R. J.; Kolarik, L. O.; Swinton, E. A., *Wat. Res.* 1982, **20**, 537.
14. Kolarik, L. O., *Wat. Res.* 1982, **17**, 141.
15. Terashima, Y.; Ozaki, H.; Sekine, M., *Wat. Res.* 1986, **20**, 537.
16. Chen, W. Y.; Anderson, P. R.; Holsen, T. M., *Research Journal WPCF* 1991, **63**, 958.
17. de Latour, C., *J. Am. Water Works Assoc.* 1976, **68**, 443.
18. Gélinas, S.; Finch, J. A.; Vreugdenhill, A. J., *Int. J. Miner. Process* 2000, **59**, 1.
19. Kim, Y.; Byunghwan, L.; Jongheop, Y., *Sep. Sci. Technol.* 2003, **38**, 2533.
20. Kaminski, M. D.; Nuñez, L., *J. Magn. Magn. Mater.* 1999, **194**, 31.
21. Lin, Q.; Xu, Z., *J. Appl. Phys.* 1996, **79**, 4702.
22. Uheida, A.; Iglesias, M.; Fontàs, C.; Zhang, Y.; Muhammed, M., *Sep. Sci. Technol.* 2006, **41**, 909.
23. Pourbaix, M., *Atlas of electrochemical equilibria in aqueous solutions.* Pergamon Press Ltd., Oxford, 1966.
24. Rasband, W., ImageJ: Image processing and analysis in Java <http://rsb.info.nih.gov/ij/>.
25. Massart, R.; Cabuil, V., *Journal de Chimie Physique et de Physico-Chimie Biologique* 1987, **84**, 967.
26. van Ewijk, G. A.; Vroege, G. J.; Philipse, A. P., *J. Magn. Magn. Mater.* 1999, **201**, 31.
27. Kramer, J.; Garcia, A. R.; Driessen, W. L.; Reedijk, J., *Chem. Commun.* 2001, **23**, 2420.
28. Kramer, J.; Driessen, W. L.; Koch, K. R.; Reedijk, J., *Hydrometallurgy* 2002, **64**, 59.
29. Kramer, J.; Dhladhla, N. E.; Koch, K. R., *Sep. Purif. Technol.* 2006, **49**, 181.
30. Cornell, R. M.; Schwertmann, U., *The iron oxides* VCH Publishers, New York, 1996.
31. Milonjic, S. K.; Kopenci, M. M.; Ilic, Z. E., *J. Radioanal. Chem.* 1983, **78**, 15.
32. Kosmulski, M., *J. Colloid Interface Sci.* 2004, **275**, 214.
33. Sun, Z.-X.; Su, F.-W.; Forsling, W.; Samskog, P.-O., *J. Colloid Interface Sci.* 1998, **197**, 151.
34. Wesolowski, D. J.; Machesky, M. L.; Palmer, D. A.; Anovitz, L. M., *Chem. Geol.* 2000, **167**, 193.
35. Kar-On Leung, B.; Hudson, M. J., *Solvent Extr. Ion Exch.* 1992, **10**, 173.
36. Sjöberg, S., *J. Non-Cryst. Solids* 1996, **196**, 51.
37. Nesterenko, P. N.; Ivanov, A. V.; Galeva, N. A.; Seneveratne, G. B. C., *J. Anal. Chem.* 1997, **52**, 736.
38. Bernardis, F. L.; Grant, R. A.; Sherrington, D. C., *React. Funct. Polym.* 2005, **65**, 205.
39. Lehto, J.; Harjula, R., *React. Funct. Polym.* 1995, **27**, 121.

## Chapter 8

### Project summary, evaluation and general discussion

---

In this thesis, the synthesis of magnetite nanoparticles and the development of systems containing these particles for transition and platinum group metal ion extraction were investigated.

The factorial design experiment in **Chapter 2** highlighted the importance of the Fe(III):Fe(II) ratio on the saturation magnetisation and percentage magnetite precipitated, with a lower Fe(III):Fe(II) ratio favouring magnetite formation. Although the Fe(III):Fe(II) ratio and iron and ammonia solution concentrations were found to be significant in terms of the resultant particle size of material, the actual particle size variation was found to be only 2 nm which would be insignificant for our applications.

The parameters highlighted in Chapter 2, were taken into account in the high pressure impinging stream reactor test work in **Chapter 3**. Reactor shape and volume were found to be critical in the large-scale, continuous precipitation of magnetite with the circular and kite-shaped reactors providing precipitate of highest percentage magnetite and saturation magnetisation.

In **Chapter 4**, it was shown that magnetite, magnetic liquid and an Aliquat 336/magnetic liquid mixture can be used for the extraction of  $[\text{Co}(\text{NCS})_4(\text{H}_2\text{O})_2]^{2-}$  from an aqueous solution to form the  $[\text{Co}(\text{SCN})_4]^{2-}$  complex in the organic phase. An increased volume of extractant showed an increase in percentage Co(II) extraction. MIBK extraction proceeded with preliminary extraction by MIBK followed by magnetic liquid addition as MIBK scavenger and Co(II) extractant. It appears that a trade-off between the concentration of magnetite in the magnetic liquid or ratio of the volume of organic extractant to the aqueous phase and the extraction time or degree of mixing may have to be made to ensure sufficient phase contact.

In **Chapter 5**, it was found that the use of a magnetic liquid in a solvent extraction setup as compared to a conventional non-magnetic system appears to promote rapid phase separation without loss of extraction potential or selectivity. Extraction kinetics were rapid with maximum extraction occurring within 10 minutes. It was found that in some cases, the rate of phase separation using the magnetic liquid system increased by up to 80 %.

In **Chapter 6**, a silica-coated diethylenetriamine-functionalised magnetite ion exchanger was synthesised through citric acid stabilisation of magnetite, coating by tetraethoxysilane and functionalising with diethylenetriamine (DETA). Resistance to acid dissolution of the iron in the magnetic core was increased by approximately 80 %, as a result of the silica coating while sintering and applying multiple coats to the particles did not significantly enhance the acid resistance.

The DETA-functionalised silica-coated magnetite ion exchanger particles were used in **Chapter 7** for the selective extraction of Pd(II) over Cu(II) with the greatest selectivity occurring in more acidic media. In general, for the successive recovery extraction/desorption tests, good (> 80 %) to quantitative Pd(II) extraction is observed, decreasing with successive cycles. The ion exchanger may deteriorate, be lost during materials handling or become saturated with the extracted metal ion due to incomplete desorption thus decreasing successive extraction capacity. Fe dissolution is again shown to decrease by approximately 80 % for single-stage extractions.

### Evaluation of thesis objectives

The research aims of this thesis were:

1. to synthesise magnetite nanoparticles on a larger scale than current conventional laboratory batch syntheses methods and to characterise the precipitated material

Synthesis of the magnetite nanoparticles on a larger scale by means of the impinging stream reactors as compared to the popular conventional laboratory batch magnetite synthesis proved successful with scale up from a batch precipitation of ~50 g to a continuous synthesis of magnetite of at least 3 kg h<sup>-1</sup>. The impinging stream reactors also allow for the continuous precipitation of particles of 8 – 12 nm diameter, suitable for use in industrial applications.

2. to synthesise and investigate the use of a magnetic liquid system for transition metal ion extraction

From the investigations conducted, it can be concluded that the magnetically modified solvent extraction system shows promise in terms of the potential it offers for more rapid organic/aqueous phase separation after solvent extraction of base metal ions. The magnetic liquid system would function optimally for the extraction of cationic metal ion species in aqueous solutions of pH > 4 (to limit magnetite solubility), with the magnetic liquid itself acting as a metal ion extractant through coordination to the magnetite surface. A potential limitation as to the use of the magnetically modified solvent extraction system, would be the acidity of aqueous solutions with which the magnetic liquid is contacted (process streams or stripping solutions) owing to the magnetite solubility at low solution pH.

3. to synthesise and investigate the use of a superparamagnetic ion exchanger for transition and/or platinum group metal ion extraction

The synthesised superparamagnetic DETA-functionalised ion exchanger material, FeSiDETA, shows great potential for use as a selective platinum group metal ion exchanger material. Alternative FeSiDETA synthesis methods should, however, be investigated as the small-scale laboratory preparation of such a

material is laborious and it would be difficult to scale such a system up for a commercial application. In addition, modifications to the FeSiDETA material, for example, in terms of acid resistance of the ion exchanger, may allow for extended reuse of this material in industrial applications of successive metal ion extraction and desorption. One of the greatest advantages of superparamagnetic ion exchangers is that they can be used in novel processing embodiments as compared to current conventional ion exchanger unit operations. Metal ion extraction could be effected by contacting such particles in, for example, a stirred tank reactor and then using an external magnetic field for removal or retention of the magnetic ion exchanger in the vessel whilst removing the supernatant. The potential for an alternative novel ion exchange processing technique allows for the ion exchanger particle size to be reduced, a factor which is currently avoided owing to the large pressure drops experienced over packed columns associated with small particle size. The small particle size which is an inherent characteristic of the FeSiDETA ion exchanger also allows for a greatly increased surface area with correspondingly increased ligand concentration per mass of ion exchanger.

The potential use of these magnetic nanoparticles in solvent extraction and ion exchange technology therefore holds great promise primarily because their superparamagnetic nature allows for particle manipulation and novel processing techniques without loss of performance under carefully selected conditions.